Marco Paulo Soares dos Santos

Um novo modelo de conceito para implantes ortopédicos instrumentados ativos

A new concept model for instrumented active orthopaedic implants

Marco Paulo Soares dos Santos

Um novo modelo de conceito para implantes ortopédicos instrumentados ativos

A new concept model for instrumented active orthopaedic implants

Tese apresentada à Universidade de Aveiro para cumprimento dos requisitos necessários à obtenção do grau de Doutor em Engenharia Mecânica, realizada sob a orientação científica do Prof. Doutor Jorge Augusto Fernandes Ferreira, Professor auxiliar do Departamento de Engenharia Mecânica da Universidade de Aveiro, e do Prof. Doutor José António de Oliveira Simões, Professor associado com agregação do Departamento de Engenharia Mecânica da Universidade de Aveiro.

Apoio financeiro da FCT e do FSE no âmbito do III Quadro Comunitário de Apoio.

o júri / the jury

presidente / president

Prof. Doutor Paulo Jorge dos Santos Gonçalves Ferreira
Professor catedrático da Universidade de Aveiro

vogais / examiners committee

Prof. Doutor Paulo Rui Alves Fernandes
Professor associado com agregação do Instituto Superior Técnico da Universidade de Lisboa

Prof. Doutor Mário Augusto Pires Vaz
Professor associado com agregação da Faculdade de Engenharia da Universidade do Porto

Prof. Doutor Raul Manuel Pereira Morais dos Santos
Professor associado com agregação da Escola de Ciências e Tecnologia da Universidade de Trás-os-Montes e Alto Douro

Prof. Doutor António Manuel de Amaral Monteiro Ramos
Professor auxiliar da Universidade de Aveiro

Prof. Doutor Jorge Augusto Fernandes Ferreira
Professor auxiliar da Universidade de Aveiro (orientador)

agradecimentos / acknowledgements

Many friends have supported me to conclude this research work, namely:

Prof. Dr. Jorge Ferreira: more than 9 years of supervision but, most important of all, a friendship for life! I hope we can keep working together for many years!

Prof. Dr. José Simões: I am always delighted with your scientific vision! Thank you for teaching me that a researcher must be a visionary!

Prof. Dr. António Ramos: how many scientific dreams we have been sharing over the last years! I hope we can keep dreaming!

Dr. Ricardo Pascoal: more than your scientific skills, I have always appreciated your generosity! Thank you!

Prof. Dr. Sandra Vieira: your scientific skills and your unstoppable enthusiasm are true inspirations for me! Thank you!

Prof. Dr. Odete da Cruz e Silva: I would like to thank you for your collaboration in this interdisciplinary project.

João Torrão: I always knew that I could trust you to support our research efforts! Thank you for your prompt assistance!

Ana Marote: Thank you for your collaboration in this project! Your support was of great importance!

Prof. Dr. Edward Furlani, your enthusiasm for science is teaching me a lot! I hope we can keep our collaboration for many years.

I would also like to thank Prof. Vítor Santos, António Festas, Jorge Almeida, Nuno Silva, Rui Cancela, Telmo Rafeiro, Susana Meireles, Mário Santos, Ana Graça, Luís Rodrigues, and many others friends that, although they are not mentioned here, they know how helpful they were. You are all in my heart.

Of course I have to emphasize the love of my parents. Thank you for your love, patience and to teach me to work hard!

I would like to thank the Portuguese Foundation for Science and Technology (FCT) for their financial support POPH/FSE under the project EXPL/EMS-SIS/2128/2013 and the grant SFRH/BD/78414/2011. My gratitude to the Department of Mechanical Engineering, Centre for Mechanical Engineering and Automation (TEMA) and Institute for Biomedicine (iBiMED) from the University of Aveiro, as well as to Motofil Robotics, for providing all the means required to carried out this thesis.

Finally, I would like to thank the *Logos*, creator of movement to the last complexity. Your love is so eccentric that call us to participate in the last complexity, the true science! Thank you for teaching us that science must research the overall universe of reason.

Palavras-chave

Artroplastia, osseointegração, implante ortopédico, implante instrumentado ativo, estimulação da regeneração óssea, estimulador capacitivo, geração de energia.

Resumo

A artroplastia total da anca (THR) é um dos procedimentos cirúrgicos mais realizados à escala global. Milhões de THRs são realizadas todos os anos em todo o mundo. Atualmente, as taxas de revisão destas artroplastias podem ser superiores a 10%. O número de THRs primárias e de revisão têm aumentado e estima-se que cresçam acentuadamente nos próximos anos, principalmente em pacientes com idades inferiores a 65 anos (incluindo aqueles com menos de 45 anos). Também se tem verificado uma tendência generalizada para o uso de fixações não cimentadas, incidência principalmente causada pelo aumento significativo de pacientes mais jovens e/ou activos. Embora se tenham realizado avanços científicos no projeto de implantes não cimentados, têm-se verificado o seu insucesso a longo-prazo. Encontram-se evidências da ineficácia dos modelos de implantes que têm sido desenvolvidos para evitar procedimentos de revisão. O desempenho dos implantes será otimizado se estes foram projetados para controlarem eficazmente o processo de osseointegração. Para se alcançar este objetivo, têm sido propostas a melhoria das técnicas cirúrgicas e dos protocolos de reabilitação, a inovação dos revestimentos (onde se incluem os revestimentos ativos projetados para a libertação controlada de fármacos e/ou outros bio-agentes) e os conceitos de Implante Instrumentado Passivo e Implante Instrumentado Ativo. Contudo, não existem demonstrações conclusivas da eficácia de tais metodologias. O principal objetivo desta tese é propor um novo modelo de conceito para implantes instrumentados para se otimizar a integração osso-implante: o implante instrumentado ativo, energeticamente auto-suficiente, com capacidade de aplicar estímulos biofísicos em tecidos-alvo de forma controlada e personalizada. A necessidade de um novo modelo é demonstrada através da realização de análises de otimalidade ao desempenho dos implantes instrumentados e não-instrumentados. Foram encontrados resultados promissores para o controlo otimizado da osseointegração usando este novo modelo, através da atuação terapêutica baseada na estimulação capacitiva com arquitetura em co-superfície, assim como para fornecer energia elétrica de forma autónoma por mecanismos de transdução baseados em indução eletromagnética usando configurações baseadas na levitação magnética.

Keywords Arthroplasty, osseointegration, orthopaedic implant, instrumented active implant, bone remodeling stimulation, capacitive stimulator, energy harvesting.

Abstract Total hip replacement (THR) is one of the most performed surgical procedures around the world. Millions of THR are carried out worldwide each year. Currently, THR revision rates can be higher than 10%. A significant increase of the number of primary and revision THRs, mainly among patients less than 65 years old (including those under 45 years old) has been predicted for the forthcoming years. A worldwide increase in the use of uncemented fixation has also been reported, incidence caused mainly by the significant increase of more active and/or younger patients. Besides the significant breakthroughs for uncemented fixations, they have not been able to ensure long-term implant survival. Up to date, current implant models have shown evidences of their inability to avoid revision procedures. The performance of implants will be optimized if they are designed to perform an effective control over the osseointegration process. To pursue this goal, improved surgical techniques and rehabilitation protocols, innovative bioactive coatings (including those for controlled delivery of drugs and/or other bio-agents in the bone-implant interface), the concepts of Passive Instrumented Implant and Active Instrumented Implant have been proposed. However, there are no conclusive demonstrations of the effectiveness of such methodologies. The main goal of this thesis is to propose a new concept model for instrumented implants to optimize the bone-implant integration: the self-powered instrumented active implant with ability to deliver controlled and personalized biophysical stimuli to target tissue areas. The need of such a new model is demonstrated by optimality analyses conducted to study the performance of instrumented and non-instrumented orthopaedic implants. Promising results on the potential of a therapeutic actuation driven by cosurface-based capacitive stimulation were achieved, as well as for self-powering instrumented active implants by magnetic levitation-based electromagnetic energy harvesting.

Contents

List of publications

The findings achieved in this Ph.D program resulted in 9 publications in international journals, 1 in a book chapter and 8 in the proceedings of congresses/conferences. Besides, 2 manuscripts were already submitted to peer-reviewed international journals. References of the papers (published and unpublished) are enumerated as follows:

1. **Marco P. Soares dos Santos**, Jorge A. F. Ferreira, José A. O. Simões, Ricardo Pascoal, João Torrão, Xiaozheng Xue, Edward P. Furlani, Magnetic levitation-based electromagnetic energy harvesting: a semi-analytical non-linear model for energy transduction, *Scientific Reports (Nature Publishing Group)* 6 (**2016**) 18579.

2. **Marco P. Soares dos Santos**, Jorge A. F. Ferreira, António Ramos, José A. O. Simões, Active Orthopaedic Implants: Towards Optimality, *Journal of the Franklin Institute*, 352(3) (**2015**) 813-834.

3. **Marco P. Soares dos Santos**, Jorge A. F. Ferreira, António Ramos, José A. O. Simões, Raul Morais, Nuno M. Silva, Paulo M. Santos, Manuel C. Reis, Tatiana Oliveira, Instrumented hip joint replacements, femoral replacements and femoral fracture stabilizers, *Expert Reviews of Medical Devices*, 11(6) (**2014**) 617-635.

4. **Marco P. Soares dos Santos**, Jorge A. F. Ferreira, A. Ramos, José A. O. Simões, Raul Morais, Nuno M. Silva, Paulo M. Santos, M. J. C. S. Reis, T. Oliveira, Instrumented Hip Implants: Electric Supply Systems, *Journal of Biomechanics*, 46(15) (**2013**) 2561-2571.

5. João N. D. Torrão, **Marco P. Soares dos Santos**, Jorge A. F. Ferreira, Instrumented knee joint implants: innovations and promising concepts, *Expert Reviews of Medical Devices*, 12(5) (**2015**) 571-584.

6. **Marco P. Soares dos Santos**, Jorge A. F. Ferreira, A. Ramos, Ricardo Pascoal, Raul Morais dos Santos, Nuno M. Silva, José A. O. Simões, M. J. C. S. Reis, António Festas, Paulo M. Santos, Multi-source Harvesting Systems for Electric Energy Generation on Smart Hip Prostheses, J. Gabriel, J. Schier, S. Van Huffel, E. Conchon, C. Correia, A. Fred, H. Gamboa (Eds.), Biomedical Engineering Systems and Technologies, Springer-Verlag Berlin Heidelberg, **2013** pp. 80-96.

7. Nuno M. Silva, Paulo M. Santos, Jorge A. F. Ferreira, **Marco P. Soares dos Santos**, A. Ramos, José A. O. Simões, M. J. C. S. Reis, Raul Morais, Power management architecture for smart hip prostheses comprising multiple energy harvesting systems, *Sensors and Actuators A: Physical* 202(1) (**2013**) 183-192.

8. M. L. Morgado, L. F. Morgado, E. Henriques, N. Silva, P. Santos, **M. Santos**, J. Ferreira, M. Reis, R. Morais, Nonlinear modeling of vibrational energy harvesters for smart prostheses, *Procedia Engineering* 47 (**2012**) 1089-1092.

9. N. Silva, P. Santos, J. Ferreira, **M. Santos**, M. Reis, R. Morais, Multi-purpose and multi-source energy management system for biomedical implants, *Procedia Engineering* 47 (**2012**) 722-725.

10. **M. Soares dos Santos**, Jorge A. F. Ferreira, José A. O. Simões, A. Ramos, Raul Morais dos Santos, Nuno M. Silva, M. J. C. S. Reis, Paulo M. Santos, Design Methodology for the Development of Long-term Hip Prosthesis Survival, *Journal of Biomechanics* 45(Suppl. 1) (**2012**) S106.

11. **Marco P. Soares dos Santos**, Jorge A. F. Ferreira, Daniel R. Fernandes, A. Ramos, José A. O. Simões, An Electrical Power Supply System for Instrumented Hip Joint Prostheses, in *Proceedings of the 7th World Congress of Biomechanics*, Boston, EUA, July 6-11, **2014**.

12. **Marco P. Soares dos Santos**, Jorge A. F. Ferreira, José A. O. Simões, A. Ramos, Próteses de anca instrumentadas, in *Proceedings of the 6th Congresso Nacional de Biomecânica (CNB2015)*, Leiria, Portugal, February 6-7 (**2015**).

13. **Marco P. Soares dos Santos**, Jorge A. F. Ferreira, A. Ramos, José A. O. Simões, Raul Morais, Nuno M. Silva, M. J. C. S. Reis, T. Oliveira, Optimality Analysis of Orthopaedic Implants, in *Proceedings of the 19th Congress of the European Society of Biomechanics (ESB2013)*, Patras, Greece, August 25-28 (**2013**).

14. Tatiana Oliveira, **Marco P. Soares dos Santos**, Jorge A. F. Ferreira, A. Ramos, José A. O. Simões, Raul Morais, Nuno M. Silva, M. J. C. S. Reis, Paulo Santos, Therapeutic Methodology for the Prevention of Aseptic Loosening of Prosthesis, in *Proceedings of the 19th Congress of the European Society of Biomechanics (ESB2013)*, Patras, Greece, August 25-28 (**2013**).

15. M. L. Morgado, L. F. Morgado, E. Henriques, N. Silva, P. Santos, **M. Santos**, J. Ferreira, M. Reis, R. Morais, Nonlinear modeling of vibrational energy harvesters for smart prostheses, in *Proceedings of the 26th European Conference on Solid-State Transducers (Eurosensors 2012)*, Kraków, Poland, September 9-12 (**2012**).

16. N. Silva, P. Santos, J. Ferreira, **M. Santos**, M. Reis, R. Morais, Multi-purpose and multi-source energy management system for biomedical implants, in *Proceedings of the 26th European Conference on Solid-State Transducers (Eurosensors 2012)*, Kraków, Poland, September 9-12 (**2012**).

17. M. L. Morgado, L. F. Morgado, E. Henriques, N. Silva, P. Santos, **M. P. S. Santos**, J. A. Ferreira, M. Reis, R. Morais, Mathematical modeling of cylindrical electromagnetic vibration energy harvesters, in *Proceedings of the 12th International Conference on Computational and Mathematical Methods in Science and Engineering (CMMSE 2012)*, La Manga - Murcia, Spain, July 2-5, pp. 900-908 (**2012**).

18. **M. Soares dos Santos**, Jorge A. F. Ferreira, José A. O. Simões, A. Ramos, Raul Morais dos Santos, Nuno M. Silva, M. J. C. S. Reis, Paulo M. Santos, Design Methodology for the Development of Long-term Hip Prosthesis Survival, in *Proceedings of the 18th Congress of the European Society of Biomechanics (ESB2012)*, Lisbon, Portugal, July 1-4, p. S106 (**2012**).

19. **Marco P. Soares dos Santos**, Ana Marote, João Torrão, Jorge A. F. Ferreira, Odete A. B. da Cruz e Silva, Sandra I. Vieira, Electromagnetic stimulation of bone remodeling in vitro: a review, submitted to the journal *Bioelectrochemistry* .

20. **Marco P. Soares dos Santos**, Ana Marote, João Torrão, Sandra I. Vieira, Odete A. B. da Cruz e Silva, A. Ramos, José A. O. Simões, Jorge A. F. Ferreira, New cosurface capacitive stimulators for the development of active osseointegrative implantable devices, submitted to the journal *Scientific Reports* (Nature Publishing Group).

Abbreviations

MSK	musculoskeletal
THR	total hip replacement
TKR	total knee replacement
NAR	Norwegian Arthroplasty Register
SOR	Swedish Arthopedic Register
REWI	National Joint Registry for England, Wales and Northern Ireland
RUS	Joint Replacement Registry for USA
DC	direct current coupling
CC	capacitive coupling
IC	inductive coupling
EF	electric field
MF	magnetic field
EMF	electromagnetic field
dcEF	electric field generated using DC
ccEF	electric field generated using CC
ccEMF	electromagnetic field generated using CC
icMF	magnetic field generated using IC
icEMF	electromagnetic field generated using IC
PEMF	pulsed EMF
CMF	combined EMF
LF EX	low-frequency voltage excitation
HF EX	high-frequency voltage excitation
NO ST	no stimulus (control)
LF ST	low-frequency stimulus
HF ST	high-frequency stimulus
MED1	without cell culture
MED2	pre-confluent cell culture
MED3	confluent cell culture
OM	osteoinductive media
MEM	minimum essential media
NSM	non-suplemented medium
HA	hydroxyapatite
ECM	extracellular matrix
MM	matriz mineralization
ALP	alkaline phosphatase
OPN	osteopontin
OPG	osteoprotegerin
ON	osteonectin
OC	osteocalcin
BSP	bone sialoprotein

Col I	type-I collagen
cbfa	core-binding factor α
FN	fibronectin
BMP	bone morphogenetic protein
IGF	insulin growth factor
TGF	transforming growth factor
Cell Nr	direct cell counting
EA	exclusion assay
MetB	metabolic activity assay
IA	DNA incorporation essay
PS	protein synthesis
WB	western blot
VGCC	voltage-gated calcium channel
DIV	days in vitro
PO	postoperatively
MBA	master active structure
SBA	slave active structure
OHB	outside human body
IHB	inside human body
HIO	instrumentation inside and outside the implant
HI	instrumentation only inside the implant
SiP	sensors in tray
SiS	sensors in stem
RF	radio frequency
FM	frequency modulation
AM	amplitude modulation
PAM	pulse amplitude modulation
PIM	pulse interval modulation
PCM	pulse code modulation
PWM	pulse width modulation
ASK	amplitude-shift keying
UHF	ultra high frequency
CSP	cartilage surface pressure
TEEH	translation-based electromagnetic energy harvester
REEH	rotation-based electromagnetic energy harvester
PEH	piezoelectric energy harvester
ANN	artificial neural network
FEM	finite element method
sD	subset-domain
sC	subset-codomain
SD	set-domain
SC	set-codomain

Chapter 1

Introduction

1.1 Scope

More than 20% of the global disability burden is due to musculoskeletal (MSK) disorders, and increasing trends of these disorders have been observed in developed and developing countries over the last 20 years [1]. Osteoarthritis is a MSK disorder with a global prevalence around 4% and the most common indication for both total hip replacement (THR) and total knee replacement (TKR) [1]. They are among the most performed surgical procedures around the world: millions of THRs and TKRs are carried out worldwide each year [2–4]. Surgical revisions are usually more complex and significantly invasive [5]. By consequence, the burden on individuals, health and social care systems is huge [1]. The incidence of primary and revision THRs and TKRs have been increasing and are predicted to increase even more in the forthcoming years, mainly among patients under 65 years old (including those under the age of 45 years) [6–8], mainly due to the considerable increases in the aged, sedentary and obese population [2, 3]. The need of hip revision procedures is currently about 6% after 5 years and 12% after 10 years following primary THR [9], although 10-year revision rates in the 5-20% range were already estimated regardless of patients' age [10]. The probability to undergo a second revision is five to six-fold higher after the first revision (similar values for THR and TKR) [11], with increasing risks for patients over 70 years old using uncemented implants [12]. According to several recognized national registers, current THR revision rates can be higher than 10%, incidences slightly higher than those being observed for TKR revisions [6, 13–16]. Besides, 90-days mortality after THR increases with age, which has achieved rates around 0.5% for patients younger than 65 years old [13, 17, 18]. Another worldwide phenomenon is the increasing use of uncemented implants in the last decade, upsurge also observed in the oldest age groups, which has been mainly explained by the increasing number of more active and/or younger patients, significant breakthroughs for uncemented fixations, as well as country-related individual surgical cultures and even oriented marketing strategies [6, 13–15, 19–22]. Recent orthopaedic registers indicate nation-dependent rates varying between 15% (Sweden) and 82% (Canada) [20].

1.2 Problem

Besides the significant increasing use of uncemented fixations, mainly among younger patients, various studies conclude that cemented implants have presented higher survival rates when compared to uncemented ones, mainly for patients older than 65 years [19, 20, 22]. Troelsen *et al.* [20] call "the uncemented paradox" to this worldwide phenomenon, highlighting the lack of consensus about which fixation method is able to achieve best performances [20, 23]. On the one hand, poorer performances of uncemented fixations seems to be related to the higher risks of revision of uncemented cups due to aseptic loosening [19]. While stress-shielding also occurs with cemented implants, uncemented fixations are more prone to induced bone loss due to this mechanical phenomena [24], although the prevalence of loosening has been reduced as solutions based on bioactive coatings have been increasingly used [6, 13, 15, 23] (e.g. the CORAIL® Hip System, a hydroxyapatite (HA) coated cementless implant). The initial mechanical stability of uncemented implants usually is a focus of more concerns [24]. Some reports also refer that fractures occur more often on uncemented stems, which increase risks of trauma during the first postoperative year, although they are also attributed to fissures produced during stem insertion [19]. Moreover, antibiotic-impregnated bone cements (e.g. the PALACOS® cement that release Gentamicin) are clinically being used to reduce infection risks [6, 13, 15, 25], but uncemented implants are currently unable to deliver drugs to the bone-implant interface, as the development of bioactive coatings for such purpose are still in preclinical testing stages [26]. It should be also noted that better mobility and reduced post-operative pain seem to be achieved by cementing implants [27]. On the other hand, better performances of uncemented stems have been reported [19, 20, 23]. This success depends upon various factors, among which must be emphasized the use of improved bioactive coatings for uncemented stems, the increased failure risk of cemented stems (mainly of smaller sizes) and the noticed minor training of clinicians to perform optimized cementing procedures [19, 20, 23]. While good stabilities can be achieved by cemented fixations at short-term following arthroplasty, the mid and long-term fixation of cemented implants can deteriorate the cement-stem and/or cement-bone interfaces, increasing the risk of aseptic loosening [24]. Albeit no significant differences in surgical complications are usually found between cemented or uncemented THRs [27], there are significantly higher mortality risks following cemented THRs [28, 29]. Another important observation is that similar risks of revision due to infection between cemented (using antibiotic-impregnated bone cements) and uncemented THA have been reported [4, 19]. Still, there is an increased risk of bacterial colonization and consequent biofilm formation due to porosity of uncemented coatings [30]. Consequently, the controversy about the higher potential of uncemented fixations for optimizing the implants' survival is not surprising [19, 24, 31]. Current therapies have shown evidences of their inability for revision-free joint replacements. This analysis strongly motivates to emphasize the need of innovative solutions for avoiding THR and TKR revisions. The increasing societal and personal burdens associated to revision procedures mainly performed in younger and/or active patients highlight the importance of developing implants to exceed 50 years survival.

The scope of this thesis is the optimization of bone-implant fixation for uncemented THRs. Osseointegration is an essential process to establish an asymptomatic and stable long-term fixation [24, 32]. An accurate control of the factors modulating the osseointegration process is mandatory for optimizing the implants' performance [32–35]. However, such purpose requires a biointegration accomplished at the micrometer and nanometer scale levels [36, 37]. As adverse bone remodeling intensifies, mainly due to wear debris and stress-shielding, the relative motion between the implant and bone increases, which can result in aseptic loosening [24, 32]. Revision rates related to stress-shielding-induced bone loss can exceed 50%, incidences confirming the implant loosening among the most common causes indicated for THR [2, 6, 13, 15]. The periprosthetic infection is also a major consequence of implant insertion [4,38–40]. Analyses using nationwide sampling have shown that THR revisions rates due to infection are around 15% [6,13,15,41]. This epidemiology also suggests the huge projection that can be achieved in the development of novel concept models that can ensure successful bonding of implants to the host skeleton.

Besides surgical techniques and rehabilitation protocols have been quite improved, the common methodologies aiming to improve the performance of hip implants have been focused on the optimization of their design and materials [24, 32, 36, 37]. Recent technology is already able to implement implants with custom-made geometries [42] and nanometer-scale textured surfaces [37]. Advanced biomaterials have been also proposed to maximize the bone-implant adhesion [43, 44]. Although these approaches are quite valuable and further research efforts can improve their long-term outcomes [45–47], they only allow to design passive implants. Implants can only be categorized as *active* if they comprise resources to perform therapeutic actuations to optimize the bone-implant fixation. The potential of actuation systems based on innovative bioactive biomaterials for coating uncemented implants has been exhaustively researched [26, 48]. Coating the implants' surface with HA has been widely used to promote osseointegration (Fig. 1a) [26]. Although their ability to enhance new bone formation, prevent formation of fibrous tissue and seal the interface from wear particles and macrophages, some recent reports have shown no improved clinical outcomes when such coatings are used [26, 49, 50]. Many other materials have been developed for enhancing bioactivity, osteoconductivity, osteoinductivity, non-cytotoxicity and non-genotoxicity of modern implant systems, such as bioactive glasses and glass-ceramics [51, 52]. The potential of active implants embedding local delivery systems has been also quite researched [26, 53, 54] (the mechanism used to perform such operation is here called 'therapeutic delivery' or 'therapeutic actuation'). This is a very relevant approach that consists in developing coating incorporating drugs (e.g. Gentamicin, tobramycin and vancomycin) and/or biomolecules (e.g. growth factors, collagen and proteins) [26,53,55,56]. For example, HA coatings incorporated with collagen, recombinant human bone morphogenetic protein (rhBMP-2) and RGD peptides, HA coatings augmented with osteogenic protein-1 (OP-1), and biodegradable PDLLA coating incorporating gentamicin were already proposed to improve the bone-implant bonding and prevent peri-operative infections [57–59]. Among the delivery methods [60], the stimuli-controlled release must be highlighted as the release rate can be controlled by

endogenous and/or exogenous stimuli, such as temperature, pH, ionic strength, ultrasound and electric or magnetic fields [53, 61–64]. Included are the drug-eluting implants that use nanocarriers (liposomes, micelles, among others) to encapsulate drugs [54, 62, 64–67]. However, these coatings-based targeted local delivery systems are still being analysed and have not been translated to clinic usage and, consequently, their clinical effectiveness is still unknown[26,53,54]. To my best knowledge, no cementless implants incorporating local delivery of drugs and/or biomolecules were already tested in human patients. The concept of Multifunctional Coating was recently proposed to produce clinically-useful systems [26]: cost-effective coatings with ability to deliver optimal temporal and dosing release without local and systemic toxicity and improve the bone-implant fixation. Although these mechanisms now opens very attractive opportunities for controlling the bone-implant bonding, they also present significant drawbacks, namely:

(a) Their design can be extremely complex, increasing as their multifunctional ability increases;

(b) Their controllability is rather reduced because: their delivery dynamics does not consider the peri-implant biochemical and biomechanical states; their behavior cannot be changed after implant insertion (their actuation is pre-established *a priori*); their ability to perform personalized release of drugs, biomolecules or biophysical stimuli is quite limited, as their long-term clinical effectiveness will most likely be unknown after arthroplasty;

(c) Their long-term controllable release of bioactive substances will most likely be quite hard to implement;

(d) Their ability to deliver different stimulations to different and nearby tissue areas will most likely be quite difficult to attain;

(e) Their temporal and dosing release can be significantly hard to monitor.

Hence, the ability of these methods to ensure long-term implant survival must be inquired. Furthermore, one must question if uncemented implants coated with local delivery systems as those above described, regardless their functionality levels, are able to achieve optimal performances.

The concept of Instrumented Implant is another approach that aims to optimize the performance of implants. Besides the inherent function of implants in replacing bone and performing load bearing functions, the main idea is to engineer a new type of implant composed by inner structures to perform monitoring operations and therapeutic actuations. Rydell (1966) [68] was the first researcher to design instrumented implants to measure forces and moments *in vivo* over the implants' neck. He collected data during several daily activities of two patients using percutaneous connections. These findings were the basis for further technological advances aiming optimize the measurement systems, measure an increasing number of quantities (forces, moments, deformations and temperatures) and communicate them wirelessly to extracorporeal systems (Fig. 1b)

[69–75]. The newest two architectures for instrumented hip implants were developed by Bergmann and co-workers [75, 76] in the last five years. However, the main goal of their technological solutions has not been the stimulation of the host tissue biointegration. Biophysical osteogenic stimulation has been studied as a potential non-drug strategy to develop therapeutic actuators for active instrumented implants, mainly based on delivery of mechanical and electromagnetic stimuli. Intracorporeal piezoelectric-based mechanical stimulation was proposed to enhance peri-implant bone formation in sheep femur and tibia [77]. Positive osteogenic effects of static magnetic fields were observed by using magnetized metals of negligible cytotoxicity (SmCo, SmFeN, stainless steel, etc.) intracorporeally (around specific animal bones) [78–81]. The peri-implant bone volume also increased by delivering static magnetic fields using permanent magnets embedded into intramedullary femoral implants [82]. The use of attractive forces between permanent magnets is another innovative fixation method currently being researched to reduce interfacial micromotions [83]. Finally, electromagnetic-stimulating implant systems (Fig. 1c) have been proposed as a groundbreaking approach to deliver controllable electric field stimulation to bone tissues [84–90]. By attaching stimulators' electrodes to implants' surfaces and embedding secondary coil(s) into the implant system, electric fields can be delivered around the implant when a primary coil, placed outside the patients' body (e.g. around the hip), provides a magnetic field to the secondary coil. Although this method has been proposed for various orthopaedic implants, only stimulative screw systems have been tested *in vivo* (e.g. the Magnetodyn® screw has been used in human patients to avoid necrosis of the femur head [85]). All these achievements must be highlighted and significant advances can be attained if these approaches are further explored. The main strengths of implanting instrumented orthopaedic implants can be enumerated as follows:

(i) They have been implanted to acquire data *in vivo*: to calibrate models defining the biomechanical and thermodynamic properties of implants; to optimize the design and materials of implants; to perform preclinical tests; and to track the healing process following THR [91–94];

(ii) They can be designed to monitor osseointegration, including the detection of implant failure states [95–99];

(iii) They can operate as stimuli delivery systems, based on the release of biomolecules, drugs and/or biophysical stimuli, to control the host tissue biointegration [90, 100];

(iv) Their operations, including therapeutic delivery, can be controlled by extracorporeal systems using wireless communication systems [75, 101–103];

(v) They can be composed by processing systems to optimize/manage their operations and analyze the monitored data [74, 75, 104].

Although instrumented implants capable of accurately control the peri-implant bone volume are highly desirable, various constraints must be addressed to develop them. Those most significant are enumerated as follows:

(a) The design of non-biological measuring systems to monitor the osseointegration process is complex (no effective solutions have been found for such purpose [95–98]);

(b) Complex implant designs may be required if drug and/or non-drug delivery systems, controlled by extracorporeal systems, were embedded into instrumented implants;

(c) The optimized/personalized stimuli delivery for highly controllable osseointegration may be complex to identify;

(d) The delivery of different stimulations to different and nearby tissue areas may be hard to achieve (such aim was never accomplished);

(e) Electric powering systems based on batteries or inductive links troubles the activities of patients and cannot be used for long-term operation [76, 94];

(f) Long-term electric self-powering of these implants is hard to develop [102, 105, 106];

(g) Their hollowed architectures increase fracture risks and, consequently, cytotoxic and genotoxic risks.

More optimized osseointegration control will be achieved as highest the ability of the stimulation system deliver different stimuli (amplitude, frequency, periodicity, exposure time, etc) to different and nearby tissue areas. No instrumented implants with ability to release drugs and/or other bio-agents in the bone-implant interface were implemented so far. This methodology could enhance controlled bone remodeling around implants and avoid adverse tissue responses to infection and foreign bodies, but controlling the temporal and dosing release to target tissue areas would most likely be a quite difficult accomplishment, mainly if fibrous tissues are formed due to other causes, such as micromovements of implants. Although it can ensure controllable dosing release (using telemetric systems [100, 107]), a highly complex implant design may be required (inner reservoirs are required, as well as mechanisms to control the delivery vehicles and routes, etc.). Besides, the functional integrity of biomolecules inside the instrumented implants does not allow long-term operability. Controlled delivery systems for personalized medicine can also be implemented by non-drug strategies. Biophysical stimulation is quite attractive for inducing a direct osteogenic effect or triggering drug releases. Electromagnetic, mechanical, ultrasound or light stimulations can promote bone adaptation [81, 108–111]. Besides, their long-term operability will most likely be easier to accomplish as there are no storage requirements, the therapeutic delivery can be controlled by clinicians (using wireless communication between the implant and extracorporeal systems) and miniaturized stimulators can be located nearby tissue areas requiring stimulation (even though they must be embedded into implants). To my best knowledge, no instrumented implants were designed to deliver mechanical, ultrasound or light stimuli. The potential of using mechanical stimulators located in the implants' surface [77] is compromised by the increased risk of weakening the interfacial bonding. Therewithal, generating mechanical stimuli inside implants to apply on target tissue areas is currently unfeasible. Mechanisms for

delivering ultrasound waves may require high complex implant designs and demand a hollowed structure that can endanger the mechanical integrity of implants. Interestingly, positive results were observed using this type of stimulus to control the release and routing of drugs and/or biomolecules [60,110], but such ability was never tested using or involving instrumented implants. Stimulation by static magnetic fields does not allow controllable and personalized therapies, although a positional control of the permanent magnets inside implants can be implemented. Regarding the delivery of electromagnetic stimuli generated by coils inside active implants, a controllable actuation can be provided, but it was never tested and certainly involves complex implant designs. The electrical stimulation obtained by extracorporeally-induced magnetic fields will most likely result in the inability to provide highly controllable stimuli to multiple tissue areas, since the complexity to design extracorporeal sources of magnetic field increases as the number of electrodes increases. Further, technological solutions based on attaching stimulators to the implants' surfaces are unable to deliver stimuli to target tissue areas. In any case, their application troubles the routine activities of the patients if optimized patient-specific clinical therapies must be administrated. Therefore, more research efforts must be conducted to design instrumented implants capable of effective long-term implant survival.

1.3 Main goals

Two main goals were defined for this thesis: to answer how to design implants for permanent bone-implant fixation and to propose an innovative therapeutic delivery system, as well as supporting systems, potentially more effective than those proposed so far. The following tasks were conducted to accomplished these goals:

1. Study the ability of both passive and active orthopaedic implants to optimize their performance. This study intend to answer if methodologies that have been used to develop implants are able to ensure effective long-term survival or, instead, different concept models for orthopaedic implants must be developed;

2. Identify the requirements that implants must fulfil to ensure implant performance optimality;

3. Carry out detailed literature reviews to identify the architectures, therapeutic actuators and supporting technologies already developed for hip implants with higher potential to control the osseintegration process[1];

4. Conduct a literature review focused on therapeutic delivery systems: (i) effective inducing positive osteogenic responses to the different stages of bone remodeling; (ii) not yet used in the design of active orthopaedic implants; (iii) with high potential to deliver different actuations to different and nearby tissue areas;

[1] I also collaborated in a similar study for knee implants (Supplement 1)

5. Develop and test *in vitro* an innovative delivery system, as well as potential supporting systems, to enhance the ability of implants to perform personalized control of the osseointegration process.

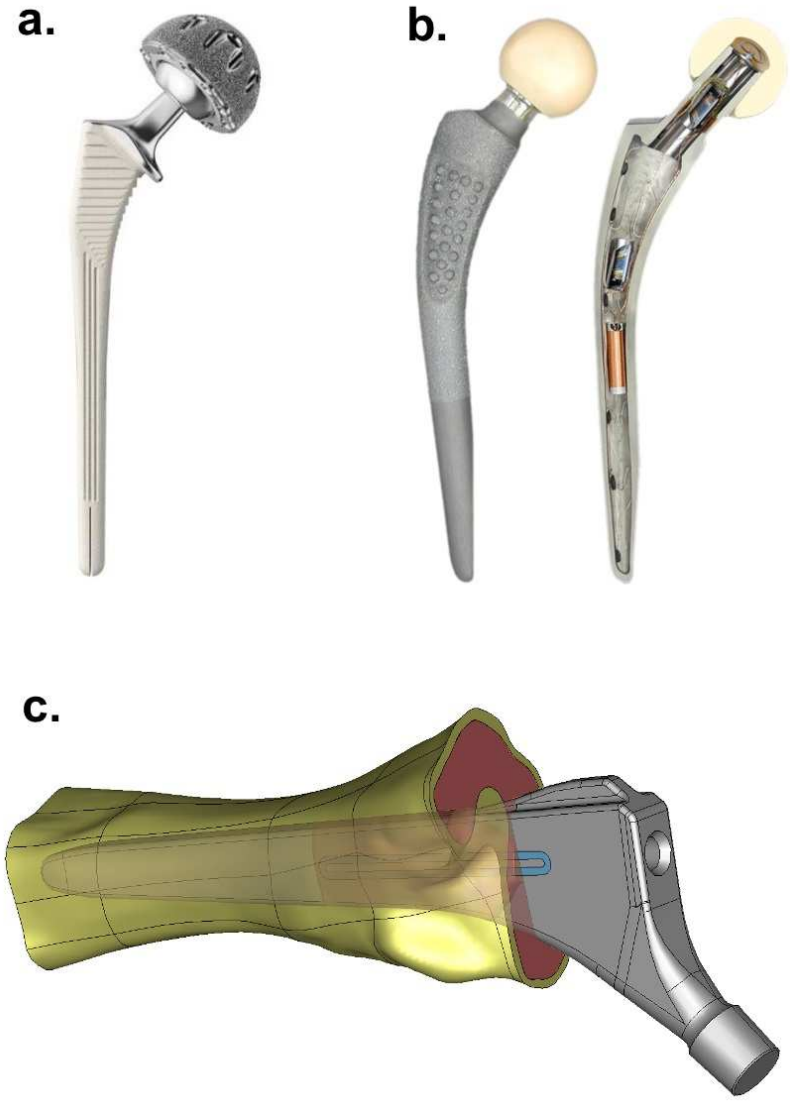

Fig. 1: Several approaches used to design THRs: a. HA coated cementless THR (Corail® Hip System, DePuy Synthes); **b.** Instrumented passive THR (Hip II, Orthoload database); **c.** Prototype of an electrostimulative THR (reproduced with permission from Zimmermann *et al.* [90]).

1.4 Outline

This thesis is divided into seven chapters. Chapters 2 to 5 are composed by a collection of papers already published or submitted manuscripts. A theoretical study to evaluate the performance optimality of orthopaedic implants is presented in chapter 2. Chapter 3 is composed by three literatures reviews that were conducted to evaluate how the implant performances could be improved, considering the conclusions obtained from the optimality analysis. An innovative therapeutic delivery system (concept, modulation, manufacturing and preliminary experimental results) with higher potential to ensure long-term implant survival is proposed in chapter 4. The various findings to develop auxiliary systems supporting the therapeutic actuation are the subject of chapter 5. A detailed discussion on the proposed methodology to design future implants with superior performance is found in chapter 6. Finally, the 7th chapter reports the list of findings and a viewpoint on how this field will most likely evolve in the forthcoming years. Besides, supplementary material is provided to support the innovations here proposed.

References

[1] L. March, E. U. Smith, D. G. Hoy, M. J. Cross, L. Sanchez-Riera, F. Blyth, R. Buchbinder, T. Vos, A. D. Woolf, Burden of disability due to musculoskeletal (MSK) disorders, Best Practice & Research in Clinical Rheumatology 28 (3) (2014) 353–366.

[2] R. Pivec, A. J. Johnson, S. C. Mears, M. A. Mont, Hip arthroplasty, Lancet 380 (2012) 1768–1777.

[3] A. J. Carr, O. Robertsson, S. Graves, A. J. Price, N. K. Arden, A. Judge, D. J. Beard, Knee replacement, Lancet 379 (2012) 1331–1340.

[4] B. H. Kapadia, R. A. Berg, J. A. Daley, J. Fritz, A. Bhave, M. A. Mont, Periprosthetic joint infection, Lancet, in press.

[5] A. R. J. Manktelow, (ii) Implant removal in revision hip surgery, Orthopaedics and Trauma 23 (5) (2009) 307–321.

[6] H. Bergen, Report June 2010, Tech. rep., The Norweigen Arthoplasty Register (2010).

[7] S. Kurtz, K. Ong, E. Lau, F. Mowat, M. Halpern, Projections of primary and revision hip and knee arthroplasty in the United States from 2005 to 2030, The Journal of Bone & Joint Surgery 89 (4) (2007) 780–785.

[8] S. M. Kurtz, E. Lau, K. Ong, K. Zhao, M. Kelly, K. J. Bozic, Future young patient demand for primary and revision joint replacement - national projections from 2010 to 2030, Clinical Orthopaedics and Related Research 467 (10) (2009) 2606–2612.

[9] G. Labek, M. Thaler, W. Janda, M. Agreiter, B. Stöckl, Revision rates after total joint replacement - cumulative results from worldwide joint register datasets, The Journal of Bone & Joint Surgery 93-B (3) (2011) 293–297.

[10] K. L. Corbett, E. Losina, A. A. Nti, J. J. Z. Prokopetz, J. N. Katz, Population-based rates of revision of primary total hip arthroplasty: a systematic review, PloS ONE 5 (10) (2010) e13520.

[11] K. L. Ong, E. Lau, J. Suggs, S. M. Kurtz, M. T. Manley, Risk of subsequent revision after primary and revision total joint arthroplasty, Clinical Orthopaedics and Related Research 468 (11) (2010) 3070–3076.

[12] K. Gromov, A. B. Pedersen, S. Overgaard, P. Gebuhr, H. Malchau, A. Troelsen, Do rerevision rates differ after first-time revision of primary THA with a cemented and cementless femoral component?, Clinical Orthopaedics and related research 473 (11) (2015) 3391–3398.

[13] G. Garellick, J. Körrholm, H. Lindahl, H. Malchau, C. Rogmark, O. Rolfson, Annual report 2013, Tech. rep., Swedish Hip Arthroplasty Register (2013).

[14] M. Sundberg, L. Lidgren, A. W-Dahl, O. Robertsson, Annual report 2014, Tech. rep., Swedish Knee Arthroplasty Register (2014).

[15] M. Porter, M. Borroff, P. Gregg, A. MacGregor, K. T. el al., 10th annual report 2013, Tech. rep., National Joint Registry for England, Wales and Northern Ireland (2013).

[16] E. W. Paxton, R. S. Namba, G. B. Maletis, M. Khatod, E. J. Yue, M. Davies, R. B. L. Jr., R. W. B. Wyatt, M. C. S. Inacio, T. T. Funahashi, A prospective study of 80,000 total joint and 5000 anterior cruciate ligament reconstruction procedures in a community-based registry in the United States, The Journal of Bone & Joint Surgery 92 (2) (2010) 117–132.

[17] L. P. Hunt, Y. Ben-Shlomo, E. M. Clark, P. Dieppe, A. Judge, A. J. MacGregor, J. H. Tobias, K. Vernon, A. W. Blom, 90-day mortality after 409 096 total hip replacements for osteoarthritis, from the National Joint Registry for England and Wales: a retrospective analysis, Lancet 382 (2013) 1097–104.

[18] J. de Gorter, M. Green, P. Gregg, M. Porter, A. Price, K. Tucker, M. Wilkinson, N. W. el al., 12th annual report 2015, Tech. rep., National Joint Registry for England, Wales and Northern Ireland (2015).

[19] N. P. Hailer, G. Garellick, J. Krrholm, Uncemented and cemented primary total hip arthroplasty in the Swedish Hip Arthroplasty Register, Acta Orthopaedica 81 (1) (2010) 34–41.

[20] A. Troelsen, E. Malchau, N. Sillesen, H. Malchau, A review of current fixation use and registry outcomes in total hip arthroplasty: the uncemented paradox, Clinical Orthopaedics and related research 471 (1) (2013) 2052–2059.

[21] M. Niemeläinen, E. T. Skyttä, V. Remes, K. Mäkelä, A. Eskelinen, Total knee arthroplasty with an uncemented trabecular metal tibial component: a registry-based analysis, The Journal of Arthroplasty 29 (1) (2014) 57–60.

[22] K. T. Mäkelä, M. Matilainen, P. Pulkkinen, A. M. Fenstad, L. Havelin, L. Engesaeter, O. F. A. B. Pedersen, S. O. J. Kärrholm, H. Malchau, G. Garellick, J. Ranstam, A. Eskelinen, Failure rate of cemented and uncemented total hip replacements: register study of combined Nordic database of four nations, BMJ 348 (f7592) (2014) 1–10.

[23] G. Green, M. Khan, F. S. Haddad, (i) Why do total hip replacements fail?, Orthopaedics and Trauma 29 (2) (2015) 79–85.

[24] D. R. Sumner, Long-term implant fixation and stress-shielding in total hip replacement, Journal of Biomechanics 48 (5) (2015) 797–800.

[25] E. Jämsen, O. Furnes, L. B. Engesæter, Y. T. Konttinen, A. Odgaard, A. Stefánsdóttir, L. Lidgren, Prevention of deep infection in joint replacement surgery, Acta Orthopaedica 81 (6) (2010) 660–666.

[26] S. B. Goodman, Z. Yao, M. Keeney, F. Yang, The future of biologic coatings for orthopaedic implants, Biomaterials 34 (13) (2013) 3174–3183.

[27] M. J. Parker, K. S. Gurusamy, S. Azegami, Arthroplasties (with and without bone cement) for proximal femoral fractures in adults, Cochrane Database of Systematic Reviews 6 (CD001706) (2010) 1–129.

[28] M. Hossain, J. G. Andrew, Is there a difference in perioperative mortality between cemented and uncemented implants in hip fracture surgery?, Injury 43 (12) (2012) 2161–2164.

[29] D. J. W. McMinn, K. I. E. Snell, J. Daniel, R. B. C. Treacy, P. B. Pynsent, R. D. Riley, Mortality and implant revision rates of hip arthroplasty in patients with osteoarthritis: registry based cohort study, BMJ 344 (e3319) (2012) 1–19.

[30] A. Braem, K. D. Cremer, N. Delattin, K. D. Brucker, B. Neirinck, K. Vandamme, J. A. Martens, J. Michiels, J. Vleugels, B. P. A. Cammue, K. Thevissen, Novel anti-infective implant substrates: controlled release of antibiofilm compounds from mesoporous silica-containing macroporous titanium, Colloids and Surfaces B: Biointerfaces 126 (1) (2015) 481–488.

[31] S. Salih, A. Hamer, Hip and knee replacement, Surgery (Oxford) 31 (9) (2013) 482–487.

[32] V. Goriainov, R. Cook, J. M. Latham, D. G. Dunlop, R. O. Oreffo, Bone and metal: an orthopaedic perspective on osseointegration of metals, Acta Biomaterialia 10 (10) (2014) 4043–4057.

[33] O. M. Omar, M. E. Lenneras, F. Suska, L. Emanuelsson, J. M. Hall, A. Palmquist, P. Thomsen, The correlation between gene expression of proinflammatory markers and bone formation during osseointegration with titanium implants, Biomaterials 32 (2) (2011) 374–386.

[34] J. Y. Kwon, H. Naito, T. Matsumoto, M. Tanaka, Estimation of change of bone structures after total hip replacement using bone remodeling simulation, Clinical Biomechanics 28 (5) (2013) 514–518.

[35] J. Wang, Y. An, F. Li, D. Li, D. Jing, T. Guo, E. Luo, C. Ma, The effects of pulsed electromagnetic eld on the functions of osteoblasts on implant surfaces with different topographies, Acta Biomaterialia 10 (2) (2014) 975–985.

[36] P. G. Coelho, R. Jimbo, Osseointegration of metallic devices: current trends based on implant hardware design, Archives of Biochemistry and Biophysics 561 (2014) 99–108.

[37] P. G. Coelho, T. Takayama, D. Yoo, R. Jimbo, S. Karunagaran, N. Tovar, M. N. Janal, S. Yamano, Nanometer-scale features on micrometer-scale surface texturing: A bone histological, gene expression, and nanomechanical study, Bone 65 (2015) 25–32.

[38] K. J. Bozic, K. Ong, E. Lau, D. J. Berry, T. P. Vail, S. M. Kurtz, H. E. Rubash, Estimating risk in Medicare patients with THA: an electronic risk calculator for periprosthetic joint infection and mortality, Clinical Orthopaedics and Related Research 471 (2) (2013) 574–583.

[39] J. C. Schrama, B. Espehaug, G. Hallan, L. B. Engesaeter, O. Furnes, L. I. Havelin, B.-T. Fevang, Risk of revision for infection in primary total hip and knee arthroplasty in patients with rheumatoid arthritis compared with osteoarthritis: a prospective, population-based study on 108,786 hip and knee joint arthroplasties from the Norwegian Arthroplasty Register, Arthritis Care & Research 62 (4) (2010) 473 479.

[40] V. Antoci, S. B. King, B. Jose, J. Parvizi, A. R. Zeiger, E. Wickstrom, T. A. F. nd Russell J. Composto, P. Ducheyne, I. M. Shapiro, N. J. Hickok, C. S. Adams, Vancomycin covalently bonded to titanium alloy prevents bacterial colonization, Journal of Orthopaedic Research 25 (7) (2007) 858–866.

[41] A. F. Kamath, K. L. Ong, E. Lau, V. Chan, T. P. Vail, H. E. Rubash, D. J. Berry, K. J. Bozic, Quantifying the burden of revision total joint arthroplasty for periprosthetic infection, The Journal of Arthroplasty, in press.

[42] P. Benum, A. Aamodt, Uncemented custom femoral components in hip arthroplasty, Acta Orthopaedica 81 (4) (2010) 427–435.

[43] S. M. Kurtz, S. Kocago, C. Arnholt, R. Huet, M. Ueno, W. L. Walter, Advances in zirconia toughened alumina biomaterials for total joint replacement, Journal of the Mechanical Behavior of Biomedical Materials 31 (2014) 107–116.

[44] J. F. Bartolomé, J. S. Moya, R. Couceiro, C. F. Gutiérrez-González, F. Guitián, A. Martinez-Insua, In vitro and in vivo evaluation of a new zirconia/niobium biocermet for hard tissue replacement, Biomaterials 76 (2016) 313–320.

[45] C. Götze, D. Rosenbaum, J. Hoedemaker, F. Bottner, W. Steens, Is there a need of custom-made prostheses for total hip arthroplasty? Gait analysis, clinical and radiographic analysis of customized femoral components, Archives of Orthopaedic and Trauma Surgery 129 (2) (2009) 267–274.

[46] B. J. McEntire, B. S. Bal, M. N. Rahaman, J. Chevalier, G. Pezzotti, Ceramics and ceramic coatings in orthopaedics, Journal of the European Ceramic Society 35 (16) (2015) 4327–4369.

[47] G. Pezzotti, K. Yamamoto, Artificial hip joints: The biomaterials challenge, Journal of the Mechanical Behavior of Biomedical Materials 31 (2014) 3–20.

[48] B. G. X. Zhang, D. E. Myers, G. G. Wallace, M. Brandt, P. F. M. Choong, Bioactive coatings for orthopaedic implants - recent trends in development of implant coatings, International Journal of Molecular Sciences 15 (7) (2014) 11878–11921.

[49] J. H. M. Goosen, A. J. Kums, B. J. Kollen, C. C. P. M. Verheyen, Porous-coated femoral components with or without hydroxyapatite in primary uncemented total hip arthroplasty: a systematic review of randomized controlled trials, Archives of Orthopaedic and Trauma Surgery 129 (9) (2009) 1165–1169.

[50] F. S. Tudor, J. R. Donaldson, S. R. Rodriguez-Elizalde, H. U. Cameron, Long-term comparison of porous versus hydroxyapatite coated sleeve of a modular cementless femoral stem (SROM) in primary total hip arthroplasty, The Journal of Arthroplasty 30 (10) (2015) 1777–1780.

[51] J. R. Jones, Review of bioactive glass: from Hench to hybrids, Acta Biomaterialia 9 (1) (2013) 4457–4486.

[52] M. C. Crovace, M. T. Souza, C. R. Chinaglia, O. Peitl, E. D. Zanotto, Biosilicate ® - A multipurpose, highly bioactive glass-ceramic. In vitro, in vivo and clinical trials, Journal of Non-Crystalline Solids 432 (2016) 90–110.

[53] J. A. Lyndon, B. J. Boyd, N. Birbilis, Metallic implant drug/device combinations for controlled drug release in orthopaedic applications, Journal of Controlled Release 179 (2014) 63–75.

[54] A. Simchi, E. Tamjid, F. Pishbin, A. R. Boccaccini, Recent progress in inorganic and composite coatings with bactericidal capability for orthopaedic applications, Nanomedicine: Nanotechnology, Biology and Medicine 7 (1) (2011) 22–39.

[55] R. A. Surmenev, M. A. Surmeneva, A. A. Ivanova, Significance of calcium phosphate coatings for the enhancement of new bone osteogenesis - A review, Acta Biomaterialia 10 (2) (2014) 557–579.

[56] J. Parvizi, V. Antoci, N. J. Hickok, I. M. Shapiro, Selfprotective smart orthopaedic implants, Expert Review of Medical Devices 4 (1) (2007) 55–64.

[57] J. He, T. Huang, L. Gan, Z. Zhou, B. Jiang, Y. Wu, F. Wu, Z. Gu, Collagen-infiltrated porous hydroxyapatite coating and its osteogenic properties: In vitro and in vivo study, Journal of Biomedical Materials Research: Part A 100A (7) (2012) 1706–1715.

[58] N. Saran, R. Zhang, R. E. Turcotte, Osteogenic protein-1 delivered by hydroxyapatite-coated implants improves bone ingrowth in extracortical bone bridging, Clinical Orthopaedics and Related Research 469 (5) (2011) 1470–1478.

[59] M. Lucke, B. Wildemann, S. Sadoni, C. Surke, R. Schiller, A. Stemberger, M. Raschke, N. P. Haas, G. Schmidmaier, Systemic versus local application of gentamicin in prophylaxis of implant-related osteomyelitis in a rat model, Bone 36 (5) (2005) 770–778.

[60] J. H. Lee, Y. Yeo, Controlled drug release from pharmaceutical nanocarriers, Chemical Engineering Science 125 (2015) 75.84.

[61] N. T. Kirkland, N. Birbilis, M. P. Staiger, Assessing the corrosion of biodegradable magnesium implants: a critical review of current methodologies and their limitations, Acta Biomaterialia 8 (3) (2012) 925–936.

[62] G. Podaru, S. Ogden, A. Baxter, T. Shrestha, S. Ren, P. Thapa, R. K. Dani, H. Wang, M. T. Basel, P. Prakash, S. H. Bossmann, V. Chikan, Pulsed magnetic field induced fast drug release from magneto liposomes via ultrasound generation, The Journal of Physical Chemistry B 118 (40) (2014) 11715–11722.

[63] D. C. Hyun, Magnetically-controlled, pulsatile drug release from poly(ε-caprolactone) (PCL) particles with hollow interiors, Polymer 74 (2015) 159–165.

[64] A. Schroeder, J. Kost, Y. Barenholz, Ultrasound, liposomes, and drug delivery: principles for using ultrasound to control the release of drugs from liposomes, Chemistry and Physics of Lipids 162 (1-2) (2009) 1–6.

[65] M. Stigter, J. Bezemer, K. de Groot, P. Layrolle, Incorporation of different antibiotics into carbonated hydroxyapatite coatings on titanium implants, release and antibiotic efficacy, Journal of Controlled Release 99 (1) (2004) 127–137.

[66] Q. Xu, Y. Tanaka, J. T. Czernuszka, Encapsulation and release of a hydrophobic drug from hydroxyapatite coated liposomes, Biomaterials 28 (16) (2007) 2687–2694.

[67] P. M. Nguyen, N. S. Zacharia, E. Verploegen, P. T. Hammond, Extended release antibacterial layer-by-layer films incorporating linear-dendritic block copolymer micelles, Chemistry of Materials 19 (23) (2007) 5524–5530.

[68] N. W. Rydell, Forces acting in the femoral head-prosthesis. A study on strain gauge supplied prostheses in living persons, Acta Orthopaedica 37 (S88) (1966) 1–132.

[69] C. E. Carlson, R. W. Mann, W. H. Harris, A look at the prosthesis-cartilage interface: design of a hip prosthesis containing pressure transducers, Journal of Biomedical Materials Research 8 (4) (1974) 261–269.

[70] M. Kilvington, R. M. Goodman, In vivo hip joint forces recorded on a strain gauged 'English' prosthesis using an implanted transmitter, Engineering in Medicine 10 (4) (1981) 175–187.

[71] D. T. Davy, G. M. Kotzar, R. H. Brown, K. G. Heiple, V. M. Goldberg, K. G. H. Jr, J. Berilla, A. H. Burstein, Telemetric force measurements across the hip after total arthroplasty, Journal of Bone and Joint Surgery 70 (1) (1988) 45–50.

[72] R. Puers, M. Catrysse, G. Vandevoorde, R. Collier, E. Louridas, F. Burny, M. Donkerwolcke, F. Moulart, A telemetry system for the detection of hip prosthesis loosening by vibration analysis, Sensors and Actuators A: Physical 85 (1-3) (2000) 42–47.

[73] G. Bergmann, F. Graichen, A. Rohlmann, Hip joint forces in sheep, Journal of Biomechanics 32 (8) (1999) 769–777.

[74] F. Graichen, G. Bergmann, A. Rohlmann, Hip endoprosthesis for in vivo measurement of joint force and temperature, Journal of Biomechanics 32 (10) (1999) 1113–1117.

[75] P. Damm, F. Graichen, A. Rohlmann, A. Bendera, G. Bergmann, Total hip joint prosthesis for in vivo measurement of forces and moments, Medical Engineering & Physics 32 (1) (2010) 95–100.

[76] G. Bergmann, F. Graichen, J. Dymke, A. Rohlmann, G. N. Duda, P. Damm, High-tech hip implant for wireless temperature measurements in vivo, PLoS One 7 (8) (2012) e43489.

[77] J. Reis, C. Frias, C. C. e Castro, M. L. Botelho, A. T. Marques, J. A. O. Simões, F. C. e Silva, J. Potes, A new piezoelectric actuator induces bone formation in vivo: a preliminary study, Journal of Biomedicine and Biotechnology 2012 (2012) 1–7.

[78] Q. C. Yan, N. Tomita, Y. Ikada, Effects of static magnetic field on bone formation of rat femurs, Medical Engineering & Physics 20 (6) (1998) 397–402.

[79] S. Xu, H. Okano, N. Tomita, Y. Ikada, Recovery effects of a 180 mT static magnetic field on bone mineral density of osteoporotic lumbar vertebrae in ovariectomized rats, Evidence-Based Complementary and Alternative Medicine 2011 (2011) 1–8.

[80] E. Puricelli, N. B. Dutra, D. Ponzoni, Histological evaluation of the influence of magnetic field application in autogenous bone grafts in rats, Head & Face Medicine 5 (1) (2009) 1–6.

[81] J. Zhang, C. Ding, L. Ren, Y. Zhou, P. Shang, The effects of static magnetic fields on bone, Progress in Biophysics and Molecular Biology 114 (3) (2014) 146–152.

[82] N. Aydin, M. Bezer, The effect of an intramedullary implant with a static magnetic field on the healing of the osteotomised rabbit femur, International Orthopaedics 35 (1) (2011) 135–141.

[83] T. Shelyakova, A. Russo, A. Visani, V. A. Dediu, M. Marcacci, Application of magnetic rods for fixation in orthopedic treatments, Computers in Biology and Medicine 61 (1) (2015) 101–106.

[84] W. Mittelmeier, S. Lehner, W. Kraus, H. P. Matter, L. Gerdesmeyer, E. Steinhauser, BISS: concept and biomechanical investigations of a new screw system for electromagnetically induced internal osteostimulation, Archives of Orthopaedic and Trauma Surgery 124 (2) (2004) 86–91.

[85] C. Windisch, W. Kolb, E. R. M. Wagner, A. Roth, G. Matziolis, A. Wagner, Invasive electromagnetic field treatment in osteonecrosis of the femoral head: a prospective cohort study, The Open Orthopaedics Journal 8 (2014) 125–129.

[86] P. C. Grunert, A. Jonitz-Heincke, Y. Su, R. Souffrant, D. Hansmann, H. Ewald, A. Kruger, W. Mittelmeier, R. Bader, Establishment of a novel in vitro test setup for electric and magnetic stimulation of human osteoblasts, Cell Biochemistry and Biophysics 70 (2) (2014) 805–817.

[87] Y. Su, R. Souffrant, D. Kluess, M. Ellenrieder, W. Mittelmeier, U. Rienen, R. Bader, Evaluation of electric field distribution in electromagnetic stimulation of human femoral head, Bioelectromagnetics 35 (8) (2014) 547–558.

[88] F. Liebrecht, W. Kraus, H. Stephan, Bone screw comprising a device for electrostimulation, US Patent 6778861 (2004).

[89] C. Potratz, D. Kluess, H. Ewald, U. van Rienen, Multiobjective optimization of an electrostimulative acetabular revision system, IEEE Transactions on Biomedical Engineering 57 (2) (2010) 460–468.

[90] C. Schmidt, U. Zimmermann, U. van Rienen, Modeling of an optimized electro-stimulative hip revision system under consideration of uncertainty in the conductivity of bone tissue, IEEE Journal of Biomedical and Health Informatics 19 (4) (2015) 1321–1330.

[91] D. D. D'Lima, B. J. Fregly, C. W. Colwell, Implantable sensor technology: measuring bone and joint biomechanics of daily life in vivo, Arthritis Research & Therapy 15 (203) (2013) 1–12.

[92] E. H. Ledet, D. D'Lima, P. Westerhoff, J. A. Szivek, R. A. Wachs, G. Bergmann, Implantable sensor technology: from research to clinical practice, Journal of the American Academy of Orthopaedic Surgeons 20 (6) (2012) 383–392.

[93] M. O. Heller, G. Bergmann, J. P. Kassi, L. Claes, N. P. Haas, G. N. Duda, Determination of muscle loading at the hip joint for use in pre-clinical testing, Journal of Biomechanics 38 (5) (2005) 1155–1163.

[94] F. Burny, M. Donkerwolcke, F. Moulart, R. Bourgois, R. Puers, K. V. Schuylenbergh, M. Barbosa, O. Paiva, F. Rodes, J. B. Bgueret, P. Lawes, Concept, design and fabrication of smart orthopedic implants, Medical Engineering & Physics 22 (7) (2000) 469–479.

[95] P. Alpuim, S. A. Filonovich, C. M. Costa, P. F. Rocha, M. I. Vasilevskiy, S. Lanceros-Mendez, C. F. A. T. Marques, R. Soares, C. Costa, Fabrication of a strain sensor for bone implant failure detection based on piezoresistive doped nanocrystalline silicon, Journal of Non-Crystalline Solids 354 (19-25) (2008) 2585–2589.

[96] C. Ruther, H. Ewald, W. Mittelmeier, A. Fritsche, R. Bader, D. Kluess, A novel sensor concept for optimization of loosening diagnostics in total hip replacement, Journal of Biomechanical Engineering 133 (10) (2011) 1–5.

[97] C. Ruther, C. Schulze, A. Boehme, H. Nierath, H. Ewald, W. Mittelmeier, R. Bader, D. Kluess, Investigation of a passive sensor array for diagnosis of loosening of endoprosthetic implants , Sensors 13 (1) (2013) 1–20.

[98] C. Ruther, C. Gabler, H. Ewald, M. Ellenrieder, M. Haenle, T. Lindner, W. Mittelmeier, R. Bader, D. Kluess, In vivo monitoring of implant osseointegration in a rabbit model using acoustic sound analysis, Journal of Orthopaedic Research 32 (4) (2014) 606–612.

[99] K. C. McGilvray, E. Unal, K. L. Troyer, B. G. Santoni, R. H. Palmer, J. T. Easley, H. V. Demir, C. M. Puttlitz, Implantable microelectromechanical sensors for diagnostic monitoring and post-surgical prediction of bone fracture healing, Journal of Orthopaedic Research 33 (10) (2015) 1439–1446.

[100] J. H. Prescott, S. Lipka, S. Baldwin, N. F. Sheppard, J. M. Maloney, J. Coppeta, B. Yomtov, M. A. Staples, J. T. Santini, Chronic, programmed polypeptide delivery from an implanted, multireservoir microchip device, Nature Biotechnology 24 (2006) 437–438.

[101] R. Morais, C. M. Frias, N. M. Silva, J. L. F. Azevedo, C. A. Serôdio, P. M. Silva, J. A. F. Ferreira, J. A. O. Simões, M. C. Reis, An activation circuit for battery-powered biomedical implantable systems, Sensors and Actuators A: Physical 156 (1) (2009) 229–236.

[102] R. Morais, N. M. Silva, P. M. Santos, C. M. Frias, J. A. Ferreira, A. M. Ramos, J. A. O. Simões, J. M. R. Baptista, M. C. Reis, Double permanent magnet vibration power generator for smart hip prosthesis, Sensors and Actuators A: Physical 172 (1) (2011) 259–268.

[103] U. Marschner, H. Grätz, B. Jettkant, D. Ruwisch, G. Woldt, W. J. Fischer, B. Clasbrummel, Integration of a wireless lock-in measurement of hip prosthesis vibrations for loosening detection, Sensors and Actuators A: Physical 156 (1) (2009) 145–154.

[104] N. M. Silva, P. M. Silva, J. Ferreira, M. P. S. dos Santos, J. A. O. S. A. Ramos, M. J. C. S. Reisa, R. Morais, Power management architecture for smart hip prostheses comprising multiple energy harvesting systems, Sensors and Actuators A: Physical 202 (1) (2013) 183–192.

[105] M. L. Morgado, L. F. Morgado, N. Silva, R. Morais, Mathematical modelling of cylindrical electromagnetic vibration energy harvesters, International Journal of Computer Mathematics 92 (1) (2015) 101–109.

[106] S. R. Platt, S. Farritor, H. Haider, On low-frequency electric power generation with PZT ceramics, IEEE/ASME Transactions on Mechatronics 10 (2) (2005) 240–252.

[107] Y. Brudno, D. J. Mooney, On-demand drug delivery from local depots, Journal of Controlled Release, in press.

[108] C. L. Ross, M. Siriwardane, G. Almeida-Porada, C. D. Porada, P. Brink, G. J. Christ, B. S. Harrison, The effect of low-frequency electromagnetic field on human bone marrow stem/progenitor cell differentiation, Stem Cell Research 15 (1) (2015) 96–108.

[109] W. R. Thompson, C. T. Rubin, J. Rubin, Mechanical regulation of signaling pathways in bone, Gene 503 (2) (2012) 179–193.

[110] F. Padilla, R. Puts, L. Vico, K. Raum, Stimulation of bone repair with ultrasound: a review of the possible mechanic effects, Ultrasonics 54 (5) (2014) 1125–1145.

[111] A. Whinfield, I. Aitkenhead, The light revival: Does phototherapy promote wound healing? A review, The Foot 19 (2) (2009) 117–124.

Chapter 2

Optimality Analysis of Orthopaedic Implants

The most promising trends towards the design of orthopaedic implants capable of optimizing the osseointegration control are not obvious to identify. The observed results achieved by the methodologies already proposed are not enough to infer their potential for such purpose. Besides, the ability of each methodology to ensure long-term implant survival seems not considered. There are not conclusive demonstrations of the ineffectiveness of passive implants. There is also no strong evidences suggesting that optimal performances of implants cannot be attained only by optimizing their design and materials. Much more research has been nevertheless conducted in order to coat passive implants with bioactive materials than to design instrumented implants, either passive or active. Considering the amount of published research, the development of coatings capable of releasing drugs and/or other bio-agents to control the peri-implant biochemical and biomechanical environments seem to be considered the most reasonable solution to minimize implant failures. Nevertheless, no reasons have been exposed to clarify why no research has been carried out to implement instrumented implants with such ability, since a higher controllability of the delivery system could be reached. Besides, the potential of organic adaptation to biophysical pathways must not be discarded without detailed studies. Hence, the performance optimality of instrumented and non-instrumented orthopaedic implants firstly must be analysed. This study was conducted in the scope of this thesis and is entitled "Active orthopaedic implants: towards optimality". It is published in the *Journal of the Franklin Institute* (volume 352, issue 3, pp. 813-834)[1]. This study intends to answer if current methodologies used for implant designing are able to perform effective long-term operability or a different concept model for orthopaedic implants must be developed. It also proposes a formulation of the architecture and operation of orthopaedic implants, which emphasizes what research lines must be primarily pursued to optimize their performance.

[1]As the content of this study is already published, the formatting rules established by the *Journal of the Franklin Institute* are used.

Available online at www.sciencedirect.com

ScienceDirect

Journal of the Franklin Institute 352 (2015) 813–834

Journal of The Franklin Institute

www.elsevier.com/locate/jfranklin

Active orthopaedic implants: Towards optimality

Marco P. Soares dos Santos[a,b,*], Jorge A.F. Ferreira[b], A. Ramos[a,b], José A.O. Simões[b]

[a]*TEMA/UA — Centre for Mechanical Technology & Automation, University of Aveiro, Campus Universitário de Santiago, 3810-193 Aveiro, Portugal*

[b]*DEM/UA — Department of Mechanical Engineering, University of Aveiro, Campus Universitário de Santiago, 3810-193 Aveiro, Portugal*

Received 29 October 2013; received in revised form 11 October 2014; accepted 7 November 2014
Available online 20 November 2014

Abstract

Although everlasting life span is a primary requirement for orthopaedic implants, their current rate of failure is relatively high. The fundamental problem of implementing optimal implants remains a top research topic. No methodology to ensure everlasting life span of orthopaedic implants has ever been proved. Joint prostheses are only being designed to operate passively, only restoring joint function. Instrumented implants have not been designed as full interactive mechanisms with the surrounding physiological environment. The purpose of this paper is twofold: (1) to prove that non-instrumented passive implants and instrumented passive implants are not able to optimize the minimization of the failures throughout the lifetime of the implants, whatever the optimization level of the implants, rehabilitation protocols or surgical procedures; and (2) to prove that active implants ensure performance optimality preventing failures. Research in the design of active implants is thus proposed as an effective methodology to characterize failures and to perform therapeutic actuations in real-time, ensuring optimal trajectories from states of failure to states of without-failure.

*Corresponding author at: DEM/UA — Department of Mechanical Engineering, University of Aveiro, Campus Universitário de Santiago, 3810-193 Aveiro, Portugal.

E-mail address: marco.santos@ua.pt (M.P. Soares dos Santos).

http://dx.doi.org/10.1016/j.jfranklin.2014.11.005
0016-0032/

1. Introduction

1.1. Demand for joint replacements

The number of arthroplasties has increased and it is estimated to increase even more in the coming years [1,2]. Kurtz et al. [2] estimated that the demand for total hip replacement (THR) will grow 174% to 572 000 per year by 2030 in the United States. The need of hip revision procedures is currently about 6% after 5 years and 12% after 10 years following arthroplasty [3]. The demand for joint replacements among patients less than 65 years old is also increasing, which is related with the increasing use of uncemented implants in primary replacements [4,5]. Some projections indicate that 50% of the primary THR and 35% of the revision THR will be performed in patients less than 65 years old between 2010 and 2030 [6]. The probability to undergo re-revision is five to six times higher after the first revision [7]. Complications following arthroplasty remain harmful for the durability of the implant [8]. Moreover, demographic changes and breakthroughs in medical technology have preceded the rising in the number of patients living longer than the lifetime of the implant.

1.2. Classes of orthopaedic implants

Classes of implants can be categorized according to its instrumentation and actuation features preventing failures. Currently, passive implants are the only class being considered for mass implantation in the human being. Non-instrumented passive implants are the class of implants comprising architectures without instrumentation and active components. They do not comprise resources: (a) to monitor their own state and the physiological states of the tissues surrounding the implants; (b) to perform therapeutic actuations in order to prevent failures, *i.e.*, to perform optimal trajectories from failure states to without-failure states; (c) to communicate with external systems, namely with medical staff. The composite hip femoral prosthesis, proposed by Simões and Marques [9], is an example of passive hip implant. The instrumentation of prostheses has begun in the 60s, when force measurements from total hip implants were first recorded [10]. Over the last 50 years, instrumented prostheses have only been designed to collect data *in vivo*, mainly from: (1) contact forces and moments in the joint [11–14]; (2) temperature distribution along the implant [15,16]; (3) misalignments [17]; (4) articular motions [18]; and (5) aseptic hip loosening [19,20]. In order to study the risk of thermally induced bone necrosis, Bergmann et al. [21] proposed the latest instrumented hip implants: an instrumented hip endoprostheses to measure the implant temperatures *in vivo*.

Up to date, only instrumented passive implants have been designed [22]: implants only comprising telemetry and electric power supply systems (Fig. 1). They have been only implanted for research issues [23–26], namely to optimize their design and preclinical testing [27], and to improve rehabilitation protocols [28,29].

No active implants have been designed so far [30]. Smart surface coating modifications can be used to implement non-instrumented active implants [31]. They are not composed by actuation, monitoring and power supply systems based on mechanical structures. The use of self-protective surfaces with the ability to monitor and act against infecting organisms [32–34] was recently proposed as a methodology to design non-instrumented active implants. Only one methodology to develop instrumented active implants has been proposed: the use of mechanical actuation systems to control bone formation surrounding the implant. The prototype of an active hip prosthesis, with the ability to prevent failures by aseptic loosening, is being designed in order to

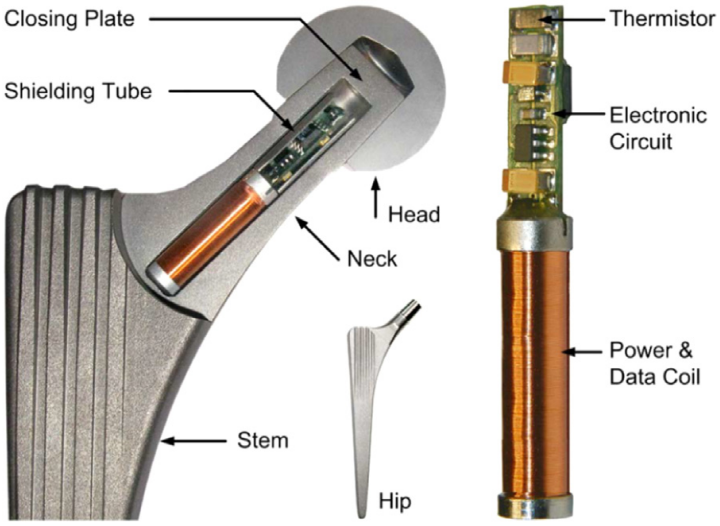

Fig. 1. Instrumented passive hip implant proposed by Bergmann et al. [21] (reproduced with permission from the authors).

demonstrate the concept. Several modules were already developed, namely: (1) two modules for the electric supply of the implant: motion-driven power generators and an energy conditioning system [35–39]; (2) two modules for the communication between the implant and external mechanisms: a dual-link telemetry system and an activation circuit [40]; (3) a module for the detection of aseptic loosening of prosthetic stem and cup [41]; and (4) a module for the active therapeutic actuation against loosening: a mechanical stimulator of bone cells, based on six polyvinylidene fluoride actuators, to induce bone formation surrounding the implant [42].

Instrumented active implants must comprise: (1) monitoring systems to measure in real-time the physiological states of the tissues surrounding the implant; (2) processing systems to identify the failures' characteristics in real-time; (3) actuators to operate therapeutic actuations when failures are detected; (4) communication systems to send/receive data to/from external systems; and (5) electrical supply systems to power monitoring, processing, actuation and transmission systems. Instrumented active implants must characterize failures in real-time and perform therapeutic actuations (also in real-time) to minimize them throughout time [43].

2. Structure of the active implants

2.1. Overall methodological design

The architecture of the active implants comprises two main structures, as shows Fig. 2(a): a Master-based Active Structure (MBA) outside the human body (OHB), and a Slave-based Active Structure (SBA) inside the human body (IHB). Passive implants do not comprise neither active therapeutic systems nor therapeutic command modes, as illustrated by Fig. 2(b). OHB mechanisms can interact with the instrumented passive implants, but these do not have command structures: master–slave architectures are only possible for active implants.

2.2. Formulation of the implants' operation

2.2.1. Mechanical features of the in situ implants' structure

Design and properties: Let α and ω be respectively a domain and a codomain. Let ${}^{\alpha}B^{t}_{b_i}$ be the subsets-domain (sDs) of mathematical models which formulate the design and operation state of

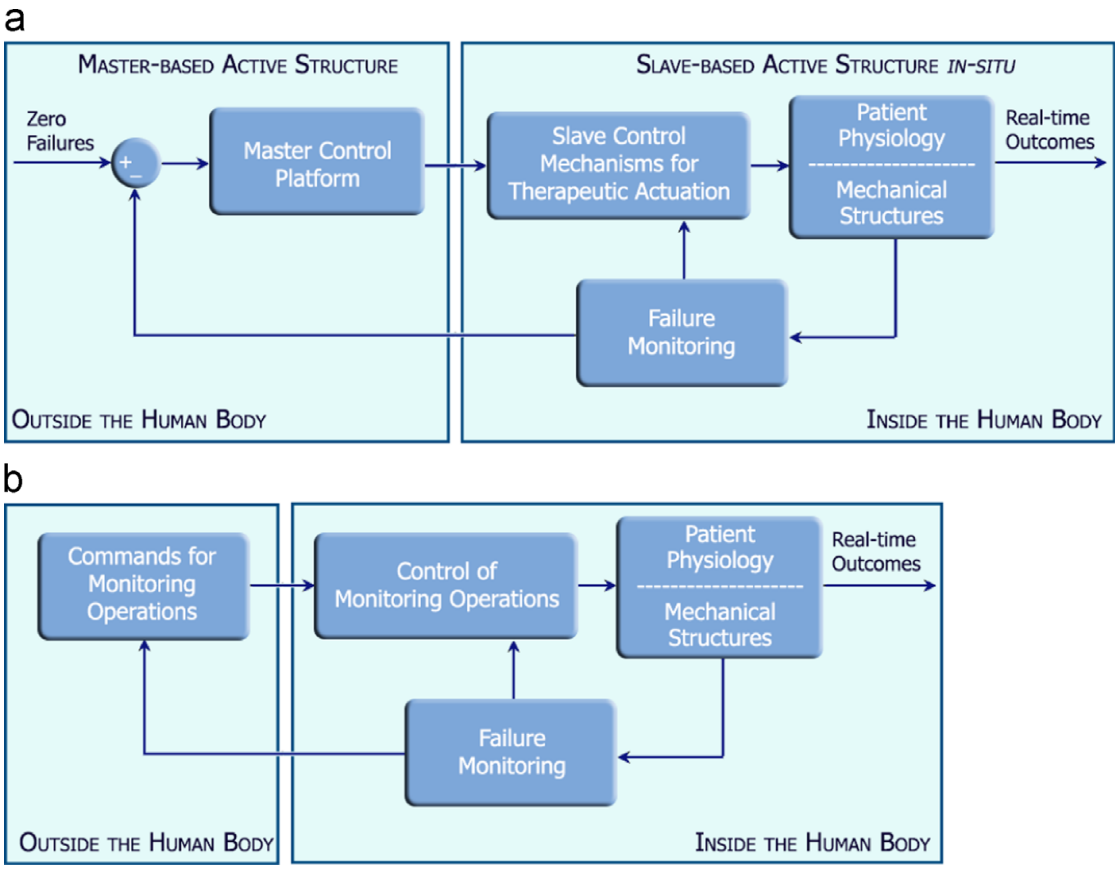

Fig. 2. Architecture of: (a) non-instrumented and instrumented active implants; (b) non-instrumented and instrumented passive implants.

the *in situ* implant's structure at time t. They must model the dimensions, geometry, type of materials and life span of all its parts, as well as: (1) the operation state of the solid structure; (2) the amount, location and operation state of its actuators, sensors, communication subsystems and harvesters; (3) and the location, amount and availability of the stored resources. Let ${}^{\omega}B_{b_j}^{t}$ be the subsets-codomain (sCs) of mathematical formulations which model the mechanical properties of the *in situ* implant's structure at time t, such as the fatigue and wear resistance, Young's modulus, tensile strength, toxicity, bioactivity and biodegradability. Let ${}^{\alpha}\mathbf{B}^{t}$ be the set-domain (SD) of sDs ${}^{\alpha}B_{b_i}^{t}$, and let ${}^{\omega}\mathbf{B}^{t}$ be the set-codomain (SC) of sCs ${}^{\omega}B_{b_j}^{t}$

$$ {}^{\alpha\omega}\mathbf{B}^{t} = \left\{ {}^{\alpha}\mathbf{B}^{t}, {}^{\omega}\mathbf{B}^{t} \right\} = \left\{ \left\{ {}^{\alpha}B_{b_i}^{t} \right\}, \left\{ {}^{\omega}B_{b_j}^{t} \right\} \right\} \tag{1} $$

Let F be a vector space of applications. Let ψ_B^t be the set of applications $F \to F$ at time t:

$$ \psi_B^t = \left\{ {}^{\alpha}B_{b_i}^{t} \to {}^{\omega}B_{b_j}^{t} : b_i \le \left| {}^{\alpha}\mathbf{B}^{t} \right|, b_j \le \left| {}^{\omega}\mathbf{B}^{t} \right| \right\} \tag{2} $$

Operators defined on ${}^{\alpha}\mathbf{B}$ *and* ${}^{\omega}\mathbf{B}$: Let $\bigvee$ and $\bigwedge$ be respectively union and intersection operators. Let $\bigvee^{\mathbf{B}^t}$ and $\bigwedge^{\mathbf{B}^t}$ be the sets of operators which define the operations on ${}^{\alpha}\mathbf{B}$ and ${}^{\omega}\mathbf{B}$ at time t:

$$ \bigvee^{\mathbf{B}^t} = \left\{ \begin{matrix} {}^{\alpha}B_{b_{i_\delta} b_{i_\varphi}} \\ \bigvee \end{matrix}, \begin{matrix} {}^{\omega}B_{b_{j_\delta} b_{j_\varphi}} \\ \bigvee \end{matrix} \right\} \Big| t, b_i, b_j, b_{i_\delta}, b_{i_\varphi}, b_{j_\delta}, b_{j_\varphi} \in \mathbb{N} : b_{i_\delta} \neq b_{i_\varphi}, b_{j_\delta} \neq b_{j_\varphi}, $$

$$1 \le b_{i_\delta}, b_{i_\varphi} \le \left|{}^{\alpha}\mathbf{B}^t\right|, 1 \le b_{j_\delta}, b_{j_\varphi} \le \left|{}^{\omega}\mathbf{B}^t\right| \tag{3}$$

$$\bigwedge^{\mathbf{B}^t} = \left\{ \bigwedge^{{}^{\alpha}B_{b_{i_\delta} b_{i_\varphi}}}, \bigwedge^{{}^{\omega}B_{b_{j_\delta} b_{j_\varphi}}} \right\} \Big| t, b_i, b_j, b_{i_\delta}, b_{i_\varphi}, b_{j_\delta}, b_{j_\varphi} \in \mathbb{N} : b_{i_\delta} \neq b_{i_\varphi}, b_{j_\delta} \neq b_{j_\varphi},$$

$$1 \le b_{i_\delta}, b_{i_\varphi} \le \left|{}^{\alpha}\mathbf{B}^t\right|, 1 \le b_{j_\delta}, b_{j_\varphi} \le \left|{}^{\omega}\mathbf{B}^t\right| \tag{4}$$

Applications between ${}^{\alpha}\mathbf{B}$ *and* ${}^{\omega}\mathbf{B}$: Let $\psi^t_{\mathbf{B}}$ be the set of applications $F \to F$ between ${}^{\alpha}\mathbf{B}^t$ and ${}^{\omega}\mathbf{B}^t$ at time t:

$$\psi^t_{\mathbf{B}} = \left\{ \bigwedge^{{}^{\alpha}B_{b_{i_\delta} b_{i_\varphi}}} \left(\bigvee^{{}^{\alpha}B_{b_{i_\delta} b_{i_\varphi}}} {}^{\alpha}B_{b_i} \right) \to \bigwedge^{{}^{\omega}B_{b_{j_\delta} b_{j_\varphi}}} \left(\bigvee^{{}^{\omega}B_{b_{j_\delta} b_{j_\varphi}}} {}^{\omega}B_{b_j} \right) \right\} \Big| t \tag{5}$$

Definition of the algebra of $\boldsymbol{B}$: Let $\mathbf{B}^t$ be the algebra of the mechanical features of the *in situ* implant's structure at time t:

$$\mathbf{B}^t = \left\langle \psi^t_{\mathbf{B}}, \bigvee^{\mathbf{B}^t}, \bigwedge^{\mathbf{B}^t} \right\rangle \tag{6}$$

2.2.2. Supply of the in situ implants' structure

Acquisition of resources and related changes: Let ${}^{\alpha}E^t_{e_i}$ be the sDs of mathematical formulations which model the acquisition of resources by the *in situ* implant's structure at time t, required to power its actuation, measurement and communication subsystems. They comprise models to predict the acquisition of resources; the type, amount and periodicity of resources required for all subsystems; amount and location of the mechanisms which perform the acquisition, and their life span; the periodicity of acquisition and the acquired amount of resources. Let ${}^{\omega}E^t_{e_j}$ be the sCs of mathematical formulations which model the effects, at time t, due to the operations to acquire resources, such as the biochemical and biomechanical changes in the patient's body; changes in the mechanical, electrical, chemical and communication subsystems of the *in situ* implant's structure. Let ${}^{\alpha}\mathbf{E}^t$ be the SD of sDs ${}^{\alpha}E^t_{e_i}$, and let ${}^{\omega}\mathbf{E}^t$ be the SC of sCs ${}^{\omega}E^t_{e_j}$. Let ψ^t_E and $\psi^t_{\mathbf{E}}$ be sets of applications and $\bigvee^{\mathbf{E}^t}$ and $\bigwedge^{\mathbf{E}^t}$ be sets of operators defined as described in Section 2.2.1, but using ${}^{\alpha}E^t_{e_i}$, ${}^{\omega}E^t_{e_j}$, ${}^{\alpha}E_{e_{i_\delta} e_{i_\varphi}}$ and ${}^{\omega}E_{e_{j_\delta} e_{j_\varphi}}$.

Definition of the algebra of $\boldsymbol{E}$: Let $\mathbf{E}^t$ be the algebra of the supply operations performed by the *in situ* implant's structure at time t:

$$\mathbf{E}^t = \left\langle \psi^t_{\mathbf{E}}, \bigvee^{\mathbf{E}^t}, \bigwedge^{\mathbf{E}^t} \right\rangle \tag{7}$$

2.2.3. Measurement operations performed by the implant

Measurement and related changes: Let ${}^{\alpha}M^t_{m_i}$ be the sDs of mathematical models which formulate the measurement of the states of the implant and the physiological states of the tissues at time t. They must model the quantities to monitor; the sensors' operation; supply and life span requirements, the amount of sensors required and their location; the measurement output values;

and periodicity and period of measurement. Let ${}^{\omega}M^{t}_{m_j}$ be the sCs of mathematical formulations which model the effects, at time t, due to the measurement operations, such as the biochemical and biomechanical changes in the patient's body; and changes in the mechanical, electrical, chemical and communication subsystems of the *in situ* implant's structure. Let ${}^{\alpha}\mathbf{M}^{t}$ be the SD of sDs ${}^{\alpha}M^{t}_{m_i}$, and let ${}^{\omega}\mathbf{M}^{t}$ be the SC of sCs ${}^{\omega}M^{t}_{m_j}$. Let ψ^{t}_{M} and $\psi^{t}_{\mathbf{M}}$ be sets of applications and $\bigvee^{\mathbf{M}^t}$ and $\bigwedge^{\mathbf{M}^t}$ be sets of operators defined as described in Section 2.2.1, but using ${}^{\alpha}M^{t}_{m_i}$, ${}^{\omega}M^{t}_{m_j}$, ${}^{\alpha}M_{m_{i_\delta}m_{i_\varphi}}$ and ${}^{\omega}M_{m_{j_\delta}m_{j_\varphi}}$.

Definition of the algebra of $\boldsymbol{M}$: Let $\mathbf{M}^{t}$ be the algebra of the measurement operations at time t:

$$\mathbf{M}^{t}=\left\langle \psi^{t}_{\mathbf{M}}, \bigvee^{\mathbf{M}^t}, \bigwedge^{\mathbf{M}^t} \right\rangle \tag{8}$$

2.2.4. Physiological states of the patient

Physiological states of tissues: Let ${}^{\alpha}S^{t}_{s_i}$ be the sDs of biochemical and biomechanical models of the patient's body at time t. Let ${}^{\omega}S^{t}_{s_j}$ be the sCs of mathematical formulations which model the physiological states of the tissues surrounding the *in situ* implant's structure. Let ${}^{\alpha}\mathbf{S}^{t}$ be the SD of sDs ${}^{\alpha}S^{t}_{s_i}$, and let ${}^{\omega}\mathbf{S}^{t}$ be the SC of sCs ${}^{\omega}S^{t}_{s_j}$. Let ψ^{t}_{S}, $\psi^{t}_{\mathbf{S}}$ be sets of applications and $\bigvee^{\mathbf{S}^t}$ and $\bigwedge^{\mathbf{S}^t}$ be sets of operators defined as described in Section 2.2.1, but using ${}^{\alpha}S^{t}_{s_i}$, ${}^{\omega}S^{t}_{s_j}$, ${}^{\alpha}S_{s_{i_\delta}s_{i_\varphi}}$ and ${}^{\omega}S_{s_{j_\delta}s_{j_\varphi}}$.

Definition of the algebra of $\boldsymbol{S}$: Let $\mathbf{S}^{t}$ be the algebra of the physiological states of the patient at time t:

$$\mathbf{S}^{t}=\left\langle \psi^{t}_{\mathbf{S}}, \bigvee^{\mathbf{S}^t}, \bigwedge^{\mathbf{S}^t} \right\rangle \tag{9}$$

2.2.5. Failures of the in situ implants' structure

Failures and related changes: Let ${}^{\alpha}L^{t}_{l_i}$ be the sDs of mathematical models which formulate the effects, at time t, due to failures, such as the modulation of biochemical and biomechanical changes on the patient's body; and changes in the mechanical, electrical, chemical and communication subsystems of the *in situ* implant's structure. Let ${}^{\omega}L^{t}_{l_j}$ be the sCs of mathematical formulations which model the failures' characteristics of the implant at time t, such as the amount, type, state and regions of failures. Let us consider that the mechanical features of the structures outside the human body do not cause failures on the *in situ* implant's structure, and *vice versa*. Let ${}^{\alpha}\mathbf{L}^{t}$ be the SD of sDs ${}^{\alpha}L^{t}_{l_i}$, and let ${}^{\omega}\mathbf{L}^{t}$ be the SC of sCs ${}^{\omega}L^{t}_{l_j}$. Let ψ^{t}_{L} and $\psi^{t}_{\mathbf{L}}$ be sets of applications and $\bigvee^{\mathbf{L}^t}$ and $\bigwedge^{\mathbf{L}^t}$ be sets of operators defined as described in Section 2.2.1, but using ${}^{\alpha}L^{t}_{l_i}$, ${}^{\omega}L^{t}_{l_j}$, ${}^{\alpha}L_{l_{i_\delta}l_{i_\varphi}}$ and ${}^{\omega}L_{l_{j_\delta}l_{j_\varphi}}$.

Definition of the algebra of $\boldsymbol{L}$: Let $\mathbf{L}^{t}$ be the algebra of the failures of the *in situ* implant's structure at time t:

$$\mathbf{L}^{t}=\left\langle \psi^{t}_{\mathbf{L}}, \bigvee^{\mathbf{L}^t}, \bigwedge^{\mathbf{L}^t} \right\rangle \tag{10}$$

2.2.6. Therapeutic prescriptions performed by the in situ implants' structure

Therapies and related changes: Let ${}^{\alpha}T^{t}_{\tau_i}$ be the sDs of mathematical models which formulate the active therapeutic actuations required to be performed by the *in situ* implant's structure to avoid failures. They must model the failures to eliminate and active therapies to administrate; quantities to control; the actuators' operation; supply and life span requirements, as well as the amount of required actuators and their location; active therapeutic actuation values; periodicity and period of actuation. Let ${}^{\omega}T^{t}_{\tau_j}$ be the sCs of mathematical formulations which model the effects, at time t, due to the active therapeutic actuations performed by the *in situ* implant's structure, such as the biochemical and biomechanical changes in the patient's body; and changes in the mechanical, electrical, chemical and communication subsystems of the *in situ* implant's structure. Let ${}^{\alpha}\mathbf{T}^{t}$ be the SD of sDs ${}^{\alpha}T^{t}_{\tau_i}$, and let ${}^{\omega}\mathbf{T}^{t}$ be the SC of sCs ${}^{\omega}T^{t}_{\tau_j}$. Let ψ^{t}_{T} and $\psi^{t}_{\mathbf{T}}$ be sets of applications and $\bigvee^{\mathbf{T}^t}$ and $\bigwedge^{\mathbf{T}^t}$ be sets of operators defined as described in Section 2.2.1, but using ${}^{\alpha}T^{t}_{\tau_i}$, ${}^{\omega}T^{t}_{\tau_j}$, ${}^{\alpha}T_{\tau_{i_\delta}\tau_{i_\varphi}}$ and ${}^{\omega}T_{\tau_{j_\delta}\tau_{j_\varphi}}$.

Definition of the algebra of $\boldsymbol{T}$: Let $\mathbf{T}^t$ be the algebra of the therapeutic actuations performed by the *in situ* implant's structure at time t:

$$\mathbf{T}^{t}=\left\langle \psi^{t}_{\mathbf{T}}, \bigvee^{\mathbf{T}^t}, \bigwedge^{\mathbf{T}^t} \right\rangle \tag{11}$$

2.2.7. Communication operations performed by the implant

Communication between structures and related changes: Let ${}^{\alpha}W^{t}_{w_i}$ be the sDs of mathematical models which formulate the communication of the implant (for active implants, between SBA the MBA structures; for passive implants, between the IHB and the OHB structures) at time t. They must model the quantities to transfer from the *in situ* structure's subsystems; rate transfer requirements; telemetric subsystems' operation; energy and life span requirements, as well as the amount and location of telemetry subsystems; quantities possible to be transferred; maximum rate transfer and periodicity of communication of such quantities. Let ${}^{\omega}W^{t}_{w_j}$ be the sCs of mathematical formulations which model the effects, at time t, due to the communication processes, such as the biochemical and biomechanical changes in the patient's body, changes in the mechanical, electrical subsystems and therapeutic functions of the *in situ* implant's structure. Let ${}^{\alpha}\mathbf{W}^{t}$ be the SD of sDs ${}^{\alpha}W^{t}_{w_i}$, and let ${}^{\omega}\mathbf{W}_{t}$ be the SC of sCs ${}^{\omega}W^{t}_{w_j}$. Let ψ^{t}_{W} and $\psi^{t}_{\mathbf{W}}$ be sets of applications and $\bigvee^{\mathbf{W}^t}$ and $\bigwedge^{\mathbf{W}^t}$ be sets of operators defined as described in Section 2.2.1, but using ${}^{\alpha}W^{t}_{w_i}$, ${}^{\omega}W^{t}_{w_j}$, ${}^{\alpha}W_{w_{i_\delta}w_{i_\varphi}}$ and ${}^{\omega}W_{w_{j_\delta}w_{j_\varphi}}$.

Definition of the algebra of $\boldsymbol{W}$: Let $\mathbf{W}^t$ be the algebra of the communication operations performed by the implant at time t:

$$\mathbf{W}^{t}=\left\langle \psi^{t}_{\mathbf{W}}, \bigvee^{\mathbf{W}^t}, \bigwedge^{\mathbf{W}^t} \right\rangle \tag{12}$$

2.2.8. Therapeutic commands performed by the implant

Generation of medical prescriptions: Let ${}^{\alpha}C^{t}_{c_i}$ be the sDs of mathematical models which predict the state of the implant, physiological state of tissues surrounding the *in situ* implant's structure and therapy results of previous therapeutic commands at time t. Let ${}^{\omega}C_{c_j}$ be the sCs of

mathematical formulations which model the generation of therapeutic commands at time t, in order to be performed by the *in situ* implant's structure. They must model the therapies to administrate and therapies possible to be administrated by the *in situ* implant's structure; actuation prescriptions to produce the required therapies, which include changes in the configuration of the *in situ* implant's structure; periodicity and period of actuation; and therapy goals. Let ${}^{\alpha}\mathbf{C}^t$ be the SD of sDs ${}^{\alpha}C^t_{c_i}$, and let ${}^{\omega}\mathbf{C}^t$ be the SC of sCs ${}^{\omega}C^t_{c_j}$. Let ψ^t_C and $\psi^t_{\mathbf{C}}$ be sets of applications and $\overset{\mathbf{C}^t}{\bigvee}$ and $\overset{\mathbf{C}^t}{\bigwedge}$ be sets of operators defined as described in Section 2.2.1, but using ${}^{\alpha}C^t_{c_i}$, ${}^{\omega}C_{c_j}$, ${}^{\alpha}C_{c_{i_\delta}c_{i_\varphi}}$ and ${}^{\omega}C_{c_{j_\delta}c_{j_\varphi}}$.

Definition of the algebra of $\boldsymbol{C}$: Let $\mathbf{C}^t$ be the algebra of the therapeutic commands performed by the implant at time t:

$$\mathbf{C}^t = \left\langle \psi^t_{\mathbf{C}}, \overset{\mathbf{C}^t}{\bigvee}, \overset{\mathbf{C}^t}{\bigwedge} \right\rangle \tag{13}$$

2.2.9. Operation of the orthopaedic implants

Operation of the instrumented active implants: Let $\mathbf{D}^t$ be the algebra of the operation of the instrumented active implants at time t:

$$\mathbf{D}^t = \left\langle \{\mathbf{B}^t, \mathbf{S}^t, \mathbf{L}^t, \mathbf{T}^t, \mathbf{M}^t, \mathbf{E}^t, \mathbf{W}^t, \mathbf{C}^t\}, \overset{\mathbf{D}^t}{\bigvee}, \overset{\mathbf{D}^t}{\bigwedge} \right\rangle \tag{14}$$

in which:

$$\overset{\mathbf{D}^t}{\bigvee} = \{\overset{\mathbf{BE}}{\bigvee}, \overset{\mathbf{BM}}{\bigvee}, \overset{\mathbf{BT}}{\bigvee}, \overset{\mathbf{BW}}{\bigvee}, \overset{\mathbf{EW}}{\bigvee}, \overset{\mathbf{ET}}{\bigvee}, \overset{\mathbf{EM}}{\bigvee}, \overset{\mathbf{TM}}{\bigvee}, \overset{\mathbf{TL}}{\bigvee}, \overset{\mathbf{TW}}{\bigvee}, \overset{\mathbf{ML}}{\bigvee}, \overset{\mathbf{MS}}{\bigvee}, \overset{\mathbf{MW}}{\bigvee}, \overset{\mathbf{LS}}{\bigvee}, \overset{\mathbf{LW}}{\bigvee}, \overset{\mathbf{SW}}{\bigvee}, \overset{\mathbf{CW}}{\bigvee}, \overset{\mathbf{CM}}{\bigvee}, \overset{\mathbf{CL}}{\bigvee}, \overset{\mathbf{CS}}{\bigvee}, \overset{\mathbf{CT}}{\bigvee}, \overset{\mathbf{CE}}{\bigvee}, \overset{\mathbf{CN}}{\bigvee}\} \Big| t \tag{15}$$

$$\overset{\mathbf{D}^t}{\bigwedge} = \left\{\overset{\mathbf{BE}}{\bigwedge}, \overset{\mathbf{BM}}{\bigwedge}, \overset{\mathbf{BT}}{\bigwedge}, \overset{\mathbf{BW}}{\bigwedge}, \overset{\mathbf{EW}}{\bigwedge}, \overset{\mathbf{ET}}{\bigwedge}, \overset{\mathbf{EM}}{\bigwedge}, \overset{\mathbf{TM}}{\bigwedge}, \overset{\mathbf{TL}}{\bigwedge}, \overset{\mathbf{TW}}{\bigwedge}, \overset{\mathbf{ML}}{\bigwedge}, \overset{\mathbf{MS}}{\bigwedge}, \overset{\mathbf{MW}}{\bigwedge}, \overset{\mathbf{LS}}{\bigwedge}, \overset{\mathbf{LW}}{\bigwedge}, \overset{\mathbf{SW}}{\bigwedge}, \overset{\mathbf{CW}}{\bigwedge}, \overset{\mathbf{CM}}{\bigwedge}, \overset{\mathbf{CL}}{\bigwedge}, \overset{\mathbf{CS}}{\bigwedge}, \overset{\mathbf{CT}}{\bigwedge}, \overset{\mathbf{CE}}{\bigwedge}, \overset{\mathbf{CN}}{\bigwedge}\right\} \Big| t \tag{16}$$

Operation of the non-instrumented active implants: Let $\mathbf{N}^t$ be the algebra of the operation of the non-instrumented active implants at time t:

$$\mathbf{N}^t = \left\langle \{\mathbf{B}^t, \mathbf{S}^t, \mathbf{L}^t, \mathbf{T}^t, \mathbf{M}^t, \mathbf{E}^t, \mathbf{C}^t\}, \overset{\mathbf{N}^t}{\bigvee}, \overset{\mathbf{N}^t}{\bigwedge} \right\rangle \tag{17}$$

in which:

$$\overset{\mathbf{N}^t}{\bigvee} = \left\{\overset{\mathbf{BE}}{\bigvee}, \overset{\mathbf{BM}}{\bigvee}, \overset{\mathbf{BT}}{\bigvee}, \overset{\mathbf{ET}}{\bigvee}, \overset{\mathbf{EM}}{\bigvee}, \overset{\mathbf{TM}}{\bigvee}, \overset{\mathbf{TL}}{\bigvee}, \overset{\mathbf{ML}}{\bigvee}, \overset{\mathbf{MS}}{\bigvee}, \overset{\mathbf{LS}}{\bigvee}, \overset{\mathbf{CM}}{\bigvee}, \overset{\mathbf{CL}}{\bigvee}, \overset{\mathbf{CS}}{\bigvee}, \overset{\mathbf{CT}}{\bigvee}, \overset{\mathbf{CE}}{\bigvee}, \overset{\mathbf{CN}}{\bigvee}\right\} \Big| t \tag{18}$$

$$\overset{\mathbf{N}^t}{\bigwedge} = \left\{\overset{\mathbf{BE}}{\bigwedge}, \overset{\mathbf{BM}}{\bigwedge}, \overset{\mathbf{BT}}{\bigwedge}, \overset{\mathbf{ET}}{\bigwedge}, \overset{\mathbf{EM}}{\bigwedge}, \overset{\mathbf{TM}}{\bigwedge}, \overset{\mathbf{TL}}{\bigwedge}, \overset{\mathbf{ML}}{\bigwedge}, \overset{\mathbf{MS}}{\bigwedge}, \overset{\mathbf{LS}}{\bigwedge}, \overset{\mathbf{CM}}{\bigwedge}, \overset{\mathbf{CL}}{\bigwedge}, \overset{\mathbf{CS}}{\bigwedge}, \overset{\mathbf{CT}}{\bigwedge}, \overset{\mathbf{CE}}{\bigwedge}, \overset{\mathbf{CN}}{\bigwedge}\right\} \Big| t \tag{19}$$

Operation of the instrumented passive implants: Let $\mathbf{I}^t$ be the algebra of the operation of the instrumented passive implants at time t:

$$\mathbf{I}^t = \left\langle \left\{\mathbf{B}^t, \mathbf{S}^t, \mathbf{L}^t, \mathbf{M}^t, \mathbf{E}^t, \mathbf{W}^t\right\}, \overset{\mathbf{I}^t}{\bigvee}, \overset{\mathbf{I}^t}{\bigwedge} \right\rangle \tag{20}$$

in which:

$$\overset{\mathbf{I}^t}{\bigvee} = \left\{ \overset{\mathbf{B}\,\mathbf{E}}{\bigvee}, \overset{\mathbf{B}\,\mathbf{M}}{\bigvee}, \overset{\mathbf{B}\,\mathbf{W}}{\bigvee}, \overset{\mathbf{E}\,\mathbf{W}}{\bigvee}, \overset{\mathbf{E}\,\mathbf{M}}{\bigvee}, \overset{\mathbf{M}\,\mathbf{S}}{\bigvee}, \overset{\mathbf{M}\,\mathbf{L}}{\bigvee}, \overset{\mathbf{M}\,\mathbf{W}}{\bigvee}, \overset{\mathbf{L}\,\mathbf{S}}{\bigvee}, \overset{\mathbf{L}\,\mathbf{W}}{\bigvee}, \overset{\mathbf{S}\,\mathbf{W}}{\bigvee} \right\} \Big| t \tag{21}$$

$$\overset{\mathbf{I}^t}{\bigwedge} = \left\{ \overset{\mathbf{B}\,\mathbf{E}}{\bigwedge}, \overset{\mathbf{B}\,\mathbf{M}}{\bigwedge}, \overset{\mathbf{B}\,\mathbf{W}}{\bigwedge}, \overset{\mathbf{E}\,\mathbf{W}}{\bigwedge}, \overset{\mathbf{E}\,\mathbf{M}}{\bigwedge}, \overset{\mathbf{M}\,\mathbf{S}}{\bigwedge}, \overset{\mathbf{M}\,\mathbf{L}}{\bigwedge}, \overset{\mathbf{M}\,\mathbf{W}}{\bigwedge}, \overset{\mathbf{L}\,\mathbf{S}}{\bigwedge}, \overset{\mathbf{L}\,\mathbf{W}}{\bigwedge}, \overset{\mathbf{S}\,\mathbf{W}}{\bigwedge} \right\} \Big| t \tag{22}$$

Operation of the non-instrumented passive implants: Let $\mathbf{P}^t$ be the algebra of the operation of the non-instrumented passive implants at time t:

$$\mathbf{P}^t = \mathbf{B}^t \tag{23}$$

3. Optimality analysis of the implants

3.1. Outcomes from implants

3.1.1. Instrumented active implants

Implant outcomes: Let ξ and γ be respectively a domain and a codomain. Let ${}^{\gamma}\mathbf{D}^t$ be the sCs of measurements of the instrumented active implant outcomes at time t following implantation, such as the life span of the implant, utility-cost rate and self-assessment scores (levels of pain; ability to perform activities of daily living, among others).

$${}^{\xi\gamma}\mathbf{D}^t = \left\{\psi^t_{\mathbf{B}}, \psi^t_{\mathbf{S}}, \psi^t_{\mathbf{L}}, \psi^t_{\mathbf{T}}, \psi^t_{\mathbf{M}}, \psi^t_{\mathbf{E}}, \psi^t_{\mathbf{W}}, \psi^t_{\mathbf{C}}, {}^{\gamma}\mathbf{D}^t\right\} \tag{24}$$

$$\boldsymbol{\psi}^t_D = \left\{ \psi^t_{\mathbf{L}} \to \left\{ {}^{\gamma}D^t_y \right\} : y \le \left| {}^{\gamma}\mathbf{D}^t \right| \right\} \tag{25}$$

Applications defined on ${}^{\xi}\mathbf{D}$: Let $\boldsymbol{\Sigma}^t_{\mathbf{D}}$ be the set of applications $F \to F$ defined on ${}^{\xi}\mathbf{D}$ at time t:

$$\boldsymbol{\Sigma}^t_{\mathbf{D}} = \left\{ \overset{{}^{\xi}D_{p_\delta}\,{}^{\xi}D_{p_\varphi}}{\bigwedge} \left(\overset{{}^{\xi}D_{p_\delta}\,{}^{\xi}D_{p_\varphi}}{\bigvee} {}^{\xi}D_p \right) \right\} \Big| t, \quad p, p_\delta, p_\varphi \in \mathbb{N} : p_\delta \neq p_\varphi, \;\; 1 \le p_\delta, p_\varphi \le 8 \tag{26}$$

Applications between ${}^{\xi}\mathbf{D}$ *and* ${}^{\gamma}\mathbf{D}$: Let f be a real function of the implant outcomes and let $\boldsymbol{\Theta}^t_{\mathbf{D}}$ be the set of applications $F \to F$ between ${}^{\xi}\mathbf{D}^t$ and f at time t:

$$\boldsymbol{\varphi}^t_{\mathbf{D}} = \left\{ \boldsymbol{\Sigma}^t_{\mathbf{D}} \to \psi^t_{\mathbf{L}} : {}^{\xi}D_{p_\varphi}, {}^{\xi}D_{p_\delta} \neq \psi^t_{\mathbf{L}} \right\} \tag{27}$$

$$\boldsymbol{\Theta}^t_{\mathbf{D}} = \left\{ \varphi^t_{\mathbf{D}} \to f \right\} \tag{28}$$

3.1.2. Non-instrumented active implants

Implant outcomes: Let ${}^{\gamma}\mathbf{N}^t$ be the sCs of measurements of the non-instrumented active implant outcomes at time t following implantation:

$$ {}^{\xi\gamma}\mathbf{N}^t = \left\{\psi_{\mathbf{B}}^t, \psi_{\mathbf{S}}^t, \psi_{\mathbf{L}}^t, \psi_{\mathbf{T}}^t, \psi_{\mathbf{M}}^t, \psi_{\mathbf{E}}^t, \psi_{\mathbf{C}}^t, {}^{\gamma}\mathbf{N}^t\right\} \tag{29} $$

$$ \boldsymbol{\psi}_N^t = \left\{\psi_{\mathbf{L}}^t \to \left\{{}^{\gamma}N_y^t\right\} : y \le \left|{}^{\gamma}\mathbf{N}^t\right|\right\} \tag{30} $$

Applications defined on ${}^{\xi}\mathbf{N}$: Let $\boldsymbol{\Sigma}_{\mathbf{N}}^t$ be the set of applications $F \to F$ defined on ${}^{\xi}\mathbf{N}$ at time t:

$$ \boldsymbol{\Sigma}_{\mathbf{N}}^t = \left\{ \bigwedge^{{}^{\xi}N_{p_\delta}\,{}^{\xi}N_{p_\varphi}} \left(\bigvee^{{}^{\xi}N_{p_\delta}\,{}^{\xi}N_{p_\varphi}} {}^{\xi}N_p \right) \right\} \Big| t, \quad p, p_\delta, p_\varphi \in \mathbb{N} : p_\delta \neq p_\varphi, \;\; 1 \le p_\delta, p_\varphi \le 7 \tag{31} $$

Applications between ${}^{\xi}\mathbf{N}$ *and* ${}^{\gamma}\mathbf{N}$: Let f be a real function of the implant outcomes and let $\boldsymbol{\Theta}_{\mathbf{N}}^t$ be the set of applications $F \to F$ between ${}^{\xi}\mathbf{N}^t$ and f at time t:

$$ \boldsymbol{\varphi}_{\mathbf{N}}^t = \left\{\boldsymbol{\Sigma}_{\mathbf{N}}^t \to \psi_{\mathbf{L}}^t : {}^{\xi}\mathrm{N}_{p_\varphi}, {}^{\xi}\mathrm{N}_{p_\delta} \neq \psi_{\mathbf{L}}^t\right\} \tag{32} $$

$$ \boldsymbol{\Theta}_{\mathbf{N}}^t = \left\{\varphi_{\mathbf{N}}^t \to f\right\} \tag{33} $$

3.1.3. Instrumented passive implants

Implant outcomes: Let ${}^{\gamma}\mathbf{I}^t$ be the sCs of measurements of the instrumented passive implant outcomes at time t following implantation:

$$ {}^{\xi\gamma}\mathbf{I}^t = \left\{\psi_{\mathbf{B}}^t, \psi_{\mathbf{S}}^t, \psi_{\mathbf{L}}^t, \psi_{\mathbf{M}}^t, \psi_{\mathbf{E}}^t, \psi_{\mathbf{W}}^t, {}^{\gamma}\mathbf{I}^t\right\} \tag{34} $$

$$ \boldsymbol{\psi}_I^t = \left\{\psi_{\mathbf{L}}^t \to \left\{{}^{\gamma}I_y^t\right\} : y \le \left|{}^{\gamma}\mathbf{I}^t\right|\right\} \tag{35} $$

Applications defined on ${}^{\xi}\mathbf{I}$: Let $\boldsymbol{\Sigma}_{\mathbf{I}}^t$ be the set of applications $F \to F$ defined on ${}^{\xi}\mathbf{I}$ at time t:

$$ \boldsymbol{\Sigma}_{\mathbf{I}}^t = \left\{ \bigwedge^{{}^{\xi}I_{p_\delta}\,{}^{\xi}I_{p_\varphi}} \left(\bigvee^{{}^{\xi}I_{p_\delta}\,{}^{\xi}I_{p_\varphi}} {}^{\xi}I_p \right) \right\} \Big| t, \quad p, p_\delta, p_\varphi \in \mathbb{N} : p_\delta \neq p_\varphi, \;\; 1 \le p_\delta, p_\varphi \le 6 \tag{36} $$

Applications between ${}^{\xi}\mathbf{I}$ *and* ${}^{\gamma}\mathrm{I}$: Let f be a real function of the implant outcomes and let $\boldsymbol{\Theta}_{\mathbf{I}}^t$ be the set of applications $F \to F$ between ${}^{\xi}\mathbf{I}^t$ and f at time t:

$$ \boldsymbol{\varphi}_{\mathbf{I}}^t = \left\{\boldsymbol{\Sigma}_{\mathbf{I}}^t \to \psi_{\mathbf{L}}^t : {}^{\xi}I_{p_\varphi}, {}^{\xi}I_{p_\delta} \neq \psi_{\mathbf{L}}^t\right\} \tag{37} $$

$$ \boldsymbol{\Theta}_{\mathbf{I}}^t = \left\{\varphi_{\mathbf{I}}^t \to f\right\} \tag{38} $$

3.1.4. Non-instrumented passive implants

Implant outcomes: Let ${}^{\gamma}\mathbf{P}^t$ be the sCs of measurements of the non-instrumented passive implant outcomes following implantation at time t:

$$ {}^{\xi\gamma}\mathbf{P}^t = \left\{\psi_{\mathbf{B}}^t, {}^{\gamma}\mathbf{P}^t\right\} \tag{39} $$

$$ \boldsymbol{\psi}_P^t = \left\{\psi_{\mathbf{L}}^t \to \left\{{}^{\gamma}P_y^t\right\} : y \le \left|{}^{\gamma}\mathbf{P}^t\right|\right\} \tag{40} $$

Applications between ${}^{\xi}\mathbf{P}$ *and* ${}^{\gamma}\mathbf{P}$: Let $\mathbf{\Theta}_{\mathbf{P}}^{t}$ be the set of applications $F \to F$ between ${}^{\xi}\mathbf{P}^{t}$ and f at time t:

$$\boldsymbol{\varphi}_{\mathbf{P}}^{t} = \left\{ \psi_{\mathbf{B}}^{t} \to \psi_{\mathbf{L}}^{t} \right\} \tag{41}$$

$$\mathbf{\Theta}_{\mathbf{P}}^{t} = \left\{ \varphi_{\mathbf{P}}^{t} \to f \right\} \tag{42}$$

3.2. Hypothesis

The following equation formulates the hypothesis that the operation outcomes from the active implants are maximized in relation with passive implants for all t:

$$\left(f\left(\varphi_{\mathbf{D}}^{t}\right) > f\left(\varphi_{\mathbf{I}}^{t}\right)\right) \overset{\mathbf{0}\ \mathbf{1}}{\bigwedge} \left(f\left(\varphi_{\mathbf{D}}^{t}\right) > f\left(\varphi_{\mathbf{P}}^{t}\right)\right) \overset{\mathbf{0}\ \mathbf{1}}{\bigwedge} \left(f\left(\varphi_{\mathbf{N}}^{t}\right) > f\left(\varphi_{\mathbf{I}}^{t}\right)\right)$$
$$\overset{\mathbf{0}\ \mathbf{1}}{\bigwedge} \left(f\left(\varphi_{\mathbf{N}}^{t}\right) > f\left(\varphi_{\mathbf{P}}^{t}\right)\right) = \mathbf{1}, \quad \forall t \tag{43}$$

in which:

$$\varrho = \left\langle \{\mathbf{0}, \mathbf{1}\}, \overset{\mathbf{0}\ \mathbf{1}}{\bigvee}, \overset{\mathbf{0}\ \mathbf{1}}{\bigwedge} \right\rangle \tag{44}$$

3.3. Configurations

3.3.1. Instrumented active implants

The autonomy of the SBA structure lays down two main groups of configurations: non-autonomous and autonomous command structures.

Non-autonomous SBA structure: Only the MBA structure is able to generate therapeutic commands. Fig. 3 shows four possible configurations to interconnect the different operations described in Section 2, namely:

$$\mathbf{D}^{t} = \left\langle \left\{ \mathbf{MBA}^{t}, \mathbf{SBA}^{t} \right\}, \overset{\mathbf{D}^{t}}{\bigvee}, \overset{\mathbf{D}^{t}}{\bigwedge} \right\rangle \tag{45}$$

in which:

Fig. 3(a): $\mathbf{SBA} = \{\mathbf{B}, \mathbf{S}, \mathbf{L}, \mathbf{T}, \mathbf{M}, \mathbf{E}, \mathbf{W}\}$, $\mathbf{MBA} = \{\mathbf{M}, \mathbf{C}\}$
Fig. 3(b): $\mathbf{SBA} = \{\mathbf{B}, \mathbf{S}, \mathbf{T}, \mathbf{M}, \mathbf{E}, \mathbf{W}\}$, $\mathbf{MBA} = \{\mathbf{L}, \mathbf{M}, \mathbf{C}\}$
Fig. 3(c): $\mathbf{SBA} = \{\mathbf{B}, \mathbf{T}, \mathbf{M}, \mathbf{E}, \mathbf{W}\}$, $\mathbf{MBA} = \{\mathbf{S}, \mathbf{L}, \mathbf{M}, \mathbf{C}\}$
Fig. 3(d): $\mathbf{SBA} = \{\mathbf{B}, \mathbf{L}, \mathbf{T}, \mathbf{M}, \mathbf{E}, \mathbf{W}\}$, $\mathbf{MBA} = \{\mathbf{S}, \mathbf{M}, \mathbf{C}\}$

The main differences among configurations are the location where **S** and **L** are performed. **M**, **S** and **L** operations can be performed both on the MBA or SBA structure; however, **E**, **B**, **T** and **W** operations have to be performed on the SBA structure. Considering the volume restrictions of the implant, lower processing requirements are demanded on the SBA structure if **S** and **L** are performed on the MBA structure. The flow direction between operations come from the operations' algebras. Other configurations are possible, such as implementing **S** and/or **B** operations both on the SBA and MBA structures. They have not been introduced because they proceed from the stated configurations and also to make the analysis easier.

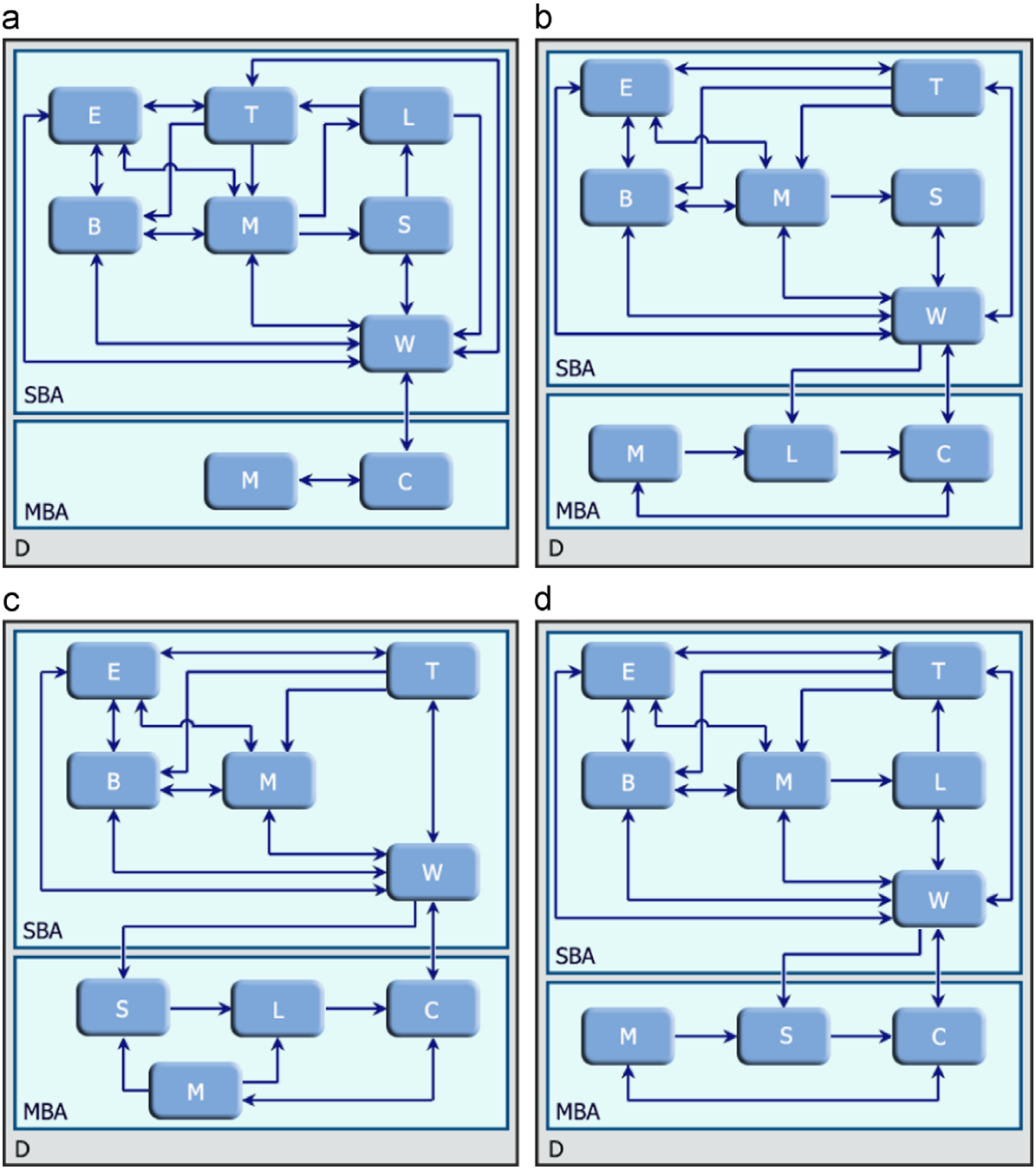

Fig. 3. Configuration 1 (a), 2 (b), 3 (c) and 4 (d) of the instrumented active implants – non-autonomous SBA structure.

Autonomous command structure: Both MBA and SBA structures are able to generate therapeutic commands. However, the generation of commands by the SBA structure must be carried out under the supervision of the MBA structure's operations. Commands from MBA structure must keep high priority over the commands generated by the SBA structure. Fig. 4 presents four possible configurations to implement a distributed implant with distributed command structure, in which:

Fig. 4(a): $\mathbf{SBA} = \{\mathbf{B}, \mathbf{S}, \mathbf{L}, \mathbf{T}, \mathbf{M}, \mathbf{E}, \mathbf{W}, \mathbf{C}\}$, $\mathbf{MBA} = \{\mathbf{M}, \mathbf{C}\}$
Fig. 4(b): $\mathbf{SBA} = \{\mathbf{B}, \mathbf{S}, \mathbf{T}, \mathbf{M}, \mathbf{E}, \mathbf{W}, \mathbf{C}\}$, $\mathbf{MBA} = \{\mathbf{L}, \mathbf{M}, \mathbf{C}\}$

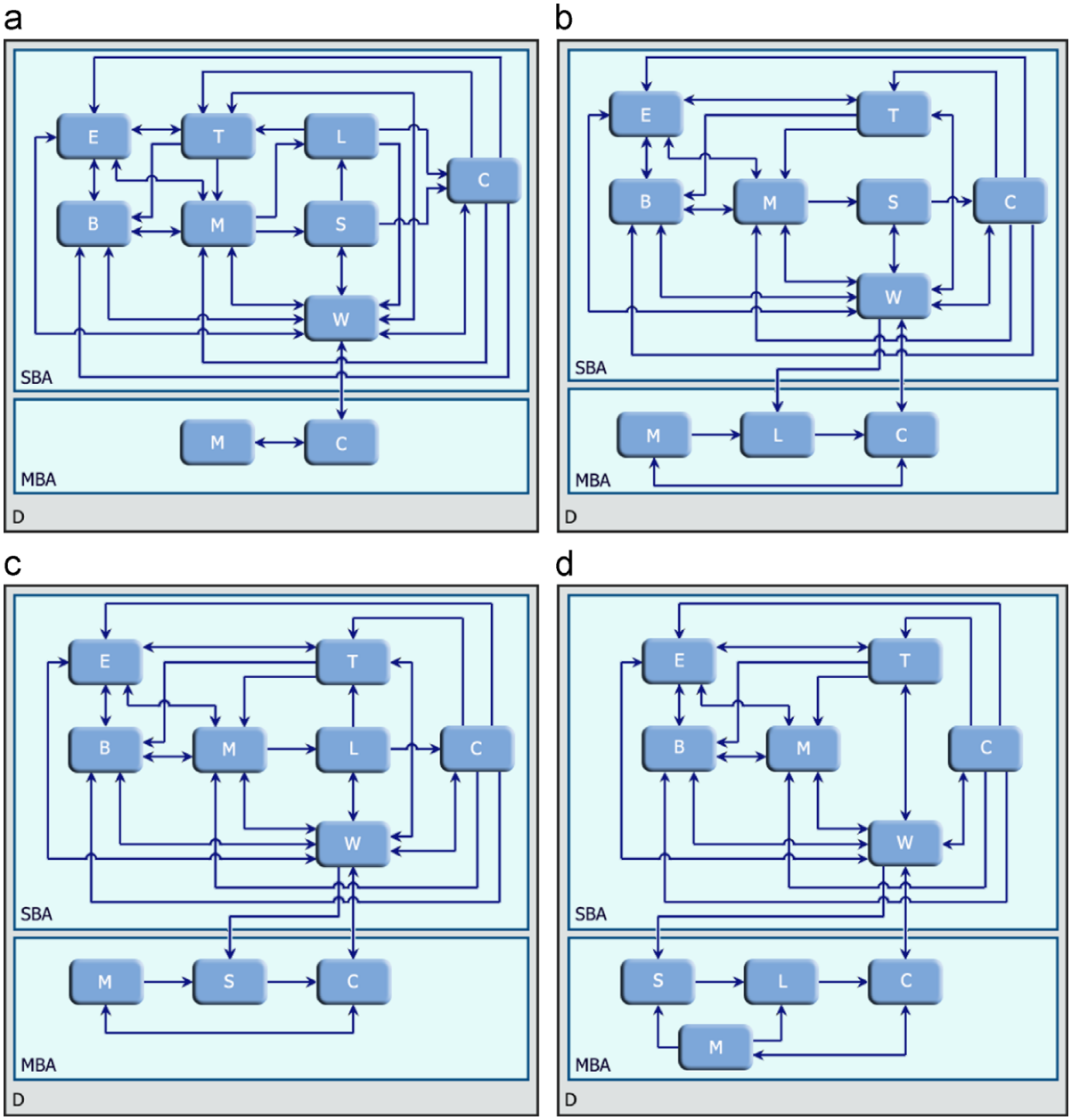

Fig. 4. Configuration 1 (a), 2 (b), 3 (c) and 4 (d) of the instrumented active implants – autonomous SBA structure.

Fig. 4(c): $\mathbf{SBA} = \{\mathbf{B}, \mathbf{L}, \mathbf{T}, \mathbf{M}, \mathbf{E}, \mathbf{W}, \mathbf{C}\}$, $\mathbf{MBA} = \{\mathbf{S}, \mathbf{M}, \mathbf{C}\}$
Fig. 4(d): $\mathbf{SBA} = \{\mathbf{B}, \mathbf{T}, \mathbf{M}, \mathbf{E}, \mathbf{W}, \mathbf{C}\}$, $\mathbf{MBA} = \{\mathbf{S}, \mathbf{L}, \mathbf{M}, \mathbf{C}\}$

3.3.2. *Non-instrumented active implants*

The SBA structure of this class of implant is fully autonomous. Because they do not comprise any MBA structure, only the SBA structure is able to generate therapeutic commands. Fig. 5 shows its only possible configuration.

$$\mathbf{N}^t = \left\langle \{\mathbf{SBA}^t\}, \bigvee^{\mathbf{N}^t}, \bigwedge^{\mathbf{N}^t} \right\rangle \tag{46}$$

in which $\mathbf{SBA} = \{\mathbf{B}, \mathbf{S}, \mathbf{L}, \mathbf{T}, \mathbf{M}, \mathbf{E}, \mathbf{C}\}$

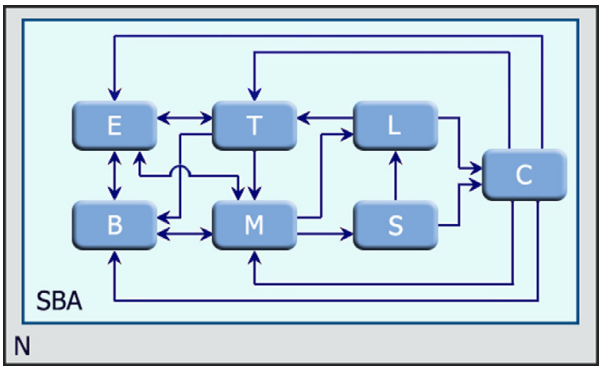

Fig. 5. Configuration of the non-instrumented active implants.

3.3.3. *Instrumented passive implants*

Fig. 6 presents four main configurations to implement instrumented passive implants (empty squares mean "no operation"). They do not comprise neither the active therapeutic operation mode nor the therapeutic command operation mode. Although mechanisms outside the human body can interact with the instrumented passive implants, they do not comprise any master structure.

3.4. *Performance analysis*

The hypothesis is true if both non-instrumented and instrumented passive implants do not satisfy the necessary conditions for optimality, while active implants satisfy necessary and sufficient conditions.

3.4.1. *Optimality of implants' performance*

The fundamental problem of implementing an implant can be stated as an optimality problem, in which one has to look into the existence of optimal trajectories between states. The performance of the implants will be optimal only if $(\psi_{\mathbf{B}}, \psi_{\mathbf{S}}, \psi_{\mathbf{L}})$ follows optimal trajectories. If sufficient conditions are satisfied, then the optimality of $(\psi_{\mathbf{B}}, \psi_{\mathbf{S}}, \psi_{\mathbf{L}})$ is possible to be implemented. Let us define: the *plants* of the SBA structures of the instrumented active implants as $(\psi^t_{\mathbf{B}}, \psi^t_{\mathbf{S}}, \psi^t_{\mathbf{L}})_D$; the *plants* of the SBA structures of the non-instrumented active implants as $(\psi^t_{\mathbf{B}}, \psi^t_{\mathbf{S}}, \psi^t_{\mathbf{L}})_N$; the *plants* of the instrumented passive implants as $(\psi^t_{\mathbf{B}}, \psi^t_{\mathbf{S}}, \psi^t_{\mathbf{L}})_I$; and the *plants* of the non-instrumented passive implants as $(\psi^t_{\mathbf{B}})_P$. Let $\mu^t_{\mathbf{S}} : {}^{\omega}\mathbf{T} \to {}^{\alpha}\mathbf{S}$ and $\mu^t_{\mathbf{B}} : {}^{\omega}\mathbf{T} \to {}^{\alpha}\mathbf{B}$ be respectively $\psi_{\mathbf{S}} - admissible$ models and $\psi_{\mathbf{B}} - admissible$ models formulating the interconnection between $\psi_{\mathbf{T}}$ and $\psi_{\mathbf{S}}$ and between $\psi_{\mathbf{T}}$ and $\psi_{\mathbf{B}}$. If we consider K as the set of all applications between two spaces and $(t+1)$ as the next time step, and taken into account that the implant is a system given by Eq. (47), then the problem of implementing an implant which is able to achieve optimality is formulated as the problem of ensuring that the set of all points $(\psi^t_{\mathbf{B}}, \psi^t_{\mathbf{S}}, \psi^t_{\mathbf{L}})$ is not empty, such that there exists a trajectory that goes from $(\psi^t_{\mathbf{B}}, \psi^t_{\mathbf{S}}, \psi^t_{\mathbf{L}})$ to the target $\left(\psi^{(t+1)}_{\mathbf{B}}, \psi^{(t+1)}_{\mathbf{S}}, \psi^{(t+1)}_{\mathbf{L}}\right)$

$$(\psi_{\mathbf{B}}, \psi_{\mathbf{S}}, \psi_{\mathbf{L}})' = g\big((\psi_{\mathbf{B}}, \psi_{\mathbf{S}}, \psi_{\mathbf{L}}), (\mu_{\mathbf{S}}, \mu_{\mathbf{B}})\big) \tag{47}$$

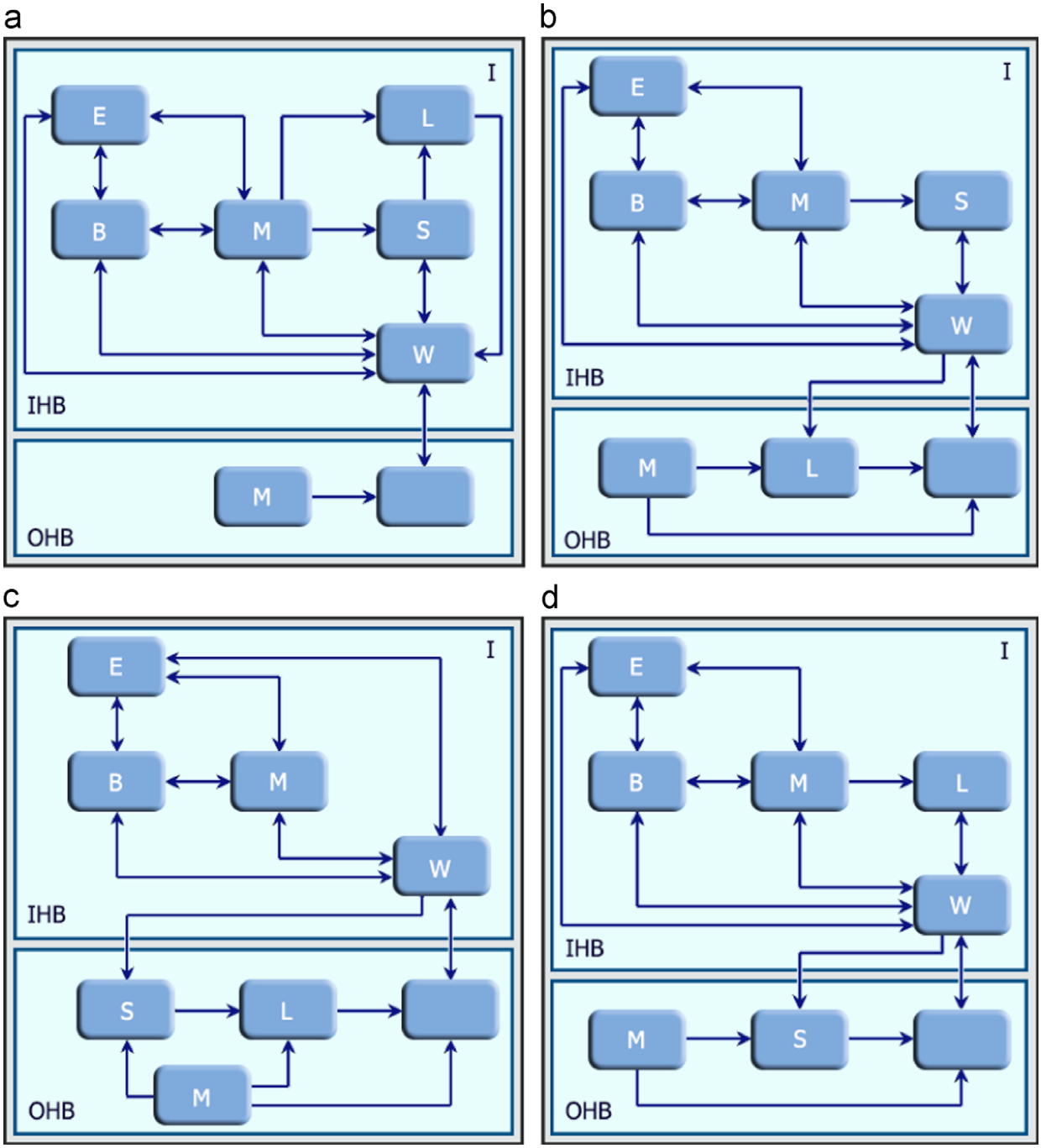

Fig. 6. Configuration 1 (a), 2 (b), 3 (c) and 4 (d) of the instrumented passive implants.

where:

$$g : \left[\left(K\left({}^{\alpha}\mathbf{B}, {}^{\omega}\mathbf{B}\right) \times K\left({}^{\alpha}\mathbf{S}, {}^{\omega}\mathbf{D}\right) \times K\left({}^{\alpha}\mathbf{L}, {}^{\omega}\mathbf{L}\right)\right) \times \left(K\left({}^{\alpha}\mathbf{S}, {}^{\omega}\mathbf{T}\right) \times K\left({}^{\alpha}\mathbf{B}, {}^{\omega}\mathbf{T}\right)\right)\right] \rightarrow \left[K\left({}^{\alpha}\mathbf{B}, {}^{\omega}\mathbf{B}\right) \times K\left({}^{\alpha}\mathbf{S}, {}^{\omega}\mathbf{S}\right) \times K\left({}^{\alpha}\mathbf{L}, {}^{\omega}\mathbf{L}\right)\right]$$

3.4.2. Diagrams of the implants' operation

The different configurations for each class of implants do not conduct to different algebras. Whatever the configuration, the diagram and optimality problem remain unchanged. The diagrams for each class of implant are introduced in Fig. 7 (empty squares mean "no operation"). They show that $\left(\psi_{\mathbf{S}}, \psi_{\mathbf{L}}\right)_P$, $\left(\mu_{\mathbf{S}}, \mu_{\mathbf{B}}\right)_I$ and $\left(\mu_{\mathbf{S}}, \mu_{\mathbf{B}}\right)_P$ do not exist.

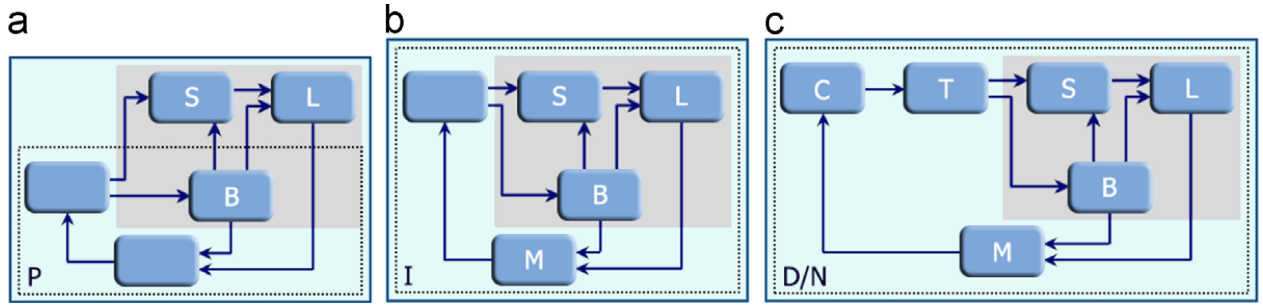

Fig. 7. Diagram of: (a) non-instrumented passive implants; (b) instrumented passive implants; (c) instrumented and non-instrumented active implants.

3.4.3. Necessary conditions for optimality

An optimality problem O is formally given by the following sixfold form [44]:

$$O = \left(\left(\psi_{\mathbf{B}}, \psi_{\mathbf{S}}, \psi_{\mathbf{L}}\right), \left(\mu_{\mathbf{S}}, \mu_{\mathbf{B}}\right), g, G, \Lambda, \phi\right) \tag{48}$$

where G is the *Lagrangian* function (it has the same domain and co-domain as g), Λ is a target, and ϕ is a function used to define the cost to achieve optimal trajectories. Because $\left(\psi_{\mathbf{S}}, \psi_{\mathbf{L}}\right)_P$, $\left(\mu_{\mathbf{S}}, \mu_{\mathbf{B}}\right)_I$ and $\left(\mu_{\mathbf{S}}, \mu_{\mathbf{B}}\right)_P$ do not exist, O_I and O_P are ill-defined, which proves that it is impossible to achieve Λ both by instrumented passive and non-instrumented passive implants. This fact can be verified based on the analysis of the Pontryagin Maximum Principle [45]: in order to implement an optimal trajectory it is necessary that there exists a *t-extremal presynthesis*, which demands:

(1) a family $\Gamma = \left\{\left(\chi_{\left(\psi^t_{\mathbf{B}}, \psi^t_{\mathbf{S}}, \psi^t_{\mathbf{L}}\right)}, \eta_{\left(\psi^t_{\mathbf{B}}, \psi^t_{\mathbf{S}}, \psi^t_{\mathbf{L}}\right)}\right)\right\}$ of admissible pairs such that the trajectory $\chi_{\left(\psi^t_{\mathbf{B}}, \psi^t_{\mathbf{S}}, \psi^t_{\mathbf{L}}\right)}$, for a control $\eta_{\left(\psi^t_{\mathbf{B}}, \psi^t_{\mathbf{S}}, \psi^t_{\mathbf{L}}\right)}$,starts at $\left(\psi^t_{\mathbf{B}}, \psi^t_{\mathbf{S}}, \psi^t_{\mathbf{L}}\right)$ and ends at the target;

(2) a normal minimized Hamiltonian H, which is given by Eq. (49) (λ is an adjoint variable):

$$H\left(\left(v_{\mathbf{S}}, v_{\mathbf{B}}\right), \left(\psi^t_{\mathbf{B}}, \psi^t_{\mathbf{S}}, \psi^t_{\mathbf{L}}\right), \lambda^t\right) \leq H\left(\left(\mu^t_{\mathbf{S}}, \mu^t_{\mathbf{B}}\right), \left(\psi^t_{\mathbf{B}}, \psi^t_{\mathbf{S}}, \psi^t_{\mathbf{L}}\right), \lambda^t\right) \tag{49}$$

(3) a solution V such that the Hamilton–Jacobi–Bellman equation is satisfied, *i.e.*,

$$H\left(\nabla V\left(\left(\psi^{(t+1)}_{\mathbf{B}}, \psi^{(t+1)}_{\mathbf{S}}, \psi^{(t+1)}_{\mathbf{L}}\right)\right), \left(\psi^{(t+1)}_{\mathbf{B}}, \psi^{(t+1)}_{\mathbf{S}}, \psi^{(t+1)}_{\mathbf{L}}\right)\right) = 0,$$
$$\forall \left(\psi^t_{\mathbf{B}}, \psi^t_{\mathbf{S}}, \psi^t_{\mathbf{L}}\right) \in \Lambda \tag{50}$$

Regarding the existence of optimal trajectories $\left(\chi^t_{\mathbf{B}}, \chi^t_{\mathbf{S}}, \chi^t_{\mathbf{L}}\right)_{opt}$, one can verify that if $\left(\chi^t_{\mathbf{B}}, \chi^t_{\mathbf{S}}, \chi^t_{\mathbf{L}}\right)_D$ and $\left(\chi^t_{\mathbf{B}}, \chi^t_{\mathbf{S}}, \chi^t_{\mathbf{L}}\right)_N$ are optimal, then:

$$\left(\psi^t_{\mathbf{B}}, \chi^t_{\mathbf{S}}, \chi^t_{\mathbf{L}}\right)_{opt} \equiv \left(\chi^t_{\mathbf{B}}, \chi^t_{\mathbf{S}}, \chi^t_{\mathbf{L}}\right)_D \tag{51}$$

$$\left(\psi^t_{\mathbf{B}}, \chi^t_{\mathbf{S}}, \chi^t_{\mathbf{L}}\right)_{opt} \equiv \left(\chi^t_{\mathbf{B}}, \chi^t_{\mathbf{S}}, \chi^t_{\mathbf{L}}\right)_N \tag{52}$$

Using a similar reasoning, one can observe that if $\left(\chi^t_{\mathbf{B}}, \chi^t_{\mathbf{S}}, \chi^t_{\mathbf{L}}\right)_I$ and $\left(\chi^t_{\mathbf{B}}\right)_P$ are optimal, then

$$\left(\chi^t_{\mathbf{B}}, \chi^t_{\mathbf{S}}, \chi^t_{\mathbf{L}}\right)_{opt} \equiv \left(\chi^t_{\mathbf{B}}, \chi^t_{\mathbf{S}}, \chi^t_{\mathbf{L}}\right)_I \tag{53}$$

$$\left(\chi^t_{\mathbf{B}}, \chi^t_{\mathbf{S}}, \chi^t_{\mathbf{L}}\right)_{opt} \equiv \left(\left(\chi^t_{\mathbf{B}}\right)_P, \left(\psi^t_{\mathbf{S}}\right)_{opt}, \left(\psi^t_{\mathbf{L}}\right)_{opt}\right) \tag{54}$$

From Eq. (54), it is deduced that non-instrumented passive implants cannot implement

trajectories that go from $\left(\chi_{\mathbf{B}}^{t},\chi_{\mathbf{S}}^{t},\chi_{\mathbf{L}}^{t}\right)$ to the target $\left(\chi_{\mathbf{B}}^{(t+1)},\chi_{\mathbf{S}}^{(t+1)},\chi_{\mathbf{L}}^{(t+1)}\right)$ because

$$\begin{aligned}&\left(\chi_{\mathbf{B}}^{t},\chi_{\mathbf{S}}^{t},\chi_{\mathbf{L}}^{t}\right)_{P}\neq\left(\chi_{\mathbf{B}}^{t},\chi_{\mathbf{S}}^{t},\chi_{\mathbf{L}}^{t}\right)_{opt}\Rightarrow\nexists V\left(\left(\psi_{\mathbf{B}}^{(t+1)},\psi_{\mathbf{S}}^{(t+1)},\psi_{\mathbf{L}}^{(t+1)}\right)\right):H=0\\&\Rightarrow\nexists\Gamma\left(\chi_{\left(\psi_{\mathbf{B}}^{t},\psi_{\mathbf{S}}^{t},\psi_{\mathbf{L}}^{t}\right)},\eta_{\left(\psi_{\mathbf{B}}^{t},\psi_{\mathbf{S}}^{t},\psi_{\mathbf{L}}^{t}\right)}\right)_{P}\Rightarrow\nexists\left(\psi_{\mathbf{B}}^{t},\chi_{\mathbf{S}}^{t},\chi_{\mathbf{L}}^{t}\right)_{opt}\end{aligned}\tag{55}$$

Regarding the existence of optimal controls $\left(\eta_{\mathbf{S}}^{t},\eta_{\mathbf{B}}^{t}\right)_{opt}$, one can state that if $\left(\eta_{\mathbf{S}}^{t},\eta_{\mathbf{B}}^{t}\right)_{D}$, $\left(\eta_{\mathbf{S}}^{t},\eta_{\mathbf{B}}^{t}\right)_{N}$, $\left(\eta_{\mathbf{S}}^{t},\eta_{\mathbf{B}}^{t}\right)_{I}$ and $\left(\eta_{\mathbf{S}}^{t},\eta_{\mathbf{B}}^{t}\right)_{P}$ are optimal, then

$$\left(\eta_{\mathbf{S}}^{t},\eta_{\mathbf{B}}^{t}\right)_{opt}=\left(\eta_{\mathbf{S}}^{t},\eta_{\mathbf{B}}^{t}\right)_{D}\tag{56}$$

$$\left(\eta_{\mathbf{S}}^{t},\eta_{\mathbf{B}}^{t}\right)_{opt}=\left(\eta_{\mathbf{S}}^{t},\eta_{\mathbf{B}}^{t}\right)_{N}\tag{57}$$

$$\left(\eta_{\mathbf{S}}^{t},\eta_{\mathbf{B}}^{t}\right)_{opt}=\left(\left(\eta_{\mathbf{S}}^{t}\right)_{opt},\left(\eta_{\mathbf{B}}^{t}\right)_{opt}\right)_{I}\tag{58}$$

$$\left(\eta_{\mathbf{S}}^{t},\eta_{\mathbf{B}}^{t}\right)_{opt}=\left(\left(\eta_{\mathbf{S}}^{t}\right)_{opt},\left(\eta_{\mathbf{B}}^{t}\right)_{opt}\right)_{P}\tag{59}$$

which means that neither instrumented passive nor non-instrumented passive implants can implement optimal controls to perform $\left(\chi_{\mathbf{B}}^{t},\chi_{\mathbf{S}}^{t},\chi_{\mathbf{L}}^{t}\right)_{opt}$, because:

$$\left(\eta_{\mathbf{S}}^{t},\eta_{\mathbf{B}}^{t}\right)_{I}\neq\left(\eta_{\mathbf{S}}^{t},\eta_{\mathbf{B}}^{t}\right)_{opt}\Rightarrow\nexists\left(\chi_{\mathbf{B}}^{t},\chi_{\mathbf{S}}^{t},\chi_{\mathbf{L}}^{t}\right)_{I}\tag{60}$$

$$\left(\eta_{\mathbf{S}}^{t},\eta_{\mathbf{B}}^{t}\right)_{P}\neq\left(\eta_{\mathbf{S}}^{t},\eta_{\mathbf{B}}^{t}\right)_{opt}\Rightarrow\nexists\left(\chi_{\mathbf{B}}^{t},\chi_{\mathbf{S}}^{t},\chi_{\mathbf{L}}^{t}\right)_{P}\tag{61}$$

These results prove that it is impossible to ensure optimal trajectories for instrumented and non-instrumented passive implants. However, these analyses cannot confirm the hypothesis (Eq. (43)). Instead, active implants $\mathbf{D}^{t}$ and $\mathbf{N}^{t}$ comprise architectures which are able to satisfy the necessary conditions to perform optimal performances, *i.e.*, they are able to find solutions V_{Γ} such that $V_{\Gamma}\equiv V$ and

$$\left(V_{\Gamma}\right)_{D}=\int G\left(\left(\chi_{\mathbf{B}}^{t},\chi_{\mathbf{S}}^{t},\chi_{\mathbf{L}}^{t}\right)_{D},\left(\eta_{\mathbf{S}}^{t},\eta_{\mathbf{B}}^{t}\right)_{D}\right)\mathrm{d}t+\phi\left(\left(\chi_{\mathbf{B}}^{(t+1)},\chi_{\mathbf{S}}^{(t+1)},\chi_{\mathbf{L}}^{(t+1)}\right)_{D}\right)\tag{62}$$

$$\left(V_{\Gamma}\right)_{N}=\int G\left(\left(\chi_{\mathbf{B}}^{t},\chi_{\mathbf{S}}^{t},\chi_{\mathbf{L}}^{t}\right)_{N},\left(\eta_{\mathbf{S}}^{t},\eta_{\mathbf{B}}^{t}\right)_{N}\right)\mathrm{d}t+\phi\left(\left(\chi_{\mathbf{B}}^{(t+1)},\chi_{\mathbf{S}}^{(t+1)},\chi_{\mathbf{L}}^{(t+1)}\right)_{N}\right)\tag{63}$$

The demonstration of both $\left(V_{\Gamma}\right)_{D}\equiv V$ and $\left(V_{\Gamma}\right)_{N}\equiv V$ are included in the demonstration that these implants satisfy the sufficient conditions to implement optimal trajectories between states (Section 3.4.4).

3.4.4. Sufficient conditions for optimality

According to Sussmann [44] (see Theorem 3.1), Γ is optimal if four sufficient conditions are satisfied:

(1) Γ be a total (*i.e.*, the largest possible) t-extremal presynthesis for O_D and O_N;
(2) the value function V_{Γ} satisfies all the weak continuity conditions for O_D and O_N;
(3) $\left(V_{\Gamma}\right)_{D}\leq V$ and $\left(V_{\Gamma}\right)_{N}\leq V$ on Λ;
(4) Γ is (g,G)-differentiable at all $\left(\psi_{\mathbf{B}},\psi_{\mathbf{S}},\psi_{\mathbf{L}}\right)$ in the complement of a *thin* subset of $\left(K\left({}^{\alpha}\mathbf{B},{}^{\omega}\mathbf{B}\right)\times K\left({}^{\alpha}\mathbf{S},{}^{\omega}\mathbf{S}\right)\times K\left({}^{\alpha}\mathbf{L},{}^{\omega}\mathbf{L}\right)\right)$.

Let us call ${}^{\Gamma_D}\psi^t_{\mathbf{T}}$ and ${}^{\Gamma_N}\psi^t_{\mathbf{T}}$ the sets of applications in which instrumented and non-instrumented active implants implement respectively Γ. Because one only has to consider the set of therapies which starts at $\left(\psi^t_{\mathbf{B}}, \psi^t_{\mathbf{S}}, \psi^t_{\mathbf{L}}\right)$ and ends at the target at time $(t+1)$, it follows necessarily that

$$\left(\bigwedge^{{}^{\Gamma_D}\mathbf{T}^t} \subseteq \bigwedge^{\mathbf{T}^t}\right) \overset{\mathbf{0}\ \mathbf{1}}{\bigwedge} \left(\bigwedge^{{}^{\Gamma_N}\mathbf{T}^t} \subseteq \bigwedge^{\mathbf{T}^t}\right) = \mathbf{1} \tag{64}$$

$$\left(\bigvee^{{}^{\Gamma_D}\mathbf{T}^t} \subseteq \bigvee^{\mathbf{T}^t}\right) \overset{\mathbf{0}\ \mathbf{1}}{\bigwedge} \left(\bigvee^{{}^{\Gamma_N}\mathbf{T}^t} \subseteq \bigvee^{\mathbf{T}^t}\right) = \mathbf{1} \tag{65}$$

$$\left({}^{\Gamma_D}\psi^t_{\mathbf{T}} \subseteq \psi^t_{\mathbf{T}}\right) \overset{\mathbf{0}\ \mathbf{1}}{\bigwedge} \left({}^{\Gamma_N}\psi^t_{\mathbf{T}} \subseteq \psi^t_{\mathbf{T}}\right) = \mathbf{1} \tag{66}$$

If there exists a therapy which implements only t-extremal presynthesis, such that $(V_\Gamma)_D \equiv V$ and $(V_\Gamma)_N \equiv V$ and Eqs. (62) and (63) are satisfied, then:

$$\left(\bigwedge^{{}^{\Gamma_{D(1)}}\mathbf{T}^t} \subseteq \bigwedge^{{}^{\Gamma_D}\mathbf{T}^t}\right) \overset{\mathbf{0}\ \mathbf{1}}{\bigwedge} \left(\bigwedge^{{}^{\Gamma_{N(1)}}\mathbf{T}^t} \subseteq \bigwedge^{{}^{\Gamma_N}\mathbf{T}^t}\right) = \mathbf{1} \tag{67}$$

$$\left(\bigvee^{{}^{\Gamma_{D(1)}}\mathbf{T}^t} \subseteq \bigvee^{{}^{\Gamma_D}\mathbf{T}^t}\right) \overset{\mathbf{0}\ \mathbf{1}}{\bigwedge} \left(\bigvee^{{}^{\Gamma_{N(1)}}\mathbf{T}^t} \subseteq \bigvee^{{}^{\Gamma_N}\mathbf{T}^t}\right) = \mathbf{1} \tag{68}$$

$$\left({}^{\Gamma_{D(1)}}\psi^t_{\mathbf{T}} \subseteq {}^{\Gamma_D}\psi^t_{\mathbf{T}}\right) \overset{\mathbf{0}\ \mathbf{1}}{\bigwedge} \left({}^{\Gamma_{N(1)}}\psi^t_{\mathbf{T}} \subseteq {}^{\Gamma_N}\psi^t_{\mathbf{T}}\right) = \mathbf{1} \tag{69}$$

where (1) in Eqs. (67)– (69) refers to condition (1) applied to Γ. The same statements are true for the other three conditions:

$$\left(\bigwedge^{{}^{\Gamma_{D(n)}}\mathbf{T}^t} \subseteq \bigwedge^{{}^{\Gamma_D}\mathbf{T}^t}\right) \overset{\mathbf{0}\ \mathbf{1}}{\bigwedge} \left(\bigwedge^{{}^{\Gamma_{N(n)}}\mathbf{T}^t} \subseteq \bigwedge^{{}^{\Gamma_N}\mathbf{T}^t}\right) = \mathbf{1}, \quad n = 1,2,3,4 \tag{70}$$

$$\left(\bigvee^{{}^{\Gamma_{D(n)}}\mathbf{T}^t} \subseteq \bigvee^{{}^{\Gamma_D}\mathbf{T}^t}\right) \overset{\mathbf{0}\ \mathbf{1}}{\bigwedge} \left(\bigvee^{{}^{\Gamma_{N(n)}}\mathbf{T}^t} \subseteq \bigvee^{{}^{\Gamma_N}\mathbf{T}^t}\right) = \mathbf{1}, \quad n = 1,2,3,4 \tag{71}$$

$$\left({}^{\Gamma_{D(n)}}\psi^t_{\mathbf{T}} \subseteq {}^{\Gamma_D}\psi^t_{\mathbf{T}}\right) \overset{\mathbf{0}\ \mathbf{1}}{\bigwedge} \left({}^{\Gamma_{N(n)}}\psi^t_{\mathbf{T}} \subseteq {}^{\Gamma_N}\psi^t_{\mathbf{T}}\right) = \mathbf{1}, \quad n = 1,2,3,4 \tag{72}$$

The desired therapies ${}^{opt}\psi^t_{\mathbf{T}}$, performed by both instrumented and non-instrumented active implants, which satisfy the sufficient conditions for optimality, can be deterministically stated as follows:

$${}^{opt}\psi^t_{\mathbf{T}} = \bigwedge^{{}^{\Gamma_{D(n)}}\mathbf{T}^t} \left(\bigvee^{{}^{\Gamma_{D(n)}}\mathbf{T}^t} {}^{\Gamma_{D(n)}}\psi^t_{\mathbf{T}}\right) \tag{73}$$

$${}^{opt}\psi^t_{\mathbf{T}} = \bigwedge^{{}^{\Gamma_{N(n)}}\mathbf{T}^t} \left(\bigvee^{{}^{\Gamma_{N(n)}}\mathbf{T}^t} {}^{\Gamma_{N(n)}}\psi^t_{\mathbf{T}}\right) \tag{74}$$

which proves that if there are optimal trajectories $\left({}^{opt}\psi_{\mathbf{T}}^{t} \neq \varnothing\right)$ (one cannot disregard that failures may become so serious that only surgical procedures are able to minimize the problem), then instrumented and non-instrumented active implants are able to implement them. From this, it follows that active implants satisfy the sufficient conditions to perform optimal performances, *i.e.*, if optimal trajectories between states of failure and states of without-failure exist, then non-instrumented active implants and instrumented active implants comprise suitable architectures to implement them. The proof is thus complete.

4. Discussion and conclusion

The concept of Instrumented Implant was first purposed as an accurate method to overcome the inaccuracy of numerical and analytical models of biomechanical quantities acting on orthopaedic implants, such as forces, moments and temperatures. Important breakthroughs have been carried out over the last decades in the optimization of such method, but neither the concept of Instrumented Implant was fully implemented nor it has evolved as a method to achieve performance optimality overcoming failures. *In vivo* data acquisition from instrumented passive implants has been used to validate biomechanical models, but no study was found about the use of such implants to validate biochemical models of the tissues surrounding the *in situ* structure. Moreover, no valuable data about the interaction between the biochemical properties of the tissues and the biomechanical properties of the implant was provided by instrumented passive implants, although their architectures allow the implementation of prediction mechanisms of failures, including those caused by its own mechanical structure. Thus, more research efforts must be conducted to implement fully operative instrumented passive implants (see Sections 2.2.9 and 3.1.3).

This study proves that active methodologies can be used to implement optimal implants. For such purpose, implants' architectures must comprise active therapeutic actuation mechanisms. Otherwise, instrumented and non-instrumented passive implants will never ensure optimal trajectories between states of failure and states of without-failure, whatever the optimization of the implants' design and materials, rehabilitation protocols or surgical procedures.

If multiple networks of different actuators were embedded into the implant, then it would be possible to implement a *multi-agent actuation mode* of operation. Prescott et al. [46] designed a microchip device comprising hundreds of arrays of discrete reservoirs, which is able to control the release of therapeutic drug doses over several months in biological environments. This study is an appropriate basis for the research of new designs of instrumented active implants implementing controlled biological therapies, such as antimicrobial therapy and suppressive antibiotic therapy. Important advances can also be achieved if research is conducted to design active implants with the ability to diagnose failures through the detection of failure-specific molecular markers, such as the detection of serum chromium levels, nitric oxide synthase, regulators of apoptosis and regulators of macrophase activity [47,48].

According to the possible configurations of the instrumented active implants, it is possible to diagnose failures and identify the physiological state of the patient outside the human body (through laboratory analysis of fluids and tissues, imaging evaluation techniques, and/or other methods), and then use the MBA structure to send these data to the SBA structure.

The definition of optimal trajectories also comprise the state of the mechanical features of the implant, *i.e.*, therapeutic actuations are performed by the active implants taking into account the optimal state of its mechanical features as a target. The greater the number of available therapies

and diagnosis methods, the greater the number of trajectories which ensure that a desired physiological state target is achievable from a current state of failure.

Declarations

The authors would like to thank the Portuguese Foundation for Science and Technology (FCT) for their financial support under the research project PTDC/EME-PME/105465/2008 and the Grant SFRH/BD/78414/2011. The authors do not have any financial or personal relationship with other people or organizations that could have inappropriately influenced this study. Ethical approval: nothing to declare.

References

[1] J.S. Day, E. Lau, K.L. Ong, G.R. Williams, M.L. Ramsey, S.M. Kurtz, Prevalence and projections of total shoulder and elbow arthroplasty in the United States to 2015, J. Shoulder Elb. Surg. 19 (8) (2010) 1115–1120.
[2] S. Kurtz, K. Ong, E. Lau, F. Mowat, M. Halpern, Projections of primary and revision hip and knee arthroplasty in the United States from 2005 to 2030, J. Bone Jt. Surg. Am. 89 (4) (2007) 780–785.
[3] G. Labek, M. Thaler, W. Janda, M. Agreiter, B. Stöckl, Revision rates after total joint replacement – cumulative results from worldwide joint register datasets, J. Bone Jt. Surg. Br. 93 (7) (2011) 293–297.
[4] H. Bergen, Report June 2010, Technical Report, The Norweigen Arthoplasty Register, 2010.
[5] G. Garellick, J. Karrholm, C. Rogmark, O. Rolfson, P. Herberts, Annual Report 2011, Technical Report, Swedish Hip Arthroplasty Register, 2011.
[6] S.M. Kurtz, E. Lau, K. Ong, K. Zhao, M. Kelly, K.J. Bozic, Future young patient demand for primary and revision joint replacement, Clin. Orthop. Relat. Res. 467 (10) (2009) 2606–2612.
[7] K.L. Ong, E. Lau, J. Suggs, S.M. Kurtz, M.T. Manley, Risk of subsequent revision after primary and revision total joint arthroplasty, Clin. Orthop. Relat. Res. 468 (11) (2010) 3070–3076.
[8] K.J. Bozic, S.M. Kurtz, E. Lau, K. Ong, T.P. Vail, D.J. Berry, The epidemiology of revision total hip arthroplasty in the United States, J. Bone Jt. Surg. Am. 91 (1) (2009) 128–133.
[9] J.A. Simões, A.T. Marques, Design of a composite hip femoral prosthesis, Mater. Des. 26 (5) (2005) 391–401.
[10] N.W. Rydell, Forces acting on the femoral head-prosthesis. A study on strain gauge supplied prostheses in living persons, Acta Orthop. Scand. 37 (88) (1966) 1–132.
[11] F. Graichen, R. Arnold, A. Rohlmann, G. Bergmann, Implantable 9-channel telemetry system for in vivo load measurements with orthopedic implants, IEEE Trans. Biomed. Eng. 54 (2) (2007) 253–261.
[12] D.D. D'Lima, S. Patila, N. Steklov, S. Chien, C.W. Colwell, In vivo knee moments and shear after total knee arthroplasty, J. Biomech. 40 (1) (2007) S11–S17.
[13] B. Kirking, J. Krevolin, C. Townsend, C.W. Colwell, D.D. D'Lima, A multiaxial force-sensing implantable tibial prosthesis, J. Biomech. 39 (9) (2006) 1744–1751.
[14] P. Damm, F. Graichen, A. Rohlmann, A. Bender, G. Bergmann, Total hip joint prosthesis for in vivo measurement of forces and moments, Med. Eng. Phys. 32 (1) (2010) 95–100.
[15] G. Bergmann, F. Graichen, A. Rohlmann, N. Verdonschot, G. van Lenthe, Frictional heating of total hip implants. Part 1. Measurements in patients, J. Biomech. 34 (4) (2001) 421–428.
[16] F. Graichen, G. Bergmann, A. Rohlmann, Hip endoprosthesis for in vivo measurement of joint force and temperature, J. Biomech. 32 (10) (1999) 1113–1117.
[17] S. Almouahed, M. Gouriou, C. Hamitouche, E. Stindel, C. Roux, Design and evaluation of instrumented smart knee implant, IEEE Trans. Biomed. Eng. 58 (4) (2011) 971–982.
[18] K.M. Varadarajan, A.L. Moynihan, D. D'Lima, C.W. Colwell, G. Li, In vivo contact kinematics and contact forces of the knee after total knee arthroplasty during dynamic weight-bearing activities, J. Biomech. 41 (10) (2008) 2159–2168.
[19] U. Marschner, H. Grätz, B. Jettkant, D. Ruwisch, G. Woldt, W.-J. Fischer, B. Clasbrummel, Integration of a wireless lock-in measurement of hip prosthesis vibrations for loosening detection, Sens. Actuators A—Phys. 156 (1) (2009) 145–154.

[20] R. Puers, M. Catrysse, G. Vandevoorde, R. Collier, E. Louridas, F. Burny, M. Donkerwolcke, F. Moulart, A telemetry system for the detection of hip prosthesis loosening by vibration analysis, Sens. Actuators A—Phys. 85 (1–3) (2000) 42–47.
[21] G. Bergmann, F. Graichen, J. Dymke, A. Rohlmann, G.N. Duda, P. Damm, High-tech hip implant for wireless temperature measurements in vivo, PLoS ONE 7 (8) (2012) e43489.
[22] M. Soares dos Santos, J.A.F. Ferreira, A. Ramos, J.A.O. Simões, R. Morais, N.M. Silva, P.M. Santos, M.C. Reis, T. Oliveira, Instrumented hip joint replacements, femoral replacements and femoral fracture stabilizers, Expert Rev. Med. Devices 11 (6) (2014) 617–635.
[23] E.H. Ledet, D. D'Lima, P. Westerhoff, J.A. Szivek, R.A. Wachs, G. Bergmann, Implantable sensor technology: from research to clinical practice, J. Am. Acad. Orthop. Surg. 20 (6) (2012) 383–392.
[24] H. Yoshida, A. Faust, J. Wilckens, M. Kitagawa, J. Fetto, E.Y.S. Chao, Three-dimensional dynamic hip contact area and pressure distribution during activities of daily living, J. Biomech. 39 (11) (2006) 1996–2004.
[25] P.D. Rushfeld, R.W. Mann, W.H. Harris, Influence of cartilage geometry on the pressure distribution in the human hip joint, Science 204 (4391) (1979) 413–415.
[26] M.O. Heller, G. Bergmann, G. Deuretzbacher, L. Claes, N.P. Haas, G.N. Duda, Influence of femoral anteversion on proximal femoral loading: measurement and simulation in four patients, Clin. Biomech. 16 (8) (2001) 644–649.
[27] M.O. Heller, G. Bergmann, J.P. Kassi, L. Claes, N.P. Haas, G.N. Duda, Determination of muscle loading at the hip joint for use in pre-clinical testing, J. Biomech. 38 (5) (2005) 1155–1163.
[28] M. Heller, G. Bergmann, G. Deuretzbacher, L. Dürselen, M. Pohl, L. Claes, N.P. Haas, G. Duda, Musculo-skeletal loading conditions at the hip during walking and stair climbing, J. Biomech. 34 (7) (2001) 883–893.
[29] F. Burny, M. Donkerwolcke, F. Moulart, R. Bourgois, R. Puers, K.V. Schuylenbergh, M. Barbosa, O. Paiva, F. Rodes, J.B. Bégueret, P. Lawes, Concept, design and fabrication of smart orthopedic implants, Med. Eng. Phys. 22 (7) (2000) 469–479.
[30] M. Soares dos Santos, J.A.F. Ferreira, A. Ramos, J.A.O. Simões, R. Morais, N.M. Silva, P.M. Santos, M.J.C.S. Reis, T. Oliveira, Instrumented hip implants: electric supply systems, J. Biomech. 46 (15) (2013) 2561–2571.
[31] J. Parvizi, V. Antoci, N.J. Hickok, I.M. Shapiro, Selfprotective smart orthopaedic implants, Expert Rev. Med. Devices 4 (1) (2007) 55–64.
[32] A. Lendlein, R. Langer, Biodegradable elastic shape-memory polymers for potential biomedical applications, Science 296 (5573) (2002) 1673–1676.
[33] J.-M. Lehn, Toward self-organization and complex matter, Science 295 (5564) (2002) 2400–2403.
[34] B. Jose, V. Antoci Jr., A.R. Zeiger, E. Wickstrom, N.J. Hickok, Vancomycin covalently bonded to titanium beads kills staphylococcus aureus, Chem. Biol. 12 (9) (2005) 1041–1048.
[35] R. Morais, N.M. Silva, P.M. Santos, C.M. Frias, J.A.F. Ferreira, A.M. Ramos, J.A.O. Simões, J.M.R. Baptista, M.C. Reis, Double permanent magnet vibration power generator for smart hip prosthesis, Sens. Actuators A—Phys. 172 (1) (2011) 259–268.
[36] N. Silva, P. Santos, J. Ferreira, M. Santos, M. Reis, R. Morais, Multi-purpose and multi-source energy management system for biomedical implants, Procedia Eng. 47 (2012) 722–725.
[37] M.L. Morgado, L.F. Morgado, E. Henriques, N. Silva, P. Santos, M. Santos, J. Ferreira, M. Reis, R. Morais, Nonlinear modeling of vibrational energy harvesters for smart prostheses, Procedia Eng. 47 (2012) 1089–1092.
[38] N.M. Silva, P.M. Silva, J.A.F. Ferreira, M.P.S. dos Santos, A. Ramos, J.A.O. Simões, M.J.C.S. Reis, R. Morais, Power management architecture for smart hip prostheses comprising multiple energy harvesting systems, Sens. Actuators A—Phys. 202 (1) (2013) 183–192.
[39] M.P. Soares dos Santos, J.A.F. Ferreira, A. Ramos, R. Pascoal, R.M. dos Santos, N.M. Silva, J.A.O. Simões, M.J.C.S. Reis, A. Festas, P.M. Santos, Multi-source harvesting systems for electric energy generation on smart hip prostheses, Biomedical Engineering Systems and Technologies, Springer-Verlag, Berlin, 2013, pp. 80–96.
[40] R. Morais, C.M. Frias, N.M. Silva, J.L.F. Azevedo, C.A. Serôdio, P.M. Silva, J.A.F. Ferreira, J.A.O. Simões, M.C. Reis, An activation circuit for battery-powered biomedical implantable systems, Sens. Actuators A—Phys. 156 (1) (2009) 229–236.
[41] P. Alpuim, S.A. Filonovich, C.M. Costa, P.F. Rocha, M.I. Vasilevskiy, S. Lanceros-Mendez, C. Frias, A.T. Marques, R. Soares, C. Costa, Fabrication of a strain sensor for bone implant failure detection based on piezoresistive doped nanocrystalline silicon, J. Non-Cryst. Solids 354 (19–25) (2008) 2585–2589.
[42] J. Reis, C. Frias, C.C. e Castro, M.L. Botelho, A.T. Marques, J.A.O. Simões, F.C. e Silva, J. Potes, A new piezoelectric actuator induces bone formation in vivo: a preliminary study, J. Biomed. Biotechnol. 2012 (2012) 1–7.
[43] M. Soares dos Santos, J.A.F. Ferreira, J.A.O. Simões, A. Ramos, R.M. dos Santos, N.M. Silva, M.J.C.S. Reis, P.M. Santos, Design methodology for the development of long-term hip prosthesis survival, J. Biomech. 45 (2012) S106.

[44] H.J. Sussmann, Nonlinear Controllability and Optimal Control, Marcel Dekker INC, New York, Basel, 1990.
[45] V.G. Boltyansky, Sufficient conditions for optimality and the justification of the dynamic programming method, SIAM J. Control 4 (2) (1966) 326–361.
[46] J.H. Prescott, S. Lipka, S. Baldwin, N.F. Sheppard, J.M. Maloney, J. Coppeta, B. Yomtov, M.A. Staples, J.T. Santini, Chronic, programmed polypeptide delivery from an implanted, multireservoir microchip device, Nat. Biotechnol. 24 (4) (2006) 437–438.
[47] S. Stea, M. Visentina, M.E. Donati, D. Granchi, G. Ciapetti, A. Sudanese, A. Toni, Nitric oxide synthase in tissues around failed hip prostheses, Biomaterials 23 (24) (2002) 4833–4838.
[48] F. Yang, W. Wu, L. Cao, Y. Huang, Z. Zhu, T. Tang, K. Dai, Pathways of macrophage apoptosis within the interface membrane in aseptic loosening of prostheses, Biomaterials 32 (35) (2011) 9159–9167.

Chapter 3

Literature review

The conclusions retrieved from the optimality analysis (section 2) state that, regardless the methodology, four requirements must be fulfilled to ensure that implants will perform actuation trajectories from states of failure to states of without-failure:

1. Implants must monitor the osseointegration process, either by using biological or non-biological mechanisms;
2. Implants must be composed by (biological and/or non-biological) therapeutic actuators to control the peri-implant bone structure and the bone-implant bonding;
3. Therapeutic actuator(s) must be highly controllable, i.e., their ability to deliver different actuations must be maximized;
4. Therapeutic actuator(s) must be able to deliver different therapeutic actuations to different and nearby tissue areas, as required for tracking an optimality actuation trajectory.

These results are quite useful as they allow to define which are the potentially most suitable methodologies to design implants capable of minimizing the uncontrolled osseointegration. Only active implants, either instrumented or non-instrumented, can optimize osseointegration. Hence, using non-organic control systems, instrumented active implants may be designed to control the bioactivity on the bone-implant interface by releasing of bio-agents and/or by delivering exogenous biophysical stimuli. Non-instrumented implants may be also designed as complex delivering systems (which may be also established to release bio-agents and/or biophysical stimuli), but they perform feedback control only using cellular pathways. However, higher controllability of the therapeutic actuation may be achieved using instrumented implants since:

(a) These implants may comprise non-cellular and/or cellular actuators (e.g. bioactive coatings and biophysical stimulators), increasing the actuation range;

(b) Non-cellular actuators (such as biophysical stimulators) may be used to control the behavior of bioactive coatings;

(c) Biophysical stimulators can be controlled extracorporeally using wireless-based communication systems, which permit time-dependent therapeutic actuations after implant's body insertion;

(d) The human knowledge (from clinicians) can be used to establish long-term personalized therapies.

Due to the inherent ability of instrumented active implants to perform highly controlled and personalized therapeutic actuations at nano- to macro-scale levels [using (nano-) miniaturized biophysical stimulators], the optimization of these implants must be firstly pursued. This thesis is then focused on enhancing the ability of instrumented implants to perform personalized control of the osseointegration process.

3.1 Instrumented implants - overview

A detailed state-of-the-art was required to identify the therapeutic actuators and supporting systems already developed for instrumented THRs, femoral replacements and femoral fracture stabilizers[1]. In a first stage, overall comparative analyses were carried out focusing on their actuation, power supply, measurement, communication and processing systems. The tests conducted by each research team to evaluate the performance and safety of their instrumented implants were also evaluated. This state-of-the-art is entitled "Instrumented hip joint replacements, femoral replacements and femoral fracture stabilizers". It is published in the *Expert Review of Medical Devices* (volume 11, issue 6, pp. 617-635)[2]. This study intends to analyse the controllability level of current instrumented implants and their ability to deliver different therapeutic actuations to different and nearby tissue areas.

[1] I also collaborated in a similar study for knee implants (Supplement 1).

[2] As the content of this study is already published, the formatting rules established by the journal *Expert Review of Medical Devices* are used.

EXPERT REVIEWS

Instrumented hip joint replacements, femoral replacements and femoral fracture stabilizers

Expert Rev. Med. Devices 11(6), 617–635 (2014)

Marco P Soares dos Santos*[1,2], Jorge AF Ferreira[2], António Ramos[1,2], José AO Simões[2], Raul Morais[3,4], Nuno M Silva[4], Paulo M Santos[3,4], Manuel C Reis[3,4] and Tatiana Oliveira[2]

[1]*Biomechanics Research Group, Centre for Mechanical Technology and Automation, Campus Universitário de Santiago, 3810-193 Aveiro, Portugal*
[2]*Department of Mechanical Engineering, University of Aveiro, Campus Universitário de Santiago, 3810-193 Aveiro, Portugal*
[3]*University of Trás-os-Montes e Alto Douro, 5001-801 Vila Real, Portugal*
[4]*Institute of Electronics and Telematics Engineering of Aveiro, 3810-193 Aveiro, Portugal*
**Author for correspondence: Tel.: +351 234 370 830 marco.santos@ua.pt*

This paper reviews instrumented hip joint replacements, instrumented femoral replacements and instrumented femoral fracture stabilizers. Examination of the evolution of such implants was carried out, including the detailed analysis of 16 architectures, designed by 8 research teams and implanted in 32 patients. Their power supply, measurement, communication, processing and actuation systems were reviewed, as were the tests carried out to evaluate their performance and safety. These instrumented implants were only designed to measure biomechanical and thermodynamic quantities *in vivo,* in order to use such data to conduct research projects and optimize rehabilitation processes. The most promising trend is to minimize aseptic loosening and/or infection following hip or femoral replacements or femoral stabilization procedures by using therapeutic actuators inside instrumented implants to apply controlled stimuli in the bone–implant interface.

KEYWORDS: arthroplasty • energy harvesting • femoral fixation • femoral replacement • hip joint replacement • instrumented implant • medical device • orthopedics • telemetry • therapeutic actuator

Need of instrumented implants

The number of primary total hip replacements (THR) has been increasing, as reported by the latest reports of several national arthroplasty registers [1–4]. By 2030, the demand for primary THR is estimated to increase by 174% (to 572,000) per year in the USA and 137% for revision THR [5,6]. Most studies report survival rates close to 100% 1 year after primary THR [1]. Although considerable research efforts have been conducted to optimize implants' design and materials, recent hip revision rates are: 14.5% in 2009, as reported by the Norwegian Arthroplasty Register (NAR) [2]; 13.6% in 2011, according to the Swedish Orthopedic Register (SOR) [3]; 12% in 2012, as reported by the National Joint Registry for England, Wales and Northern Ireland (REWI) [4]; 11.5% in 2008, as published by the Joint Replacement Registry for USA (RUS) [6]. Most of these registers have registered increases in hip revisions [2,3,6]. Labek *et al.* [7] reported revision rates of about 6% after 5 years and 12% after 10 years, using data from worldwide joint registers; and Ong *et al.* [8] found 95.9% for 5-year survival probabilities, by analyzing the Medicare database. The risk of subsequent revisions is reported to be five- to six-times higher after the first revision [8]. The number of primary THR at younger ages (less than 65 years old) is increasing as well [9]. In the USA, younger patients underwent 44.7% of primary THR and 38.5% of revision procedures from 2001 to 2008 [6]. Recent projections indicate that young patients will demand 50% of primary THR and 35% of revisions between 2010 and 2030 [10].

Aseptic loosening and infection are among the most common causes for THR. The following aseptic loosening rates were recently registered: NAR [2]: approximately 50% in 2009; SOR [3]: 58.1% in 2011; REWI [4]: 40% in 2012; RUS [6]: 28.3% in 2008. However, THR outcomes are influenced by patient-related and device factors, as well as by surgeons' expertise, health systems and demographic factors [11]. Aseptic loosening rates seem to be gradually decreasing [2–4]. Revision

rates due to infection are: NAR [2]: approximately 17% in 2009; SOR [3]: 13.1% in 2011; REWI [4]: 12% in 2012; RUS [6]: 19.6% in 2008. Revision risks due to infection have been increasing [2,3,12,13]. SOR also reported that 61% of reoperations without implant replacement are due to infections [3].

The use of cement in primary and revision THR has been decreasing. NAR has been reporting this trend since 2003. In 2009, they used about 50% of uncemented and hybrid hip implants in primary THR, of which 80% were implanted in younger patients [2]. Such a long-term trend was also observed by SOR [3], which also found higher risks for revision due to loosening with cemented cups and due to infection with cemented stems.

Different methods must be considered to optimize the performance of implants. Rydell [14] was the first researcher to design instrumented hip implants to monitor biomechanical quantities *in vivo*. He acquired orthogonal compressive forces and moments *in vivo* over the neck of Austin Moore endoprostheses during several daily activities of two patients. Data were communicated by using percutaneous connections to external data acquisition systems. Many other researchers succeeded Rydell in this research line. They have designed instrumented implants in order to collect data having the following applications [15–20]:

- Calibration of models defining the implants' biomechanical and thermal environment;
- Optimization of mechanical design and materials' behavior of implants;
- Preclinical testing;
- Tracking of the healing evolution and improvement of rehabilitation processes after arthroplasty.

Considering current revision rates, the growing need of long-term survival of implants (which is also related with demographic changes) and the advances in electronic systems, instrumented implants may maximize outcomes following THR, if they are designed to control their biochemical environment. The epidemiology of revision THR suggests that instrumented hip implants must be first implemented to prevent aseptic loosening and infection in the bone–implant interface.

Femoral bone loss is one of the most complex problems that may occur after THR. Mechanical loosening, osteolysis secondary to particle debris and stress-shielding with adaptive bone remodeling are some mechanisms influencing the maintenance of femoral bone mass after THR [21,22]. Femoral replacements and femoral fracture fixation implants are being recommended for sedentary patients with severe bone loss [22]. Then, adjustable-based instrumented femoral replacements and instrumented femoral fracture stabilizers, comprising ability to control bone growth, may be designed to minimize the risk of complex revision surgeries due to bone loss.

Review structure

Literature search strategy

Relevant publications were selected in order to identify the design features, architectures, functions, achievements and future breakthroughs in instrumented hip joint replacements, instrumented femoral replacements and instrumented femoral fracture stabilizers. No time period restriction was introduced in the search parameters, because there is no previously published in-depth review about this subject. The collection was completed in December 2013.

Selection criteria

The selection of studies was based on the following criteria:

- Literature reporting instrumented hip joint replacements, instrumented femoral replacements and instrumented femoral fracture stabilizers that were already implanted, that is, implants experimentally validated *in vivo*. *In vitro* studies were only considered if later *in vivo* studies, using the same instrumented implants, were published;
- Literature focusing on instrumented implants without percutaneous wired connections (the use of percutaneous wiring is considered unacceptable for clinical applications);
- Literature reporting recent advances for future instrumented implants.

Data extraction & analyses

The key mechanical modifications to standard implants are described in this document. Tests that were conducted to evaluate their performance and safety for implantation in human patients were identified. Their power supply, measurement, communication, data processing and therapeutic operations were comparatively analyzed. Knowledge obtained from *in vivo* operation of these implants was considered outside the scope of this work (see the review of Ledet *et al.* [18] for such subject).

Instrumented hip joint replacements

Overview

Five research groups have designed a total of 12 architectures for total hip joint replacements, arranged as follows according to generations of technological breakthroughs:

- Mann *et al.* [23–38] proposed three architectures for instrumented endoprostheses: [23–27,30] for the first generation, [28–32,36–38] for the second generation and [32–35] for the third generation;
- Goodman *et al.* [39–41] developed an architecture for instrumented hip implants;
- Puers *et al.* [42] developed an architecture for instrumented hip implants;
- Davy *et al.* [43–47] reported four architectures for total hip prostheses: [44] for the first generation, [44] for the second generation, [43–45] for the third generation and [44–47] for the fourth generation;
- Bergmann *et al.* [11,48–66] designed three architectures for instrumented implants (total hip prostheses and endoprostheses): [11,48–50,55–63,65] for the first generation, [11,51,52,61–65] for the second generation and [53,54,66] for the third generation.

These authors implemented instrumented hip implants based on two types of architectures [12]: instrumentation was housed both in cavities inside and outside the implant; instrumentation was totally sealed as a one-piece implant. Hereafter, they will be referred to as 'HIO' and 'HI', respectively. These architectures comprise measurement, communication and electric power supply systems. Electronic circuitries have been housed in hollow regions machined into the implants, mainly inside the neck and head.

Implants designed by Mann *et al.* [23–38] are based on an HI architecture. They were designed for spatial and temporal measurement of pressures over the cartilage surface in human hip joint. They modified Austin-Moore endoprostheses by spherically hollowing the hemisphere and cylindrically hollowing the stem tip. They developed the instrumented hip joint replacements with the largest number of transducers. They conducted fatigue and calibration tests on the three generations of implants. Novelties of their research include the development of the first hip implant comprising a telemetric system, the first implant to measure spatial pressures over human acetabula and the first implant electrically supplied by an inductive power link.

An HIO architecture for hip prostheses was designed by Goodman *et al.* [39–41] to measure axial forces over the prosthetic neck. They modified an English prosthesis by designing the head as a removable piston and cylindrically hollowing the neck and stem. They conducted calibration tests on the load measurement system. Their research resulted in the following novelties: acquisition of the first data from loads acting *in vivo* on human hip joints using telemetric systems (these results were published before those published by Mann *et al.* [23–38]); design of the first battery supplied instrumented implant; design of the first instrumented implant with an externally activated power switch, in order to minimize the electric power consumption; the first use of the 'piston in cylinder' component (head is designed as a removable piston, which in turn is fitted into a cylindrically hollowed neck) for implants' structures without percutaneous connections; design of an instrumented implant based on an HIO structure. However, all electronic circuits were housed in the tissues surrounding the implant and cables were used to connect transducers to the transmitter system. This method is liable to fatigue and sealing problems, significantly increasing the risk of biological problems. Instrumentation remains disabled if the activation system fails.

Bergmann *et al.* have been contributing intensively to the technological breakthroughs of instrumented implants [11,48–66]. They implanted the first instrumented implants in sheep and dogs using percutaneous wired connections [67,68]. Since then, they have implanted three HI generations of instrumented hip implants in human patients. First, they modified total hip prostheses (Uni-hip, Mecron) as follows: the head was cone-shaped hollowed and it was designed to be removable; the top of the stem was cylindrically hollowed and the neck was oversized and cylindrically hollowed. They conducted fatigue, load calibration, sealing, corrosion, heating, acceleration and biocompatibility tests on implants, and finally they implanted them in three sheep over 3 years before the implantation in human patients. The second generation was designed using modified CENOS endoprostheses (ARTOS, Berlin) and ceramic heads (CERASIV GmbH, Plochingen, Germany): the head was hollowed in cone shape and was designed to be removable; the neck was oversized and cylindrically hollowed and the stem was hollowed lengthwise, according to its own geometry. Heating, sealing, mechanical shocks, load and temperature calibration tests were carried out on implants before implantation. 'Cementless Tapered Wedge' total hip prostheses (Merete Medical GmbH, Berlin), with ceramic head, were customized by modifying the head (it was hollowed in cone shape and designed to be removable) and neck (it was oversized and cylindrically hollowed). This third generation was approved to be implanted in human patients after sealing, endurance, fatigue and calibration tests. The number of sensors and biomechanical quantities under tracking were different among architectures. Considerable amount of biomechanical and thermodynamic data (forces, moments and temperatures) have been acquired *in vivo*, which can be downloaded from the OrthoLoad database [69]. These data have been widely used in orthopedic and biomedical engineering research. This research team was the first to: propose the 'MATRIX' method for 3D force measurement using only three single strain gauges [50,67]; develop the 'current difference' method for low power consumption using strain gauges [50]; acquire data from loads acting *in vivo* on animal hip joints, using instrumented prostheses; compare hip joint forces in man, sheep and dogs; miniaturize telemetric systems (4, 8 and 9 channels) for instrumented implants; use a telemetric system inside implants comprising different induction power link and data link and measure temperatures along the entire length of implants.

Davy *et al.* [43–47] have designed four generations of instrumented implants based on HI architecture. The first and the second are modified T-28 total hip prostheses; the third and fourth are modified DF-80 (Zimmer) total hip prostheses. All architectures were implemented to measure three orthogonal forces on the neck; the third and fourth architectures also monitor rectified supply voltage and temperature inside the neck. Their necks were cylindrically hollowed; heads were cylindrically and spherically hollowed, and they were designed to be removable; only the neck of the first generation was not oversized. Load calibration tests were conducted on all architectures. Pacemaker-type batteries were used to power implants based on the third generation. Magnetic reed switches were replaced by momentary reed switches and additional circuitry was introduced to power implants for an adjustable period of time. Davy *et al.* were the first to use miniaturized pacemaker-type batteries inside hip joint replacements. The instrumentation of their implants is disabled if the activation system fails.

Puers *et al.* [42] modified cemented hip prosthesis (the head and top of the neck were hollowed) in order to design an HI architecture with the ability to detect loosening. Prediction is obtained by analyzing head accelerations when external mechanical vibrations are applied at the distal end of the femoral bone.

They have found a relation between loosening and distortion rate of head's accelerations. Later research concluded that this method is only reliable when the size of failures is more than one-third of the stem length, although detection of failures located at the stem central portion is likely to fail [70]. Nevertheless, they were the first to propose hip prostheses comprising internal mechanisms to measure some failure states.

Measurement features

Table 1 lists measurement features of the 12 architectures experimentally validated *in vivo*. Strain gauges (based on resistive methods) have been used in most implants (only Puers *et al.* [42] applied a capacitive method). Most of them have been housed in the inner walls of the neck. Loads and moments over hip implants, as well as temperatures inside implants, have been the main monitored quantities. Head's acceleration and rectified supply voltage (inside implants) were also under tracking. Architectures designed by Mann *et al.* [23–38], and the second architecture designed by Bergmann *et al.* [11,51,52,61–65], housed the highest number of transducers inside instrumented implants (14, 13 and 12, respectively). Bergmann *et al.* [11,48–52,55–65] achieved load errors lower than 1% and temperature errors lower than 0.1°C. Data acquisition was sampled up to 4.2 kHz. Mann *et al.* [32–35] simultaneously monitored 13 quantities up to 500 Hz and Bergmann *et al.* [11,48–52,55–65] monitored 12 signals up to 250 Hz.

Data storage inside implants has not been reported. Processing of data acquired *in vivo* has not been reported, namely one cannot find characteristics of failures determined by implants (such as extension, type, state and regions of failures), as well as physiological states of tissues surrounding implants' structures.

Communication features

Table 2 introduces a comparative basis between the communication features of instrumented implants. All architectures use radiofrequency (RF) transmission circuitry and antenna(s). Mann *et al.* [23–38] designed the transmitter with the highest number of channels (16). Bergmann *et al.* [11,51,52,61–65] decided to use two transmitters, each of them with eight channels. The authors housed them in different locations, namely in the head, neck and shaft, and even outside the implants. Transmitters embedded outside implants may dislocate from its initial position, as reported by Goodman *et al.* [41]. Inside implants, antennas were located in upper regions, namely at the end of the stem, head and upper neck region. Bergmann *et al.* [11,48–66] and Puers *et al.* [42] magnetically and mechanically shielded the circuitry, using metallic protective hollowed cylinders. Data monitored *in vivo* have been transmitted to instrumentation located outside the patients' body: the main goal has been to use these data for research projects [13,14,26,62]. Data acquisition was not performed throughout the daily living of patients, but only in research laboratories.

Therapeutic features

No architecture comprising therapeutic actuation systems was reported. Although new designs and materials for orthopedic implants have been researched, implants have not been designed to perform real-time therapy *in vivo*. They do not comprise actuation mechanisms to prevent failures in real-time, that is, to ensure controlled trajectories between states of failure and states of without-failure, whatever the failures' characteristics.

Supply features

Table 3 presents a comparative analysis between the supply features that allow the implants' operation. Implants have been supplied only by electric energy. No other acquisition of resources (e.g., chemicals) has been managed. Data monitored *in vivo* have not been considered as resources required by implants to operate successfully, that is, the current operation of implants is not function of previously monitored data.

Only inductive power links and batteries have been used as electrical power supply systems to operate *in vivo*. No published studies reporting failures of power supply systems were found. Inductive powering requires circuitry outside the patients' body, namely primary coil(s), power oscillator(s), antenna(s) and processing circuitries. Oscillation frequencies between 3 and 750 kHz were used. Secondary power coils and power regulation systems were housed inside the patients' body: power coils were housed in different regions, namely at the top of the stem, shaft and neck; regulation systems were located in head, neck and shaft. Battery-based power systems were designed to power the instrumentation inside implants when reed switches were activated (inside the patients' body) by magnets (outside the patients' body). In order to maximize the power to supply electronics embedded inside implants, Bergmann *et al.* [11,51–54,61–66] used microcontrollers (outside the patients' body) controlling the oscillator frequency to compensate for effects of relative displacement between primary and secondary coils. Power consumption of instrumentation has been minimized: the first architecture designed by Mann *et al.* [23–27,30] required 500 mW to operate; the second architecture developed by Bergmann *et al.* [11,51,52,61–65] only needed 10 mW (although it comprises three strain gauges, nine thermistors and two transmitter systems requiring power supply). However, power needs are related with the number of components and, consequently, with the number of operations possible to be carried out by implants.

Methods that were used to power implants constrain their operation. By using inductive power systems:

- the period between data monitoring operations increases, because they disturb daily activities of patients after hip replacement;
- high power consumption is demanded due to their poor efficiency, which can be dangerous if human tissues are exposed to high levels of RF electromagnetic fields [71].

By using battery-based power systems:

- autonomy for long-term operation of implants is not ensured;
- the number of systems requiring electric power is fully related with the lifespan of batteries.

Table 1. Instrumented hip joint replacements – measurement features[†].

Features	Mann *et al.* [23–38]	Goodman *et al.* [39–41]	Bergmann *et al.* [11,48–66]	Davy *et al.* [43–47]	Puers *et al.* [42]
Measuring method	(1, 2, 3) Resistive (wheatstone bridges)	Resistive (wheatstone bridges)	(1, 2, 3) Resistive (wheatstone bridges)	(1, 2, 3) Resistive (wheatstone bridges)	Capacitive
Components of measurement systems	(1, 2) 14 pressure transducers[‡]; (3) 13 pressure transducers[‡]; temperature transducer (thermistor)	4 sets of strain gauges	(1) 3 strain gauges, temperature transducer (thermistor NTC); (2) 3 strain gauges, 9 NTC transducers; (3) 6 strain gauges; NTC transducer	(1, 2, 3, 4) 3 sets of strain gauges; (3, 4) temperature transducer (model: N/D)	Accelerometer
Locations of components	(1, 2, 3) Inside the hemisphere	Inside the neck	(1) Inside the neck; (2) strain gauges: inside the neck; NTCs: 2 inside the neck and 6 inside the stem; (3) inside the neck	(1, 2) in the cap; (3, 4) inside the neck	Inside a titanium container, in the head
Measured quantities	(1) 14 CSP; (2) 10 CSP; (3) 12 CSP; temperature inside the hemisphere	Mean axial load on the neck	(1) 3 spatial orthogonal forces on the neck; temperature in the neck; (2) 3 spatial orthogonal forces on the neck; 8 temperatures along neck and shaft; 2 temperatures in circuitry boards; rectified supply voltage; (3) 3 spatial orthogonal forces and 3 moments on the neck; temperature inside the neck; rectified supply voltage; synchronization signal	(1, 2, 3, 4) 3 spatial orthogonal forces on the neck; (3, 4) rectified supply voltage and temperature inside the neck	Head acceleration[§]
Transmitted quantities[¶]	All measured quantities were transmitted	The measured quantity was transmitted	All measured quantities were transmitted	All measured quantities were transmitted	The measured quantity was transmitted
Sampling period	(1, 2) 253 Hz; (3) 500 Hz	1 kHz	(1, 2) 250 Hz; (3) 120 Hz	(1, 2, 3, 4) N/D	4.2 kHz
Errors	(1, 2) Maximum offset error: 0.7 MPa; (3) maximum noise level: 0.2 MPa	Maximum calibration error: 7%; maximum accuracy error (load): 10%	(1) Maximum accuracy error (load): 3%; maximum accuracy error (temperature): 0.1°C; maximum calibration error (load): 1.5%; (2) maximum calibration error (load): 1%; maximum accuracy error (temperature): 0.1°C; (3) maximum calibration error (load): 1.9%; maximum calibration error (moments): 1.5%	(1, 2) N/D; (3, 4) maximum calibration error (load): 2.5%	N/D

[†]Terminology: (n) – implant of the nth generation.
[‡]They were designed as cantilever beams with strain gauges.
[§]They are used to monitor loosening by vibration analysis.
[¶]They were transmitted to signal acquisition systems outside the patients' body.
CSP: Cartilage surface pressures; N/D: Information not reported; NTC: Negative temperature coefficient.

Power needs have not been high because database storage, prediction algorithms and therapeutic actuation systems were not implemented inside implants. These approaches are suitable for research purposes focused on studying the dynamics of biomechanical quantities, and, in an extended scope, for research requiring data that can be monitored in a laboratory or in very limited extent during activities of daily living of patients.

Each power supply system was customized to power the respective instrumented implant. However, over the past decades, there were significant technological breakthroughs in monitoring, processing and communication systems composing such

Table 2. Instrumented hip joint replacements – communication features[†].

Features	Mann *et al.* [23–38]	Goodman *et al.* [39–41]	Bergmann *et al.* [11,48–66]	Davy *et al.* [43–47]	Puers *et al.* [42]
Method of communication	(1, 2, 3) Telemetric (radio transmission of inductive link): radio transmission of data from implants to a receiver	Telemetric: radio transmission of data from the implant to a receiver	(1, 3) Telemetric (radio transmission of inductive link): radio transmission of data from implants to a receiver. (2) Telemetric (radio transmission of inductive link): radio transmission of data from the implant to a twin receiver	(1, 2, 3, 4) Telemetric: radio transmission of data from implants to a receiver	Telemetric (radio transmission of inductive link): radio transmission of data from the implant to a receiver
Components of communication systems	(1, 2, 3) 16-channel 100 MHz PAM/FM transmitter; antenna (the secondary coil)	Single channel 102.3 MHz FM transmitter; antenna; antenna cable	(1) 4-channel 150 MHz RF transmitter; antenna; (2) 2× 8-channel 130–150 MHz PIM Coder transmitter; 2 antennas; (3) 9-channel 150 MHz PIM transmitter; antenna	(1, 2, 4) 76–90 MHz FM transmitter (number of channels: N/D); (3) 4-channel 76–90 MHz FM transmitter; (1, 2, 3, 4) antenna	10–11.5 MHz RF transmitter (number of channels: N/D); antenna
Locations of components	(1, 2, 3) Circuitry: inside the hemisphere; antenna: end of the stem	Outside the implant (inside the transmitter system housing)	(1) Circuitry: inside a metallic cylinder[‡] in the neck; antenna: inside the head; (2) circuitry: 1 transmitter inside a metallic cylinder in the neck, 1 transmitter inside a metallic cylinder in the shaft; 2 antennas: inside the head; (3) circuitry: inside a metallic cylinder in the neck; antenna: inside the head	(1, 2, 3, 4) Circuitry: inside the head, in the upper neck region	Inside a titanium container, in the head
Acquisition mode[§]	(1, 2, 3) During tests[¶]	During tests[¶]	(1, 2, 3) During tests[¶]	(1, 2, 3, 4) During tests[¶]	During tests[¶]
Resolution	(1, 2, 3) 16 bits	N/D	(1, 2, 3) 12 bits	(1, 2, 3, 4) N/D	8 bits

[†]Terminology: (n) – implant of the nth generation.
[‡]The metallic cylinder was designed in order to shield magnetically and mechanically the circuitry, as well as to improve power transfer between primary and secondary coils.
[§]Period between data monitoring operations.
[¶]Communication with implants was only carried out in the research laboratory.
FM: Frequency modulation; N/D: Information not reported; PAM: Pulse-amplitude modulation; PIM: Pulse interval modulation; RF: Radiofrequency.

implants, which imposed the development of more complex power supply systems. No published studies reporting comparisons between power supply systems for a given implant were found, thus one cannot conclude about their relative performance. Even so, Bergmann *et al.* implemented the most complex power systems. They also seem to be the most reliable and safe because they conducted the highest number of tests on implants before their implantation in human patients, according to literature. However, one must emphasize that inductive power links and/or batteries are not suitable for instrumented implants operating throughout the daily living of patients.

In vivo operation details

Implants designed by Mann *et al.* [23–38] operate when they are powered by an inductive link. Their first architecture was tested with six human acetabular components, taken directly from the autopsy room to a hip simulator. Their second architecture was implanted into a human patient, allowing *in vivo* data acquisition throughout 2 weeks [37], 1 year [28], 3 years [29] and 5 years [32,36,38] postoperatively. Their third architecture was also implanted into a human patient and the data acquisition was carried out throughout 1 year [32], 2.5 years [33,34] and 3 years [35] following THR.

Goodman *et al.* [39–41] implanted its instrumented English prosthesis into a human patient and, then, they acquired *in vivo* data throughout the first 40 days postoperatively. This architecture of instrumented implant can only operate while batteries provide energy and when switches enable supply.

Implants designed by Bergmann *et al.* [11,48–66] are able to operate if they are powered by inductive link. Four sheep and

Table 3. Instrumented hip joint replacements – supply features†.

Features	Mann *et al.* [23–38]	Goodman *et al.* [39–41]	Bergmann *et al.* [11,48–66]	Davy *et al.* [43–47]	Puers *et al.* [42]
Type of supply	(1, 2, 3) Electric energy	Electric energy	(1, 2, 3) Electric energy	(1, 2, 3, 4) Electric energy	Electric energy
Method for power supply	(1, 2, 3) Inductive powering, using a 100 kHz modulation	Powered by batteries	(1, 2, 3) Inductive powering using a 3–5 kHz modulator	(1, 2, 3, 4) Powered by a battery	Inductive powering, using a 750 kHz modulation
Components of supply systems inside the patient's body	(1, 2, 3) Coil on a ferrite core; regulation systems	3 batteries (1.35 V, mercury); 2 reed switches	(1, 2, 3) (Secondary) power coil; regulation systems	(1, 2) Battery; (3, 4) pacemaker-type battery (3.6 V lithium); (2, 3) magnetic reed switch; (4) momentary reed switch; (1, 2, 3, 4) regulation systems, power coil	(Secondary) power coil; regulation systems
Locations of components inside the patients' body	(1, 2, 3) Power induction link: end of the stem; circuitry: inside the hemisphere	Outside the implant (inside the transmitter system embedded around the implant)	(1) Power coil: top of the stem, inside a metallic cylinder; circuitry: in the neck, inside a metallic cylinder; (2) in the shaft, inside a metallic cylinder; (3) power coil: in the neck; circuitry: inside a metallic cylinder in the neck	(1, 2) Battery, circuitry: inside the head, in the upper neck region; (3, 4) battery: inside the neck; (1, 2) power coil: N/D; (3, 4) power coil: base of the prosthesis ball; (1, 2, 3, 4) circuitry: inside the head, in the upper neck region; (2, 3, 4) switch: inside the head, in the upper neck region	Power coil: inside the neck; circuitry: inside a titanium container, in the head
Components of supply systems outside the patients' body	(1, 2, 3) 100 kHz power oscillator; (primary or driver) coil (around the thigh)	Magnet (to latch reed switches)	(1) 4 kHz power oscillator; (primary) coil (around thigh); (2) 3.5–4.5 kHz power oscillator; (3) 3–5 kHz power oscillator; (2, 3) (primary) coil (around thigh); antenna, RF receiver and controllers	(1, 2, 3, 4) Magnet (to latch reed switches)	750 kHz power oscillator; (primary) coil (around thigh)
Power regulation circuitries	(1, 2, 3) Inside the implant: circuitry to regulate output voltage; outside the implant: N/D	Inside the implant: N/D; outside the implant: N/D	(1, 2, 3) Inside the implant: circuitry to regulate output voltage; (2, 3) outside the implant: control of oscillator frequency to compensate displacements of coils	(1, 2, 3, 4) Inside the implant: circuitry to regulate output voltage; outside the implant: N/D	Inside the implant: circuitry for power control; outside the implant: N/D
Power generation	(1, 2) 500 mW; (3) 30 mW	N/D	(1) 7 mW; (2) 10 mW; (3) N/D (5 mW for communication operations)	(1, 2, 3, 4) N/D	22.5 mW
Lifespan	(1, 2, 3) N/D	70 h	(1, 2, 3) N/D	(1, 2, 3, 4) N/D	N/D
Efficiency	(1, 2, 3) 10%	N/D	(1) 0.06%; (2) N/D; (3) between 0.03% and 0.09%	(1, 2, 3, 4) N/D	0.25%

†Terminology: (n) – implant of the nth generation.
N/D: Information not reported; RF: Radiofrequency.

three human patients underwent the implantation of the first architecture and acquisition of data took place over 11 months [61,62], 22 months [59], 30 months [55], 33 months [58], 58 months [63], 5 years [57] and 9 years [65] postoperatively. Their second architecture was implanted into four patients, which allowed *in vivo* monitoring over 11 months [61], 14 months [61], 22 months [63], 36 months [64] and 6 years [65] after THR. Their last architecture was implanted into 10 patients (see database OrthoLoad [69]) and data were monitored throughout 12 months postoperatively [66].

Hip prostheses designed by Davy *et al.* [43–47] require battery-based supply. Each of the last three architectures was implanted into a human patient. They monitored data *in vivo* up to 58 days postoperatively. Puers *et al.* [42] implanted their instrumented hip prosthesis into a human patient, but they have not reported how long it already operated *in vivo*.

Bergmann *et al.* [11,48–66] have acquired the largest amount of *in vivo* data (9 years of measurements). Although 24 patients underwent the implantation of instrumented hip joint replacements, no side effects were reported in literature.

Breakthroughs in instrumented hip joint implants have increased their complexity. Those developed by Bergmann *et al.* are the most complex implants ever implemented and tested *in vivo*. Their implants seem to be the most reliable, taken into account that: they operated successfully during the longest time period; they withstood the highest number of tests before their implantation in human patients; they were implanted in the highest number of patients without side effects and they presented the lowest measurement errors. However, no performance comparisons between instrumented hip joint implants have been found in literature. Instrumented hip joint implants were designed for different purposes. No studies reporting comparisons between relative performances of instrumented implants were published. Besides, each instrumented implant was not implanted in a number of patients that allows significant statistical analyses. By consequence, one cannot conclude about the best implant design.

Instrumented femoral replacements & fracture stabilizers

Overview

Only Taylor *et al.* [15,72–77] designed instrumentation for femoral replacements. They proposed two architectures for instrumented (proximal and distal) femoral replacements: [15,72,74,75] for the first generation (proximal); [15,73,76,77] for the second generation (distal). Two research groups have designed two architectures for femoral fixation implants: Brown *et al.* [44,78] developed an architecture for instrumented nail plate implants; Schneider *et al.* [79–81] designed an architecture for instrumented intramedullary nails.

These authors implemented HI architectures: their measurement, communication and electric power supply systems were housed in hollow regions machined inside implants.

Only Brown *et al.* [44,78] designed instrumentation for nail plates. They have designed an HI architecture to measure forces and moments in the nail plate junction. They modified nail plate implants as follows: the plate and nail were hollowed; the plate was machined with four screw holes and non-uniform hollow regions between screws; a cover was designed to enclose the hollowed plate sections; an heavier side plate was used and a hollowed square section was designed in the nail closest to the plate junction. They conducted fatigue, calibration, biocompatibility and signal attenuation tests on implants before their implantation in human patients. They were the first authors to: acquire *in vivo* data from an instrumented femoral fracture stabilizer; use miniaturized batteries inside instrumented implants and propose an instrumented femoral fracture stabilizer using activation systems.

Only Schneider *et al.* [79–81] proposed an HI architecture to instrument intramedullary nails. They modified an AO/ASIF universal femoral nail by sectioning lengthwise the curved tube and hollowing five circular cavities around the mid-diaphyseal cross-section. The distal end and the proximal end were designed to be removed, as well. They conducted fatigue tests on the instrumented nail. They acquired a large database of 3-axis orthogonal forces and moments acting *in vivo* in the mid-diaphyseal cross-section, providing valuable information for accurate estimations of long bone forces during healing processes.

Breakthroughs in instrumentation of femoral replacements were carried out by Taylor *et al.* [15,72–77]. First, they modified proximal femoral replacements (Stanmore bone tumor replacement prostheses): the main shaft and intramedullary stem were hollowed; a large cavity was machined into the proximal part of the main shaft; a smaller cavity was machined into the distal end of the stem; a stem tip assembly was designed to connect electrically to an encapsulated coil (located outside the implant's body), through a metal-in-glass feedthrough. The second generation was based on modifications to distal femoral replacements (Stanmore bone tumor replacement prostheses): the main shaft and intramedullary stem were hollowed; the proximal shaft encloses a cavity in order to embed electronic systems, as well as four flats to house sensors for force, torque and moment measurements; a cavity at the end of the intramedullary stem was also designed to house a force measurement system. Both generations are based on HI architectures. According to literature, the reliability of implants was achieved by performing fatigue, sealing, calibration and signal attenuation tests before implantation in human patients. They have applied the 'MATRIX' method, proposed by Bergmann *et al.* [67], in the design of both generations. The number and location of transducers, as well as the location of coils/antennas, differ among architectures. Their main goal has been the *in vivo* measurement of forces and moments throughout femoral replacements, and to assess progressive loosening of intramedullary stems postoperatively [74,77]. They were the first authors to implant instrumented femoral replacements and acquired *in vivo* data from such implants. They also developed the instrumented implant with the largest number of transducers.

Measurement features

Measurement features of instrumented femoral replacements and instrumented femoral fracture stabilizers are presented in Table 4. Stain gauges were used in all implants and, apart from the instrumented implant designed by Brown *et al.* [44,78], they were housed in several regions of implants. Loads and moments on implants were the main quantities under tracking. Rectified supply voltage was monitored by the implant designed by Schneider *et al.* [79–81], although no feedback control of external oscillator frequency was reported. The second architecture designed by Taylor *et al.* [15,73,76,77] housed 24 transducers inside instrumented implants. Schneider *et al.* [79–81] achieved accuracy errors lower than 0.1% and linearity errors up to 2.5%. Data acquisition was sampled up to 200 Hz.

Instrumented femoral replacements and instrumented femoral fixation implants have been designed to measure biomechanical quantities *in vivo*. The implants' physiological environment has not been monitored. Data storage inside implants has not been reported. Data monitored *in vivo* was not post-processed in order to model characteristics of implants' failures.

Communication features

Table 5 introduces a comparative analysis between the communication features of implants. All instrumented implants comprise RF transmitters. Both circuitry and antennas were housed in several regions of implants. The induction coils for both generations proposed by Taylor *et al.* [15,72–75] were housed outside the implants, supported by the tip of the modified stem (first generation) and by the main shaft (second generation). All measured quantities have been transmitted to instrumentation located outside the patients' body: the main goal has been to use these *in vivo* data to optimize the design and testing of femoral replacements and total knee replacements [82]. Data acquisition was only conducted in research laboratories, following the same communication method implemented for instrumented hip joint replacements.

Table 4. Instrumented femoral replacements and instrumented fracture stabilizers – measurement features†.

Features	Brown *et al.* [44,78]	Schneider *et al.* [79–81]	Taylor *et al.* [15,72–77]
Implant type	Nail plate implant (model: N/D)	Intramedullary femoral nail (AO/ASIF universal nail)	(1) Proximal femoral replacement (Stanmore bone tumor replacement prosthesis); (2) Distal femoral replacement (Stanmore bone tumor replacement prosthesis)
Measuring method	Resistive (wheatstone bridges)	Resistive (wheatstone bridges)	(1, 2) Resistive (wheatstone bridges)
Components of measurement systems	Strain gauges (quantity: N/D)	5 strain gauges; temperature transducer (model: N/D); data conversion circuitry	(1) 8 strain gauges (2 full bridges); (2) 24 strain gauges (5 full bridges)
Locations of components	Inside the nail, close to junction of the plate	Strain gauges: in the mid-diaphyseal cross-section and 15 mm apart from the mid-diaphyseal cross-section; temperature transducer: N/D; circuitry: in a cavity at intermediate location between the proximal end and the mid-diaphyseal cross-section, and in a cavity at the intermediate location between the distal end and the mid-diaphyseal cross-section	(1) Cavities in the main shaft and above the tip of the intramedullary stem; (2) 20 strain gauges in the shaft cavity and 4 strain gauges in the stem tip cavity
Measured quantities	Two orthogonal bending moments in nail plate junction	Three orthogonal forces and three moments acting in mid-diaphyseal cross-section; temperature and rectified supply voltage	(1) Axial force over the prosthesis shaft and stem tip; (2) axial force, axial torque and orthogonal bending moments over the shaft, and axial force over the stem tip
Sampling period	N/D	0.375 Hz	(1) 200 Hz; (2) 100 Hz
Errors	N/D	Maximum accuracy error (load): 0.1%; maximum linearity error: 2.5% for axial loads, 0.25% for bending loads and 0.6% for torsion loads	(1,2) Maximum accuracy error (load): 10 N; Maximum accuracy error (torque): 0.1 Nm

†Terminology: (n) – implant of the nth generation.
N/D: Information not reported.

Table 5. Instrumented femoral replacements and instrumented fracture stabilizers – communication features[†].

Features	Brown *et al.* [44,78]	Schneider *et al.* [79–81]	Taylor *et al.* [15,72–77]
Implant type	Nail plate implant (model: N/D)	Intramedullary femoral nail (AO/ASIF universal nail)	(1) Proximal femoral replacement (Stanmore bone tumor replacement prosthesis); (2) Distal femoral replacement (Stanmore bone tumor replacement prosthesis)
Method of communication	Telemetric: radio transmission of data from the implant to a receiver	Telemetric (radio transmission of inductive link): radio transmission of data from the implant to a receiver	(1, 2) Telemetric (impedance modulation of inductive link): radio transmission of data from subject to base station
Components of communication system	2-channel 88–108 MHz AM/FM transmitter; antenna	8-channel 100 kHz Pulse code modulation transmission system; antenna	(1, 2) Single channel 418 MHz UHF transceiver
Locations of components	Inside the plate	In a cavity at intermediate location between the proximal end and the mid-diaphyseal cross-section, near data conversion circuitries	(1, 2) Circuitry: cavity in the main shaft; induction coil: outside the implant (beneath the intramedullary stem), encapsulated to the end-cap by silicone rubber
Transmitted quantities	Two orthogonal bending moments in nail plate junction	Three orthogonal forces and three moments acting in mid-diaphyseal cross-section; temperature and rectified supply voltage.	(1) Axial force over the prosthesis shaft and stem tip; (2) axial force, axial torque and orthogonal bending moments over the shaft, and axial force over the stem tip
Period	During tests[‡]	During tests[‡,§]	(1, 2) During tests[‡]
Resolution	N/D	14 bits	(1, 2) Analog PWM

[†]Terminology: (n) – implant of the nth generation.
[‡]Communication with implants was only performed in the research laboratory.
[§]Only 10 ms in every 333 ms were used for transmission of data.
AM: Amplitude modulation; FM: Frequency modulation; N/D: Information not reported; PWM: Pulse width modulation; UHF: Ultra high frequency.

Therapeutic features

No instrumentation for femoral replacements and femoral fixation implants was designed in order to implement therapeutic actuation. Research on the optimization of femoral implants is being carried out [82], but no actuation mechanisms were embedded in the structure of these instrumented implants, in order to prevent failures in real-time. Their current operations do not take into account previous data monitored *in vivo* as well.

Supply features

Table 6 presents a comparative basis between the supply features designed for instrumented femoral implants and instrumented femoral fracture stabilizers. These implants only require electric energy to operate: they were not designed to use other resources, such as chemicals. The authors used induction-based and battery-based supply systems to power implants. Induction-based supply systems comprise circuitry outside the patients' body: primary coils and/or antennas and power oscillators were required by all architectures. Schneider *et al.* [79–81] and Taylor *et al.* [15,72–77] housed secondary power coils and conditioning systems inside the implants, but both generations proposed by Taylor *et al.* [15,72–75] positioned the secondary coils outside (beneath the stem tip and around the main shaft). Power regulation circuitries were housed in several regions of implants. The battery-based power system, designed by Brown *et al.* [44,78], requires a switch operation to enable power (a magnet, outside the patients' body, must enable/disable the activation circuitry, inside the patients' body). No circuitry to maximize the energy available inside the implants' structure was reported. The minimization of power consumption was not reported.

These power supply systems were customized to power measurement and communication systems and were selected according to desired autonomy and available space. The drawbacks of using inductive-based power supply or battery-based power supply are the same as those reported for instrumented hip joint replacements. These power supply methods can be used also in research focused on monitoring of biomechanical or biochemical quantities possible to be acquired *in vivo* by instrumented implants.

In vivo operation details

Instrumented nail plate implants proposed by Brown *et al.* [44,78] operate if batteries have sufficient energy and the activation

Table 6. Instrumented femoral replacements and instrumented fracture stabilizers – power supply features†.

Features	Brown *et al.* [44,78]	Schneider *et al.* [79–81]	Taylor *et al.* [15,72–77]
Implant type	Nail plate implant (model: N/D)	Intramedullary femoral nail (AO/ASIF universal nail)	(1) Proximal femoral replacement (Stanmore bone tumour replacement prosthesis); (2) Distal femoral replacement (Stanmore bone tumour replacement prosthesis)
Type of supply	Electric energy	Electric energy	(1, 2) Electric energy
Method for power supply	Powered by batteries	Inductive powering, using a 2 kHz modulator	(1, 2) Inductive powering, using a modulator externally located
Components of supply systems inside the patients' body	Set of batteries (1.35 V, mercury) (quantity: N/D); magnetic reed switch	Power coil; regulation systems	(1, 2) Coil and ferrite core; regulation systems
Locations of components inside the patients' body	Batteries: inside the nail; switch: inside the plate	In a cavity at the intermediate location between the distal end and the mid-diaphyseal cross-section	(1) Coil and ferrite: outside the implant; (1, 2) circuitry: midshaft cavity; (2) coil and ferrite: distal portion in the shaft
Components of supply systems outside the patients' body	Magnet (to latch the reed switches)	(1) 2 kHz power oscillator; (primary) coil (around thigh)	(1, 2) (Primary) coil, power oscillator (frequency: 1.2 MHz) and battery (coil around thigh)
Power regulation circuitries	Inside the implant: N/D; outside the implant: N/D	Inside the implant: circuitry to regulate output voltage; outside the implant: N/D	(1, 2) Inside the implant: circuitry to regulate output DC voltage; outside the implant: linear regulator
Power generation	N/D	100 mW	(1) 151 mW (8 mA); (2) N/D (6 mA)
Lifespan	N/D	N/D	(1) Over 3 years; (2) over 2 years
Efficiency	N/D	N/D	(1) 10%; (2) 13%

†Terminology: (n) – implant of the nth generation.
N/D: Information not reported.

system is switched on. They performed *in vivo* data acquisition throughout postoperative and convalescent recovery of three human patients.

The architecture for instrumented intramedullary nails, proposed by Schneider *et al.* [79–81], operates when it is powered by an inductive power link. They implanted this instrumented implant into a patient and performed data acquisition *in vivo* throughout 6 months postoperatively.

All architectures developed by Taylor *et al.* [15,72–77] require inductive powering in order to operate. Instrumented proximal femoral replacements, based on the first architecture, were implanted into two patients, which allowed the acquisition of *in vivo* data up to 3 years postoperatively [15]. Instrumented distal femoral replacements, based on the second architecture, were implanted into two patients and data from each patient was recorded over 2 years before revision was required [76,77].

No side effects on patients were reported in literature about the operation of instrumented femoral implants and instrumented fracture stabilizers.

Expert commentary

The newest architecture for instrumented hip joint implants was proposed by Bergmann *et al.* [83,84]. It is able to measure implant temperatures *in vivo* required to study the risk of thermally induced bone necrosis (Figure 1). The newest instrumented intramedullary nail was developed by Faroug *et al.* [85]. By modifying a TriGen® META Nail (Smith & Nephew®), they embedded a strain measurement system into each of eight cavities that they machined onto the surface of the nail. They demonstrated *in vitro* that such instrumented nail is able to predict fracture healing. Currently, they are working toward implementation of a device for *in vivo* operation.

Instrumented implants analyzed in this review have been designed mainly to measure biomechanical and thermodynamic quantities, that is, besides their main function in the articulation motion, these implants were designed as transducers. The first concepts of instrumented hip joint replacement, instrumented femoral replacement and instrumented femoral fracture stabilizer (Figure 2) defined these implants as medical devices composed by:

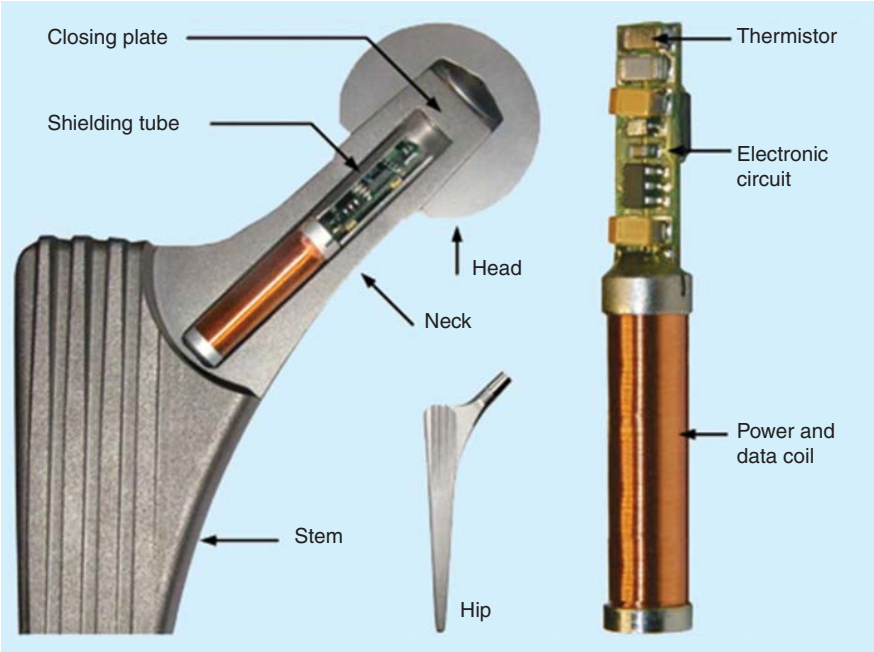

Figure 1. Cross-section of instrumented hip endoprostheses for temperature measurements *in vivo*.
Reproduced with permission from Bergmann *et al.* [83].

- Resource acquisition systems;
- Measurement systems, to monitor the states of implants and physiological states of tissues around implants;
- Processing systems, to model physiological states of tissues surrounding the implants' *in situ* structure, as well as to model failures' characteristics of implants;
- Communication systems between electronic circuitries inside and outside human body.

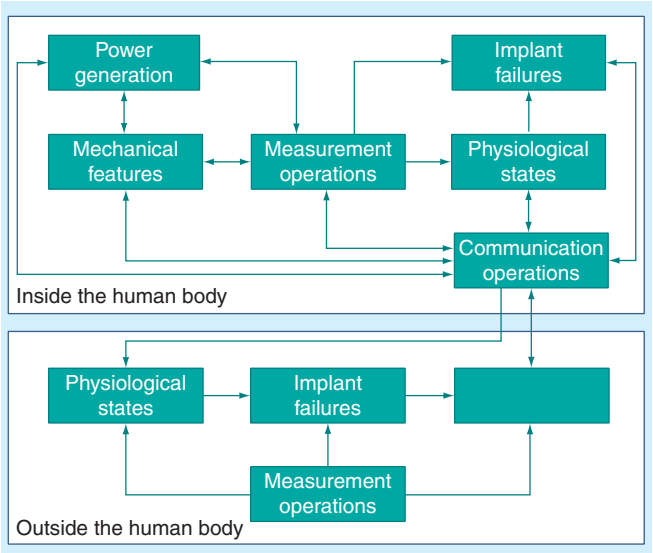

Figure 2. General architecture of instrumented non-active implants.
Empty square means 'no operation'.

Following this first concept, new telemetric systems were developed for *in vivo* monitoring: Marschner *et al.* [86] designed a new telemetric system for instrumented hip prostheses similar to the one proposed by Puers *et al.* [42]; Valdastri *et al.* [87] proposed a ZigBee wireless technology to design telemetric systems. Research on novel transducers for measuring biomechanical quantities has also been conducted: Cristofolini *et al.* [88] developed a piezoelectric transducer to measure forces in the cement–implant interface; Gattiker *et al.* [89] developed a sensing system for measurement of loads on hip implants, by transducing load into a varying amount of fluid in a channel housed inside transducer. Although these achievements are quite significant, no implants have been proposed as instruments to: validate biochemical models of tissues surrounding implants; identify the interaction between biochemical properties of tissues and biomechanical properties of implants; characterize failures; transfer the diagnose of failures, as well as the states of tissues surrounding implants, to/from implants (these data can be acquired by laboratory analyses, and then they can be sent to implants; or they can be acquired by measurement systems housed inside implants, and then they can be sent to processing units outside the human body).

Breakthroughs in real-time characterization of aseptic loosening and infection are relevant to increase the lifetime of implants. Alpuim *et al.* [90] designed a thin-film strain sensor, based on piezoresistive doped nanocrystalline silicon, for aseptic loosening detection on prosthetic stem and cup. They used relative motions in bone–implant interface as the characterizing feature. However, this sensor must be optimized to ensure accurate characterization of this type of failure along critical regions. Hao *et al.* [91] proposed real-time prediction of aseptic loosening through *in vivo* evaluation of the implant stability (migration and micromotion measurement). They developed a differential variable reluctance transducer for that purpose, but it has the limitation of not being appropriate for accurate identification of regions where aseptic loosening occurs. Recently, Ruther *et al.* [92] demonstrated the potential of acoustic sound analyses to monitor osseointegration of different orthopedic implant surfaces *in vivo*.

New methods to harvest electric energy *in vivo* inside instrumented implants have been published (Figure 3): Morais *et al.* [93–95], Silva *et al.* [95,96], Morgado *et al.* [97] and Soares dos Santos *et al.* [98–100] designed motion-driven electromagnetic energy harvesting systems; Silva *et al.* [95,96], Soares dos Santos *et al.* [98–100] and Platt *et al.* [101] proposed piezoelectric energy harvesting systems. New conditioning interface

circuitries have also been developed: Le *et al.* [102] designed CMOS circuitry to interface with piezoelectric energy harvesting systems and Silva *et al.* [95,96] designed power management architectures for instrumented hip prostheses powered by multiple energy harvesters.

Novel energy storage systems were recently proposed by Silva *et al.* [96] to maximize the amount of available energy harvested *in vivo*: they developed a storage circuitry based on supercapacitors to avoid using energy reservoirs based on batteries. New telemetric systems were already tested by Morais *et al.* [94,103] and Silva *et al.* [96] for instrumented hip prostheses powered by electromagnetic energy harvesting systems.

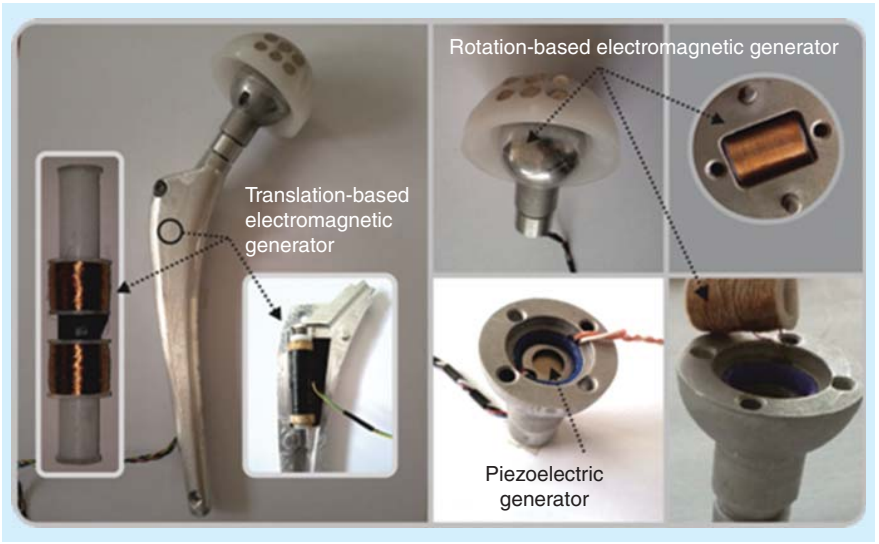

Figure 3. Hip prosthesis prototype, comprising three energy harvesting systems. Reproduced with permission from Silva *et al.* [96].

The most significant recent advance is the concept of instrumented active implant (Figure 4). Resource acquisition, measurement, communication and processing systems are also required in the design of active implants. However, they must also provide actuation with ability to implement clinical therapies in real-time. Instrumented hip joint replacements, instrumented femoral replacements and instrumented femoral fracture stabilizers can be designed as active implants. They can evolve toward the minimization of failures in real-time by using:

- Actuators as an integral part of the implant, in order to apply therapeutic stimuli in bone–implant interface;
- Therapeutic command generators, in order to control actuators embedded into instrumented implants.

Instrumented active implants can be configured according to non-autonomous or autonomous architectures. In non-autonomous architectures, an extracorporal master-based active structure must be able to generate therapeutic commands, and an intracorporal slave-based active structure must be able to execute such commands. In autonomous architectures, both master-based active structure and slave-based active structure must be able to generate therapeutic commands, although generation of commands by the slave-based active structure must be carried out under supervision of the master-based active structure. Figures 5 & 6 illustrate the main structural differences among instrumented active and non-active implants. A promising advance would be the development of implants with ability to prevent aseptic loosening and/or infections: if they occur, then instrumented active implants must characterize them and perform controlled therapeutic actuations. They must be smart implants to ensure customization and optimization of their performance throughout their lifetime. Reis *et al.* [104] and Frias *et al.* [105,106] used piezoelectric-based mechanical stimulation to control bone formation surrounding hip implants. They support their research on previous studies

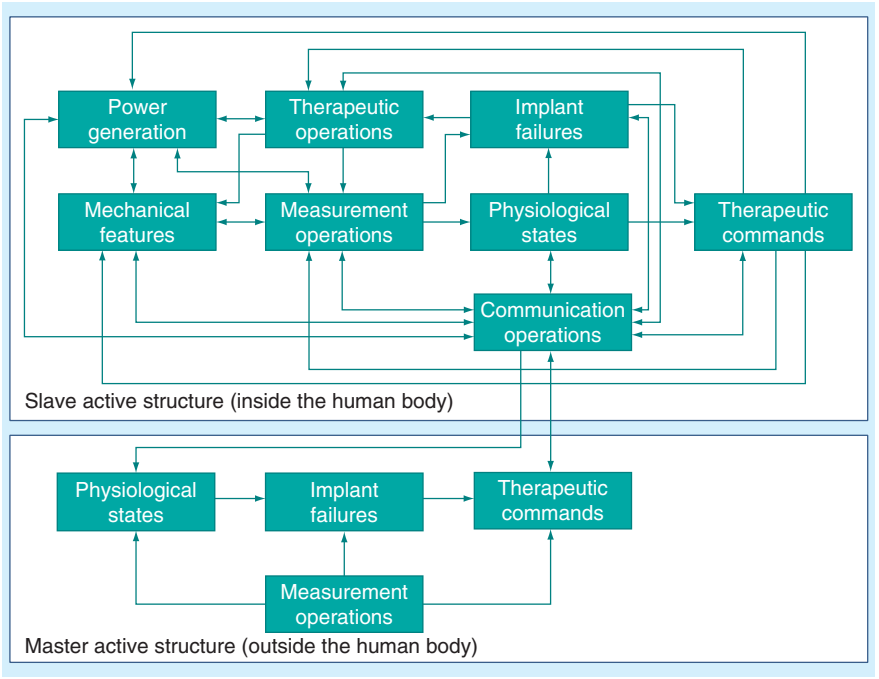

Figure 4. General architecture of instrumented active hip implants.

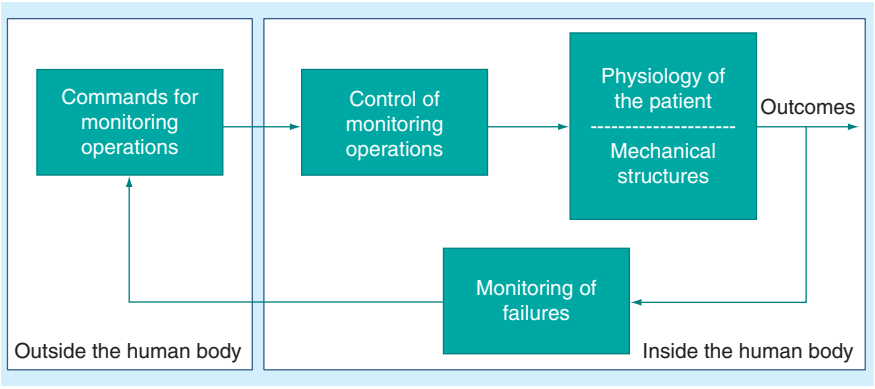

Figure 5. Structure and functions of instrumented non-active implants.

about effects of mechanical stimulation on bone cells [107,108]. Bone cell proliferation and differentiation can also be achieved by electrical stimulation [109,110]. These two actuation methods could be applied to design instrumented active implants comprising a network of mechanical and/or electrical stimulators of bone cells along the critical regions where aseptic loosening occurs. Soares dos Santos *et al.* [100,111] proposed such an architecture for instrumented hip implants. Another appropriate basis for research of new therapeutic actuations is the study published by Prescott *et al.* [112]. They designed a microchip device comprising hundreds of arrays of discrete reservoirs, which is able to control the release of therapeutic drug doses over several months in biological environments. This achievement can be used to design instrumented active implants with ability to implement controlled biological therapies, such as antimicrobial therapies and suppressive antibiotic therapies.

Instrumented active implants require powerful and miniaturized processing capability. In this scope, novel miniaturized CMOS System-on-Chip architectures for orthopedic implants were recently proposed by Zhao *et al.* [113]. Additionally, the telemetric system, proposed by Weiss *et al.* [114], is also noteworthy because it maximizes the RF coupling, which in turn can be used to reduce size and complexity of communication systems.

Five-year view

Instrumented implants are promising devices for advanced therapies toward minimization of revision rates. Optimality analyses of architectures and configurations of instrumented active and non-active implants would allow to define the ability of each implant to prevent failures in real-time. The controllability of implants when aseptic loosening and infection occur is expected to be analyzed. Taking into account the breakthroughs in circuit design for miniaturized and high-performance electronic systems, as well as the progress in intelligent actuation and sensing systems, the design of active implants may become achievable.

Additional methods for loosening detection may be explored in the coming years, such as measurement *in vivo* of failure-specific molecular markers surrounding implants (e.g., nitric oxide synthase [115] and peroxynitrite [116]). In addition to the need of electric energy, other resources will have to be stored inside implants, such as chemicals for biosensing [117]. Some research projects are predicted to be focused on the accurate characterization of aseptic loosening and/or infection in real-time, namely on the design of miniaturized sensors and networks of sensors around critical regions where these causes of failure occur.

Energy harvesting systems are maintenance-free and harvest electric power without the need of interaction with the bone–implant interface. It is noteworthy that power generation naturally accompanies the active lives of patients besides these advantages, one must emphasize their ease of implementation and low cost. To date, translational-based

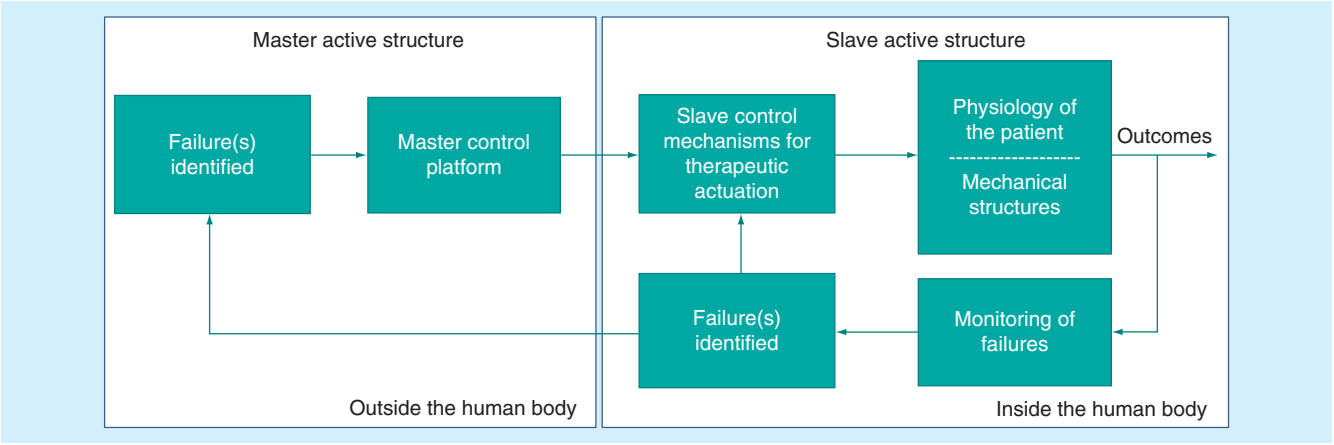

Figure 6. Structure and functions of instrumented active implants.

electromagnetic harvesters (designed to power instrumented hip implants) were only configured as mass-spring-damper systems [94,99] and magnetic levitation systems [96]. Other configurations may be studied. Further research may include the optimization of energy harvesters according to the gait patterns of patients during their routine activities. For this purpose, following efforts will probably concentrate on the development and validation of non-linear models, which can be used to accurately predict electric power harvesting. According to the maximum power harvested *in vivo* by each configuration, a specific energy harvester can be design for each instrumented implant, either for active or non-active implants.

In coming years, actuation systems for stimulation of bone growth around implants, by enhancing the proliferation and differentiation of bone cells, may be studied. One can expect proposals of new electrical stimulation systems, since current electrical stimulation apparatus [109,110] are not appropriate for *in vivo* actuation. Finally, further steps may be taken toward identification of suitable stimuli for each aseptic loosening characterization.

Acknowledgements

The authors would like to thank the Portuguese Foundation for Science and Technology (FCT) for their financial support under the grants PTDC/EME-PME/105465/2008 and SFRH/BD/78414/2011. The permission for reproduction of Figure 3 by Elsevier is appreciated. Finally, the authors would also like to thank the peer reviewers and R Pascoal for their useful suggestions and constructive remarks.

Financial & competing interests disclosure

The authors have no relevant affiliations or financial involvement with any organization or entity with a financial interest in or financial conflict with the subject matter or materials discussed in the manuscript. This includes employment, consultancies, honoraria, stock ownership or options, expert testimony, grants or patents received or pending or royalties.

No writing assistance was utilized in the production of this manuscript.

Key issues

- Although considerable research efforts have been conducted to optimize the design and materials of hip implants, revision rates are about 6% after 5 years and 12% after 10 years following THR. The number of primary THR at younger ages (less than 65 years old) is increasing. The use of uncemented primary and revision THR is also increasing. Aseptic loosening has been the most important reason for hip revision. An increased risk of revision due to infection after THR has been verified in the last years.
- Instrumented hip joint replacements, instrumented femoral replacements and instrumented femoral fracture stabilizers were proposed for research purposes focused on studying the dynamics of biomechanical and thermodynamic quantities when such implants operate *in vivo*. They have been designed to: collect data (mainly forces, moments and temperatures) for calibration of models defining the implants' biomechanical and thermal environment; optimize the mechanical design and materials' behavior of implants; carry out preclinical testing; track the healing evolution and improve the rehabilitation processes after arthroplasty.
- Twelve architectures for instrumented hip joint replacements, without percutaneous wired connections, were implanted into 24 human patients. Two architectures for instrumented femoral replacements were implanted into four human patients. Two architectures for instrumented femoral fixation implants were implanted into four human patients.
- More than 9 years of successful operation was achieved by instrumented hip joint replacements. Up to 9 years of data were acquired *in vivo* from these implants. No side effects were reported.
- All instrumented implants were designed with measurement, communication and electric power supply systems. However, no therapeutic actuation systems were embedded in the structure of these instrumented implants in order to maximize their ability to overcome failures in real-time.
- Instrumented implants are being developed as medical devices for advanced therapies toward the minimization of revision rates.
- The most promising trend in this field is focused on the design of instrumented active implants to prevent aseptic loosening and/or infection: implants comprising therapeutic actuation systems with ability to induce trajectories from each state of loosening/infection to states of without-loosening/infection.
- Optimization of electric power supply systems must be conducted toward self-powering. Energy harvesting systems are noteworthy in this scope.
- Measurement systems must be developed toward the characterization of the implants' biomechanical environment, as well as the design of a network of sensors around critical regions where loosening and infection occur.
- Design of electrical and mechanical stimulation systems for instrumented implants may effectively induce and control bone growth in regions where aseptic loosening occurs.

References

Papers of special note have been highlighted as:
• of interest
•• of considerable interest

1. Rolfson O, Kärrholm J, Dahlberg LE, Garellick G. Patient-reported outcomes. in the Swedish hip arthroplasty register: results of a nationwide prospective observational study. J Bone Joint Surg Br 2011;93-B(7): 867-87
2. Bergen H. Report June 2010. The Norwegian arthroplasty register. 2010
3. Garellick G, Karrholm J, Rogmark C, et al. Annual report 2011. Swedish Hip Arthroplasty Register. 2011
4. Porter M, Borroff M, Gregg P, et al. 10th annual report 2013. National Joint Registry for England, Wales and Northern Ireland. 2013
5. Kurtz S, Ong K, Lau E, et al. Projections of primary and revision hip and knee arthroplasty in the United States from 2005 to 2030. J Bone Joint Surg 2007; 89(4):780-5
6. Paxton EW, Namba RS, Maletis GB, et al. A prospective study of 80,000 total joint and 5000 anterior cruciate ligament reconstruction procedures in a community-based registry in the united states. J Bone Joint Surg 2010;92(2):117-32
7. Labek G, Thaler M, Janda W, et al. Revision rates after total joint replacement – cumulative results from worldwide joint register datasets. J Bone Joint Surg 2011; 93-B(3):293-7
8. Ong KL, Lau E, Suggs J, et al. Risk of subsequent revision after primary and revision total joint arthroplasty. Clin Orthop Relat R 2010;468(11):3070-6
9. Philpott A, Weston-Simons JS, Grammatopoulos G, et al. Predictive outcomes of revision total hip replacement – a consecutive series of 1176 patients with a minimum 10-year follow-up. Maturitas 2014;77(2):185-90
10. Kurtz SM, Lau E, Ong K, et al. Future young patient demand for primary and revision joint replacement – national projections from 2010 to 2030. Clin Orthop Relat R 2009;467(10):2606-12
11. Bozic KJ, Lau E, Ong K, et al. Risk factors for early revision after primary total hip arthroplasty in Medicare patients. Clin Orthop Relat R 2014;472(2):449-54
12. Schrama J, Espehaug B, Hallan G, et al. Risk of revision for infection in primary total hip and knee arthroplasty in patients with rheumatoid arthritis compared with osteoarthritis: A prospective, population-based study on 108,786 hip and knee joint arthroplasties from the Norwegian arthroplasty register. Arthritis Care Res 2010;62(4):473-9
13. Bozic KJ, Ong K, Lau E, et al. Estimating risk in medicare patients with THA – an electronic risk calculator for periprosthetic joint infection and mortality. Clin Orthop Relat R 2013;471(2):574-83
14. Rydell NW. Forces acting in the femoral head-prosthesis. A study on strain gauge supplied prostheses in living persons. Acta Orthop Scand 1966;37(Suppl 88):1-132
15. Heller MO, Bergmann G, Kassi JP, et al. Determination of muscle loading at the hip joint for use in pre-clinical testing. J Biomech 2005;38(5):1155-63
16. Heller MO, Bergmann G, Deuretzbacher G, et al. Musculo-skeletal loading conditions at the hip during walking and stair climbing. J Biomech 2001;34(7):883-93
17. Burny F, Donkerwolcke M, Moulart F, et al. Concept, design and fabrication of smart orthopedic implants. Med Eng Phys 2000;22(7):469-79
18. Ledet EH, D'Lima D, Westerhoff P, et al. Implantable sensor technology: from research to clinical practice. J Am Acad Orthop Sur 2012;20(6):383-92
19. Yoshida H, Faust A, Wilckens J, et al. Three-dimensional dynamic hip contact area and pressure distribution during activities of daily living. J Biomech 2006;39(11): 1996-2004
20. Shah AD, Taylor SJ, Hua J. Correlation of radiographic and telemetric data from massive implant fixations. J Biomech 2006; 39(7):1304-14
21. Rubash HE, Sinha RK, Shanbhag AS, Kim S. Pathogenesis of bone loss after total hip arthroplasty. Orthop Clin North Am 1998;29(2):173-86
22. Parvizi J, Mortazavi SJ. Massive femoral bone loss: solutions of last resort. Semin Arthroplasty 2010;21(1):51-6
23. Carlson CE. A proposed method for measuring pressures on the human hip joint. Exp Mech 1971;11(11):499-506
24. Carlson CE, Mann RW, Harris WH. A look at the prosthesis-cartilage interface: design of a hip prosthesis containing pressure transducers. J Biomed Mater Res 1974;8(4):261-9
25. Carlson CE, Mann RW, Harris WH. A radio telemetry device for monitoring cartilage surface pressures in the human hip. IEEE Trans Bio-med Eng 1974;21(4): 257-64
26. Rushfeldt PD, Mann RW, Harris WH. Influence of cartilage geometry on the pressure distribution in the human hip joint. Science 1979;204(4391):413-15
27. Rushfeldt PD, Mann RW, Harris WH. Improved techniques for measuring in vitro the geometry and pressure distribution in the human acetabulum – II. Instrumented endoprosthesis measurement of articular surface pressure distribution. J Biomech 1981;14(5):315-23
28. Hodge WA, Fijan RS, Carlson KL, et al. Contact pressures in the human hip joint measured in vivo. Proc Natl Acad Sci USA 1986;83(9):2879-83
29. Hodge WA, Carlson KL, Fijan RS, et al. Contact pressures from an instrumented hip endoprosthesis. J Bone Joint Surg 1989; 71(9):1378-86
30. Mann RW, Burgess RG. A instrumented prosthesis for measuring pressure on acetabular cartilage in vivo. In: Bergmann G, Graichen F, Rohlmann A, editors. Implantable telemetry in orthopaedics. Freie Universität; Berlin, Germany: 1990. p. 65-75
31. Mann RW, Hodge WA. In vivo pressures on acetabular cartilage following endoprosthesis surgery, during recovery and rehabilitation, and in the activities of daily living. In: Bergmann G, Graichen F, Rohlmann A, editors. Implantable telemetry in orthopaedics. Freie Universität; Berlin, Germany: 1990. p. 181-204
32. Carlson KL. Human hip joint mechanics – an investigation into the effects of femoral head endoprosthetic replacements using in vivo and in vitro pressure data. Ph.D. thesis. Massachusetts Institute of Technology; London, UK: 1993
33. Tackson SJ, Krebs DE, Harris BA. Acetabular pressures during hip arthritis exercises. Arthritis Care Res 1997;10(5): 308-19
34. McGibbon CA, Krebs DE, Mann RW. In vivo hip pressures during cane and load-carrying gait. Arthritis Care Res 1997; 10(5):300-7
35. McGibbon CA, Krebs DE, Trahan CA, et al. Cartilage degeneration in relation to repetitive pressure – case study of a unilateral hip hemiarthroplasty patient. J Arthroplasty 1999;14(1):52-8
36. Krebs DE, Elbaum L, Riley PO, et al. Exercise and gait effects on in vivo hip contact pressures. Phys Ther 1991;71(4): 301-9
37. Strickland EM, Fares M, Krebs DE, et al. In vivo acetabular contact pressures during

rehabilitation, part I: acute phase. Phys Ther 1992;72(10):691-9

38. Givens-Heiss DL, Krebs DE, Riley PO, et al. In vivo acetabular contact pressures during rehabilitation, part II: postacute phase. Phys Ther 1992;72(10):700-5

39. Goodman RM, English TA, Kilvington M. An implantable FM telemetry system for measuring forces on prosthetic hip joints. In: Amlaner CJ Jr, Macdonald DW, editors. A handbook on biotelemetry and radio tracking. Pergamon Press; Oxford, UK: 1979. p. 297-306

40. English TA, Kilvington M. In vivo records of hip loads using a femoral implant with telemetric output (a preliminary report). J Biomed Eng 1979;1(2):111-15

41. Kilvington M, Goodman RM. In vivo hip joint forces recorded on a strain gauged 'English' prosthesis using an implanted transmitter. Eng Med 1981;10(4):175-87

42. Puers R, Catrysse M, Vandevoorde G, et al. A telemetry system for the detection of hip prosthesis loosening by vibration analysis. Sensor. Actuat A Phys 2000;85(1-3):42-7

• **First architecture of instrumented hip implants for failure detection. In this study, the first attempt to monitor prosthesis loosening was carried out.**

43. Davy DT, Kotzar GM, Brown RH, et al. Telemetric force measurements across the hip after total arthroplasty. J Bone Joint Surg 1988;70(1):45-50

44. Davy DT, Kotzar GM, Berilla J, Brown RH. Telemeterized orthopaedic implant work at case Western Reserve University. In: Bergmann G, Graichen F, Rohlmann A, editors. Implantable telemetry in orthopaedics. Freie Universität; Berlin, Germany: 1990. p. 205-19

45. Kotzar GM, Davy DT, Goldberg VM, et al. Telemeterized in vivo hip joint force data: a report on two patients after total hip surgery. J Orthop Res 1991;9(5):621-33

46. Brand RA, Pedersen DR, Davy DT, et al. Comparison of hip force calculations and measurements in the same patient. J Arthroplasty 1994;9(1):45-51

47. Kotzar GM, Davy DT, Berilla J, Goldberg VM. Torsional loads in the early postoperative period following total hip replacement. J Orthop Res 1995;13(6): 945-55

48. Bergmann G, Graichen F, Siraky J, et al. Multichannel strain gauge telemetry for orthopaedic implants. J Biomech 1988; 21(2):169-76

49. Graichen F, Bergmann G. Four-channel telemetry system for in vivo measurement of hip joint forces. J Biomed Eng 1991;13(5): 370-4

50. Bergmann G, Graichen F, Rohlmann A. Instrumentation of a hip joint prosthesis. In: Bergmann G, Graichen F, Rohlmann A, editors. Implantable telemetry in orthopaedics. Freie Universität; Berlin: 1990. p. 35-63

51. Graichen F, Bergmann G, Rohlmann A. Dual 8 channel telemetry system for in vivo load measurements with two instrumented implants. In: Bergmann G, Graichen F, Rohlmann A, editors. Implantable telemetry in orthopaedics. Freie Universität; Berlin, Germany: 1990. p. 153-62

52. Graichen F, Bergmann G, Rohlmann A. Hip endoprosthesis for in vivo measurement of joint force and temperature. J Biomech 1999;32(10):1113-17

•• **First instrumented hip implant with ability to measure biomechanical and thermal quantities along its entire length.**

53. Graichen F, Arnold R, Rohlmann A, Bergmann G. Implantable 9-channel telemetry system for in vivo load measurements with orthopedic implants. IEEE Trans Bio-med Eng 2007;54(2): 253-61

54. Damm P, Graichen F, Rohlmann A, et al. Total hip joint prosthesis for in vivo measurement of forces and moments. Med Eng Phys 2010;32(1):95-100

•• **The latest instrumented hip prosthesis implanted *in vivo*. It was developed to measure 3D forces and moments acting between head and cup.**

55. Bergmann G, Graichen F, Rohlmann A. Hip joint loading during walking and running, measured in two patients. J Biomech 1993;26(8):969-90

56. Bergmann G, Correa da Silva M, Neff G, et al. Evaluation of ischial weight-bearing orthoses, based on in-vivo joint force measurements. Clin Biomech 1994;9(4): 225-34

57. Bergmann G, Kniggendorf H, Graichen F, Rohlmann A. Influence of shoes and heel strike on the loading of the hip joint. J Biomech 1995;28(7):817-27

58. Bergmann G, Graichen F, Rohlmann A. Is staircase walking a risk for the fixation of hip implants. J Biomech 1995;28(5):535-53

59. Bergmann G, Graichen F, Rohlmann A, Linke H. Hip joint forces during load carrying. Clin Orthop Relat Res 1997;335: 190-201

60. Bergmann G, Graichen F, Rohlmann A. Hip joint forces in sheep. J Biomech 1999; 32(8):769-77

61. Bergmann G, Deuretzbacher G, Heller M, et al. Hip contact forces and gait patterns from routine activities. J Biomech 2001; 34(7):859-71

62. Heller MO, Bergmann G, Deuretzbacher G, et al. Influence of femoral anteversion on proximal femoral loading: measurement and simulation in four patients. J Biomech 2001; 16(8):644-9

63. Bergmann G, Graichen F, Rohlmann A, et al. Frictional heating of total hip implants. Part 1. measurements in patients. J Biomech 2001;34(4):421-8

64. Stansfield BW, Nicol AC, Paul JP, et al. Direct comparison of calculated hip joint contact forces with those measured using instrumented implants. An evaluation of a three-dimensional mathematical model of the lower limb. J Biomech 2003;36(7): 929-36

65. Bergmann G, Graichen F, Rohlmann A. Hip joint contact forces during stumbling. Langenbeck Arch Surg 2004;389(1):53-9

66. Damm P, Ackermann R, Bender A, et al. In vivo measurements of the friction moment in total hip joint prostheses during walking. J Biomech 2012;45(Suppl 1):S268

67. Bergmann G, Siraky J, Kölbel R, Rohlmann A. Measurement of joint forces with implants – a new method of instrumentation and its application in sheep. Biomechanics Symposium, ASCE Mechanics Conference; 1981. 43:225-8

68. Bergmann G, Siraky J, Rohlmann A, Koelbel R. A comparison of hip joint forces in sheep, dog and man. J Biomech 1984; 17(12):907-21

69. Bergmann G. editor. Charit Universitaetsmedizin Berlin "OrthoLoad". Available from: www.orthoload.com [Last accessed December 2013]

70. Qi G, Mouchon WP, Tan TE. How much can a vibrational diagnostic tool reveal in total hip arthroplasty loosening? Clin Biomech 2003;18(5):444-58

71. IEEE-SA Standard Board. C95.1-2005 – IEEE standard for safety levels with respect to human exposure to radiofrequency electromagnetic fields, 3 kHz to 300 GHz. Institute of Electrical and Electronics Engineers; NJ, USA: 2005

72. Taylor SJ, Donaldson NN. Instrumenting STANMORE-prostheses for long-term strain measurement in vivo. In: Bergmann G, Graichen F, Rohlmann A, editors. Implantable telemetry in

orthopaedics. Freie Universität; Berlin, Germany: 1990. p. 93-102

73. Taylor SJ. A telemetry system for measurement of forces in massive orthopaedic implants in vivo. Conf Proc 18th IEEE Eng Med Biol Soc 1996;1:290-2
74. Taylor SJ, Perry JS, Meswania JM, et al. Telemetry of forces from proximal femoral replacements and relevance to fixation. J Biomech 1997;30(3):225-34
75. Bassey EJ, Littlewood JJ, Taylor SJ. Relations between compressive axial forces in an instrumented massive femoral implant, ground reaction forces, and integrated electromyographs from vastus lateralis during various 'osteogenic' exercises. J Biomech 1997;30(3):213-23
76. Taylor SJ, Walker PS, Perry JS, et al. The forces in the distal femur and the knee during walking and other activities measured by telemetry. J Arthroplasty 1998; 13(4):428-37
77. Taylor SJ, Walker PS. Forces and moments telemetered from two distal femoral replacements during various activities. J Biomech 2001;34(7):839-48

•• **Design of instrumented femoral replacements with 24 transducers (the highest number of transducers ever embedded in instrumented hip or femoral implants).**

78. Brown RH, Burstein AH, Frankel VH. Telemetering in vivo loads from nail plate implants. J Biomech 1982;15(11):815-23
79. Schneider E, Michel MC, Genge M, Perren SM. Loads acting on an intramedullary femoral nail. In: Bergmann G, Graichen F, Rohlmann A, editors. Implantable telemetry in orthopaedics. Freie Universität; Berlin: Germany: 1990. p. 221-7
80. Genge M, Schneider E, Michel MC, Genge H Perren SM. Multi-channel telemetry system for load measurements in intramedullary nails. In: Bergmann G, Graichen F, Rohlmann A, editors. Implantable telemetry in orthopaedics. Freie Universität; Berlin: Germany: 1990. p.133-6
81. Schneider E, Michel MC, Genge M, et al. Loads acting in an intramedullary nail during fracture healing in the human femur. J Biomech 2001;34(7):849-57
82. Wehner T, Claes L, Simon U. Internal loads in the human tibia during gait. Clin Biomech 2009;24(3):299-302
83. Bergmann G, Graichen F, Dymke J, et al. High-tech hip implant for wireless temperature measurements in vivo. PLoS One 2012;7(8):e43489

•• **The newest instrumented hip joint prosthesis proposed in literature. It was designed to evaluate the risk of thermally induced bone necrosis.**

84. Bergmann G, Graichen F, Rohlmann A, et al. Hip implant for temperature measurements. J Biomech 2012;45(1):S1
85. Faroug R, McCarthy I, Meswania J, et al. Strain response of an instrumented intramedullary nail to three-point bending. J Med Eng Technol 2011;35(5):275-82

•• **The newest instrumented intramedullary nail proposed in literature. It was designed to predict fracture healing.**

86. Marschner U, Grätz H, Jettkant B, et al. Integration of a wireless lock-in measurement of hip prosthesis vibrations for loosening detection. Sensor Actuat A-Phys 2009;156(1):145-54
87. Valdastri P, Rossi S, Menciassi A, et al. An implantable ZigBee ready telemetric platform for in vivo monitoring of physiological parameters. Sensor Actuat A-Phys 2008;142(1):369-78
88. Cristofolini L, Marchetti A, Cappello A, Viceconti M. A novel transducer for the measurement of cement-prosthesis interface forces in cemented orthopaedic devices. Med Eng Phys 2000;22(7):493-501
89. Gattiker F, Umbrecht F, Neuenschwander J, et al. Novel ultrasound read-out for a wireless implantable passive strain sensor (WIPSS). Sensor Actuat A-Phys 145-2008;146:291-8
90. Alpuim P, Filonovich SA, Costa CM, et al. Fabrication of a strain sensor for bone implant failure detection based on piezoresistive doped nanocrystalline silicon. J Non-Cryst Solids 2008;354(19-25):2585-9
91. Hao S, Taylor JT, Bowen CR, et al. Sensing methodology for in vivo stability evaluation of total hip and knee arthroplasty. Sensor Actuat A-Phys 2010; 157(1):150-60
92. Ruther C, Gabler C, Ewald H, et al. In vivo monitoring of implant osseointegration in a rabbit model using acoustic sound analysis. J Orthop Res 2014;32(4):606-12

•• **Successful in vivo detection of loose instrumented implants using a magnetic sphere inside the implant and external magnetic fields.**

93. Morais R, Silva N, Santos P, et al. Permanent magnet vibration power generator as an embedded mechanism for smart hip prosthesis. Proc Eng 2010;5: 766-9
94. Morais R, Silva NM, Santos PM, et al. Double permanent magnet vibration power generator for smart hip prosthesis. Sensor Actuat. A-Phys 2011;172(1):259-68
95. Silva N, Santos P, Ferreira J, et al. Multi-purpose and multi-source energy management system for biomedical implants. Proc Eng 2012;47:722-5
96. Silva NM, Santos PM, Ferreira JA. Power management architecture for smart hip prostheses comprising multiple energy harvesting systems. Sensor Actuat A-Phys 2013;202:183-92

•• **First motion-driven magnetic levitation system to power instrumented hip joint prostheses. The authors also developed an advanced conditioning circuitry to manage electric power generated by multiple energy sources.**

97. Morgado ML, Morgado LF, Henriques E, et al. Nonlinear modeling of vibrational energy harvesters for smart prostheses. Procedia Engineering 2012;47:1089-92
98. Soares dos Santos M, Ferreira JA, Ramos A, et al. Multi-source energy harvesting power generators for instrumented implants – towards the development of a smart hip prosthesis. Conf Proc 5th Biodevices; 2012. p. 71-81
99. Soares dos Santos M, Ferreira JA, Ramos A, et al. Multi-source harvesting systems for electric energy generation on smart hip prostheses. In: Gabriel J, Schier J, Van Huffel S, et al. editors. Biomedical engineering systems and technologies 357. Springer-Verlag Berlin Heidelberg; NY, USA: 2013. p. 80-96
100. Soares dos Santos M, Ferreira JA, Ramos A, et al. Instrumented hip implants: electric supply systems. J Biomech 2013;46(15): 2561-71
101. Platt SR, Farritor S, Haider H. On low-frequency electric power generation with PZT ceramics. IEEE-ASME Trans Mech 2005;10(2):240-52
102. Le TT, Han J, von Jouanne A, et al. Piezoelectric micro-power generation interface circuits. IEEE J Solid-St Circ 2006;41(6):1411-20
103. Morais R, Frias CM, Silva NM, et al. An activation circuit for battery-powered biomedical implantable systems. Sensor Actuat A-Phys 2009;156(1):229-36
104. Reis J, Frias C, Canto e Castro C, et al. A new piezoelectric actuator induces bone

formation in vivo: a preliminary study. J Biomed Biotechnol 2012;2012:1-7

105. Frias C, Reis J, Capela e Silva F, et al. Polymeric piezoelectric actuator substrate for osteoblast mechanical stimulation. J Biomech 2010;43(6):1061-6
106. Frias C, Reis J, Capela e Silva F, et al. Piezoelectric actuator: searching inspiration in nature for osteoblast stimulation. Compos Sci Technol 2010;70(13):1920-5
107. Ehrlich PJ, Lanyon LE. Mechanical strain and bone cell function: a review. Osteoporosis Int 2002;13(9):688-700
108. Ignatius A, Blessing H, Liedert A, et al. Tissue engineering of bone: effects of mechanical strain on osteoblastic cells in type I collagen matrices. Biomaterials 2005; 26(3):311-18
109. Hronik-Tupaj M, Kaplan DL. A review of the responses of two- and three-dimensional engineered tissues to electric fields. Tissue Eng Part B Rev 2012;18(3):167-80
110. Balint R, Cassidy NJ, Cartmell SH. Electrical stimulation: a novel tool for tissue engineering. Tissue Eng Part B Rev 2013; 19(1):48-57
111. Soares dos Santos M, Ferreira JA, Simões JA, et al. Design methodology for the development of long-term hip prosthesis survival. J Biomech 2012;45(1):S106
112. Prescott JH, Lipka S, Baldwin S, et al. Chronic, programmed polypeptide delivery from an implanted, multireservoir microchip device. Nat Biotechnol 2006; 24(4):437-8
113. Zhao K, Luo H, Chen H, et al. A SoC for pressure balance measurement application in total knee arthroplasty. AASRI Proc 2012;1: 267-75
114. Weiss MD, Smith JL, Bach J. RF coupling in a 433-MHz biotelemetry system for an artificial hip. IEEE Antenn Wirel Pr 2009;8:916-19
115. Stea S, Visentin M, Donati ME, et al. Nitric oxide synthase in tissues around failed hip prostheses. Biomaterials 2002; 23(24):4833-8
116. Yang F, Wu W, Cao L, et al. Pathways of macrophage apoptosis within the interface membrane in aseptic loosening of prostheses. Biomaterials 2011;32(35): 9159-67
117. Ponmozhi J, Frias C, Marques T, Frazão O. Smart sensors/actuators for biomedical applications: rev measurement. 2012;45(7): 1675-88

3.2 Electromagnetic stimulation of bone cells

Results found in section 3.1 have shown that no therapeutic actuators have been developed so far for *in vivo* operation, such that instrumented THRs could control osseointegration. Currently, it is unknown if bioactivity on the bone-implant is more effective by delivering exogenous biophysical stimuli or by the action mechanisms of bioactive coatings. The design of instrumented implants for controlled release of drugs and/or other bio-agents may be quite complex, as stated in chapter 1. Alternatively, it is worth exploring if controllable biophysical stimulation systems can be designed using non-complex architectures. Among the biophysical stimulation methods that proved to induce osteogenic effects, and according to the analyses reported in section 1.2, the deliver of electric and/or magnetic fields to stimulate bone cells seems the most promising method. Since the rational identification of parameters for optimized osteogenic stimulation of tissues or organs firstly requires a solid background on how bone cells activity is electrically and/or magnetically controllable, a detailed review was carried out for: identifying the apparatuses already used to deliver electric and/or magnetic stimuli to bone cells; and analysing the interrelationship between the established stimuli parameters and obtained biological outcomes (including possible adverse events). This study shows how stimuli promote osteogenicity throughout the main stages of osteoblastic maturation in culture (cellular proliferation, matrix maturation and matrix mineralization), as well as the osteogenic effects when key experimental factors are varied (stimulation method, frequency and field strengths of the stimulus, cell model, cell density and maturation stages, serum concentration and osteoinductive factors). Some relevant transduction mechanisms of osteogenicity were subjects also broached. Finally, the main limitations of the current state-of-the-art in this scope were identified and new perspectives for its improvement were proposed. This review paper is entitled "Electromagnetic stimulation of bone remodeling *in vitro*: a review" and it was already submitted to a peer-reviewed international journal (*Bioelectrochemistry*).

Electromagnetic stimulation of bone remodeling *in vitro*: a review

Marco P. Soares dos Santos[1,2], Ana Marote[3], João Torrão[1,2], Jorge A. F. Ferreira[1,2], Odete A. B. da Cruz e Silva[3], Sandra I. Vieira[3]

[1] Centre for Mechanical Technology and Automation, Universidade de Aveiro, 3810-193 Aveiro, Portugal.
[2] Department of Mechanical Engineering, Universidade de Aveiro, 3810-193 Aveiro, Portugal.
[3] Neurociences and Cellular Signaling Group, Institute for Biomedicine (iBiMED), SACS, Universidade de Aveiro, 3810-193 Aveiro, Portugal

Corresponding author: Marco P. Soares dos Santos
Email: marco.santos@ua.pt

* Equally contributing authors

Abstract

The natural occurrence of electromagnetic fields in bone tissues has triggered considerable research addressing their effects on bone remodeling. Electric and/or magnetic stimulation has been proposed as a therapeutic strategy for conditions in which active bone remodeling is critical, namely osteoporosis, bone fracture and poor osseointegration in bone-implant interfaces. Positive effects of electric and magnetic stimulation on bone physiology have been reported, and the variation of specific stimuli parameters, such as frequency, electric or magnetic field strengths, and exposure time, yields different biological outcomes. Despite the volume of work in this field, a systematic evaluation of the correlation between the stimuli parameters and their biological output is lacking. In this review, we provide for the first time a unique insight into the results of the most relevant studies using direct current coupling, capacitive coupling and inductive coupling apparatuses to deliver electric and/or magnetic stimuli to bone cells in culture (cell lines, stem cells and primary cells). The stimuli parameters used and their biological outcomes, concerning the three principal stages of bone remodeling (cellular proliferation, matrix maturation and matrix mineralization) were object of a comprehensive survey here presented. The potential molecular mechanisms underlying the biological outcomes were also addressed. Some major conclusions could be drawn regarding the biological and stimuli factors applied, and the resulting osteogenic responses. This review intends to support the identification of parameters that induce optimum osteogenic stimulation of tissues and organs for future personalized biophysical therapies.

Keywords: Electromagnetic stimulation; bone cells; osteogenic effects; bone remodeling; nondrug therapy.

1. Introduction

Musculoskeletal disorders account for more than 20% of the global disability burden, and over the last 20 years this contribution has increased in developed and developing countries [1]. Their frequency, chronicity and resultant disability are increasing the costs due to loss of productivity and associated health care services, placing the latter amongst the most expensive across developed countries [1–3]. Given that the socioeconomic impact of these disorders is expected to increase dramatically in the forthcoming years [1, 2], it is mandatory to pursue methods that increase the efficiency of the therapies employed against these disorders.

Bone electric properties

Exogenously delivered electric stimulation is thought to mimic endogenous electric currents that normally occur in bone, inducing similar biological effects that ultimately regulate bone remodeling. Bone is a dynamic and highly specialized connective tissue, which can be macroscopically divided into two types: cortical and trabecular. Cortical bone has densely packed collagen fibrils that form concentric lamellae, and surrounds the central marrow cavity providing mechanical and protective functions. Trabecular (or cancellous) bone, located at the ends of long bones, has a loosely organized porous matrix, and provides metabolic functions. At the microscopic level, bone is composed of osteocytes (mature bone cells), crystalline and amorphous mineral phases (hydroxyapatite), crystalline and amorphous organic phases (collagen), and liquids [4, 5]. Bone composition provides characteristic electro-mechanical properties that depend, to a great extent, on mechanical loading (compression or tension). Two main hypotheses have been put forward to explain the electrical potentials measured in loaded bone: the piezoelectric effect and the streaming potentials. Bone piezoelectricity, a bilinear interaction between electrical and mechanical variables, was first proposed by Fukada and Yasuda and attributed to the crystalline micelle of collagen molecules [6, 7]. The magnitude of the electrical potential is influenced by the rate and magnitude of the deformation, while its polarity is determined by the direction: electronegative potentials occur in areas subjected to compression, and electropositive ones occur in areas under tension [8, 9]. Dry bone has piezoelectric constants around $\approx$100 mV, while the loading of moist cortical bone generates much smaller potentials ($\approx$100 μV) that are putatively explained by streaming potentials [7]. These potentials arise from changes in the spatial charge density followed by ionic movement, and can be produced by the bending of hydrated bone or the fluid movement through bone [4, 7, 10, 11].

There are many factors that affect the electrical behavior of bone tissue. Electric and dielectric properties of bone vary according to its macrostructure (cortical vs. trabecular) [12, 13]. Intrinsic factors, such as tissue age, moisture content (wet or dry), fluid conductivity, mineral and organic content interact with electric current and determine the bone dielectric properties [14–17]. Fat and collagen contents are strongly related to relative permittivity, while water content is significantly related to conductivity. These relationships can be used as diagnostic tools, such as to predict trabecular bone water

or fat contents during implant surgery [16] and to assess fracture healing and new bone formation [18].

Therapeutic applications of electromagnetic stimulation

The therapeutic value of electric and/or magnetic stimulation has been recognized for pain relief, wound healing, neuromuscular dysfunctions, pharmaceuticals delivery (iontophoresis), among other conditions [19–26]. Fukada's and Yasuda's studies on the piezoelectric effect of bone have encouraged many researchers to explore the effects of electric current on bone remodeling [27–29]. The Food and Drug Administration (FDA) has approved bone growth stimulation devices based on the following three methods of administering these biophysical stimuli to bone: Direct Current (DC), Capacitive Coupling (CC) and Inductive Coupling (IC) [30]. The DC method is invasive whereas the CC and IC methods are non-invasive. The effectiveness of these methods has been demonstrated both *in vivo* and *in vitro*, and they have been proposed as therapeutic strategies for minimizing osteoporosis, promoting bone fracture healing and improving osseointegration in bone-implant interfaces [31–36].

Bone remodeling is a tightly orchestrated process of bone resorption and bone formation. This turnover is essential to remove microdamage, replace dead and hypermineralized bone, adapt the bone architecture to local stresses, and regulate calcium homeostasis and hematopoiesis, among others. Osteoporosis, one of the major musculoskeletal disorders, is characterized by low bone mass and structural deterioration, due to an imbalanced bone remodeling. Importantly, several authors have reported the efficacy of electrical and/or magnetic stimulation to prevent and even reverse osteoporosis in animal models [31–36].

Electric and/or magnetic stimulation are also valuable in bone healing upon fracture, including fracture repair of osteoporotic bone. The process of bone regeneration is initiated by an acute inflammatory response, in which relevant signaling molecules are produced and released, followed by mesenchymal stem cells recruitment and subsequent proliferation and differentiation into osteogenic cells to generate a primary cartilaginous callus. Callus remodeling is then necessary to fully restore normal bone structure, which may take years to be accomplished [37, 38]. If the regulation of this complex process is compromised, in particular under osteoporotic conditions, healing is delayed or impaired, leading to bone nonunion or disabled union. In combination with pharmacotherapy, several methods have been proposed to treat these conditions, including invasive therapies such as surgical repair, allografts and autogenous bone grafts, or non-invasive therapies such as ultrasound stimulation. Electrical and/or magnetic stimulation has proven to be an effective treatment for both nonunions [39–41] and spinal fusions [42, 43]. Additionally, when compared to ultrasound stimulation and drug administering treatments, therapies involving electrical stimulation are more cost-effective for fracture nonunions due to their lower total health care resource use and lower overall costs [44].

Bone electrical and/or magnetic stimulation may also assist osseointegration, one of the most important phenomenon affecting long-term behavior of implantable orthopedic implants [45]. Current bone-implant interfaces cannot ensure a timeless stable

performance, mainly when interfacing osteoporotic bones [45]. Loss of primary stability and early migration of the implant occurs frequently, leading to revision procedures due to implant loosening [46–49]. Instrumented active implants, with the ability to apply personalized electrical and/or magnetic stimuli in the bone implant interface, may be a future innovative method to optimize osseointegration. Further, their application can be quite significant when revision procedures endanger the patients' life or deeply deprive their life quality, especially when suffering from osteoporosis and with less than 65 years old [48]. Inductive coupling stimulation has been the delivery method more intensively studied as a therapy to enhance osseointegration (as reviewed in [50]).

Characteristics and optimization of osteogenic electromagnetic stimulation

The application of electric and/or magnetic stimulation to promote bone healing has many advantages over pharmacological or chemical therapeutics. Firstly, most of them can be designed as non-invasive, avoiding the production of toxic chemicals and the induction of immunogenic responses [51, 52]. Further, these stimulators can apply painless stimuli, employing non-complex apparatuses that are less expensive than growth factors and drug interventions [51]. Incorporated electrodes can be used in operations where both constant monitoring and application of therapeutic stimuli to the same specific volume co-exist [51]. Nonetheless, the application of electrical and/or magnetic stimuli as a nondrug intervention requires a deep understanding of the correlation between specific stimulation parameters and resulting osteogenic effects, and this is still far from an optimized level that ensures effective bone turnover.

Osteogenic parameters to be used with DC, CC and IC stimuli-delivery devices are usually first tested *in vitro* in bone cells cultures. Osteoblasts are the main cells used, as these are responsible for bone matrix production [5]. *In vitro* studies using the DC, CC and IC stimulators have explored particular features of bone remodeling, particularly osteoblasts proliferation, differentiation (matrix maturation), and matrix mineralization, the main stages of osteoblastic maturation in culture [53–55]. However, the studies use quite different stimuli and biological setups in their experimental designs, and evaluate different biological outcomes. Consequently, it is difficult to infer on potential correlations between electric and/or magnetic stimuli and osteogenic outcomes. The rational identification of parameters for optimized osteogenic stimulation of tissues or organs requires a solid background on how osteoblast and osteoclast activities are influenced by electric and/or magnetic fields. Therefore, this paper provides for the first time a unique insight into the main results of studies using DC, CC and IC apparatuses to stimulate osteoblast-like cell lines, stem cells and primary bone cells in culture. Critical analyses on the influence of the experimental design factors on the biological outcome are also presented. This added knowledge will hopefully help future designs of studies on cultured cells stimulated electrically and/or electromagnetically, and support its translation to tissue or organ levels. The ultimate goal is to aid in the development of innovative medical devices, such as implantable orthopedic implants comprising intelligent stimulators [46, 48].

2. Electromagnetic stimulation of bone remodeling *in vitro*

In order to identify electrical and/or magnetic stimulation conditions effective in bone remodeling, many *in vitro* studies have been performed in which different stimulus parameters were applied to cultured bone cells. Variables encompassed quite different cell culture and stimuli conditions, and quite distinct biological outcomes were observed. To more easily extract comparative conclusions from these studies, the most relevant characteristics were systematized (supplementary Tables S1-S9). This analysis was conducted considering various cell culture features, including the cellular model used and confluence state at the time of the stimulus onset. Several stimuli characteristics were also considered for each stimulation method, namely waveform, frequency, periodicity, electric field (EF) strength and/or magnetic field (MF) strength, current density, time of stimuli exposure and total assay duration.

Biological outcome evaluation was categorized based on the three specific stages of osteoblasts *in vitro* maturation: proliferation, differentiation and matrix mineralization [53, 54]. In these studies, proliferation was assessed by: direct cell counting ('Cell Nr.'), trypan blue exclusion assay ('EA'), metabolic cell viability assays ('MetB'), quantification of the DNA content ('DNA'), quantification of incorporated exogenously added labeled-DNA (incorporation assay, 'IA'), or by quantifying protein synthesis ('PS').

Cellular differentiation, which takes place after cell confluence or upon osteogenic factors medium addition, is characterized by the formation of an organic matrix. Most surveyed studies evaluated this stage by analyzing the expression or localization of matrix-associated proteins. Collagen type I comprises around 90% of the organic matrix and thus its expression and medium secretion are well-recognized differentiation markers [56, 57]. The organic matrix is also composed of other collagen proteins (type III, V and X), proteoglycans, and numerous noncollagenous proteins such as osteonectin, osteocalcin, bone sialoprotein, and osteopontin, which can be used to assess differentiation. Osteonectin and osteopontin, for example, mediate signal cascades for the full expression of the mature osteoblast phenotype and mineralization of the extracellular matrix (ECM). The expression and activity of alkaline phosphatase (ALP) are other widely used early biomarkers of osteoblast differentiation. This enzyme hydrolyzes organic phosphates to increase the local phosphate concentration to a level required for the generation of hydroxyapatite crystals [58, 59].

Mineralization of the mature matrix is the end phase of osteoblastic differentiation. In the analyzed studies, mineralization was inferred by measuring osteocalcin expression and/or the amount of extracellularly deposited calcium. Osteocalcin, a type-1 noncollagenous protein secreted by osteoblasts, actively participates in this stage. In the presence of calcium, osteocalcin combines with hydroxyapatite, modulating the hydroxyapatite growth and crystal morphology [59, 60]. Matrix mineralization was also assessed using Alizarin red and von Kossa staining for calcium deposits in the matrix. In a few studies, electron microscopy was employed to visualize the morphology of mineral

spherules [61]. Of note, cell migration and related intracellular calcium levels were also measured and extracted from studies using DC stimulation.

A summary of some of the major features found are described below, but for a detail and complete analysis of the content presented in this review paper please refer to Tables S1-S9, which can be found in the on-line version.

2.1. Direct current coupling

2.1.1. Design of DC stimulation systems

The direct current coupling systems refer to all stimulators composed of electrodes which are all in direct ohmic contact with the cell culture medium, such that electrical currents are transferred to ionic currents through an electrode-electrolyte interface. Usually, this current flow is achieved by using agar salt bridges to isolate cells from harmful electrochemical by-products generated by the direct exposure of the electrode(s) to the culture (Fig. 1) [51, 62–64]. However, biocompatible and highly conductive materials immersed into the culture, mostly arranged in parallel configuration, have also been used to carry out the electrodes-culture contact. This method ensures that bone cells are stimulated by (constant or time-dependent) ionic currents and DC electric fields (dcEFs).

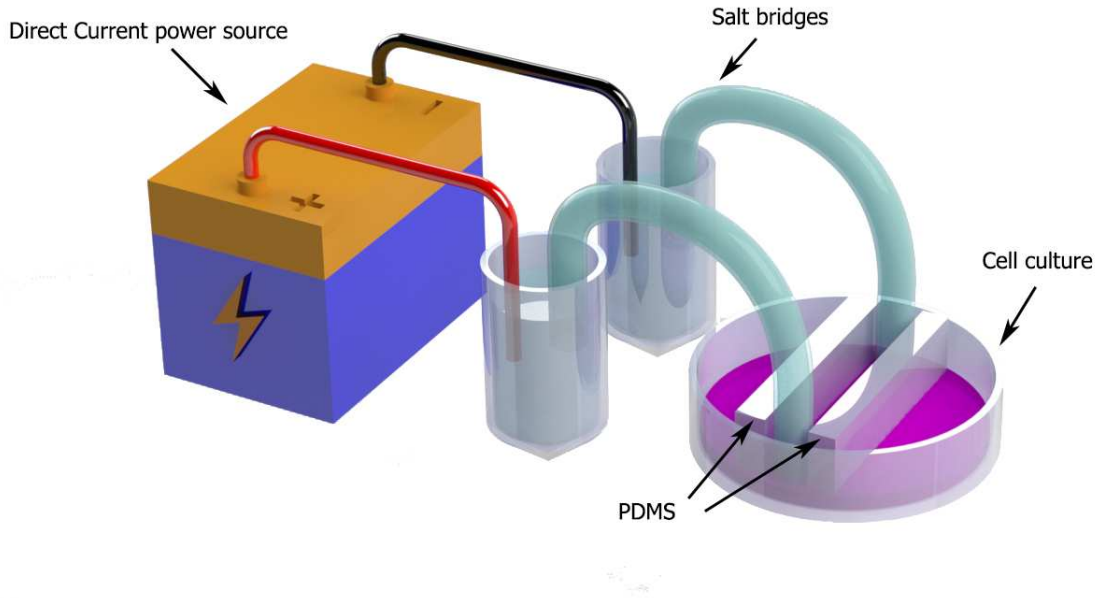

Fig. 1: Experimental setup for direct current stimulation systems. A power source provides the required current for bone cell stimulation. To avoid cytotoxicity, salt bridges are used to ensure the delivery of electric current without direct contact with the electrodes. PDMS - polydimethylsiloxane.

2.1.2. Cellular responses to DC stimulation

From the surveyed data, specific DC experimental setups were able to induce positive responses in the three cell models, particularly in terms of proliferation and Ca^{2+} content (Fig. 2, supplementary Tables S1-S3).

Cell alignment and migration

Most studies using DC stimulation evaluate cell alignment and cell migration, as well as the potential involvement of calcium in these processes. The application of short-duration (few seconds) dcEFs is enough to promote cell alignment and elongation perpendicularly to the EF lines (Tables S1 and S2) [65,66]. This effect is suggested to occur before migration and to result from the alteration of cell tensions, in a pattern related to both the direction of the stimulus and the direction of the future movement [65].

Endogenous EFs generated at wounds are known to act as migratory stimuli for fibroblasts and macrophages [67]. Similarly, externally applied dcEFs also induce osteoblast and osteoclast electrotaxis in culture. However, there are differences in the direction of the migration between cell types and between species. The application of EF strengths similar to those found in wounds (≈1 V/cm) resulted in opposite directions of migration for rat (RCJ 1.20 and RCB 2.2A) and human (SaOS-2) osteoblast like cell-lines (Table S1). Rat osteoblasts migrate towards the cathode [68], while human osteoblasts migrate anodally [69].

Human bone marrow-derived mesenchymal stem cells (hBM-MSCs) (Table S2) also presented anodal galvanotaxis at low EFs strengths (0.25 V/cm), with a maximal migratory response at 3 V/cm [70]. Accordingly, the application of a 0.1 V/cm EF strength for 5 days (3 h/day) promoted the expression of migration- and invasion-related genes in hBM-MSCs [71]. As for rat osteoblast-like cells, primary osteoblasts (Table S3) from rat calvaria migrated towards the cathode [69], while primary rabbit osteoclasts presented anodal-directed migration [68].

Concluding, externally applied dcEFs induce bone cells migration in a cell-type specific manner and dependent on voltage, time, and calcium levels, as already suggested elsewhere [70]. Calcium is an important second messenger, suggested to participate in the signal transduction of electrical signals (further discussed in section 4.1). No directed migration is observed in calcium-free conditions; however, only EFs strengths around 14 V/cm were able to trigger a rapid increase in intracellular calcium levels [69] (Table S1), possibly through the activation of voltage-gated calcium channels (VGCCs) [66, 72, 73]. In this study, Özkucur *et al.* [69] have observed that the initial intracellular calcium elevation occurs in the cell side that does not face the electrode towards which the cell migrates; this initial calcium rise is thus initiated at opposite sides in rat calvarial and human SaOS-2 cells, resulting in their differential directionality.

Proliferation

Positive effects of dcEFs on the proliferation of osteoblast-like cells lines were observed in few studies. The application of low EF strengths (0.015-0.02 V/cm) for 34 h to rat osteosarcoma cells enhanced DNA synthesis by +10-40% above control levels [63] (Table

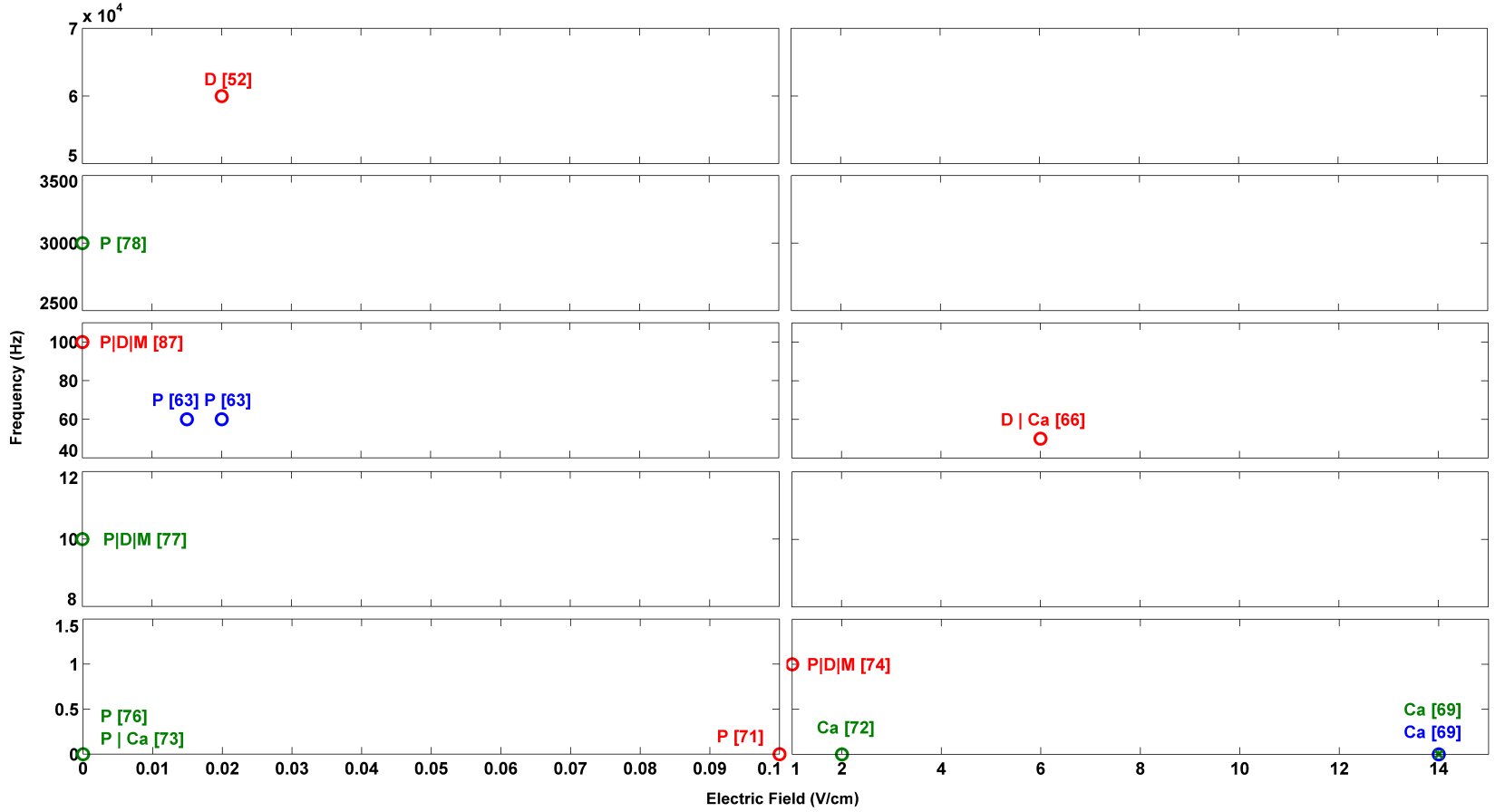

Fig. 2: Schematic representation of the osteogenic electric field strengths and frequencies applied in direct current studies. Positive cellular responses to a defined electric field are divided into proliferation (P), differentiation (D) and mineralization (M). Positive intracellular calcium concentration (Ca) is also represented. The colors correspond to the cellular model used: immortalized cell lines in blue; stem cells in red and primary cells in green. Several references indicated on the axes refer to studies in which the EF strength or the frequency, or both, are not described. Frequencies and periodicities were standardized according to supplementary Fig. S1.

S1). dcEFs also induced proliferative effects on hBM-MSCs, either in the presence (up to 200%) or absence (up to 78%) of osteoinductive media (OM). Increased cell number [74] and metabolic activity [71] of hBM-MSCs grown in OM were observed when using EF strengths of 0.1 and 2 V/cm, respectively. The increase under normal growth media is usually lower, but 24 h/day exposure to a current density of either 1.5 or 15 $\mu A/cm^2$ at 100 Hz increased cell number after 6 days of stimulation [75]. However, these cells presented no alterations in their metabolic activity when exposed 40 min/day (for 28 days) at a high frequency (60 kHz) [52] (Table S2). For primary osteoblasts (Table S3), positive proliferative effects were achieved by delivering quite different stimuli: low (10 Hz) or high frequencies (3 kHz) during short (1 h/day) or long (24 h/day) time exposures increased the cell number up to 46% [73, 76].

Matrix maturation and mineralization

Increases in ALP activity were observed in human bone marrow-derived and mouse adipose-derived MSCs incubated with OM and daily exposed to dcEFs (Table S2) [66, 74]. Increases in the expression of ALP and collagen type I were observed for a EF exposure of 0.02 V/cm/60 kHz (40 min/day) and 6 V/cm/50 Hz (6 h/day) [52] (Table S2). When primary osteoblasts were stimulated 6 h/day at 10 Hz, the expression of collagen type I increased either at day 2 or day 21 [77]. A much higher frequency (3 kHz) failed to increase collagen and ALP expression after 4 days of 6 h or 24 h/day exposures [78] (Table S3). Of note, cellular differentiation has not been evaluated in osteoblast-like cell lines.

Regarding hBM-MSCs matrix mineralization, only five studies analyzed matrix mineralization, and all used osteoinductive media (Table S2). Of those, none detected up-regulations in osteocalcin levels, and only two observed increased mineralization, although with quite different stimuli (100 Hz, 24 h/day [75] and 1 Hz/1 V/cm, 30 min/day [74]). However, either cells exposure 40 min/day for 28 days to a lower 0.02 V/cm EF strength at a high 60 kHz frequency [52] or to a single-day EF exposure of 2 h followed by 28 days of incubation in OM, failed to increase matrix mineralization [70]. Matrix mineralization was never evaluated in osteoblast-like cell lines; in primary osteoblasts it was only evaluated for one stimulus – a EF of 10 Hz, 6 h/day during 21 days – that induced osteocalcin levels and calcium deposition in the extracellular matrix [77] (Table S3).

In synthesis, DC stimuli of EF strengths between 1-14 V/cm can induce proliferative effects (+38 to 200%) and increases in differentiation markers or intracellular Ca^{2+}, mainly when applied to stem and primary cell cultures (Fig. 2; Tables S1-S3) [66,69,72,74]. These studies have used either constant DC stimuli or sinusoidal and square stimuli waveforms. However, other studies using EF strengths of 1-12 V/cm observed no effects (or even detrimental ones) on Ca^{2+} content [51,62–66,69,74], differentiation [78], and mineralization outcomes [65, 66, 69, 74]. Further, it is difficult to infer on other stimuli characteristics, since very few studies using DC stimulation had information on both the EF strength and frequency, and a broad spectrum of osteogenic frequencies was tested (from 1 to 60 kHz) but in a small number of studies. The exposure time may also be an important factor to test in future experiments, since an increase of the stimulus duration may result in augmented cellular proliferation [78].

2.2. Capacitive coupling

2.2.1. Design of CC stimulation systems

The capacitive coupling systems refer to all stimulators composed of electrodes such that either they are not in ohmic contact with the cell culture medium or just one of the electrodes is immersed into the culture to establish an electrode-culture contact. The electrodes are plates usually arranged in parallel, and cells are placed between these electrodes (Fig. 3) such that homogeneous distributions of charges and stimuli are provided [51, 52, 78]. Cell stimulation is performed either by capacitive coupling EFs (ccEFs) or electromagnetic fields (ccEMFs), and displacement currents (when time-dependent EFs are applied), although ion translocation can also take part in this process.

2.2.2. Cellular responses to CC stimulation

Sinusoidal, square and sawtooth CC waveforms were applied successfully in osteogenesis in various experimental setups using the three cell models (Fig. 4, supplementary Tables S4-S6).

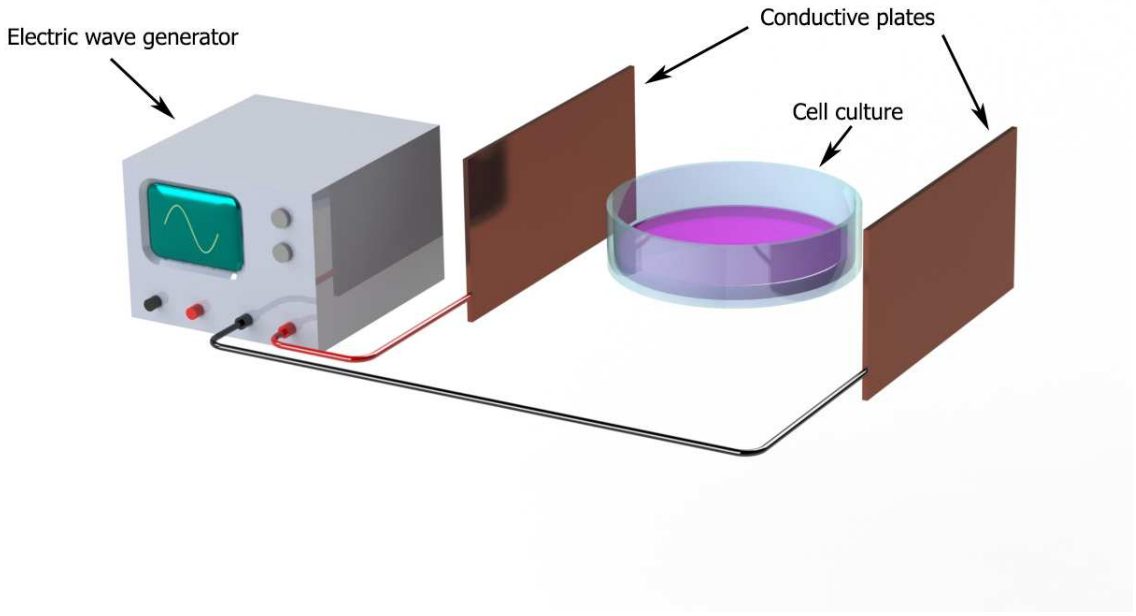

Fig. 3: Experimental setup for capacitive coupled stimulation systems. A power generator provides the voltage (sine wave, square, sawtooth, etc.) required to generate the electric field to stimulate the cells placed between two parallel plates. The plates can be on opposite sides of the culture dish or at the top and bottom.

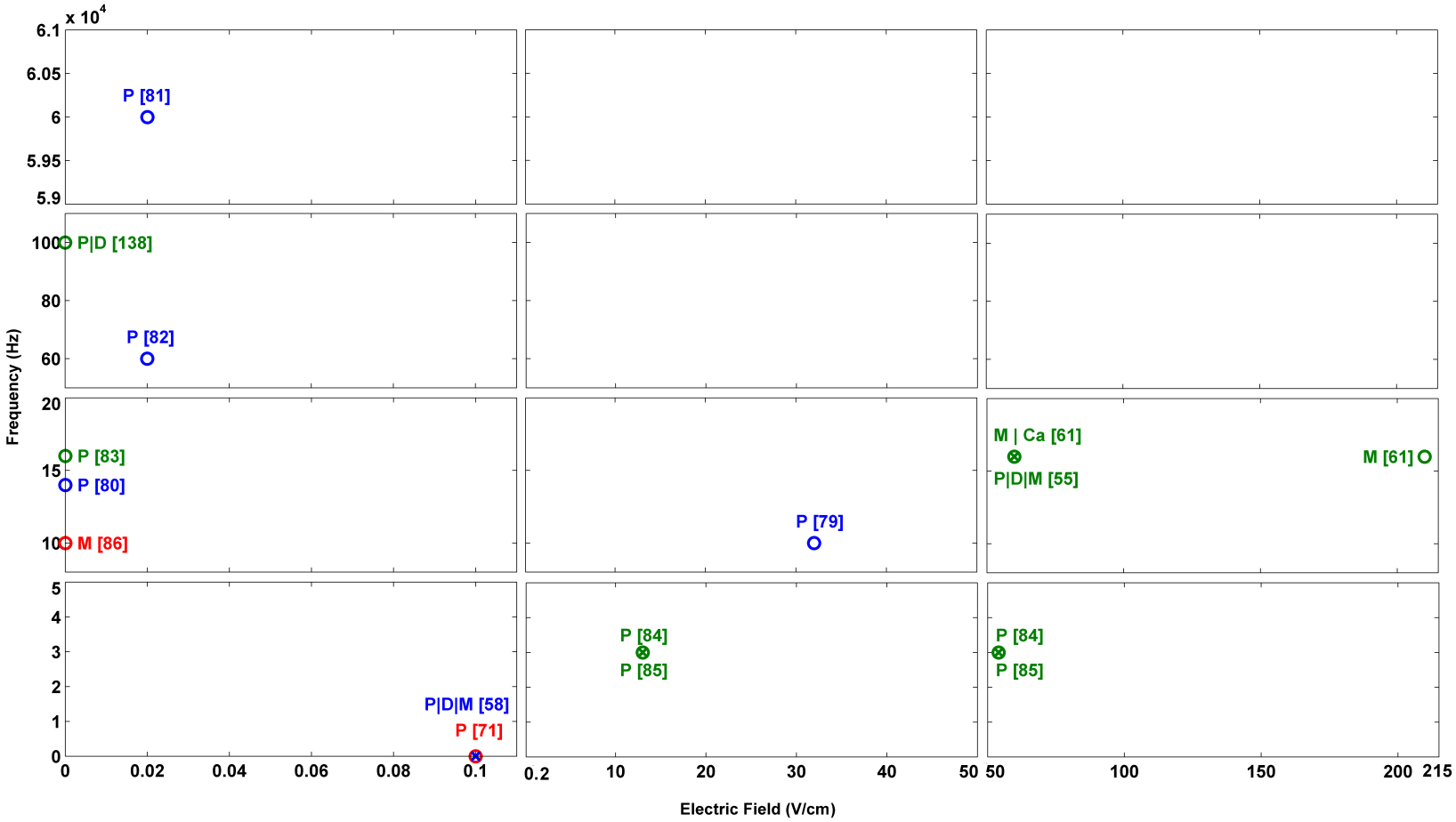

Fig. 4: Schematic representation of the osteogenic electric field strengths and frequencies applied in capacitive coupling studies. Positive cellular responses to a defined electric field are divided into proliferation (P), differentiation (D) and mineralization (M). The colors correspond to the cellular model used: immortalized cell lines in blue; stem cells in red and primary cells in green. Several references indicated on the axes refer to studies in which the EF strength or the frequency is not described. Reference [80] appears on the frequency axis since it uses a quite low EF strength (1×10^{-7} V/cm). Frequencies and periodicities were standardized according to supplementary Fig. S1.

Proliferation

Most of the studies using capacitive coupling systems to stimulate osteoblast-like cell lines reported increases in DNA synthesis, even though with different stimuli (Table S4). Besides other characteristics, such as biological ones, the conjugation of the stimulus' frequency and EF strength seems very important. Using a frequency of 10 Hz, Ozawa *et al.* [79] observed a two-fold increase in MC3T3-E1 cells' DNA synthesis, whereas the same frequency was not sufficient to promote DNA synthesis in TE-85 cells [80]. Differences between the applied EF strengths may explain this discrepancy: 31.9 V/cm of the former, contrasting to the extremely low strength of 1×10^{-7} V/cm of the latter [79, 80]. At equal EF strengths (0.02 V/cm) and duration of field exposure (24 h), an increase in the stimulus frequency from low (60 Hz) to high (60 kHz) led to a decrease in the positive effects on MC3T3 cells DNA synthesis: from +49% to +18.7% [81]. The exposure time is also important: when using the low 60 Hz frequency, increases in the stimulus duration (from 30 min to 2, 6 and 24 h) led to gradual increases in DNA incorporation, from +17% to +49% [82].

Very few studies used stem cells to analyze the osteogenic effects of CC stimulation (Table S5), but one of these reported increased metabolic activity for hBM-MSCs after 5 days (3 h/day) of exposure to an EF strength of 0.1 V/cm using degenerate waves [71].

Studies on primary cell cultures were also conducted using distinct stimuli characteristics (Table S6). The application of two EFs with quite different strengths, 1×10^{-7} V/cm and 60 V/cm, at the same frequency (16 Hz), resulted in similar increases in DNA synthesis (+30%) and cell number (+10 to 30%) after 18 h and 7 days of field exposure, respectively [55,83]. Frequency and EF strength may induce nonlinear behaviors on cellular proliferation. On one hand, using very low EF strength (1×10^{-7} V/cm), Fitzsimmons *et al.* [83] observed no increase in DNA synthesis at frequencies immediately below (8, 12 Hz) or above (20, 24 Hz) the proliferative 16 Hz value (+30% in this value) in primary cells; these authors observed a similar behavior in osteoblast-like cells (around the 14 Hz proliferative frequency). On the other hand, using a low frequency (3 Hz), Binderman *et al.* [79, 84, 85] reported increases in DNA synthesis (+40 and +240%) for EF strengths below (13 V/cm) and above (54 V/cm) an intermediate non-proliferative EF strength (22-24 V/cm).

In synthesis, proliferative effects (+17 to 240% of proliferation) were observed throughout a wide range of EF strengths (from 1×10^{-7} to 210 V/cm), with an incidence in values in the tens of V/cm (Fig. 4). For setups with EFs in this range, a few trends could be inferred: 1) more EF strength generally resulted in increased proliferative outcome, although this behavior may not be linear [79, 84, 85]; 2) at a given EF strength and frequency, more exposure time to the stimulus might induce more cellular proliferation [78,79,82]. Noteworthy, when using extremely low EF strengths (1×10^{-7} V/cm; sinusoidal wave), very narrow and cell-type specific intervals of successful proliferative frequencies occurred [80, 83]. Regarding frequency, proliferative effects were observed at low (tens to hundreds) and high (in the thousands) frequencies. High frequencies were usually used with lower EF strengths (and exposure periods) and vice-versa. Since the number of studies using ccEF stimulation is relatively low (13) to infer more general trends on the effects

of these parameters on cells proliferation, more systematic approaches that independently vary each of the stimuli parameters (such as the waveform, frequency and EF strength) are needed.

Matrix maturation and mineralization

Regarding cell lines and stem cells, only two studies using CC stimulators (one for each cell model) evaluated osteoblastic differentiation and matrix mineralization. Increases in various osteogenic differentiation markers, and a 480% increase in matrix mineralization, were observed in human SaOS-2 immortalized cells after 28 h of field exposure (0.1 V/cm, 16 Hz, 4 h/day) (Table S4) [58]. Osteocalcin expression increased in hBM-MSCs after 14 days of culture on a hydrogel when these cells underwent 6 h/day exposure to a ccEMF at 10 Hz (Table S5) [86]. In primary cultures, only three studies evaluated matrix maturation and mineralization. ALP activity, several differentiation markers and osteocalcin levels increased in bovine primary cells exposed for 18 days to a EF strength of 60 V/cm at 16 Hz (Table S6) [55]. The same researchers have later reported that this stimulus settings (or altering the EF strength to 210 V/cm) also increased the matrix calcium content and the number of nodules and mineral spherules, typical of the *in vivo* onset of mineralization [61].

In summary, very few studies have monitored and reported positive effects of CC stimulation on bone cells differentiation or mineralization (Fig. 4). These studies generally exhibited a wide disparity of settings, and sometimes not all the information was available. In these, frequency varied from 10 to 100 Hz, and EF strength from 0.1 to 210 V/cm. Time of daily exposure also varied, although cells were usually stimulated over two or three weeks in culture. Therefore, a very small amount of information is available, and it urges to perform more systematic studies on CC stimulation effects on osteogenic differentiation and mineralization.

2.3. Inductive coupling

2.3.1. Design of IC stimulation systems

The inductive coupling systems refer to all stimulators designed either as coil(s), formed by winding conductive wire, or as permanent magnet(s). Usually, they are not in ohmic contact with the cell culture medium (Fig. 5). While only magnetostatic interactions stimulate cells when using permanent magnet(s), coil(s) can promote cell stimulation either by magnetic or electromagnetic fields (icEMFs), because time-dependent magnetic fields induce nonconservative EFs in the coils. Besides, ion translocations can also take part in this process. The main stimuli waveforms applied to bone cells in the studies here presented were pulsed electromagnetic fields (PEMF) [87, 88] and combined electromagnetic fields (CMF) [89].

2.3.2. Cellular responses to IC stimulation

Osteogenic effects were observed when applying sinusoidal, square, triangular and sawtooth IC stimuli waveforms, mostly PEMF but also CMF, to the three cell model types (Fig. 6, supplementary Tables S7-S9).

Proliferation

The IC stimulation has been the mostly used method to stimulate bone cells, and increased DNA synthesis is reported in approximately half of the studies using osteoblast-like cell lines (Table S7). Using CMF stimuli, some authors observed 58-71% increases in DNA synthesis in TE-85 cells [89, 90]. Increasing PEMF field exposure duration, from 30 min to 9 h and 24 h, promoted larger increases in DNA synthesis: +276%, 284% and 355%, respectively [91]. As usual, some authors also reported decreased cell number (up to -48%) and protein synthesis (up to -17%) in rat and human osteosarcoma cell lines exposed to PEMFs [87, 92–94].

Regarding stem cells (Table S8), increases in DNA synthesis, cell number and metabolic activity were observed in hBM-MSCs exposed to PEMFs for different stimuli parameters. Various studies using 4.4 kHz and 1.6 or 1.8 mT are included [71, 95, 96], but one other study using a very similar PEMF stimulus presented a decrease in cell number [88,97]. The confluent state of the cells in this later, in opposition to the pre-confluent state in most of the former studies, may be a key factor promoting on these differences (see section 3.5).

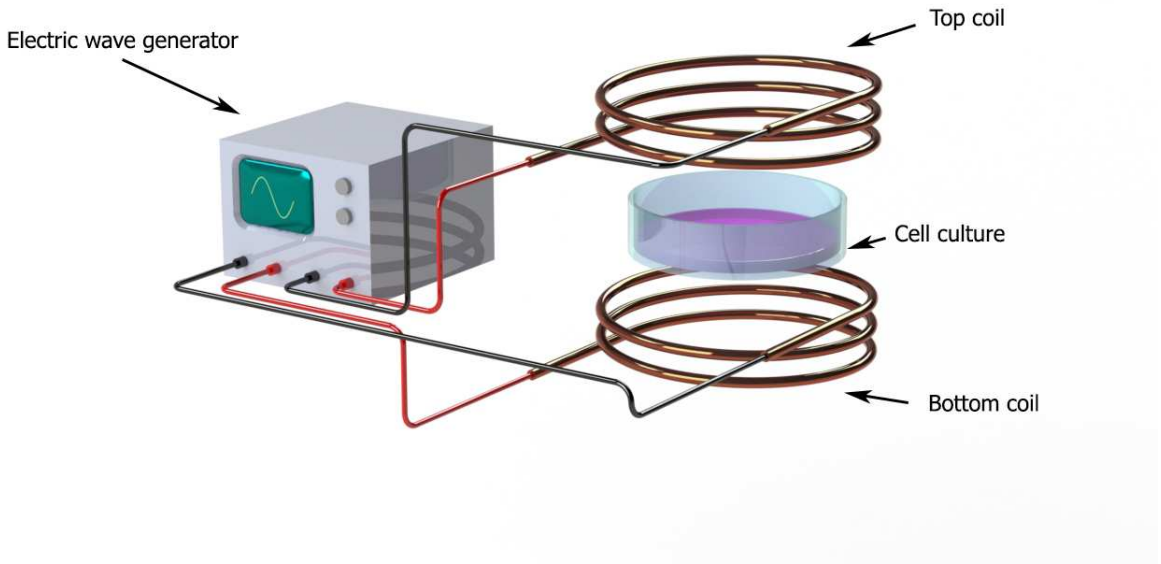

Fig. 5: Experimental setup for inductive coupled stimulation systems. Magnetic fields are generated by electric currents flowing through one or more wire coils. Electric fields also stimulate the cultures placed aligned with the axis of the coil(s) when time-varying magnetic fields are generated.

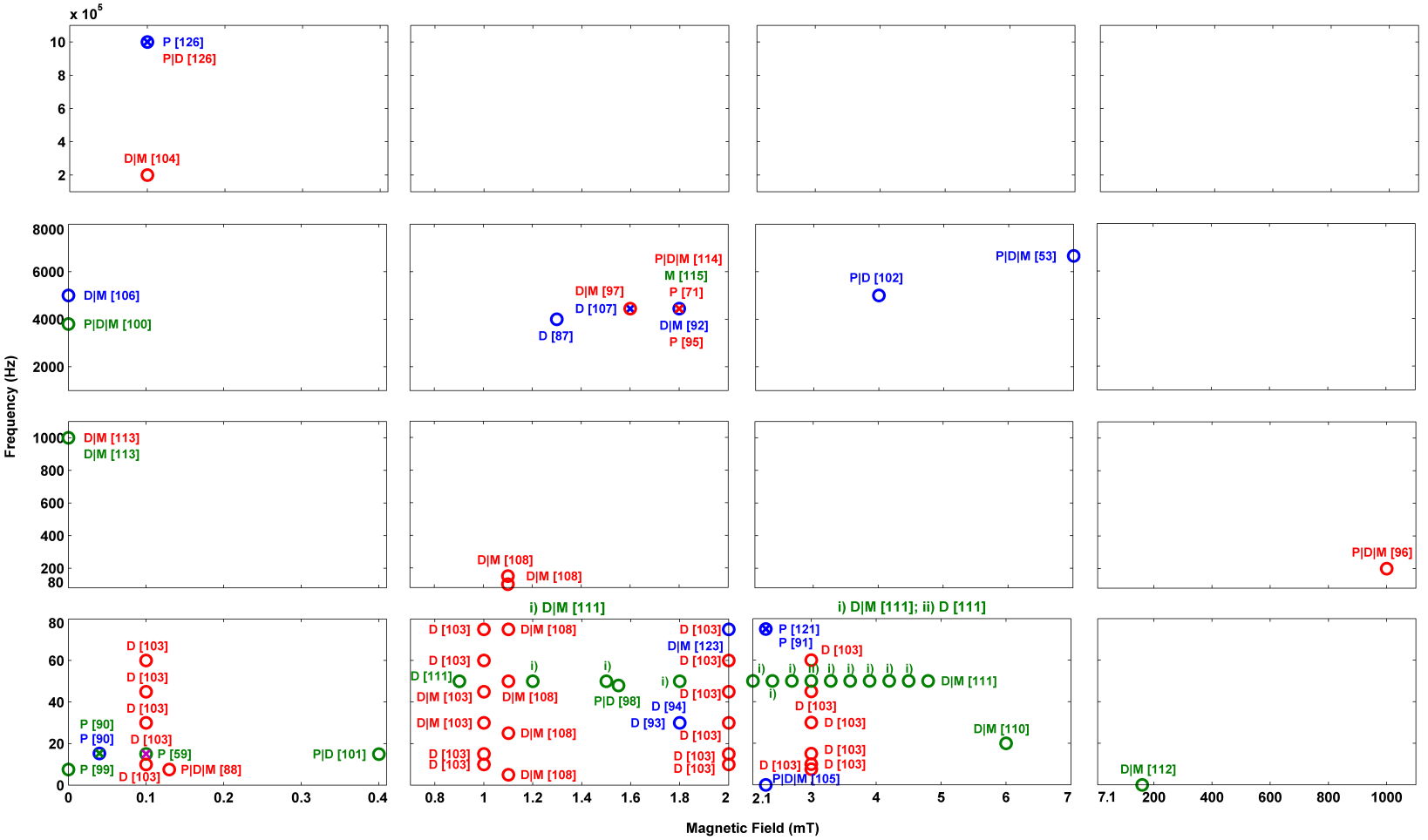

Fig. 6: Schematic representation of the osteogenic electric field strengths and frequencies applied in inductive coupling studies. Positive cellular responses to a defined electric field are divided in proliferation (P), differentiation (D) and mineralization (M). The colors correspond to the cellular model used: immortalized cell lines in blue; stem cells in red and primary cells in green. Several references indicated on the axes refer to studies in which the MF field strength or the frequency are not described. Frequencies and periodicities were standardized according to supplementary Fig. S1.

Proliferative results in stem cells were quite diverse, with 50% of the icEMFs studies in stem cells resulting in positive effects (using low and high frequencies and EF strengths), 33% in no alteration, and around 16% in negative effects.

Most studies involving primary cultures reported increases in proliferation (Table S9). For example, osteoblasts from rat calvaria increased their metabolic activity and cell number when exposed for 3 days to icEMFs of lower MF strengths (and generally low frequencies) [59, 98–100]. Using very low MF strengths, increased DNA synthesis (+26%) was observed in human bone cells after 30 min of CMF stimulation and a subsequent 18 h rest period [90], and an increase in their cell number (+29%) was reported upon 7 days of exposure to PEMFs [101].

With respect to the EF/MF field strengths, frequency and time of exposure to the stimulus, some major conclusions can be drawn (Fig. 6). Proliferative effects (up to +355% [91]) were mainly observed for MF strengths lower than 4 mT, using frequencies either low (up to 222 Hz) or high (4-7 kHz). Both short (30 min/day) and long (24 h/day) exposure time increased cell proliferation [53,89,90,101,102], but for some icEMFs settings, proliferation may increase as the exposure time increases [91]. Importantly, variations in the PEMF proliferative effects may derive not only from the PEMF characteristics but also from biological factors, such as the percentage of serum in the medium, cell density, cell type and differentiation stage [103]. Further, the time when the biological outcome is measured is also important, since decreased proliferation at later stages seems necessary for PEMF-induced osteodifferentiation of primary and stem cells [103, 104].

Matrix maturation

Most studies using IC stimulation reported increases in ALP activity and/or expression for all cell types tested. For example, PEMFs enhanced ALP activity of human and rat osteosarcoma cell lines by 21% to 108% (Table S7) [87, 92–94, 105, 106]. 108% increase was observed in the rat osteosarcoma cell line ROS 17/2.8 after 3 days of 24 h/day icEMF exposure (30 Hz, 1.8 mT, 6 μV/cm) [94]. ALP activity of the osteocyte-like cell line MYLO-Y4 also increased (200%) after 1 day of 8 h exposure to PEMF of 1.6 mT at 4.4 kHz [107]. A 1.6 fold increase was reported for collagen type I expression in human osteosarcoma MG63 cells exposed to PEMFs for 4 days (8 h/day, 4.4 kHz, 1.8 mT) [92].

An increase in ALP activity was observed in hBM-MSCs exposed to different MFs (0.13 to 1000 mT) (Table S8) [88, 96, 97, 103]. Importantly, data from Jansen *et al.* [104] suggest that the strongest effect of PEMF on hBM-MSCs differentiation is exerted in the period prior to mineralization. Using very similar experimental setups, Sun *et al.* [95] (MF of 1.8 mT at 4.4 kHz; 8 h/day) did not observe increased hBM-MSCs differentiation upon 24 days, but Schwartz *et al.* [97] (1.6 mT, 4.4 kHz; 8 h/day) did (increased ALP and OC). The fact that in the former study cells were only exposed to the stimulus in the first 3 days (contrasting to the all 24 days in the later) might explain this difference, together with the addition of the growth factor BMP-2 to the media in this later (discussed in section 4.2). In hASCs, osteogenesis-related genes and ALP were up-regulated by a 1.0 mT MF strength at both 30 and 45 Hz [104]. Noteworthy, some genes were more up-regulated at 30 Hz (Col-I, RUNX2), whereas the 45 Hz frequency was more effective for others (OSX and

OC) [103]. Most interestingly, systematic approaches testing for intervals of frequencies or strength values revealed 'pyramid-like' responses of osteogenic markers. By exposing hBM-MSCs cells to a MF strength of 1.1 mT at frequencies ranging from 5 to 150 Hz, Luo *et al.* (2012) [108] unraveled a symmetric behavior in the cells' osteogenic response (ALP activity, OC levels). In this, the 50 Hz value corresponded to the symmetry axis, presenting the maximum osteogenic response, and frequencies above or below it induced lower osteogenic effects. Kang *et al.* [103] observed this same behavior when assessing ALP expression and activity in hASCs, upon application of a MF strength of 1.0 mT at frequencies in the 7.5-75 Hz range. This group also observed that ALP expression also followed a pyramid-like curve in response to a narrow interval of MF strengths (from 0.1 to 3.0 mT). Although significantly increased over control levels from 0.8 to 3.0 mT, ALP expression levels increased until 1.0/2.0 mT [when using supplemented e non-suplemented medium (NSM), respectively], the MF strengths with the highest/optimal ALP responses, and decreased thereafter [103]. Later on (2014) it has also demonstrated that osteoclast formation, differentiation, and activity are regulated by frequency in an opposite manner to osteoblasts [109]. While stimulation at 7.5 Hz decreased osteoblastic differentiation, it induced osteoclastic differentiation and activity; the 45 Hz frequency, previously reported as positive for osteoblastic differentiation, was observed to inhibit osteoclast formation [103, 109].

Regarding primary cultures, ALP activity also increased in primary human osteoblasts after 10 days of exposure to PEMF (14.9 Hz, 0.4 mT; Table S9) [101]. Collagen type I expression was found considerably increased (+370%) in other primary human osteoblasts exposed to PEMF for 21 days to similar frequency conditions (20 Hz, 6 mT, 0.113 mV/cm; Table S9) [110]. Up to date, the previously reported 'pyramid-response' was observed on stem cell and primary cultures, and was found along the MF strength and frequency axes. Zhou *et al.* [111] observed that ALP activity behaved like a wave in response to increasing MF strengths, presenting two maximum values at 1.8 and 3.6 mT.

Summarizing, positive differentiation effects (up to 540% [110]) were mainly achieved with MFs higher than 0.13 mT, at frequencies either low (up to 200 Hz) or high (1-6.7 kHz) (Fig. 6). Noticeably, most studies used more than 8 h/day of stimulus and, for a given MF strength and frequency, exposure times higher than 4 h/day and throughout several days may induce more cell differentiation [106]. Higher differentiation levels were found with 1.3-7 mT MF strengths [53,87] at frequencies lower than 75 Hz [93,105] (or 4-6.7 kHz for cell lines). Primary cells presented enhanced differentiation with MF strengths belonging to a wider interval (0.4-160 mT) and again at low and high frequencies [98, 100, 101, 110, 112]. For stem cells, differentiating effects were found at very different conditions in terms of MF strengths and frequencies [88, 96, 97, 113]. Importantly, in these and in primary bone cells, the amplitude of the osteogenic effects may vary in pyramid- or even wave-like manners (as consecutive pyramid-like behaviours) around key MF strengths or frequency values that render high responses [103, 108]. In this way, as the MF strength or frequency linerary increases, the maturation response is not linear, but behaves like a wave, with periodic maximum responses occurring at key MF strengths or frequency values. These type of characteristics should be further explored using systematic approaches even in other cell

models. Also and related, there are various gaps in the range of stimuli setups tested so far, namely in the 7-150 mT and 200-990 mT ranges, and in the 250-950 Hz and 1.05-3.5 kHz ranges.

Matrix mineralization

The effects on matrix mineralization may depend on the stage of maturation at which the icEMF is applied, as suggested by Diniz *et al.* [53]. An increase in matrix mineralization (51%) was observed in MC3T3-E1 cells when a PEMF stimulus (6.67 kHz, 7 mT) was applied to early culture stages (1-15 days) (Table S7) [53]. Up regulation of osteocalcin expression (up to 260%) was found for low MF strengths (<2.3 mT) at low and high frequencies (75 Hz; 4.4 kHz) when the stimuli was also applied in the early culture stages (Table S7) [92, 105]. Matrix mineralization also increased in a hBM-MSC culture at the 28th day, after a period of 15 days of PEMF stimulation (2 h/day, 7.5 Hz, 0.13 mT, 2 mV/cm) (Table S8) [88]. These cells showed increased osteocalcin expression and/or matrix mineralization in response to icEMFs of a wide range of strengths (0.13 mT to 1 T) and at a wide frequency spectrum (5 to 4.4 kHz) [88, 96, 97, 103, 114] (Table S8). Stimulating hASCs with a MF of 1.0 mT/30-45 Hz, Kang *et al.* [103] observed increased mineralization and calcium content, either in normal growth media or in OM, although always at higher amplitudes in OM conditions.

Likewise, rat calvarial osteoblastic cells presented increased matrix mineralization (c.a. +50%) either upon magnetostatic (160 mT) or PEMF stimuli (1.8 mT; Table S9) [112,115]. icEMFs of low MF strengths (up to 4.5 mT), at a wide frequency spectrum (from 50 to 4444 Hz), were able to enhance osteocalcin expression and/or matrix mineralization in these cells [100, 111, 115] (Table S9). A 'wave-like' effect was also found for matrix mineralization in response to a MF strength 0.9-4.8 mT interval and, as before for matrix maturation, the maximum values occurred at 1.8 and 3.6 mT [111].

From the surveyed studies, the most significant mineralization effects were found for MF strengths in the 1.8-7.0 mT and frequencies in the 4.4-6.7 kHz ranges [53, 92, 115]. Higher mineralization levels in primary cells were found within a wider MF strength range (1.8-160 mT) at low (up to 20 Hz [110,112]) or high (3.8-4.4 kHz [100,115]) frequencies. Stem cells enhanced mineralization at two very different MF strengths (1 T or lower than 1.8 mT), and at frequencies of various orders of magnitude [88,96,97,113]. Importantly, osteoblastic mineralization may also occur in a wave-like manner in response to MFs [111], what should be further experimentally explored. Also, at a given MF strength and frequency, a period of exposure higher than 4 h/day (for at least 3 days) may induce more cell mineralization [53, 92, 100, 105, 106, 110, 113]. Finally, to apply the stimulus at an early stage of culture appears to be a positive factor, but not sufficient, since other IC-related studies did not report matrix mineralization effects, though the stimuli were also applied in the early stages [59, 95].

As general conclusions from the studies using IC stimulation, Fig. 6 shows that frequencies up to 6.7 kHz and MF strengths up to 1 T can induce cell proliferation, matrix differentiation and/or mineralization in osteoblast-like cell lines and stem cells, respectively. However, most stimulations with positive osteogenic effects were carried out

for MF strengths lower than 7 mT. Further, much higher frequencies (up 1 GHz) can also promote positive effects on specific maturation stages, but are less explored. Also to highlight that no effects (or even negative ones) may also occur with similar stimuli if some of the stimulation parameters are altered [53, 88, 99]. Particular interesting is the data from stem and primary cells differentiation studies where nonlinear responses also occur. In these, particular frequencies and MF strengths can be highly osteogenic, while frequencies and MF strengths close to these maximum values loose part of the osteogenic effect, according to a pyramid-like, or even wave-like behaviors [103, 108, 111]. Therefore, all the experimental design must be carefully stipulated, and the stimulus settings subject to optimization, specially in what concerns these type of behaviors.

3. Factors that influence the electrical stimulation outcome

As observed above, there is great variation regarding the biological outcomes obtained when applying different electric and/or magnetic stimuli to bone cells, and several factors must be considered to compare the findings and define effective stimulation parameters. The stimulus's characteristics can strongly influence the biological outcome, including the stimulation method, the stimulus's frequency, the EF/MF strengths, and the duration of field exposure. The biological setup must also be considered, with main factors including: the cell model, the cellular density, the serum concentration, and the presence of osteoinductive factors in the cell culture media.

3.1. Stimulation method

The stimulation method (DC, CC, IC) may induce different osteogenic responses for similar frequency, EF strength, exposure time, etc. due to their dissimilar apparatuses, which result in distinct field strength distributions. Besides, these methods have specific advantages and disadvantages that must be taken into account. Due to their effects on cell migration, dcEFs have been proposed as an effective mechanism to recruit bone marrow MSCs to the sites of injury, encouraging the use of dcEFs in vivo to guide MSCs migration in bone regeneration therapies [70]. Nevertheless, there are some proposed drawbacks of applying EFs directly to cells, including the generation of electro-chemical products that contribute to increase both the number of reactive oxygen species (hydrogen peroxide, hydroxyl and oxygen ions, free radicals, etc. [116]) and the pH, which can raise the resistance to the current flow at the electrodes' surfaces [78]. Conversely, other authors proposed that these products – often referred to as faradic products – contribute to the dcEF-induced bone remodeling effects. It was hypothesized that hydrogen peroxide-stimulated osteoclastic resorption releases calcium into the medium, potentially priming the surface for increased pH-stimulated osteoblasts to lay down new bone [64].

Capacitive coupled stimulation is suitable for delivering EFs to cultured cells, and promote osteoblastic maturation in vitro. Nevertheless, as the distance between electrodes

increases, the electrodes must be supplied with higher voltages, what can result in an unsafe in vivo stimulus. This can be problematic since in the existing CC stimulators for extracorporeal therapies the electrodes must be accommodated to the human bodys limbs. However, this may be circumvented by housing electrodes inside implants, such that they can be used to deliver intracorporeal therapies [117, 118]. New solutions for the in vivo use of CC systems will certainly boost the scarce research on its effects on osteogenic differentiation.

IC stimulation has been used in clinical practice since 1979 [119]. Nevertheless it may also endanger the patients' tissues in extracorporeal therapies, since the EMF is dependent on the distance between the coil(s) and the cells/tissues. Furthermore, potential uncontrolled cell proliferation on target and adjacent tissues may occur when inappropriate stimuli are applied *in vivo* [96]. This method is being proposed in new electroinduction systems that operate inside orthopedic implants and require much lower EMFs [117].

3.2. Frequency of the stimulus

It has been postulated that the most effective PEMF frequency should be similar to that associated with normal body action frequencies. Bone physiological frequencies range between 1-2 Hz during locomotion and 15-20 Hz during the maintenance of posture [120]; upon injury, generated extracellular currents are in the range of mHz [93]. In vitro, osteogenic effects can be obtained by using electric and/or magnetic fields at either low frequencies (most up to 60-75 Hz), that simulate in vivo frequencies, or at much higher, namely up to 60 kHz. Moreover, the frequency at which the most significant effects are achieved varies between cell types, stimulation method and EF and/or MF strengths. Up to date, studies using DC stimulation induced proliferation, matrix maturation and mineralization for frequencies up to 100 Hz (Fig. 2). Nevertheless, the higher frequencies already evaluated (3 and 60 kHz) also enhanced proliferation and matrix maturation. Most studies using CC stimulation reported osteogenic effects for frequencies lower than 100 Hz, mostly bellow 20 Hz, with the exception of a tested 60 kHz frequency that induced proliferation. Some CC studies proposed a frequency-dependent effect on osteoblast-like cells proliferation. However, the frequency at which the most significant osteogenic effects are achieved varies in a cell-dependent manner [80, 83] (Fig. 4). Importantly, the small amount of studies available does not allow to infer trends for the frequencies used in DC and CC stimulation (Tables S1-S6 and Fig. 2 and 4), and systematic approaches on stimuli parameters, such as frequency, are mandatory.

Using the IC method, osteogenic effects can be found with frequencies from 7.5 Hz to 1 GHz. Nevertheless, most IC stimuli enhancing proliferation, differentiation and mineralization used low frequencies in the 7.5-75 Hz range, or high frequencies around 5 kHz. It was proposed that low-frequency PEMF stimulation (30-75 Hz) acts as an external regulatory signal, inducing both osteoblast-like cells proliferation [94] and the overexpression of proliferation markers, such as c-myc and c-fos [121]. Regarding osteoblastic maturation, some authors suggest that low frequency stimuli are only able to induce differentiation when using osteoinductive factors [97, 115]. Nevertheless, there are

reports on increased differentiation in the absence of osteoinductive cofactors [87, 92–94, 105, 106], although in the absence of OM the frequency values may need to increase (shift right) in order for the same osteogenic effect to be obtained [103]. On the other hand, high-frequency PEMF stimulation (≈1 kHz) can increase osteoblastic differentiation (ALP activity; osteocalcin and osteopontin expression; matrix mineralization) without the aid of additional co-stimulants or osteogenic media [113]. In two studies that systematically evaluated the effects of PEMF stimulation varying frequencies on stem cells' osteogenic differentiation, low frequency intervals from 5 to 150 Hz [108] and 7.5 to 75 Hz [103] were tested. In both, as the frequency initially increased, the inductive effect on differentiation also increased (from 5 to 50 Hz using hBM-MSCs [108], and from 7.5 to 30/45 Hz using ASCs [103]). However, from 50 to 150 Hz [108] and from 30/45 to 75 Hz [103], as the frequency increased, the inductive differentiation effect decreased. In the later study, the 7.5 Hz frequency was even inhibitory to hASCs osteogenic differentiation [103]. Due to this 'pyramid-like' behavior, optimal frequencies for in vitro induction of human MSCs bone differentiation must be carefully selected, as slight variations might greatly affect the osteodifferentiation outcome. Moreover, optimal frequency values also depend on the stipulated MF strengths [103], and repeated 'pyramid-like' behaviors, resulting in wave-like osteogenic response curves, may also exist as for the MF strength axis [111].

3.3. Electric and magnetic field strength of the stimulus

From the cellular level, weak EFs are preferred over strong ones as they more closely resemble the endogenously produced EFs in bone tissues (1-10 μV/cm during normal activity [94, 122]), and are able to induce beneficial responses without damaging the cells. Noteworthy, none of the studies here included, using EF strengths from 1×10^{-7} to hundreds of V/cm, reported any damage for the cells or cell death.

The EFs strengths with reported osteogenic effects ranged from 1×10^{-7} to 210 V/cm. Both these lowest and highest EF strengths were found using the CC method. However, the very low 1×10^{-7} V/cm EF strengths were only proliferative at specific (and cell-type dependent) frequency values, corresponding to intermediate frequencies around which no other frequency was osteogenic. Further, half of the CC studies applied EF strengths ranging from 13 to 60 V/cm, more similar to the DC stimuli values applied in these studies, which ranged from 0.015 to 14 V/cm (Tables S4-S6, Fig. 2 and 4). The proliferative output generally increased, although sometimes nonlinearly, with the EF strength when using ccEFs ranging from 0.02 to 60 V/cm. This increase is more consistent if no other stimulus characteristics are altered. Additionally, at a given EF strength and frequency, increasing the stimulus duration may result in an augmented cellular proliferation. Nevertheless, more systematic studies are needed to confirm any of these trends, and no trend could be depicted for osteoblastic differentiation, with differentiating EFs strengths varying from low (0.02, 0.1 V/cm) to high (60, 210 V/cm).

Most of the MF strengths delivered by IC stimulation were lower than 3 mT. Although no explanation was found in the literature, it may involve protection of cells from damage when using stronger MFs. The icMF strengths that induced proliferative effects were

mainly lower than 2.3 mT, and in the 0.1-1.8 mT range for stem and 0.05-1.5 mT for primary cells. Similarly, positive differentiation and mineralization responses were obtained with MF strengths within the 0.13-7.0 mT range. However, it is important to highlight that no studies were found using MF strengths in the 7-150 mT and the 200-990 mT intervals. Various studies using IC stimulation observed that not only the time of exposure to the stimulus could influence the outcome, but also the period at which the stimulus was delivered [53, 87, 88, 91, 94, 98, 100, 123]. Further, two systematic studies, one on adipose-derived MSCs and other in primary osteoblasts, revealed that at a given frequency the osteogenic response to a linear variation of the EF strength may be non-linear, as above for the frequency variation. The osteogenic response may in fact occur in a symmetric 'pyramid-like' curve, alone or repeated along the EF strength axis, as in a wave-like curve, what again demonstrates the need for systematic approaches of this parameter in each experimental setup [103, 111].

3.4. Cell model

A number of factors, such as developmental stage, species, skeletal site of origin, state of differentiation, and phenotype (as non-transformed versus transformed), may contribute to variations in the osteogenic response to the electric and/or magnetic stimulation. These factors are suggested to influence the cell membrane composition or surface charge density, altering the interaction between the biological system and the applied EFs and/or MFs [80]. The selection of the appropriate and most relevant in vitro osteoblast model for studying the effect of electrical and/or magnetic stimulation in bone is thus of utmost importance. Various cell culture models have been employed, including primary cells from different species, mesenchymal and other stem cells, and immortalized cell lines. Each cell model presents advantages and disadvantages that need to be considered before performing the biological assays and upon evaluation of the stimulation outcome.

Human osteosarcoma cell lines (SaOS-2, MG63, TE-85) are easily available, do not require time consuming isolation or ethical approval, and provide reliable reproducibility [124]. However, these transformed cell lines present unrepressed replicative activity and fail to display the normal coupling of growth arrest and differentiation [125]. Several studies have been performed using these cell lines to study migration [65, 69], as well as the three stages of osteoblast maturation [58, 80, 87, 89–92, 105, 106, 121, 126]. Even though they are not considered good models to study osteoblast differentiation, there are also reports of increased ALP activity and matrix mineralization upon CC and IC stimulation of SaOS-2 and MG63 cell lines [58,87,92,105,106]. MC3T3-E1 is a non-transformed cell line derived from newborn murine calvariae, which has been reported to display osteoblast-like characteristics after repeated culturing passages. It therefore provides an useful model to study the transition between proliferation and differentiation, the molecular mechanism of osteoblastic maturation, and the formation of bone-like extracellular matrix [125]. These cells are frequently used as models to study proliferation upon CC stimulation [79, 81, 82], and proliferation and differentiation upon IC stimulation [53, 98, 102].

Human mesenchymal stromal/stem cells have stem cell-like characteristics, including

self- renewal, and are able to differentiate into bone, cartilage, fat and skeletal tissues [52]. MSCs can be derived from a variety of different sources, including bone marrow (BM), adipose tissue and peripheral blood. hBM-MSCs are found in the stromal compartment of bone marrow and play a vital role in the process of bone regeneration [71]. Since these cells are recruited to the fracture site to proliferate and differentiate into osteoblasts, they are good models to study the effectiveness of electrical and/or magnetic stimulation in bone regeneration. While DC stimulation experiments have studied hMSCs migratory responses [70, 71], CC and IC stimulation have focused on their proliferation and osteoblastic differentiation under osteogenic media [52, 71, 75, 86, 88, 95–97, 103, 104, 108, 123]. It has been suggested that hMSCs migratory responses are more pronounced than in primary osteoblasts, as they present stiff actin fibers that are more susceptible to external EFs [62].

The magnitude of the osteogenic response of human MSCs to an EF/MF stimulus also depends on the origin of the cells. Following an IC stimulus of 2 mT and 75 Hz for 21 days (in OM), bone-marrow derived MSCs responded significantly better than adipose-derived MSCs (ASCs) in terms of proliferation, osteogenic differentiation and matrix mineralization. These were analyzed using an extensive battery of osteogenic markers [123]. The authors proposed that, although ASCs and BM-MSCs share many biological characteristics, there are some differences in their differentiation potential, transcriptome, proteome, and immunomodulatory activity that result in differential efficiency in the PEMF to induce MSCs commitment into osteoblasts, higher for BM-MSCs [123]. Nevertheless, ASCs and BM-MSCs osteodifferentiation, follow similar patterns, such as the pyramid-like responses, in which the highest observed osteogenic responses were observed at frequencies in the 30-45 Hz range for hASCs [103] and 50 Hz for hB-MSCs [108].

Primary cells reflect the *in vivo* niche and have therefore more preclinical applicability [124]. As with the other cell types, significant osteogenic responses were achieved by stimulating primary bone cells with DC, CC and IC stimulation (Tables S3, S6, S9). However, some drawbacks exist regarding the use of primary osteoblast cultures. Firstly, differences between species complicate the extrapolation to human clinical disease and treatment outcomes [124]. Secondly, the presence of various cell populations (fibroblasts, chondroblasts, and osteoblasts) in isolated calvarial and primary cell cultures, limits the interpretation of the results [125]. Finally, subcultivation of primary cultures may result in loss of osteoblast specific characteristics [125].

3.5. Cell density and maturation stages

The state of cell confluence (density) upon stimulation influences cell-environment and cell-cell communication and, consequently, the cellular response to the stimuli [94]. The growth of adherent cultured cells, such as osteoblast-like cells and stem cells, comprises various stages, including: a 'lag' phase of cell adaptation to the culture conditions; a 'logarithmic (log) growth' phase of active proliferation and exponential increase in cell density; and a 'plateau' phase, when cellular proliferation slows down due to the occupation of all the available space ('confluent cells'). The duration of both 'lag' and 'log' phases

greatly depends on the initial cell seeding density. Enhanced proliferation is expected to occur when cells are stimulated in the 'log growth' phase, i.e., when the stimuli is applied in non-confluent cultures [53, 55, 59, 63, 76, 79, 80, 89–91]. This general rule may not apply to some osteoblastic cell lines, which partially lose the contact-contact inhibition feature that impedes growth when confluence is reached. Consequently, increases in these cells' proliferation can be observed in two days post-confluent cultures [81, 82]. Additionally, decreased proliferation rates were observed even when electrical stimulation was applied to non-confluent cultures [87, 88, 93].

McLeod and colleagues [94] have reported that bone cell function is modulated by EFs in a cell density-dependent manner: no effect on cell activity was observed for sparse cultures (lower than 50×10^3 cells.cm^{-2}), whereas denser cultures (in the 50-350×10^3 cells.cm^{-2} range) had decreased proliferation (25%) and doubled ALP activity. Nevertheless, up-regulation of ALP activity disappeared in more highly confluent cultures. Alterations in the internal biological and physical states were advanced as two possible interpretations for this cell density-dependency [94]. As regards the cells physical state, gap junctional coupling between cells (i.e. increased cell-cell communication with increasing cell density) alters the magnitude of the cellular responses to extracellular EFs [93,107]. Gap junctional coupling provides electrical continuity within networks of cells, allowing ions to pass from cell to cell via their channels [93]. Another possible justification is the influence of shape and size of individual cells in the overall population, as they may affect the EFs distribution around the cells, as well as the amount of the charged cell surface exposed to the field [75, 94]. In low-density cultures, cells are only sparsely distributed over the bottom of the culture dish, and leave some areas in direct contact with the highly conductive culture medium. As cell density increases towards maximum confluence, the cellular population generates a compact layer of high electrical resistance, stimulating the growth of the organic extracellular matrix; this matrix further enhances resistivity, and hence the osteogenic efficiency of the electric stimulation [55]. Another study, conducted by Kaivosoja and colleagues [126], points to the importance of low density cultures to induce differentiation, as spreading of adherent cells exerts tension in actin cytoskeleton, which might induce osteogenesis.

The differentiation stage at which cells are stimulated is also important on the effect of PEMF stimulation on gene expression and mineralization [114]. Following an initial up-regulation period, Jansen *et al.* [104] observed a down-regulation of osteogenic gene markers in BMSCs exposed to PEMF stimulation, suggesting that the strongest effect on differentiation is exerted in the period prior to mineralization. Due to the lack of studies in this scope, it would be very interesting to perform studies aiming to identify correlation(s) between the period at which the stimulus is applied and its osteodifferentiating abilities.

3.6. Serum concentration and osteoinductive factors

Together with cell density, the presence of serum and osteoinductive factors in the cell culture media can also greatly affect the osteogenic response. Serum consists of a mixture of hundreds of proteins, including several factors needed for the proliferation of various

cells in culture [127]. Its inclusion in the culture media can hence influence the effects of electrical and/or magnetic stimulation. The presence of serum in the culture media is suggested to reverse cell migration and actin distribution in response to a DC stimulus of 2 V/cm EF strength [62]. The enhancement of bone cell proliferation in response to EF stimulation is often associated with low concentrations (lower than 0.2%) or serum-free culture media, since low serum concentration decreases the cells' basal growth rate [63, 83, 128]. Accordingly, high serum concentrations may inhibit EF effects after longer exposures to this type of stimulus [94]. However, short periods (30 min) of PEMF exposure are able to stimulate the proliferation of human osteosarcoma cell lines (TE-85 and MG63) grown in normal 10% serum-containing media [91]. Hence, the influence of serum concentration in the outcome of electrical and magnetic stimulation depends on the duration of the experiment and on the ability of each cell type to grow under serum-free conditions.

Several biochemical compounds, such as ascorbic acid, β-gylcerophosphate, dexamethasone and bone morphogenetic protein 2 (BMP-2) can be added to the culture medium and act as pro-osteogenic cofactors to stimulate bone cell function [52, 66, 77]. Consequently, when cultures are maintained in differentiation (or osteoinductive) media, containing osteogenic factors, better differentiation outputs are obtained though proliferation might be impaired or delayed [52]. For example, either IC stimulation or OM alone are able to induce hASCs matrix maturation and mineralization, but the simultaneously treatment of cells with both results in a synergistic effect [103]. The presence of OM can greatly increase the regulatory effect of IC stimulation on osteogenic genes (COL-I, RUNX2, OSX and OC), an effect reproduced by adding growth factors such as BMP-2 [97, 103]. Further, in this study the presence of OM decreased the MF strength and frequency that induced the highest osteogenic responses, from around 2.0 mT at 45 Hz (NSM conditions) to 1.0 mT at 30 Hz (OM conditions) [103].

4. Transduction of electrical signals inside bone cells

The identification of the mechanisms that mediate EF- and/or MF-induced cellular responses would greatly facilitate the selection of the appropriate stimulation parameters, such as strength, frequency and exposure duration [62]. Several molecular mechanisms have been proposed, but there is still much uncertainty. DC stimulation delivering EFs at low frequency are likely to initiate molecular signaling pathways at the cell surface, as these are unable to penetrate into the cell due to the high resistivity of the cell membrane, with a conductivity $\approx 1\times10^{6}$-1×10^{8} times smaller to the cytoplasm one [62]. Some authors have thus explored the effects of EFs in primary messengers, such as growth factors' metabolism, while others have focused on studying second messengers and effectors. The regulation of intracellular calcium levels is possibly a key cellular event involved in the transduction of electric and/or magnetic stimuli, but heat shock proteins are also emerging as potential key factors mediating stimulatory cellular effects.

4.1. Calcium as a second messenger of osteogenic effects induced by electromagnetic fields

Calcium acts as a second messenger in many biochemical signal-transduction pathways, and appears to mediate cell responses to EFs and/or MFs. Strong dcEFs (higher than 10 V/cm) may cause membrane depolarization in osteoblasts and activate voltage-gated Ca^{2+} channels (VGCCs), which in turn induce rapid Ca^{2+} influxes across the membrane [69, 72]. However, the application of smaller EFs is not expected to cause VGCC activation in the plasma membrane. Accordingly, VGCCs inhibition with Verapamil or $CdCl_2$ blocks the immediate increase of intracellular calcium levels that follows the application of a strong EF strengths (10 V/cm), but fails to prevent the induction of intracellular calcium levels by an EF strength of 2 V/cm [69, 72].

Other mechanisms have been put forward to explain the changes in calcium levels upon stimulation with weaker EFs, including stimulation of stretch-activated cation channels (SACCs) and cell surface receptors coupled to phospholipase C (PLC) [72]. SACCs are non-specific channels that can detect and transduce mechanical forces into biochemical signals (influx of extracellular calcium) and therefore modulate cell locomotion [72, 129]. Electric stimuli may activate SACC by altering cellular mechanisms that induce SACC redistribution and clustering (i.e., electroosmosis) [72]. However, the treatment of human osteoblasts with a SACC's blocker (Gd^{3+}) partially inhibited EF-induced intracellular calcium concentration ($[Ca^{2+}]i$), suggesting the involvement of other mechanisms [72]. PLC selective inhibition prevents $[Ca^{2+}]i$ induction by applying a 2 V/cm EF, suggesting that an electric stimulation induces conformational transitions on specific PLC-coupled receptors [72, 74]. PLC consequent activation leads to the formation of membrane diacylglycerol (DAG), which stimulates PKC and soluble inositol trisphosphate IP3. The latter diffuses rapidly in the cytosol and binds to its receptors (e.g. in the endoplasmic reticulum), stimulating Ca^{2+} release from internal stores [72, 130]. Therefore, Khatib *et al.* [72] proposed a model in which dcEF-induced intracellular calcium are mediated by extracellular Ca^{2+} influx via mechanically operated SACCs, and by PLC-dependent Ca^{2+} release from internal stores.

Less is discussed regarding the involvement of calcium in the effects of CC and IC stimulation. However, Brighton and colleagues [82] suggest that the initial transduction of CC and IC stimuli is different. While the signal transduction of CC stimuli occurs at the bone cell membrane through VGCCs, the EMFs applied by IC stimulation pass through the bone cell membrane and generate an EF within the cytosol, which in turn induces the release of Ca^{2+} from internal stores [82].

Effects of Ca^{2+} on cytoskeleton dynamics and migration

As described before, EFs generated by DC stimulation induce cell orientation and migration in a calcium-dependent manner (Tables S1-S3). Alterations in cytoskeleton and membrane dynamics, resultant from increased $[Ca^{2+}]i$ and decreased ATP levels, are put forward to explain the regulation of cell mechanics in response to electric stimulation [62].

After cells exposure to a 2 V/cm dcEF for 60 min in serum-free HBSS, disassembly

of actin scaffolds was visible in both primary osteoblasts and hMSCs, similarly to what occurred upon cell treatment with ionomycin [62]. The application of the same stimulus also caused ATP depletion, possibly due to ATP consumption or ATP release to the extracellular medium, which inhibits actin-linker proteins (such as Ezrin/radixin/moesin (ERM) proteins), causing membrane separation from the cytoskeleton and further decreases in membrane tension [62]. Additional activation of myosin light chain kinase (MLCK), by increased [Ca^{2+}]i, triggers actin-activated myosin ATPase that regulates cell contraction and migration [69]. The cellular migration direction, which is species- and cell type-specific (section 2.1.2), is thought to be determined by differential polarization of the zone of the cell membrane that faces the anode and the cathode [69, 76]. Nevertheless, it remains unclear how and why [Ca^{2+}]i rises on opposite sides of the membrane. One possible explanation involves local activation of various charged receptors or ion channels acting as voltage sensors [69].

Ca^{2+} effects on proliferation

Elevated intracellular calcium levels may also transduce electric signals into bone cell proliferation. Increased [Ca^{2+}]i induces an increase in phospholipase A2 [82]. The products generated by this enzyme activate the prostaglandin E2 synthesis, which acts as an autocrine and/or paracrine factor to stimulate bone cell proliferation [82]. Additionally, an increase in cytosolic calcium also leads to calmodulin activation, an effector known to promote nucleotide synthesis [82, 99].

Ca^{2+} effects on differentiation

Concomitant changes in Ca^{2+} dynamics and in MAP kinases activation state have been suggested to induce hMSC differentiation in response to dcEF exposure. A prolonged exposure to a 0.1 V/cm dcEF might induce enzymatic activity of assembled proteins involved in cellular adhesion, such as focal adhesion kinase (FAK), paxillin, vinculin and src, which in turn induce MAP kinase activation [74]. Additionally, calcium might influence osteogenesis by playing a structural role of extracellular matrix formation [131].

4.2. Growth factors in electromagnetic signal transduction

Human bone matrix is known to contain many polypeptide growth factors, which bind to their high affinity receptors and elicit multiple effects besides stimulation or inhibition of growth [132]. These molecules may also initiate apoptosis, differentiation and gene expression not only in a specific target cell, but also in the neighboring cells [133]. Several investigators have already studied the synthesis and secretion of insulin growth factor (IGF)-II, transforming growth factor β1 (TGF-β1), and bone morphogenetic proteins (BMPs) on electrically- and/or magnetically-stimulated bone cells.

Insulin growth factor II

IGF-II plays a key role in mammalian growth, influencing fetal cell division and differentiation, and possibly metabolic regulation [134]. As the predominant bone-derived mitogen, it is most probably involved in mediating EF effects on bone cell proliferation

[80, 89, 90]. Fitzsimmons *et al.* [80, 89] proposed that EFs induce the release of IGF-II into the medium, through a calcium-dependent mechanism, in sufficient concentrations to promote cell proliferation. Upon ccEF exposure at 14 Hz for 30 minutes, IGF-II levels were observed to increase in the cell culture medium, reaching a plateau (1.10 $ng.ml^{-1}$) approximately 1 h after CC exposure. Additionally, an accumulation of IGF-II transcripts was also observed within a few hours of exposure [80]. In a TE-85 cell culture exposed to CMF at 15.3 Hz for 10 min, the IGF-II medium levels increased up to 3.5 $ng.ml^{-1}$ [89]. Subsequent studies also revealed the increased number of IGF-II receptors in TE-85 cell's membrane subjected to CMF stimuli at low frequencies [128].

Transforming growth factor β

TGF-β superfamily is composed of extracellular signaling molecules that play widespread roles in development regulation [135]. Additionally, TGF-β is an important growth factor involved in tissue remodeling and wound healing, as it induces fibronectin and collagen production, thus regulating cell matrix deposition [136]. TGF-β can be released from cells as a latent complex of dimers attached to their propeptides and to TGF-β-associated proteins. Proteolytic activity or interaction with integrin proteins releases and activates the TGF-β ligand [137]. The levels of TGF-β1 mRNA and activity significantly increase after 1 day of CC exposure (60 kHz, 20 mV/cm) or 8 h of PEMF stimulation (4.4 kHz, 1.8 mT) [81, 92]. Two observations suggest that this signaling molecule mediates electrically- and/or magnetically-induced osteoblast differentiation effects rather than proliferative ones. Zhuang *et al.* [81] failed to demonstrate a connection between proliferation and increased TGF-β1 activity in CC-stimulated MC3T3 cells. Lohmann *et al.* [92] suggested a correlation between collagen deposition and the levels of latent TGF-β1, as they both peak simultaneously in cells stimulated with an IC apparatus. PEMF induces TGF-β1 levels during the maturation period until the beginning of mineralization, upon which the levels drop and cannot be up-regulated by IC stimulation [104].

Bone morphogenetic proteins

BMP is another member of the TGF-β superfamily with the ability to induce bone formation in cultured cells [135]. Some authors support that PEMF's positive *in vivo* osteogenic effects may be secondary to an endogenous stimulation of these BMP osteoinductive cytokines [104]. Approximately 20 isoforms of BMP have been identified with varying osteoinductive potentials. The most osteogenic BMPs are BMP-2, BMP-6, BMP-9, BMP-4 and BMP-7. BMP-2 induces bone formation and promotes osteoblastic proliferation, and their expression levels are up-regulated upon CC and IC stimulation of rat-derived primary osteoblasts [100, 115, 138]. PEMF was reported to strongly induce BMP-2 until the day 9, at the onset of the mineralization process [104]. Other study, using icEMFs at high frequency to promote osteogenic differentiation of C3H10T1/2 mouse stem cells, also observed BMPs up-regulation at specific differentiation phases. While BMP-6, BMP-7 and BMP-9 expression levels increased during the early and late differentiation phases (days 3 and 10), BMP-2 and BMP-4 levels increased only in the later differentiation

stages (days 7, 10 and 14) [113]. In addition, BMP-2 and BMP-4 may also mediate the osteoinductive effects of magnetic fields at low frequencies [139].

4.3. A role for Heat Shock proteins in electrical signal transduction

Heat shock proteins react to stress conditions in order to maintain cellular homeostasis, regulate protein folding, degradation and secretion, and are involved in differentiation responses. Two heat shock proteins – hsp27 and hsp70 – have been studied as potential mediators of electrical stimuli-induced proliferation and osteodifferentiation effects. Hronik-Tupaj *et al.* [52] observed up-regulation of hsp27 mRNA levels on days 10, 15 and 20 in hMSCs stimulated with dcEFs. Both in control and stimulation groups, hsp27 peaked at the 10th day; however, in the stimulated group hsp27 levels were maintained high, while in the control group a significant drop occurred from day 10 on. Hsp70 mRNA levels were only significantly up-regulated in comparison to the control group at day 20. These authors proposed the increased hsp27 to explain the morphological and biochemical changes in osteoblasts upon electrical stimulation, as this protein affects gene expression, differentiation, growth, and actin cytoskeleton reorganization [52, 140].

5. Conclusions and future perspectives

The translational value of electric and magnetic stimulation for osteoporosis, fracture repair, and osseointegration therapies is currently unknown but of high potential. An extensive understanding of the cellular responses to electrical and magnetic fields is essential for optimizing stimuli parameters for therapeutic stimulation of the bone tissue. This requires improving the state-of-the-art by researching the influence of a broad range of values for each parameter and stimulation method. The ability of electrical and magnetic stimulation to promote bone remodeling in vitro was here explored. A wide variety of stimuli setups were osteogenic (increased proliferation, matrix maturation and/or matrix mineralization) for various cell model systems (immortalized lines, stem cells, and primary cultures), using DC, CC or IC stimulation methods. Only isolated trends could be observed regarding the stimuli characteristics and the osteogenic responses. However, a few systematic studies suggest that EF strengths and frequencies may induce 'pyramidal' osteogenic responses, or 'wave-like' ones resulting from repeats of these pyramid-like behaviors over the EF strength-axis and frequency-axis. Indeed, these response curves may explain why linear increases or decreases in these parameters are not linearly permissive or inhibitive. More systematic studies of the stimulus' parameters, including the stimulus exposure time, are thus crucial, along with studies of a wide range of EF/MF strengths and frequencies not yet explored. The osteogenic response of a successful EF/MF strength/frequency pair should also be screen at nearby values of strength and frequency, for therapeutic optimization purposes. Further, since the aim is to translate the work to *in vivo* assays and some stimuli parameters may deliver the desired opposite effects to

osteoclast and osteoblast activities [110], the effects of electrical and magnetic stimulation on osteoclasts should be studied more thoroughly. Methodology standardization will facilitate the development and clinical application of electrical and/or magnetic stimulation devices, such as medical devices with ability to control the bone remodeling unbalances, and active orthopaedic implants. This later could be able to promote personalized osseointegration in a safe, reproducible and automated manner using these biophysical stimulations. Research on permanent magnets is also pertinent, since various implantable medical devices have been proposed to stimulate osteoregeneration by using these methods [141, 142]. However, we must highlight that CC and IC stimulators can deliver more controllable stimuli to bone. IC stimulation has been the most used method to study the ability of electromagnetic fields to promote osteogenesis; however, no feasible solutions have yet been found for their use in highly controllable stimuli delivery systems, as for the use of biophysical stimulators inside implantable devices to control osteointegration and combat osteoporosis [36, 143]. In a nearby future, innovative electrical stimulation systems currently under design might fulfil such purposes [144]. Currently, we are designing and testing new CC stimulators to be used in intracorporeal systems able to administer personalized stimulation therapies.

Acknowledgments

This work is supported by the Institute for Biomedicine iBiMED UID/BIM/04501/2013 and funded by FEDER funds through the Operational Programme Competitiveness Factors (COMPETE) and the Portuguese Foundation for Science and Technology (FCT) - project reference EXPL/EMS-SIS/2128/2013; grant reference SFRH/BD/78414/2011.

References

[1] L. March, E. U. Smith, D. G. Hoy, M. J. Cross, L. Sanchez-Riera, F. Blyth, R. Buchbinder, T. Vos, A.D. Woolf, Burden of disability due to musculoskeletal (MSK) disorder, Best Practice & Research Clinical Rheumatology 28(3)(2014) 353-366.

[2] A. D. Woolf, J. Erwin, L. March, The need to address the burden of musculoskeletal conditions, Best Practice & Research Clinical Rheumatology 26(2)(2012) 183-224.

[3] A. D. Woolf, B. Pfleger, Burden of major musculoskeletal conditions, Bulletin of the World Health Organization 81(9)(2003) 646-656.

[4] J. Behari, Biophysical bone behaviour: Principles and applications, John Wiley & Sons, 2009.

[5] S. C. Marks, P.R. Odgren, Principles of Bone Biology, 2nd Edition, Academic Press, 2002, Ch. Structure and Development of the Skeleton.

[6] E. Fukada, I. Yasuda, On the piezoelectric effect of bone, Journal of the Physical Society of Japan 12(10)(1957) 1158-1162.

[7] D. Gross, W. S. Williams, Streaming potential and the electromechanical response of physiologically-moist bone, Journal of Biomechanics 15(4)(1982) 277-295.

[8] C. A. Bassett, R. O. Becker, Generation of electric potentials by bone in response to mechanical stress, Science 137(3535) (1962) 1063-1064.

[9] I. Yasuda, The classic fundamental aspects of fracture treatment, Clinical Orthopaedics and Related Research 124(1977) 5-8.

[10] G. W. Hastings, F. A. Mahmud, The electromechanical properties of fluid-filled bone: A new dimension, Journal of Materials Science: Materials in Medicine 2(2)(1991) 118-124.

[11] Z. B. Friedenberg, C. T. Brighton, Bioelectric potentials in bone, The Journal of Bone & Joint Surgery 48(5)(1966) 915-923.

[12] S. Saha, P. A. Williams, Electric and dielectric properties of wet human cancellous bone as a function of frequency, Annals of Biomedical Engineering 17 (1989) 143-158.

[13] S. Saha, P. A. Williams, Electric and dielectric properties of wet human cortical bone as a function of frequency, IEEE Transactions on Biomedical Engineering 39(12)(1992) 1298-1304.

[14] P. Williams, S. Saha, The electrical and dielectric properties of human bone tissue and their relationship with density and bone mineral content, Annals of Biomedical Engineering 24(2)(1996) 222-233.

[15] C. Gabriel, S. Gabriel, E. Corthout, The dielectric properties of biological tissues: I. Literature survey, Physics in Medicine and Biology 41(11)(1996) 2231-2249.

[16] J. Sierpowska, M. J. Lammi, M. A. Hakulinen, J. S. Jurvelin, R. Lappalainen, J. Töyräs, Effect of human trabecular bone composition on its electrical properties, Medical Engineering & Physics 29(8)(2007) 845-852.

[17] G. T. Swanson, J. F. Lafferty, Electrical properties of bone as a function of age, immobilization and vibration, Journal of Biomechanics 5(3)(1972) 261-266.

[18] S. Kumaravel, S. Sundaram, Monitoring of fracture healing by electrical conduction: A new diagnostic procedure, Indian Journal of Orthopaedics 46(4)(2012) 384-390.

[19] L. R. Nascimento, S. M. Michaelsen, L. Ada, J. C. Polese, L. F. Teixeira-Salmela, Cyclical electrical stimulation increases strength and improves activity after stroke: a systematic review, Journal of Physiotherapy 60(1)(2014) 22-30.

[20] C. Zeng, H. li, T. Yang, Z.-h. Deng, Y. Yang, Y. Zhang, G.-h. Lei, Electrical stimulation for pain relief in knee osteoarthritis: systematic review and network meta-analysis, Osteoarthritis and Cartilage 23(2)(2015) 189-202.

[21] K. Robb, S. G. Oxberry, M. I. Bennett, M. I. Johnson, K. H. Simpson, R. D. Searle, A cochrane systematic review of transcutaneous electrical nerve stimulation for cancer pain, Journal of Pain and Symptom Management 37(4)(2009) 746-753.

[22] J. A. Obes Deep-brain stimulation of the subthalamic nucleus or the pars interna of the globus pallidus in Parkinson's disease, The New England Journal of Medicine 345(13)(2001) 956-963.

[23] L. E. Augustinsson, P. Bohlin, P. Bundsen, C. A. Carlsson, L. Forssman, P. Sjöberg, N. O. Tyreman Pain relief during delivery by transcutaneous electrical nerve stimulation, Pain 4(1)(1977) 59-65.

[24] A. L. Benabid, A. Benazzouz, D. Hoffmann, P. Limousin, P. Krack, P. Pollak, Long-term electrical inhibition of deep brain targets in movement disorders, Movement Disorders 13(3)(1998) 119-125.

[25] R. Melzack, Prolonged relief of pain by brief, intense transcutaneous somatic stimulation, Pain 1(4)(1975) 357-373.

[26] M. Zhao, B. Song, J. Pu, T. Wada, B. Reid, G. Tai, F. Wang, A. Guo, P. Walczysko, Y. Gu, T. Sasaki, A. Suzuki, J. V. Forrester, H. R. Bourne, P. N. Devreotes, C. D. McCaig, J. M. Penninger, Electrical signals control wound healing through phosphatidylinositol-3-OH kinase-γ and PTEN, Nature 442 (2006) 457-460.

[27] I. D. Gelalis, A. N. Politis, C.M. Arnaoutoglou, A. V. Korompilias, E. E. Pakos, M. D. Vekris, A. Karageorgos, T. A. Xenakis, Diagnostic and treatment modalities in nonunions of the femoral shaft. A review, Injury 43(7) (2012) 980-988.

[28] J. Reis, C. Frias, C. Canto e Castro, M. L. Botelho, A. Torres Marques, J. A. Simões, F. Capela e Silva, J, Potes, A new piezoelectric actuator induces bone formation in vivo: a preliminary study, Journal of Biomedicine and Biotechnology 2012(2012) 1-7.

[29] J. C. Gan, P. A. Glazer, Electrical stimulation therapies for spinal fusions: current concepts, European Spine Journal 15(9)(2006) 1301-1311.

[30] M. Griffin, A. Bayat, Electrical stimulation in bone healing: critical analysis by evaluating levels of evidence, Eplasty 11 (2011) e34.

[31] C. T. Brighton, G. T. Tadduni, S. R. Pollack, Treatment of sciatic denervation disuse osteoporosis in the rat tibia with capacitively coupled electrical stimulation. Dose response and duty cycle., The Journal of Bone & Joint Surgery 67 (7) (1985) 1022-1028.

[32] C. T. Brighton, G. T. Tadduni, S. R. Goll, S. R. Pollack, Treatment of denervation/disuse osteoporosis in the rat with a capacitively coupled electrical signal: effects on bone formation and bone resorption, Journal of Orthopaedic Research 6(5)(1988) 676-684.

[33] C. T. Brighton, C. E. Nichols, G. A Arangio, Amelioration of oxygen-induced osteoporosis in the in vitro fetal rat tibia with a capacitively coupled electrical field, Journal of Orthopaedic Research 3(3)(1985) 311-320.

[34] C. T. Rubin, K. J. McLeod, L. E. Lanyon, Prevention of osteoporosis by pulsed electromagnetic fields, The Journal of Bone & Joint Surgery 71(3)(1989) 411-417.

[35] K. Chang, W. H-S. Chang, M-T. Tsai, C. Shih, Pulsed electromagnetic fields accelerate apoptotic rate in osteoclasts, Connective tissue research 47(4)(2006) 222-228.

[36] C. T. Rubin, S. Judex, Y-X. Qin, J. Rubin, Osteoporosis, 4th Edition, Academic Press, 2013, Ch. Prevention of Osteoporosis by Physical Signals: Defining a Potential Role for Nondrug Strategies in the Treatment of Musculoskeletal Injury and Disease.

[37] R. Marsell, T. A. Einhorn, The biology of fracture healing, Injury 42(6)(2011) 551-555.

[38] C. Andrew, L. Bassett, Development and Growth, 2nd Edition, Academic Press, 1971, Ch. Biophysical Principles Affecting Bone Structure.

[39] W. J. Sharrard, A double-blind trial of pulsed electromagnetic fields for delayed union of tibial fractures, The Bone & Joint Surgery 72(3)(1990) 347-355.

[40] W. J. Sharrard, M. L. Sutcliffe, M. J. Robson, A. G. Maceachern, The treatment of fibrous non-union of fractures by pulsing electromagnetic stimulation, The Bone & Joint Surgery 64(2)(1982) 189-193.

[41] W. G. de Haas, J. Watson, D. M. Morrison, Non-invasive treatment of ununited fractures of the tibia using electrical stimulation, The Bone & Joint Surgery 62-B(4)(1980) 465-470.

[42] C. B. Goodwin, C. T. Brighton, R. D. Guyer, J. R. Johnson, K. I. Light, H. A. Yuan, A double-blind study of capacitively coupled electrical stimulation as an adjunct to lumbar spinal fusions, Spine 24(13)(1976) 1349-1356.

[43] W. J. Kane, Direct Current Electrical Bone Growth Stimulation for Spinal Fusion, Spine 13(3)(1988) 363-365.

[44] N. Wu, Y. Lee, D. Segina, H. Murray, T. Wilcox, L. Boulanger, Economic burden of illness among US patients experiencing fracture nonunion, Orthopaedic Research and Reviews 5 (2013) 21-33.

[45] P. G. Coelho, R. Jimbo, "Osseointegration of metallic devices: current trends based on implant hardware design, Archives of Biochemistry and Biophysics 561(2014) 99-108.

[46] M. P. Soares dos Santos, J. A. Ferreira, A. Ramos, J. A. Simões, Active orthopaedic implants: towards optimality, Journal of the Franklin Institute 352(3)(2015) 813-834.

[47] A. J. Carr, O. Robertsson, S. Graves, A. J. Price, N. K. Arden, A. Judge, D. J. Beard, Knee replacement, Lancet 379(2012) 1331-1340.

[48] M. P. Soares dos Santos, J. A. Ferreira, A. Ramos, J. A. Simões, R. Morais, N. M. Silva, P. M. Santos, M. C. Reis, T. Oliveira, Instrumented hip joint replacements, femoral replacements and femoral fracture stabilizers, Expert Review of Medical Devices 11(6)(2014) 617-635.

[49] V. Goriainov, R. Cook, J. M. Latham, D. G. Dunlop, R. O. Oreffo, Bone and metal: an orthopaedic perspective on osseointegration of metals, Acta Biomaterialia 10(10)(2014) 4043-4057.

[50] R. Dimitriou, G. C. Babis, Biomaterial osseointegration enhancement with biophysical stimulation, Journal of Musculoskeletal and Neuronal Interactions 7(3)(2007) 253-265.

[51] M. Hronik-Tupaj, D. L. Kaplan, A Review of the responses of two- and three-dimensional engineered tissues to electric fields, Tissue Engineering Part B: Reviews 18(3) (2012) 167-180.

[52] M. Hronik-Tupaj, W. L. Rice, M. Cronin-Golomb, D. L Kaplan, I. Georgakoudi, Osteoblastic differentiation and stress response of human mesenchymal stem cells exposed to alternating current electric fields, Biomedical Engineering Online 10(9)(2011) 1-22.

[53] P. Diniz, K. Shomura, K. Soejima, G. Ito, Effects of pulsed electromagnetic field (PEMF) stimulation on bone tissue like formation are dependent on the maturation stages of the osteoblasts, Bioelectromagnetics 23(5)(2002) 398-405.

[54] G. S. Stein, J. B. Lian, J. L. Stein, A. J. Van Wijnen, M. Montecino, Transcriptional control of osteoblast growth and differentiation, Physiological Reviews 76(2)(1996) 593-629.

[55] M. Hartig, U. Joos, H-P Wiesmann, Capacitively coupled electric fields accelerate proliferation of osteoblast-like primary cells and increase bone extracellular matrix formation in vitro, European Biophysical Journal 29(7)(2000) 499-506.

[56] S. Pina, S. I. Vieira, P. Rego, P. M. Torres, O. A. da Cruz e Silva, E. F. da Cruz e Silva, J.M. Ferreira, Biological responses of brushite-forming Zn-and ZnSr-substituted β-tricalcium phosphate bone cements, European Cells and Materials 20 (2010) 162-177.

[57] S. C. Cowin, Bone mechanics handbook, 2nd Edition, CRC Press 2001, Ch. Integrated Bone Tissue Physiology: Anatomy and Physiology.

[58] M. Griffin, A. Sebastian, J. Colthurst, A. Bayat, Enhancement of Differentiation and Mineralisation of Osteoblast-like Cells by Degenerate Electrical Waveform in an In Vitro Electrical Stimulation Model Compared to Capacitive Coupling, PloS One 8(9)(2013) e72978.

[59] W. H-S. Chang, L-T. Chen, J-S. Sun, F-H. Lin, Effect of pulseburst electromagnetic field stimulation on osteoblast cell activities, Bioelectromagnetics 25(6)(2004) 457-465.

[60] Q. Q. Hoang, F. Sicheri, A. J. Howard, D. S. Yang, Bone recognition mechanism of porcine osteocalcin from crystal structure, Nature 425(6961)(2003) 977-980.

[61] H-P. Wiesmann, M. Hartig, U. Stratmann, U. Meyer, U. Joos, Electrical stimulation influences mineral formation of osteoblast-like cells in vitro, Biochimica et Biophysica Acta (BBA) - Molecular Cell Research 1538(1)(2001) 28-37.

[62] I. Titushkin, M. Cho, Regulation of cell cytoskeleton and membrane mechanics by electric field: role of linker proteins, Biophysical Journal 96(2)(2009) 717-728.

[63] M. Noda, D. E. Johnson, A. Chiabrera, G. A. Rodan, Effect of electric currents on DNA synthesis in rat osteosarcoma cells: Dependence on conditions that influence cell growth, Journal of Orthopaedic Research 5(2)(1987) 253-260.

[64] T. Bodamyali, J. M. Kanczler, B. Simon, D. R. Blake, C. R. Stevens, Effect of faradic products on direct current-stimulated calvarial organ culture calcium levels, Biochemical and Biophysical Research Communications 264(3)(1999) 657-661.

[65] S. Curtze, M. Dembo, M. Miron, D. B. Jones, Dynamic changes in traction forces with DC electric field in osteoblast-like cells, Journal of Cell Science 117(13)(2004) 2721-2729.

[66] K. E. Hammerick, A. W. James, Z. Huang, F. B. Prinz, M. T. Longaker, F. B. Prinz, M. T. Longaker, Pulsed direct current electric fields enhance osteogenesis in adipose-derived stromal cells, Tissue Engineering: Part A 16(3)(2010) 917-931.

[67] M. R. Cho, H. S. Thatte, R. C. Lee, D.E. Golan, Integrin-dependent human macrophage migration induced by oscillatory electrical stimulation, Annals of Biomedical Engineering 28(3)(2000) 234-243.

[68] J. Ferrier, S. M. Ross, J. Kanehisa, J. E. Aubin, Osteoclasts and osteoblasts migrate in opposite directions in response to a constant electrical field, Journal of Cellular Physiology 129(3)(1986) 283-288.

[69] N. Özkucur, T. K. Monsees, S. Perike, H. Q. Do, R. H. Funk, Local calcium elevation and cell elongation initiate guided motility in electrically stimulated osteoblast-like cells, PloS One 4(7)(2009) e6131.

[70] Z. Zhao, C. Watt, A. Karystinou, A. J. Roelofs, C. D. McCaig, I. R. Gibson, C. De Bari, Directed migration of human bone marrow mesenchymal stem cells in a physiological direct current electric field, European Cells and Materials 22 (2011) 344-358.

[71] M. Griffin, S. A. Iqbal, A. Sebastian, J. Colthurst, A. Bayat, Degenerate wave and capacitive coupling increase human MSC invasion and proliferation while reducing cytotoxicity in an in vitro wound healing model, PloS One 6(8)(2011) e23404.

[72] L. Khatib, D. E. Golan, M. Cho, Physiologic electrical stimulation provokes intracellular calcium increase mediated by phospholipase C activation in human osteoblasts, FASEB Journal 18(15)(2004) 1903-1905.

[73] Q. Wang, S. Zhong, W. Zhang, G. Wang, DNA Synthesis and Ca^{2+} Metabolism of Isolated Rat Osteoblast-Like Cells Under Direct Current Stimulation, Electro- and Magnetobiology 16(2)(1997) 87-93.

[74] S. Sun, Y. Liu, S. Lipsky, M. Cho, Physical manipulation of calcium oscillations facilitates osteodifferentiation of human mesenchymal stem cells, FASEB Journal 21(7)(2007) 1472-1480.

[75] I. S. Kim, J. K. Song, Y. M. Song, T. H. Cho, T. H. Lee, S. S. Lim, S. J. Kim, S. J. Hwang, Novel effect of biphasic electric current on in vitro osteogenesis and cytokine production in human mesenchymal stromal cells, Tissue Engineering: Part A 15(9)(2009) 2411-2422.

[76] Q. Wang, S. Zhong, Y. Xie, Z. Zhang, G. Yang, Electrochemical reactions during constant DC current stimulation: An in vitro experiment with cultured rat calvarial cells, Electro- and Magnetobiology 14(1)(1995) 31-40.

[77] P. Supronowicz, P. Ajayan, K. Ullmann, B. Arulanandam, D. Metzger, R. Bizios, Novel currentconducting composite substrates for exposing osteoblasts to alternating current stimulation, Journal of Biomedical Materials Research: Part A 59(3)(2002) 499-506.

[78] I. S. Kim, J. K. Song, Y. L. Zhang, T. H. Lee, T. H. Cho, Y. M. Song, D. K. Kim, S. J. Kim, S. J. Hwang, Biphasic electric current stimulates proliferation and induces VEGF production in osteoblasts, Biochimica et Biophysica Acta (BBA) - Molecular Cell Research 1763(9)(2006) 907-916.

[79] H. Ozawa, E. Abe, Y. Shibasaki, T. Fukuhara, T. Suda, Electric fields stimulate DNA synthesis of mouse osteoblastlike cells (MC3T3E1) by a mechanism involving calcium ions, Journal of Cellular Physiology 138(3)(1989) 477-483.

[80] R. J. Fitzsimmons, D. D. Strong, S. Mohan, D. J. Baylink, Low-amplitude, low-frequency electric field-stimulated bone cell proliferation may in part be mediated by increased IGF-II release, Journal of Cellular Physiology 150(1)(1992) 84-89.

[81] H. Zhuang, W. Wang, R. M. Seldes, A. D. Tahernia, H. Fan, C. T. Brighton, Electrical stimulation induces the level of TGF-β1 mRNA in osteoblastic cells by a mechanism involving calcium/calmodulin pathway, Biochemical and Biophysical Research Communications 237(2)(1997) 225-229.

[82] C. T. Brighton, W. Wang, R. Seldes, G. Zhang, S. R. Pollack, Signal transduction in electrically stimulated bone cells, The Journal of Bone & Joint Surgery 83(10)(2001) 1514-1523.

[83] R. J. Fitzsimmons, J. R. Farley, W. R. Adey, D. J. Baylink, Frequency dependence of increased cell proliferation, in vitro, in exposures to a low-amplitude, low-frequency electric field: evidence for dependence on increased mitogen activity released into culture medium, Journal of Cellular Physiology 139(3)(1989) 586-591.

[84] I. Binderman, D. Somjen, Z. Shimshoni, J. Levy, H. Fischler, R. Korenstein, Stimulation of skeletal-derived cell cultures by different electric field intensities is cell-specific, Biochimica et Biophysica Acta (BBA)-Molecular Cell Research 844(3)(1985) 273-279.

[85] R. Korenstein, D. Somjen, H. Fischler, I. Binderman, Capacitative pulsed electric stimulation of bone cells. Induction of cyclic-AMP changes and DNA synthesis, Biochimica et Biophysica Acta (BBA)-Molecular Cell Research 803(4)(1984) 302-307.

[86] C. M. Creecy, C. F. O'Neill, B. P. Arulanandam, V. L. Sylvia, C. S. Navara, R. Bizios, Mesenchymal stem cell osteodifferentiation in response to alternating electric current, Tissue Engineering: Part A 19(3-4)(2013) 467-474.

[87] G. Hannay, D. Leavesley, M. Pearcy, Timing of pulsed electromagnetic field stimulation does not affect the promotion of bone cell development, Bioelectromagnetics 26(8)(2005) 670-676.

[88] M-T. Tsai, W-J. Li, R. S. Tuan, W. H. Chang, Modulation of osteogenesis in human mesenchymal stem cells by specific pulsed electromagnetic field stimulation, Journal of Orthopaedic Research 27(9)(2009)1169-1174.

[89] R. J. Fitzsimmons, J. T. Ryaby, S. Mohan, F. P. Magee, D. J. Baylink, Combined magnetic fields increase insulin-like growth factor-II in TE-85 human osteosarcoma bone cell cultures, Endocrinology 136(7)(1995) 3100-3106.

[90] J. T. Ryaby, R. J. Fitzsimmons, N. A. Khin, P. L. Culley, F. P. Magee, A. M. Weinstein, D. J. Baylink, The role of insulin-like growth factor II in magnetic field regulation of bone formation, Bioelectrochemistry and Bioenergetics 35(1-2)(1994) 87-91.

[91] M. De Mattei, A. Caruso, G. C. Traina, F. Pezzetti, T. Baroni, V. Sollazzo, Correlation between pulsed electromagnetic fields exposure time and cell proliferation increase in human osteosarcoma cell lines and human normal osteoblast cells in vitro, Bioelectromagnetics 20(3)(1999) 177-182.

[92] C. H. Lohmann, Z. Schwartz, Y. Liu, H. Guerkov, D. Dean, B. Simon, B. D. Boyan, Pulsed electromagnetic field stimulation of MG63 osteoblastlike cells affects differentiation and local factor production, Journal of Orthopaedic Research 18(4)(2000) 637-646.

[93] M. A. Vander Molen, H. J. Donahue, C. T. Rubin, K. J. McLeod, Osteoblastic networks with deficient coupling: differential effects of magnetic and electric field exposure, Bone 27(2)(2000) 227-231.

[94] K. J. Mcleod, H. J. Donahue, P. E. Levin, M. A. Fontaine, C. T. Rubin, Electric fields modulate bone cell function in a densitydependent manner, Journal of Bone and Mineral Research 8(8)(1993) 977-984.

[95] L-Y. Sun, D-K. Hsieh, T-C. Yu, H-T. Chiu, S-F. Lu, G-H. Luo, T. K. Kuo, O. K. Lee, T-W. Chiou, Effect of pulsed electromagnetic field on the proliferation and differentiation potential of human bone marrow mesenchymal stem cells, Bioelectromagnetics 30(4)(2009) 251-260.

[96] Y-C. Fu, C.-C. Lin, J-K. Chang, C-H. Chen, I-C. Tai, G-J. Wang, M-L. Ho, A Novel Single Pulsed Electromagnetic Field Stimulates Osteogenesis of Bone Marrow Mesenchymal Stem Cells and Bone Repair, PloS One 9(3)(2014) e91581.

[97] Z. Schwartz, B. J. Simon, M. A. Duran, G. Barabino, R. Chaudhri, B. D. Boyan, Pulsed electromagnetic fields enhance BMP2 dependent osteoblastic differentiation of human mesenchymal stem cells, Journal of Orthopaedic Research 269()(2008) 1250-1255.

[98] Y. Wei, H. Xiaolin, S. Tao, Effects of extremely low-frequency-pulsed electromagnetic field on different-derived osteoblast-like cells, Electromagnetic Biology and Medicine 27(3)(2008) 298-311.

[99] J. K-J. Li, J. C-A. Lin, H-C. Liu, J-S. Sun, R-C. Ruaan, C. Shih, W. H-S. Chang, Comparison of ultrasound and electromagnetic field effects on osteoblast growth, Ultrasound in Medicine & Biology 32(5)(2006) 769-775.

[100] N. Selvamurugan, S. Kwok, A. Vasilov, S. C. Jefcoat, N. C. Partridge, Effects of BMP-2 and pulsed electromagnetic field (PEMF) on rat primary osteoblastic cell proliferation and gene expression, Journal of Orthopaedic Research 25(9)(2007) 1213-1220.

[101] S. Barnaba, R. Papalia, L. Ruzzini, A. Sgambato, N. Maffulli, V. Denaro, Effect of pulsed electromagnetic fields on human osteoblast cultures, Physiotherapy Research International 18(2)(2013) 109-114.

[102] M. Y. Esmail, L. Sun, L. Yu, H. Xu, L. Shi, J. Zhang, Effects of PEMF and glucocorticoids on proliferation and differentiation of osteoblasts, Electromagnetic Biology and Medicine 31(4)(2012) 375-381.

[103] K. S. Kang, J. M. Hong, J. A. Kang, J. W. Rhie, Y. H. Jeong, D. W. Cho, Regulation of osteogenic differentiation of human adipose-derived stem cells by controlling electromagnetic field conditions, Experimental & Molecular Medicine 45(2013) e6.

[104] J. H. Jansen, O. P. van der Jagt, B. J. Punt, J. A. Verhaar, J. P. van Leeuwen, H. Weinans, H. Jahr, Stimulation of osteogenic differentiation in human osteoprogenitor cells by pulsed electromagnetic fields: an in vitro study, MC Musculoskeletal Disorders 11 (2010) 188

[105] P. Torricelli, M. Fini, G. Giavaresi, R. Botter, D. Beruto, R. Giardino, Biomimetic PMMA-based bone substitutes: a comparative in vitro evaluation of the effects of pulsed electromagnetic field exposure, Journal of Biomedical Materials Research: Part A 64(1)(2003) 182-188.

[106] C. F. Martino, D. Belchenko, V. Ferguson, S. Nielsen-Preiss, H. J. Qi, The effects of pulsed electromagnetic fields on the cellular activity of SaOS2 cells, Bioelectromagnetics 29(2)(2008) 125-132.

[107] C. H. Lohmann, Z. Schwartz, Y. Liu, Z. Li, B. J. Simon, V. L. Sylvia, D. D. Dean, L. F. Bonewald, H. J. Donahue, B. D. Boyan, Pulsed electromagnetic fields affect phenotype and connexin 43 protein expression in MLO-Y4 osteocyte-like cells and ROS 17/2.8 osteoblast-like cells, Journal of Orthopaedic Research 21(2)(2003) 326-334.

[108] F. Luo, T. Hou, Z. Zhang, Z. Xie, X. Wu, J. Xu, Effects of pulsed electromagnetic field frequencies on the osteogenic differentiation of human mesenchymal stem cells, Orthopedics 35(4)(2012) e526-e531.

[109] J. M. Hong, K. S. Kang, H-G. Yi, S-Y. Kim, D-W. Cho, Electromagnetically controllable osteoclast activity, Bone 62 (2014) 99-107.

[110] K. Heermeier, M. Spanner, J. Träger, R. Gradinger, P. G. Strauss, W. Kraus, J. Schmidt, Effects of extremely low frequency electromagnetic field (EMF) on collagen type I mRNA expression and extracellular matrix synthesis of human osteoblastic cells, Bioelectromagnetics 19(4)(1998) 222-231.

[111] J. Zhou, L-G. Ming, B-F. Ge, J-Q. Wang, R-Q. Zhu, Z. Wei, H-P. Ma, C. J. Xian, K-M. Chen, Effects of 50 Hz sinusoidal electromagnetic fields of different intensities on proliferation, differentiation and mineralization potentials of rat osteoblasts, Bone 49(4)(2011) 753-761.

[112] Y. Yamamoto, Y. Ohsaki, T. Goto, A. Nakasima, T. Iijima, Effects of static magnetic fields on bone formation in rat osteoblast cultures, Journal of dental research 82(12)(2003) 962-966.

[113] C. M. Teven, M. Greives, R. B. Natale, Y. Su, Q. Luo, B-C. He, D. Shenaq, T-C. He, R. R. Reid, Differentiation of osteoprogenitor cells is induced by high-frequency pulsed electromagnetic fields, Journal of Craniofacial Surgery 23(2)(2012) 586-593.

[114] L-Y. Sun, D-K. Hsieh, P-C. Lin, H-T. Chiu, T-W. Chiou, Pulsed electromagnetic fields accelerate proliferation and osteogenic gene expression in human bone marrow mesenchymal stem cells during osteogenic differentiation, Bioelectromagnetics 31(3)(2010) 209-219.

[115] T. Bodamyali, B. Bhatt, F. J. Hughes, V. R. Winrow, J. M. Kanczler, B. Simon, J. Abbott, D. R. Blake, C. R. Stevens, Pulsed electromagnetic fields simultaneously induce osteogenesis and upregulate transcription of bone morphogenetic proteins 2 and 4 in rat osteoblasts in vitro, Biochemical and Biophysical Research Communication 250(2)(1998) 458-461.

[116] J. Spadaro, R. Becker, Function of implanted cathodes in electrode-induced bone growth, Medical and Biological Engineering and Computing 17(6)(1979) 769-775.

[117] P. C. Grunert, A. Jonitz-Heincke, Y. Su, R. Souffrant, D. Hansmann, H. Ewald, A. Krüger, W. Mittelmeier, R. Bader, Establishment of a Novel In Vitro Test Setup for Electric and Magnetic Stimulation of Human Osteoblasts, Cell Biochemistry and Biophysics 70(2)(2014) 805-817.

[118] D. Madjar, M. Nathan, E. Peled, H. Terkel, Self powered osteogenesis and osseointegration promotion and maintenance device for endosseous implants, Patent US7917223 B2 2011.

[119] V. Sollazzo, A. Palmieri, F. Pezzetti, L. Massari, F. Carinci, Effects of pulsed electromagnetic fields on human osteoblastlike cells (MG-63): a pilot study, Clinical Orthopaedics and Related Research 468(8)(2010) 2260-2277.

[120] S. Weinbaum, S. C. Cowin, Y. Zeng, A model for the excitation of osteocytes by mechanical loading-induced bone fluid shear stresses, Journal of Biomechanics 27(3)(1994) 339-360.

[121] M. De Mattei, N. Gagliano, C. Moscheni, C. Dellavia, C. Calastrini, A. Pellati, M. Gioia, A. Caruso, G. Stabellini, Changes in polyamines, c-myc and c-fos gene expression in osteoblast-like cells exposed to pulsed electromagnetic fields, Bioelectromagnetics 26(3)(2005) 207-214.

[122] R. A. Luben, C. D. Cain, M. C. Chen, D. M. Rosen, W. R. Adey, Effects of electromagnetic stimuli on bone and bone cells in vitro: inhibition of responses to parathyroid hormone by low-energy low-frequency fields, Proceedings of the National Academy of Sciences USA 79(13)(1982) 4180-4184.

[123] G. Ceccarelli, N. Bloise, M. Mantelli, G. Gastaldi, L. Fassina, M. G. De Angelis, D. Ferrari, M. Imbriani, L. Visa, A comparative analysis of the in vitro effects of pulsed electromagnetic field treatment on osteogenic differentiation of two different mesenchymal cell lineages, BioResearch Open Access 2(4)(2013) 283-294.

[124] E. Czekanska, M. Stoddart, R. Richards, J. Hayes, In search of an osteoblast cell model for in vitro research, European cells & materials 24 (2012) 1-17.

[125] L. D. Quarles, D. A. Yohay, L. W. Lever, R. Caton, R. J. Wenstrup, Distinct proliferative and differentiated stages of murine MC3T3-E1 cells in culture: An in vitro model of osteoblast development, Journal of Bone and Mineral Research 7(6)(1992) 683-692.

[126] E. Kaivosoja, V. Sariola, Y. Chen, Y. T. Konttinen, The effect of pulsed electromagnetic fields and dehydroepiandrosterone on viability and osteo-induction of human mesenchymal stem cells, Journal of Tissue Engineering and Regenerative Medicine 9(1)(2015) 31-40.

[127] H. Lodish, A. Berk, S. L. Zipursky, P. Matsudaira, D. Baltimore, J. Darnell. Molecular Cell Biology, 4th Edition Molecular Cell Biology, W. H. Freeman and Company, 2000.

[128] R. J. Fitzsimmons, J. T. Ryaby, F. P. Magee, D. J. Baylink, IGF-II receptor number is increased in TE-85 osteosarcoma cells by combined magnetic fields, Journal of Bone and Mineral Research 10(5)(1995) 812-819.

[129] J. Lee, A. Ishihara, G. Oxford, B. Johnson, K. Jacobson, Regulation of cell movement is mediated by stretch-activated calcium channels, Nature 400(6742)(1999) 382-386.

[130] P. J. Cullen, P. J. Lockyer, Integration of calcium and RAS signalling, Nature Reviews Molecular Cell Biology 3 (2002) 339-348.

[131] X. Sun, E. McLamore, V. Kishore, K. Fites, M. Slipchenko, D. M. Porterfield, XXX, O. Akkus, Mechanical stretch induced calcium efflux from bone matrix stimulates osteoblasts, Bone 50(3)(2012) 581-591.

[132] R. D. Finkelman, S. Mohan, J. C. Jennings, A. K. Taylor, S. Jepsen, D. J. Baylink, Quantitation of growth factors IGF-I, SGF/IGF-II, and TGF-β in human dentin, Journal of Bone and Mineral Research 5(7)(1990) 717-723.

[133] B. D. Gomperts, I. M. Kramer, P. E. Tatham, Signal Transduction, 2nd Edition, Academic Press, 2009, Ch. First Messengers.

[134] S. D. O'Dell, I. N. Day, Insulin-like growth factor II (IGF-II), The International Journal of Biochemistry & Cell Biology 30(7)(1998) 767-771.

[135] H. Lodish, A. Berk, S. L. Zipursky, P. Matsudaira, D. Baltimore, J. Darnell. Molecular Cell Biology, 4th Edition Molecular Cell Biology, W. H. Freeman and Company, 2000.

[136] B. D. Gomperts, I. M. Kramer, P. E. Tatham Signal Transduction, 2nd Edition, Academic Press, 2009, Ch. Growth factors: Setting the Framework.

[137] B. D. Gomperts, I. M. Kramer, P. E. Tatham Signal Transduction, 2nd Edition, Academic Press, 2009, Ch. Signalling Through Receptor Serine/Threonine Kinases.

[138] J. Cao, Y. Man, L. Li, Electrical stimuli improve osteogenic differentiation mediated by aniline pentamer and PLGA nanocomposites, Biomedical reports 1(3)(2013) 428-432.

[139] M. Nagai, M. Ota, Pulsating electromagnetic field stimulates mRNA expression of bone morphogenetic protein-2 and -4, Journal of Dental Research 73(10)(1994) 1601-1605.

[140] E. T. Maizels, C. A. Peters, M. Kline, R.E. Cutler, M. Shanmugam, M. Hunzicker-Dunn, Heat-shock protein-25/27 phosphorylation by the δ isoform of protein kinase C, Biochemical Journal 332(3)(1998) 703-712.

[141] N. Aydin, M. Bezer, The effect of an intramedullary implant with a static magnetic field on the healing of the osteotomised rabbit femur, International Orthopaedics 35(1)(2011) 135-141.

[142] T. Shelyakova, A. Russo, A. Visani, V. A. Dediu, M. Marcacci, Application of magnetic rods for fixation in orthopedic treatments, Computers in Biology and Medicine 61 (2015) 101-106.

[143] W. R. Thompson, C. T. Rubin, J. Rubin, Mechanical regulation of signaling pathways in bone, Gene 503(2)(2012) 179-193.

[144] C. Schmidt, U. Zimmermann, U. van Rienen, Modeling of an Optimized Electro-Stimulative Hip Revision System Under Consideration of Uncertainty in the Conductivity of Bone Tissue, IEEE Journal of Biomedical and Health Informatics 19(14)(2015) 1321-1330.

3.3 Electric powering of instrumented implants

Besides the need of innovative biophysical stimulation systems, other systems must be developed to support their operation. The osseointegration process must be monitored to ensure that optimal therapeutic actuations can be driven, as proved in chapter 2. However, a significant funding support is required to conduct research in this scope, which was not possible to get during this PhD program. Sophisticated communication systems were already developed, as shown in section 3.1, and major problems are not expected in their optimization for ensuring the operation of the new concept model of orthopaedic implant here proposed. Electric powering of instrumented active implants is also a subject of great importance, as their actuation, monitoring, processing and communication systems must be supplied to operate. But, as one has realized from section 3.1, finding a method to power such implants remains an unsolved problem. Therefore, a detailed analysis of the electric supply systems already developed to power instrumented THRs was also carried out. A review paper focusing on this scope was then written. It is entitled "Instrumented Hip Implants: Electric Supply Systems" and is published in the *Journal of Biomechanics* (volume 46, issue 15, pp. 2561-2571)[3].

[3]As the content of this study is already published, the formatting rules established by the *Journal of Biomechanics* are used.

Journal of Biomechanics 46 (2013) 2561–2571

Contents lists available at ScienceDirect

Journal of Biomechanics

journal homepage: www.elsevier.com/locate/jbiomech
www.JBiomech.com

Review

Instrumented hip implants: Electric supply systems

Marco P. Soares dos Santos [a,b,*], Jorge A.F. Ferreira [b], A. Ramos [a,b], José A.O. Simões [b], Raul Morais [c,d], Nuno M. Silva [d], Paulo M. Santos [c,d], M.J.C.S. Reis [c,d], T. Oliveira [b]

[a] TEMA/UA—Centre for Mechanical Technology and Automation, Campus Universitário de Santiago, 3810-193 Aveiro, Portugal
[b] DEM/UA—Department of Mechanical Engineering, University of Aveiro, Campus Universitário de Santiago, 3810-193 Aveiro, Portugal
[c] UTAD—University of Trás-os-Montes e Alto Douro, 5001-801 Vila Real, Portugal
[d] IEETA—Institute of Electronics and Telematics Engineering of Aveiro, 3810-193 Aveiro, Portugal

ARTICLE INFO

Article history:
Accepted 13 August 2013

Keywords:
Instrumented prosthesis
Active implant
Electric power supply
Inductive powering
Energy harvesting

ABSTRACT

Instrumented hip implants were proposed as a method to monitor and predict the biomechanical and thermal environment surrounding such implants. Nowadays, they are being developed as active implants with the ability to prevent failures by loosening. The generation of electric energy to power active mechanisms of instrumented hip implants remains a question. Instrumented implants cannot be implemented without effective electric power systems. This paper surveys the power supply systems of seventeen implant architectures already implanted *in-vivo*, namely from instrumented hip joint replacements and instrumented fracture stabilizers. Only inductive power links and batteries were used *in-vivo* to power the implants. The energy harvesting systems, which were already designed to power instrumented hip implants, were also analyzed focusing their potential to overcome the disadvantages of both inductive-based and battery-based power supply systems. From comparative and critical analyses of the methods to power instrumented implants, one can conclude that: inductive powering and batteries constrain the full operation of instrumented implants; motion-driven electromagnetic energy harvesting is a promising method to power instrumented passive and active hip implants.

Contents

* Corresponding author at: University of Aveiro, Centre for Mechanical Technology & Automation (TEMA), Department of Mechanical Engineering, Campo Universitário de Santiago, 3810-193 Aveiro, Portugal. Tel.: +351 234370830; fax: +351 234370953.
E-mail address: marco.santos@ua.pt (M.P. Soares dos Santos).

0021-9290/$ - see front matter © 2013 Elsevier Ltd. All rights reserved.
http://dx.doi.org/10.1016/j.jbiomech.2013.08.002

1. Introduction

1.1. Need of instrumented hip implants

The number of total hip joint replacements (THR) has increased and it is predicted to increase even more in the coming years (Kurtz et al., 2007). Currently, the need of hip revision procedures is rated about 6% after 5 years and 12% after 10 years following arthroplasty (Labek et al., 2011). In the last 10 years, an increase about 13.6% in the number of revisions was reported by the Swedish Orthopedic Register (Kärrholm, 2010). In addition, the probability to undergo re-revision is five to six times higher after the first revision (Ong et al., 2010).

Some Arthroplasty Registers are reporting the increasing use of uncemented and hybrid (cemented acetabulum) hip implants in primary replacements (Bergen, 2010; Garellick et al., 2011). They are also highlighting that most patients, undergoing the implantation of uncemented implants, are patients less than 60 years old. This trend is also verified in projections for the future profile of patients: 50% of the primary THR and 35% of the revision THR will be performed in patients less than 65 years old between 2010 and 2030 (Kurtz et al., 2009).

The optimization of the design and material properties of hip joint implants, as well as the surgical procedures to implant them, has been a subject of paramount importance for the research community. The current revision rates suggest the use of different methodologies to optimize the performance of hip joint implants. Considering the advances in the electronic systems, as well as in the monitoring and actuation methods, the instrumented implant may become an effective methodology to maximize the outcomes following THR. If uncemented implants are developed to adjust, by themselves, to the biochemical environment surrounding them, then the maximization of their performance will be achieved.

Aseptic loosening is the main reason for revision in hip replacements (Havelin et al., 2009), being currently reported around 70% of all revisions (although it is probably more critical if it is associated to deep infection) (Bergen, 2010). Then, instrumented implants must be primarily addressed to patients who are at risk of early implant loosening. However, it is difficult to predict the long-term behavior of the bone-implant interface, in order to identify previously the group of patients that will likely undergo aseptic loosening. Considering the requirement of long-term implant survival and the idiosyncrasies of patients, uncemented hip replacements can be instrumented in order to operate personalized failure prevention in real-time. The main goal is to minimize the need of revision procedures.

1.2. Potential of instrumented hip implants

The concept of Instrumented Hip Implant was proposed as an accurate method to model the biomechanical and thermal environment surrounding hip implants and to optimize the rehabilitation processes following arthroplasty (Bergmann et al., 2012; Damm et al., 2010; Graichen et al., 1999; Heller et al., 2005). Rydell (1966) was the first researcher who designed and implanted the first two instrumented hip implants in two patients, in order to measure orthogonal compressive forces and moments over the neck of the implants. The newest architecture for instrumented hip implants was proposed by Bergmann et al. (2012). In order to study the risk of thermally induced bone necrosis, they developed instrumented hip endoprostheses to measure the implant temperatures *in-vivo*. So far, only passive implants have been instrumented. This class of implants comprises architectures without active mechanisms, namely actuation systems and command structures. Currently, research is being conducted towards the development of instrumented active implants (Frias et al., 2010; Reis et al., 2012). This approach aims the development of instrumentation for implants with the ability to apply stimuli in the bone-implant interface, in order to control the bone remodeling. The architectures of instrumented active solutions are defined according to Fig. 1, but no prototype was already fully designed. A full active hip implant must comprise (Soares dos Santos et al., 2012): (1) measurement systems to monitor the physiological states of the tissues surrounding the implant; (2) processing systems to model the physiological states of the tissues surrounding the implant, as well as to model the failures' characteristics, namely the state and regions of failures by aseptic loosening; (3) actuation systems to perform therapeutic prescriptions against states of failures by loosening; (4) communication systems between the implant and external systems; and (5) electrical supply systems to power sensors, actuators, transmitters and processing systems. If aseptic loosening occurs in the interface, then the instrumented active implant must characterize it (in real-time) and perform a therapeutic actuation

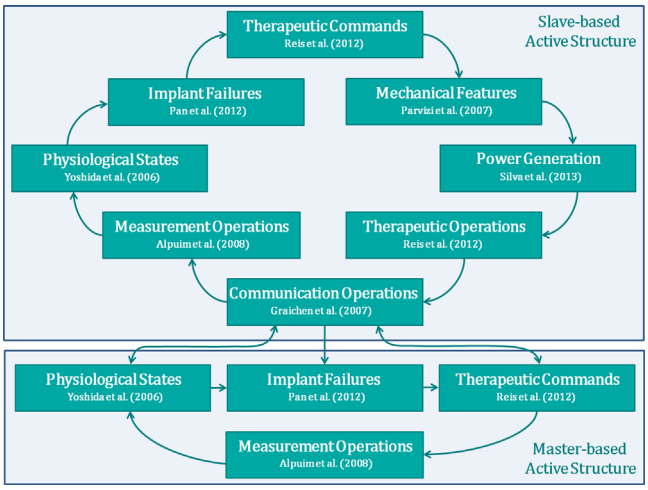

Fig. 1. Architecture of the instrumented hip implants to overcome failures. The Master-based Active Structure is housed outside the human body; the Slave-based Active Structure is housed inside the implants. 'Physiological States' refers to the processing operations that use biochemical and biomechanical measures of the patient's body in order to model the physiological states of the tissues surrounding the instrumented implants. 'Implant Failures' refers to the processing operations that use the effects due to failures (such as the modulation of biochemical and biomechanical changes in the tissues surrounding the implants; and changes in the mechanical, electrical, chemical and communication subsystems of the instrumented implant) to model the failures' characteristics (such as the type, state and regions of failures). 'Therapeutic Commands' uses data about the state of the implants, physiological state of tissues surrounding the implants and therapy results of previous therapeutic commands, in order to generate medical prescriptions to be carried out by the 'Therapeutic Operations'. These therapeutic commands must be conducted primarily by medical specialists, although instrumented implants can be designed with the ability to "learn" throughout time, by using artificial learning algorithms. The module 'Mechanical Features' evaluates the operation state of the actuators, sensors, communication systems and power supply systems (Alpuim et al., 2008; Pan et al., 2012; Yoshida et al., 2006).

(also in real-time) to minimize the state of failure, according to a closed-loop control methodology. The actuators, inside the instrumented implants, must operate suitable (then controlled) therapeutic actuations, in order to minimize the state of loosening throughout time. Bone cell proliferation and differentiation can be carried out by electrical or mechanical stimulation of bone cells (Balint et al., 2013; Hronik-Tupaj and Kaplan, 2012; Ignatius et al., 2005; Reis et al., 2012). Instrumented active implants could be developed to comprise a network of electrical and/or mechanical stimulators of bone cells along the critical regions where loosening occurs. Because they comprise communication systems that allow the data transfer between the implant and the external systems, medical specialists can program therapeutic actuations, in order to be performed by the actuators inside the implant. Because these implants comprise measurement systems, medical specialists can monitor the evolution of the loosening characteristics without the need of other diagnosis methods or invasive procedures.

According to this concept of Instrumented Active Implant, one can conclude that instrumented passive hip implants can also be optimized to model the biochemical behavior of the tissues surrounding the implant; to model *in-vivo* the interaction between the biochemical properties of the tissues and the biomechanical properties of the implant; to model *in-vivo* the failures' characteristics; and to communicate *in-vivo* the failure diagnoses during the routine activities of the patients.

Non-instrumented active implants are also able to exhibit controlled therapeutic actuation in the bone-implant interface throughout time. Their architectures do not comprise electronics, sensors, actuators and power supply systems based on mechanical structures. Smart surface coating modifications can be used to implement non-instrumented active implants (Lehn, 2002; Lendlein and Langer, 2002; Parvizi et al., 2007). The main drawback of this class of implants is the difficulty to implement accurate therapeutic actuations in response to particular biochemical properties of the bone-implant interface when loosening occurs.

Whatever the class of the instrumented hip implants, they require electric powering in order to operate: instrumented passive implants have to power monitoring, processing and communication systems; instrumented active implants have to power monitoring, processing, communication and actuation systems. The goal of this survey is to analyze the electric power systems which were already designed for the particular application of powering instrumented hip replacements and instrumented fracture stabilizers; and to analyze which methods are most feasible for future designs of instrumented implants.

2. Methods

2.1. Literature search strategy

Relevant publications were selected in order to compare all the power supply methods and mechanisms already implemented and validated in instrumented hip joint replacements and instrumented fracture stabilizers, as well as to identify the new trends towards their optimization. The search was also carried out reviewing the reference section of all papers eligible from the selection criteria. The collection was completed in June 2013.

2.2. Selection criteria

Studies, focusing on the following three criteria, were selected:

(1) instrumented hip joint replacements and instrumented fracture stabilizers, which were experimentally validated *in-vivo*. *In-vitro* studies were considered if later *in-vivo* studies, using the same instrumented implants, were published.
(2) instrumented implants without percutaneous wired connections. The use of percutaneous wiring is not acceptable for clinical applications.
(3) recent advances on power supply systems for instrumented hip joint replacements and instrumented fracture stabilizers.

2.3. Assessment of other literature reviews

To our knowledge, only Ledet et al. (2012) briefly reported how telemetric systems of instrumented passive implants were powered. Neither comparative nor critical analyses were conducted so far to the electric power supply systems of the instrumented hip joint replacements or instrumented fracture stabilizers. No authors carried out a survey about all the methods, for electric power generation, that were already applied to both instrumented passive and active hip implants. Moreover, no viability analysis of the methods to power instrumented hip implants was already accomplished.

3. Results

3.1. Instrumentation of hip joint replacements

Twelve architectures of instrumented hip joint replacements, comprising electric power supply systems, were designed by five research groups. They were arranged according to generations of technological breakthroughs, as follows:

(a) three architectures for instrumented endoprostheses were proposed by: Carlson et al. (1974), and Mann and Burgess (1990) for the 1st generation; Carlson (1993), Hodge et al. (1989), and Mann and Burgess (1990) for the 2nd generation; Carlson (1993) and McGibbon et al. (1999) for the 3rd generation.
(b) Kilvington and Goodman (1981) and Puers et al. (2000) developed, respectively, only one architecture for hip prostheses.
(c) four architectures for total hip prostheses were designed by: Davy et al. (1988) for the 1st generation; Davy et al. (1988) for the 2nd generation; Davy et al. (1990) for the 3rd generation; Davy et al. (1988) for the 4th generation.
(d) Friedmar Graichen, and associated research group, contributed with three new designs for total hip prostheses and endoprostheses: Bergmann et al. (1988) and Graichen and Bergmann (1991) for the 1st generation; Graichen et al. (1999) for the 2nd generation; Damm et al. (2010) and Graichen et al. (2007) for the 3rd generation.

A comparative analysis of these electric power supply features can be carried out using Table 1.

From the comparative analysis, one can find the following considerations:

(1) All architectures have been powered by inductive power links or batteries. Although the choice of the method to power instrumented orthopedic implants has been under discussion, only these two methods were used in *in-vivo* tests;
(2) The electric supply systems were used to power instrumentation housed both inside and outside the implants;
(3) Up to 9 years of continuous operation of the electric supply systems were already reported;
(4) The electric supply systems were used only to power measuring implants, i.e., passive architectures which were only designed to collect *in-vivo* data (no actuation systems for therapeutic purposes were implemented);
(5) These power supply systems were customized only to power measurement (which were composed mainly by strain gauges and temperature sensors), communication and processing systems;
(6) These power supply systems are suitable for research purposes related to the modulation of biomechanical quantities, namely forces and temperatures, and, in general, for all research requiring data monitoring that can be conducted only in laboratory or limitedly during the daily life of patients;
(7) Processing units were only designed for power regulation;

Table 1
Electric supply features of the instrumented hip joint replacements[a].

Features	Mann et al.	Kilvington and Goodman	Graichen et al.	Davy et al.	Puers et al.
Implant type	(1,2,3) Austin-Moore endoprosthesis (model: ND)	English prosthesis (model: ND)	(1) Total hip prosthesis (Uni-hip, Mecron); (2) CENOS endoprosthesis (ARTOS, Berlin); ceramic head (CERASIV GmbH, Plochingen, Germany); (3) 'Cementless Tapered Wedge' (CTW) total hip prosthesis (Merete Medical GmbH, Berlin); ceramic head	(1) T-28 total hip prosthesis; (2) total hip prosthesis (model: ND); (3,4) DF-80 (Zimmer) total hip prosthesis	Hip prosthesis (model and type: ND)
Method for power supply	(1,2,3) Inductive powering, using a 100 kHz modulation externally located	Powered by batteries	(1,2,3) Inductive powering, using a 3–5 kHz modulator externally located	(1,2,3,4) Powered by a battery	Inductive powering, using a 750 kHz modulation externally located
Components of the supply system inside the patient's body	(1,2,3) (secondary) coil wound on a ferrite core; regulation systems	3 Batteries (1.35 V mercury); 2 reed switches	(1,2,3) (secondary) power coil; regulation systems	(1,2) Battery; (3,4) pacemaker-type battery (3.6 V lithium); (2,3) magnetic reed switch; (4) momentary reed switch; (1,2,3,4) regulation systems; power coil	(Secondary) power coil; regulation systems
Locations of the components inside the patients' body	(1,2,3) Power induction link: end of the stem; circuitry: inside the hemisphere	Outside the implant (inside the transmitter system housing)	(1) Power coil: in the top of the stem, inside a metallic cylinder; circuitry: in the neck, inside a metallic cylinder; (2) in the shaft, inside a metallic cylinder; (3) power coil: in the neck; circuitry: inside a metallic cylinder in the neck	(1,2) Battery, circuitry: inside the head, in the upper neck region; (3,4) battery: inside the neck; (1,2) power coil: ND; (3,4) power coil: in the base of the prosthesis ball; (1,2,3,4) circuitry: inside the head, in the upper neck region; (2,3,4) switch: inside the head, in the upper neck region	Power coil: inside the neck; circuitry: inside the titanium can, in the head.
Components of the supply system outside the patients' body	(1,2,3) 100 kHz power oscillator; (primary or driver) coil (around the thigh)	Magnet (to latch the reed switches)	(1) 4 kHz power oscillator; (primary) coil (around the thigh); (2) 3.5–4.5 kHz power oscillator; (3) 3–5 kHz power oscillator; (2,3) (primary) coil (around the thigh); antenna, RF receiver and microcontroller (to control the current supply voltage of the electronics)	(1,2,3,4) Magnet (to latch the reed switches)	750 kHz power oscillator; (primary) coil (around the thigh)
Systems of the instrumented implant requiring power supply	(1,2) 14 pressure transducers[i]; (3)13 pressure transducers[i]; temperature transducer (thermistor); (1,2,3) 16-channel 100 MHz PAM/FM transmitter and antenna	4 Sets of strain gauges; single channel 102.3 MHz FM transmitter; antenna; antenna cable	(1) 3 strain gauges, temperature transducer (thermistor NTC); 4-channel 150 MHz RF transmitter; antenna; (2) 3 strain gauges, 9 NTC transducers; 2 × 8 channel 130–150 MHz PIM Coder transmitter; 2 antennas; (3) 6 strain gauges; NTC transducer; 9-channel 150 MHz PIM transmitter; antenna	(1,2,3,4) 3 sets of strain gauges; (3,4) temperature transducer (model: ND); (1,2,4) 76–90 MHz FM transmitter (number of channels: ND); (3) 4-channel 76–90 MHz FM transmitter; (1,2,3,4) antenna	Accelerometer; 10–11.5 MHz RF transmitter (number of channels: ND); antenna
Electric power needs[b]	(1,2) 500 mW; (3) 30 mW	ND	(1) 7 mW; (2) 10 mW; (3) ND (5 mW for communication operations)	(1,2,3,4) ND	22.5 mW
Power regulation circuitries	(1,2,3) Inside the implant: circuitry to regulate the output voltage; outside the implant: NP	Inside the implant: ND; outside the implant: NP	(1,2,3) Inside the implant: circuitry to regulate the output voltage; (2,3) Outside the implant: feedback control of the oscillator frequency to compensate the displacements of the coils	(1,2,3,4) Inside the implant: circuitry to regulate the output voltage; outside the implant: NP	Inside the implant: circuitry to regulate the output voltage; outside the implant: NP
Life span	(1,2,3) ND	70 h	(1,2,3) ND	(1,2,3,4) ND	ND
Tests over the implants[l]	(1,2,3) Fatigue	ND	(1) Fatigue; sealing; corrosion; temperature resistance; acceleration; burn-in; biocompatibility; implantation in 3 sheep over 3 years; (2) temperature resistance; burn-in; sealing; mechanical shocks; (3) sealing; endurance; fatigue	ND	ND
Implantations	(1) NA (6 human acetabular components were used[k]); (2) 1 patient; (3) 1 patient	1 Patient	(1) 4 Sheep; 3 patients; (2) 4 patients; (3) 10 patients	(1) ND; (2) 1 patient; (3) 1 patient; (4) 1 patient	1 Patient
Operation period *in-vivo*	(1) ND; (2) over 5 years[d] PO; (3) up to 3 years[e] PO.	40 Days PO.	(1) Up to 9 years[f] PO; (2) over 6 years[g] PO; (3) up to 12 months[h] PO	(1) ND; (2) up to 3 days PO; (3) up to 31 days PO; (4) up to 58 days PO	ND
Period of power acquisition[c]	(1,2,3) NA	NA	(1,2,3) NA	(1,2,3,4) NA	NA

Table 1 (*continued*)

Features	Mann et al.	Kilvington and Goodman	Graichen et al.	Davy et al.	Puers et al.
Efficiency	(1,2,3) 10%.	ND	(1,2,3) ND	(1,2,3,4) ND	0,25%
Availability of power	(1,2,3) During the tests[j]	While batteries are able to power[j]	(1,2,3) During the tests[j]	(1,2,3,4) While batteries are able to power[j]	During the tests[j]
Other functions	(1,2,3) Antenna, for data communication.	NA	(1,2,3) NA	(1,2,3,4) NA	NA
Side effects	(1) ND (2,3) non-existent	ND	(1) ND; (2,3) non-existent	(1,2,3,4) ND	ND

[a] Terminology: (*n*)—*n*th architecture; NA—not applicable; ND—information not reported; NP—operation not projected; PO—postoperatively.
[b] Average power consumption.
[c] Time required to the acquisition of enough energy to power all the circuitry.
[d] Five years (Givens-Heiss et al., 1992).
[e] McGibbon et al. (1999).
[f] Bergmann et al. (2004).
[g] Bergmann et al. (2004).
[h] Damm et al. (2012).
[i] They were designed as cantilever beams with strain gauges.
[j] The communication with the implant was only carried out in the research laboratory.
[k] Taken directly from the autopsy room to a hip simulator.
[l] Concerning the electric power systems of the implants.

(8) Lower levels of power were demanded because predicting algorithms, database storage and therapeutic actuation systems were not implemented;
(9) No side effects, concerning the operation of the power generators *in-vivo*, were reported in the 24 patients who undergone the implantation of these instrumented hip implants;
(10) High power consumption is demanded by the inductive powering systems due to their poor efficiency;
(11) The life span of the battery-based power supply systems is related with the number of systems requiring electric power;
(12) The design of these power supply systems is not suitable to perform data acquisition throughout the daily living of the patients.

3.2. Instrumentation of fracture stabilizers

Three architectures for distal and proximal femoral replacements were proposed by: Taylor (1996) for the 1st generation; Bassey et al. (1997) for the 2nd generation; Taylor et al. (1998), and Taylor and Walker (2001) for the 3rd generation. Two research groups have conducted the instrumentation of other fracture stabilizers: Brown et al (1982) proposed an architecture for instrumented nail plate implants; Schneider et al. (2001) proposed an architecture for instrumented intramedullary nails. Their electric power supply features can be compared using Table 2.

Considerations 1–6, 8–12 from the previous section, which details a critical analysis of the power supply systems for hip joint replacements, are also true for instrumented fracture stabilizers. No processing capability was reported.

3.3. Energy harvesting systems to power instrumented hip implants

Recently, the suitability of the energy harvesting methods to power instrumented implants started out being studied. Instrumented hip joint replacements were already instrumented with energy harvesting systems, although without *in-vivo* results. Four motion-driven electromagnetic and piezoelectric harvesters were already designed and tested *in-vitro* (Fig. 2):

(a) A multi-source energy harvesting system, composed by two electromagnetic harvesters (a translational and a rotational) and a piezoelectric harvester, was proposed by Soares dos Santos et al. (2013). The translational-based electromagnetic harvester was configured as a mass-spring-damper system.
(b) An electromagnetic harvester, based on a mass-spring-damper configuration but with a braking magnet, was proposed by Morais et al. (2009, 2010, 2011). Inductive powering was used for activation and deactivation of the data acquisition and processing systems.
(c) An electromagnetic harvester, based on a magnetic levitation configuration, was proposed by Silva et al. (2012, 2013) and Morgado et al. (2012). Inductive powering was also used for activation and deactivation of the data acquisition and processing systems.

Their electric power generation features can be compared using Table 3.

One can state the following considerations about the ability of the motion-driven electromagnetic harvesting systems to power instrumented hip implants:

(1) The amount of energy harvested is based on the acceleration profile that excites the generators;
(2) None of these energy harvesters has been optimized according to the gait patterns of patients who undergone THR;
(3) These powering methods avoid the constraints related with the operation period of the instrumentation embedded into the implants;
(4) These harvesting systems ensure long-term energy generation: they are maintenance-free; the energy source is (theoretically) everlasting; the energy is generated inside the implants, which ensures autonomy and safety, and avoids biological changes in the bone-implant interface; they are not expensive; and, finally, they are easy to implement (Morais et al., 2011);
(5) Motion-driven energy harvesters can be designed according to different dimensions, up to nanoscale;
(6) The performance of the electromagnetic harvesters, based on mass-spring-damper configurations, will probably decrease throughout time, due to the mechanical fatigue characteristics of the springs. The magnetic levitation configuration overcomes this problem, because neodymium magnets keep their magnetism practically indefinitely and because of the non-contact nature of this configuration (the only mechanical contact is between the free magnet(s) and the cylindrical tube);
(7) The major drawback of these powering methods is to require hip movements of the patients, according to nonzero

Table 2
Electric supply features of the instrumented fracture stabilizers[a].

Features	Brown, Burstein and Frankel.	Schneider et al.	Taylor et al.
Implant type	Nail plate implant (model: ND)	Intramedullary Femoral Nail (AO/ASIF universal nail)	(1) Proximal Femoral Replacement (Stanmore prosthesis); (2) Distal Femoral Replacement (Stanmore prosthesis). (3) Distal Femoral Replacement (model: ND)
Method for power supply	Powered by batteries	Inductive powering, using a 2 kHz modulator externally located	(1,2,3) Inductive powering, using a modulator externally located
Components of the supply system inside the patient's body	Set of batteries (1.35 V mercury) (quantity: ND); magnetic reed switch	(Secondary) power coil; regulation systems	(1,2,3) (Secondary) coil and ferrite core; regulation systems
Locations of the components inside the patients' body	Batteries: inside the nail; switch: inside the plate	In a cavity at the intermediate location between the distal end and the mid-diaphyseal cross-section	(1,2) Coil and ferrite: outside the implant; (1) circuitry: cavity above the tip of the smaller diameter stem; (2) circuitry: midshaft cavity; (3) circuitry: in the distal shaft cavity; coil and ferrite: distal portion in the shaft
Components of the supply system outside the patients' body	Magnet (to latch the reed switches)	(1) 2 kHz power oscillator; (primary) coil (around the thigh)	(1,2,3) (Primary) coil, power oscillator (frequency: ND) and battery (all around the thigh)
Systems of the instrumented implant requiring power supply	Strain gauges (quantity: ND); 2-channel 88–108 MHz AM/FM transmitter and antenna	5 Strain gauges; temperature transducer; data conversion circuitry; 8-channel 100 kHz transmission system (pulse code modulation) and antenna	(1) 4 Strain gauges; (2,3) 24 strain gauges; (1) single channel 418 MHz UHF transmitter and antenna; (2) multi-channel 418 MHz UHF transmitter (number of channels: ND); antenna; (3) multi-channel UHF transmitter (frequency: ND) and antenna
Electric power needs[g]	ND	100 mW	(1) 151 mW (8 mA); (2) ND (6 mA); (3) ND
Power regulation circuitries	Inside the implant: ND; outside the implant: NP	Inside the implant: circuitry to regulate the output voltage; outside the implant: ND	(1,2,3) Inside the implant: circuitry to regulate the output voltage; outside the implant: ND
Life span	ND	ND	(1,2,3) ND
Tests over the implant[h]	Fatigue; biocompatibility	Fatigue	(1) ND; (2) Fatigue; sealing; (3) Fatigue
Implantations	3 Patients	1 Patient	(1) 2 Patients; (2) 2 patients; (3) 2 patients.
Operation period *in-vivo*	During the PO and convalescent recovery process	6 Months PO.	(1) 9 Years[c] PO; (2) 30 months[d] PO; (3) 30 months[e] PO.
Period of power acquisition[b]	NA	NA	(1,2,3) NA
Efficiency	ND	ND	(1) 10%; (2) 13%; (3) ND
Availability of power	While batteries are able to power	During the tests[f]	(1,2,3) During the tests[f]
Other functions	NA	NA	(1,2,3) Antenna, for data communication
Side effects	ND	ND	(1,2,3) ND

[a] Terminology: (*n*)–*n*th architecture; NA—not applicable; ND—information not reported; NP—operation not projected; PO—postoperatively.
[b] Time required to the acquisition of enough energy to power all the circuitry.
[c] Shah et al. (2006).
[d] Bassey et al. (1997).
[e] Taylor and Walker (2001).
[f] The communication with the implant was only carried out in the research laboratory.
[g] Average power consumption.
[h] Concerning the electric power systems of the implants.

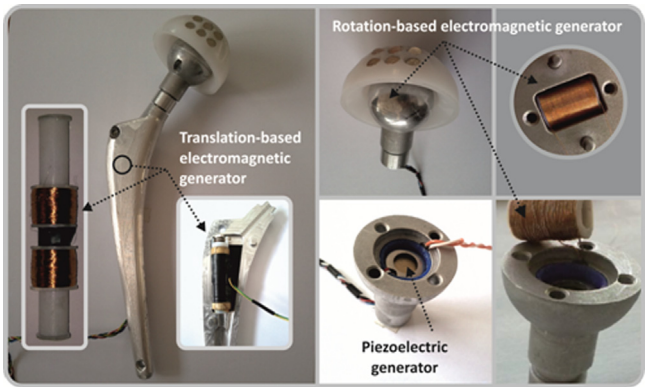

Fig. 2. The four motion-driven electromagnetic and piezoelectric harvesters already designed to power instrumented hip prostheses (Silva et al., 2013).

acceleration profiles. Consequently, only very low levels of energy will be generated if patients are not able to perform their routine activities. This problem arises mainly in the recovery period following THR and it becomes critical with the aging of patients;

(8) Currently, no conclusions can be reported about the amount of energy possible to be generated by these powering methods, because no accurate nonlinear models have been developed and validated in order to conduct optimization studies.

Considerations 1–5, 7 and 8, which were stated for the electromagnetic harvesting systems, are also true for piezoelectric harvesting. The progressive degradation rate of the piezoelectric materials, to repeated mechanical and electrical cycling, cannot be disregarded, as proved by Platt et al. (2005). No fracture stabilizers were instrumented with energy harvesting systems.

4. Discussion

4.1. Methods already used to power instrumented hip implants

The use of inductive powering or batteries constrains the full operation of instrumented implants. Although Bock et al. (2012) recently highlighted the importance of the battery systems for medical

Table 3
Features of the energy harvesters for instrumented hip joint replacements[a].

Features	Soares dos Santos et al.	Morais et al.	Silva et al. and Morgado et al.
Implant type	Metabloc™ hip prosthesis (Zimmer Corporate, EUA)	Freeman hip prosthesis	Freeman hip prosthesis
Method for power supply	Motion-driven electromagnetic and piezoelectric harvesting	Motion-driven electromagnetic harvesting and inductive powering	Motion-driven electromagnetic harvesting and inductive powering
Components of the supply system inside the patient's body	Translational generator: 1 coil spring, 2 neodymium magnets, 1 winding; rotational generator: 1 winding, 24 neodymium magnets; piezoelectric generator: piezoelectric diaphragm	Harvester: 1 coil spring, 2 neodymium magnets, 2 windings, power management circuitry, (Li-ion rechargeable) battery and 2 Aluminum Electrolytic capacitors; inductive generator: (control link) receiver antenna	Harvester: 3 neodymium magnets, 2 windings, power management circuitry, 2 supercapacitors; inductive generator: (control link) receiver antenna
Locations of the components inside the patients' body	Translational generator: in the stem; rotational generator: upper half of the head and acetabular component; piezoelectric generator: lower half of the ball head	In the stem	In the stem
Components of the supply system outside the patients' body	NA	Emitter antenna; 125 kHz power oscillator; ASK receiver, microprocessors	Emitter antenna; 125 kHz power oscillator; ASK receiver, microprocessors
Systems of the instrumented implant requiring power supply	ND (the prototype was only designed with these power generators)	RF transmitter, data processing circuitry, activation circuitry	RF transmitter, data processing circuitry, activation circuitry
Average power generation	Up to 53.7 μW	Up to 108.9 μW	Up to 200 μW
Power regulation circuitries	NA	Inside the implant: circuitry to regulate the output voltage; outside the implant: NP	Inside the implant: circuitry to regulate the output voltage; outside the implant: NP
Life span	ND (theoretically everlasting)	ND (theoretically everlasting)	ND (theoretically everlasting)
Implantations	NA	NA	NA
Tests over the implants	ND	ND	ND
Operation period *in-vivo*	NA	NA	NA
Period of power generation[b]	ND (no circuitry was included)	5,5 s in every 294,44 s (considering only the generation of power for starting-up, signal conditioning, conversion, processing and RF transmission)	ND
Efficiency	ND (no circuitry for signal conditioning was included)	NA	NA
Availability of power	During the movements of the patients' body	During the movements of the patients' body, or while batteries and storage capacitors are able to power	During the movements of the patients' body, or while storage capacitors are able to power
Other functions	NA	NA	NA
Side effects	NA	NA	NA

[a] Terminology: NA—not applicable; ND—information not reported; NP—operation not projected.
[b] Time required to harvest enough energy to power all the circuitry.

devices requiring high reliability, their use does not ensure long-term operation of the instrumented implants. Batteries cannot be charged and discharged often without damage and reduction in capacity, which makes them unsuitable for everlasting operation. Besides, specialized circuitry is required to charge batteries. The use of inductive power supply strongly reduces the periodicity of operation of the instrumented implants, because it is uncomfortable for patients (Almouahed et al., 2011b) and it troubles their routine activities, as shown in Fig. 3. However, one must emphasize the suitability of the induction-based and battery-based supply systems for research purposes requiring data that can be monitored in laboratory or limitedly during the daily life of patients. Following this methodology, the newest instrumented hip endoprostheses, developed by Bergmann et al. (2012), uses an inductive power link to supply temperature sensors inside the implants.

The supply problem becomes critical if one consider that the concept of Instrumented Hip Implant allows the design of architectures with the ability to monitor the biochemical behavior of the tissues surrounding the implants. The same problem also arises if one design instrumentation for implants with the ability to perform therapeutic actuations, in order to overcome detected failures (Reis et al., 2012; Soares dos Santos et al., 2012, 2013). The power consumption increases as the number of sensors, transducers and actuators increase. Moreover, the greater the number of operations of the instrumented hip implants, the larger the consumption and required availability of the power supply systems to operate. Besides, the everlasting life span of orthopedic implants must be considered a validation criterion. One can conclude that induction-based and battery-based supply systems are not able to promote the optimization of both instrumented passive and instrumented active implants, because the monitoring and therapeutic actuation systems must be ready to perform when command orders are prescribed. Of course the maximum prescription rate of therapeutic commands can be decreased to the maximum operation rate of the therapeutic actuators. However, the maximum operation rate of the therapeutic actuators must be higher than the maximum prescription rate of therapeutic commands if optimal performances are required. Finally, the use of inductive power links can be dangerous for patients if their tissues are exposed to high levels of RF electromagnetic fields for a long time. The low efficiency of this method, as well as the higher levels of energy required by active implants when compared to passive implants, may impair the bone-implant interface.

Fig. 3. The primary power coil around a patient's hip (Bergmann et al., 2012). Having a coil around the hip is uncomfortable and troubles the activities of the patients.

Although there are no conclusive proofs of the effectiveness of the motion-driven energy harvesting systems to power instrumented passive or active hip implants, they are being studied for these particular applications because they can generate energy without any of the disadvantages of both inductive supply and batteries. However, their performances are strongly reduced in the recovery period following THR and when patients are not able to perform their routine activities. Therefore, motion-driven energy harvesting systems are best suitable for patients less than 60 years old with good mobility. More efforts must be conducted to validate them as an effective method (within their limitations) to power instrument implants. Firstly, the energy needs for a measurement system (in order to detect the aseptic loosening), a processing system (in order to characterize the loosening) and an actuation system (in order to perform therapeutic actuations to prevent loosening) must be estimated. Then, each configuration must be optimized taken into account the hip movements during routine activities of patients. The validation of accurate nonlinear models to predict their power generation is mandatory. According to the maximum power harvested by each configuration and the energy needs for each design of instrumented passive or active implant, a particular energy harvester can be selected to supply a particular instrumented hip implant. Moreover, models will clarify if it is advantageous to implement only few macroscale harvesters or many micro/nanoscale harvesters.

4.2. New conditioning systems

New conditioning systems are being developed to interface with the energy generators operating *in-vivo*. The main breakthroughs about this subject are listed below:

(a) Le et al. (2006) proposed a CMOS circuitry to interface the piezoelectric energy harvesting;
(b) Silva et al. (2012, 2013) proposed power management systems to interface multiple energy harvesters;
(c) Telemetry systems for instrumented hip prostheses, powered by *in-vivo* energy sources, were also proposed by Morais et al. (2009, 2011) and Silva et al. (2013);
(d) Silva et al. (2013) have proposed storage systems based on supercapacitors, in order to overcome the problems related to the use of batteries as energy reservoirs. The storage of the energy harvested is also a requirement for the maximization of the amount of available energy. Otherwise, energy is lost if it is not used thereupon the generation, or the system will not be reliable if harvesters do not generate enough energy to meet the power needs.
(e) Zhao et al. (2012) developed a miniaturized System-on-Chip (SoC) that can be customized to operate in instrumented hip implants. They embedded a processor, ADC, RF transceiver, EEPROM and SRAM memories, and SPI peripheral interfaces within a 9 mm^3 SoC.

4.3. Methods already used to power other instrumented implants

Prior the optimization of the power supply systems for instrumented hip implants, one must take into account the power systems already developed for other orthopaedic implants. To our knowledge, only inductive power links (comprising components inside and outside the patients′ body) were designed to power instrumented knee implants *in-vivo*. The main contributions were provided by Heinlein et al. (2009, 2007), Kutzner et al. (2010), D′Lima et al. (2008), D′Lima et al. (2005) and Kirking et al. (2006). Although without *in-vivo* results, three piezoelectric harvesting systems were already designed to power instrumented knee implants:

(a) Almouahed et al. (2011a, 2011b) embedded four piezoelectric elements within the anteromedial, posteromedial, anterolateral, and posterolateral compartments of the tibial baseplate. Their main purpose was to instrument knee implants with the ability to measure *in-vivo* the anteroposterior and mediolateral distributions of tibiofemoral force on the tibial baseplate, using self-powered methods. They conducted the optimization of this piezoceramic generator, but only using the axial force applied by the tibial component during the gait cycle: they harvested about 11 mW of maximum average raw power. Such piezoelectric generators can be customized to power instrumented fracture stabilizers. Their application to power instrumented hip joint implants will result in lower power generation, because of the volume restrictions on the hip joint implant. Their performance degradation is a serious drawback for long-term applications. The major potential of this study is the use of piezoelectric materials both for monitoring and power generation operations.
(b) Platt et al. (2005a, 2005b) designed a force-based piezoelectric harvesting system similar to the power generation system proposed by Almouahed et al. (2011a, 2011b). They embedded three PZT elements inside an instrumented knee implant, but with larger dimensions than those used by Almouahed et al. (2011a, 2011b). They reported power generation levels up to 4.8 mW of raw electric power under axial loading conditions.
(c) Luciano et al. (2012) proposed a motion-driven electromagnetic harvesting system which uses the relative motion between the femur and tibia to generate electric power. In the tibial plate, they embedded two cylindrical coils between two condyles; near the outer surface of each condyle, prismatic magnets were embedded. No generated power levels were reported. The main advantage of this method is to avoid the movement of the coils and magnets during power generation, which in turn minimizes the maintenance needs. It is a preliminary study which may became an important breakthrough for instrumented knee replacements. However, it is not feasible for instrumented hip joint implants, because there is no relative motion inside them or is quite difficult to create relative motion inside them.

Only inductive power supply systems were implemented to power instrumented shoulder implants (Westerhoff et al., 2009a, 2009b) and instrumented vertebral body replacements (Rohlmann et al., 2012; Rohlmann et al., 2007). No other breakthroughs were found about electric supply methods to power these implants.

4.4. Viability analysis of other methods to power instrumented hip implants

Rasouli and Phee (2010) reported the main energy sources to power medical devices. Morais et al. (2011) enumerated the methods that can be used to supply smart prostheses. The feasibility of these methods must be analyzed in order to power instrumented hip implants:

(a) Biofuel cells require organic components to generate electric power. Long-term storage of enzymatic biofuel cells inside the implants is quite hard to accomplish. The use of organic components outside the implants requires power generation outside the implants, as well as energy transfer into the implants, which may conduct to biocompatibility and safety problems. No biofuel system was already developed using organic components of bone. Sakai et al. (2009) proposed a biofuel cell system from activated human macrophages. Bone marrow-derived macrophages could be used for energy generation (Weischenfeldt and Porse, 2008). However, such biological systems are quite difficult to implement and they will cause biochemical changes in the bone-implant interface.
(b) The use of radioisotope (such as the plutonium 238) energy conversion raises many toxicity problems (Rasouli and Phee, 2010) and it is expensive (Wei and Liu, 2008), although its safety and reliability were already reported (Wei and Liu, 2008). Research efforts have been conducted to harness its high energy density (Wacharasindhu et al., 2009), but no generation system was designed to ensure more than 30 years of power generation.
(c) Thermoelectric generation systems could be designed by harnessing the temperature increase inside the implants during the routine activities of patients (Bergmann et al., 2001). Several drawbacks hinder the development of feasible thermoelectric generators inside the implants: the temperature gradients and rates of temperature change are small; it is quite hard to implement and to keep a cold junction inside the implants; hip motion is required; thermoelectric generation exhibits low conversion efficiencies, mainly at low temperature differences (Rasouli and Phee, 2010). Another approach is to install the warm junction outside the implant, but safety problems and biochemical changes in the bone-implant interface will arise.
(d) Power generation based on magnetic coupling (Rasouli and Phee, 2010; Wei and Liu, 2008) presents similar problems as described for the inductive powering.

4.5. Future research

Many electromechanical harvesters have been proposed in the last years, but most were designed for vibration-based powering. Sue and Tsai (2012) reviewed those powered by human body motion. They showed that electromagnetic and electrostatic energy harvesters have been designed to operate at frequencies much higher than the frequencies of the hip joint. Saha et al. (2008) also proposed a magnetic levitation harvester, similar with the generators designed by Silva et al. (2012, 2013) and Morgado et al. (2012), to generate energy from human motion, but they optimized it to generate energy inside backpacks. The mechanical deformation of piezoelectric cantilever beams is being quite studied for mechanical to electrical energy conversion. However, the literature has shown that they maximize the power generation within vibration spectrums not matching with the frequencies of the hip joint (Gu and Livermore, 2011; Ly et al., 2011; Morris et al., 2008; Moss et al., 2011; Sue and Tsai, 2012; Zhu et al., 2010). Considering all constraints presented in this Section 4, one can conclude that customized harvesters must be studied specifically for orthopaedic implants. Power generation systems, comprising motion-driven electromagnetic energy harvesters, secondary batteries and/or supercapacitors, are potential solutions to power instrumented hip implants for long-term requirements. Magnetic levitation configurations are particularly interesting because they keep their performance throughout time (their performance changes are insignificant) and they are maintenance-free. We propose the development and optimization of the following three configurations of motion-driven electromagnetic harvesters: (i) magnetic levitation systems using several free permanent magnets, in order to optimize the characteristics of each magnet according to the hip motions (Fig. 4a); (ii) magnetic levitation systems using several independent windings, so that the optimization of the characteristics of each winding, as well as their operation mode, can be conducted (Fig. 4b); (iii) magnetic levitation systems using hollow permanent magnets around independent windings (Fig. 4c). The research for a match between the use of several free magnets and several independent windings is encouraged. It must also be optimized the relation between the minimization of the generators' dimensions and the maximization of their power generations. The implementation of electrostatic energy harvesters is an alternative approach to power passive or active implants. However, due to their limited ability to power medical devices by human body motion (Mitcheson et al., 2004; Sue and Tsai, 2012), they are best suitable as secondary power generators. So, the study of the motion-driven magnetic levitation generators must be conducted firstly.

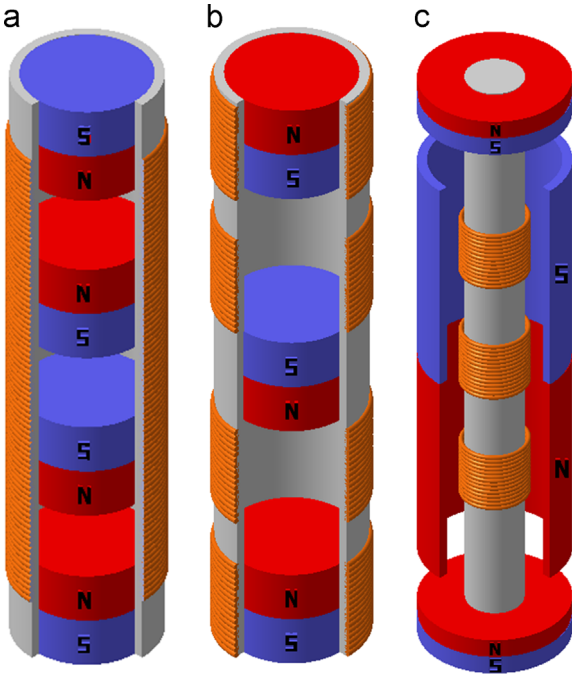

Fig. 4. Promising motion-driven electromagnetic harvesters to power instrumented hip joint replacements and instrumented fracture stabilizers (in section view): (a) magnetic levitation system comprising four permanent magnets, two of which are free magnets; (b) magnetic levitation system comprising four independent windings and one free permanent magnet; (c) magnetic levitation system composed by three hollowed permanent magnets and three independent windings around one free magnet.

Conflict of interest statement

We do not have any financial or personal relationship with other people or organizations that could have inappropriately influenced this study.

Acknowledgements

The authors would like to thank the Portuguese Foundation for Science and Technology (FCT) for their financial support under the research project PTDC/EME-PME/105465/2008 and the grant SFRH/BD/78414/2011. The authors would also like to thank Marco Coutinho (University of Aveiro) for his valuable help in the design of the figures.

References

Almouahed, S., Gouriou, M., Hamitouche, C., Stindel, E., Roux, C., 2011a. Design and evaluation of instrumented smart knee implant. IEEE Transactions on Biomedical Engineering 58, 971–982.
Almouahed, S., Gouriou, M., Hamitouche, C., Stindel, E., Roux, C., 2011b. The use of piezoceramics as electrical energy harvesters within instrumented knee implant during walking. IEEE/ASME Transactions on Mechatronics 16, 799–807.
Alpuim, P., Filonovich, S., Costa, C., Rocha, P., Vasilevskiy, M., Lanceros-Mendez, S., Frias, C., Marques, A., Soares, R., Costa, C., 2008. Fabrication of a strain sensor for bone implant failure detection based on piezoresistive doped nanocrystalline silicon. Journal of Non-Crystalline Solids 354, 2585–2589.
Balint, R., Cassidy, J., Cartmell, H., 2013. Electrical stimulation: a novel tool for tissue engineering. Tissue Engineering Part B: Reviews 19, 48–57.
Bassey, E., Littlewood, J., Taylor, S., 1997. Relations between compressive axial forces in an instrumented massive femoral implant, ground reaction forces, and integrated electromyographs from vastus lateralis during various 'osteogenic' exercises. Journal of Biomechanics 30, 213–223.
Bergen, H. 2010. Report June 2010. The Norweigen Arthoplasty Register.
Bergmann, G., Graichen, F., Dymke, J., Rohlmann, A., Duda, G., Damm, P., 2012. High-tech hip implant for wireless temperature measurements *in vivo*. PLoS One 7, e43489.
Bergmann, G., Graichen, F., Rohlmann, A., 2004. Hip joint contact forces during stumbling. Langenbeck's Archives of Surgery 389, 53–59.
Bergmann, G., Graichen, F., Rohlmann, A., Verdonschot, N., van Lenthe, G., 2001. Frictional heating of total hip implants. Part 1. Measurements in patients. Journal of Biomechanics 34, 421–428.
Bergmann, G., Graichen, F., Siraky, J., Jendrzynski, H., Rohlmann, A., 1988. Multichannel strain gauge telemetry for orthopaedic implants. Journal of Biomechanics 21, 169–176.
Bock, D., Marschilok, A., Takeuchi, K., Takeuchi, E., 2012. Batteries used to power implantable biomedical devices. Electrochimica Acta 84, 155–164.
Brown, R., Burstein, A., Frankel, V., 1982. Telemetering *in vivo* loads from nail plate implants. Journal of Biomechanics 15, 815–823.
Carlson, C., Mann, R., Harris, W., 1974. A radio telemetry device for monitoring cartilage surface pressures in the human hip. IEEE Transactions on Biomedical Engineering, BME-21, 257–264.
Carlson, K., 1993. Human Hip Joint Mechanics—An Investigation into the Effects of Femoral Head Endoprosthetic Replacements Using *in vivo* and *in vitro* Pressure Data. Ph.D. Thesis. MIT, Massachusetts.
Damm, P., Graichen, F., Rohlmann, A., Bender, A., Bergmann, G., 2010. Total hip joint prosthesis for *in vivo* measurement of forces and moments. Medical Engineering & Physics 32, 95–100.
Damm, P., Ackermann, R., Bender, A., Graichen, F., Bergmann, G., 2012. *In vivo* measurements of the friction moment in total hip joint prostheses during. Journal of Biomechanics 45, S268.
Davy, D., Kotzar, G., Brown, R., Heiple, K., Goldberg, V., Heiple, K., Berilla, J., Burstein, A., 1988. Telemetric force measurements across the hip after total arthroplasty. Journal of Bone and Joint Surgery 70, 45–50.
Davy, D., Kotzar, G., Berilla, J., Brown, R., 1990. Telemeterized orthopaedic implant work at case Western Reserve University. In: Bergmann, G., Graichen, F., Rohlmann, A. (Eds.), Implantable Telemetry in Orthopaedics. Freie Universität Berlin, pp. 205–219.
D'Lima, D., Steklov, N., Patil, S., Colwell, C., 2008. The Mark Coventry Award: *in vivo* knee forces during recreation and exercise after knee arthroplasty. Clinical Orthopaedics and Related Research 466, 2605–2611.
D'Lima, D., Townsend, C., Arms, S., Morris, B., Colwell, C., 2005. An implantable telemetry device to measure intra-articular tibial forces. Journal of Biomechanics 38, 299–304.
Frias, C., Reis, J., Capela e Silva, F., Potes, J., Simões, J., Marques, A., 2010. Polymeric piezoelectric actuator substrate for osteoblast mechanical stimulation. Journal of Biomechanics 43, 1061–1066.
Garellick, G., Karrholm, J., Rogmark, C., Rolfson, O., Herberts, P., 2011. Annual Report 2011. Swedish Hip Arthroplasty Register.
Givens-Heiss, D., Krebs, D., Riley, P., Strickland, E., Fares, M., Hodge, W., Mann, R., 1992. *In vivo* acetabular contact pressures during rehabilitation, part II: Postacute phase. Physical Therapy 72, 700–705.
Graichen, F., Bergmann, G., 1991. Four-channel telemetry system for *in vivo* measurement of hip joint forces. Journal of Biomedical Engineering 13, 370–374.
Graichen, F., Bergmann, G., Rohlmann, A., 1999. Hip endoprosthesis for *in vivo* measurement of joint force and temperature. Journal of Biomechanics 32, 1113–1117.
Graichen, F., Arnold, R., Rohlmann, A., Bergmann, G., 2007. Implantable 9-channel telemetry system for *in vivo* load measurements with orthopedic implants. IEEE Transactions on Biomedical Engineering 54, 253–261.
Gu, L., Livermore, C., 2011. Impact-driven, frequency up-converting coupled vibration energy harvesting device for low frequency operation. Smart Materials and Structures 20, 045004.
Havelin, L., Fenstad, A., Salomonsson, R., Mehnert, F., Furnes, O., Overgaard, S., Pedersen, A., Herberts, P., Karrholm, J., Garellick, G., 2009. The Nordic Arthroplasty Register Association: a unique collaboration between 3 national hip arthroplasty registries with 280,201 THRs. Acta Orthopaedica 80, 393–401.
Heinlein, B., Graichen, F., Bender, A., Rohlmann, A., Bergmann, G., 2007. Design, calibration and pre-clinical testing of an instrumented tibial tray. Journal of Biomechanics 40, S4–S10.
Heinlein, B., Kutzner, I., Graichen, F., Bender, A., Rohlmann, A., Halder, A., Beier, A., Bergmann, G., 2009. ESB clinical biomechanics award 2008: Complete data of total knee replacement loading for level walking and stair climbing measured *in vivo* with a follow-up of 6–10 months. Clinical Biomechanics 24, 315–326.
Heller, M., Bergmann, G., Kassi, J., Claes, L., Haas, N., Duda, G., 2005. Determination of muscle loading at the hip joint for use in pre-clinical testing. Journal of Biomechanics 38, 1155–1163.
Hodge, W., Carlson, K., Fijan, R., Burgess, R., Riley, P., Harris, W., Mann, R., 1989. Contact pressures from an instrumented hip endoprosthesis. Journal of Bone and Joint Surgery 71, 1378–1386.
Hronik-Tupaj, M., Kaplan, L., 2012. A review of the responses of two- and three-dimensional engineered tissues to electric fields. Tissue Engineering Part B: Reviews 18, 167–180.
Ignatius, A., Blessing, H., Liedert, A., Schmidt, C., Neidlinger-Wilke, C., Kaspar, D., Friemert, B., Claes, L., 2005. Tissue engineering of bone: effects of mechanical strain on osteoblastic cells in type I collagen matrices. Biomaterials 26, 311–318.
Kärrholm, J., 2010. The Swedish hip arthroplasty register. Acta Orthopaedica 81, 3–4.
Kilvington, M., Goodman, R., 1981. *In vivo* hip joint forces recorded on a strain gauged 'english' prosthesis using an implanted transmitter. Engineering in Medicine 10, 175–187.
Kirking, B., Krevolin, J., Townsend, C., Colwell, C., D'Lima, D., 2006. A multiaxial force-sensing implantable tibial prosthesis. Journal of Biomechanics 39, 1744–1751.
Kurtz, S., Lau, E., Ong, K., Zhao, K., Kelly, M., Bozic, K., 2009. Future young patient demand for primary and revision joint replacement—national projections from 2010 to 2030. Clinical Orthopaedics and Related Research 467, 2606–2612.
Kurtz, S., Ong, K., Lau, E., Mowat, F., Halpern, M., 2007. Projections of primary and revision hip and knee arthroplasty in the united states from 2005 to 2030. Journal of Bone & Joint Surgery 89, 780–785.
Kutzner, I., Heinlein, B., Graichen, F., Bender, A., Rohlmann, A., Halder, A., Beier, A., Bergmann, G., 2010. Loading of the knee joint during activities of daily living measured *in vivo* in five subjects. Journal of Biomechanics 43, 2164–2173.
Labek, G., Thaler, M., Janda, W., Agreiter, M., Stöckl, B., 2011. Revision rates after total joint replacement—cumulative results from worldwide joint register datasets. The Journal of Bone & Joint Surgery 93-B, 293–297.
Le, T., Han, J., von Jouanne, A., Mayaram, K., Fiez, T., 2006. Piezoelectric micro-power generation interface circuits. IEEE Journal of Solid-State Circuits 41, 1411–1420.
Ledet, E., D'Lima, D., Westerhoff, P., Szivek, J., Wachs, R., Bergmann, G., 2012. Implantable sensor technology: from research to clinical practice. Journal of the American Academy of Orthopaedic Surgeons 20, 383–392.
Lehn, J., 2002. Toward self-organization and complex matter. Science 295, 2400–2403.
Lendlein, A., Langer, R., 2002. Biodegradable, elastic shape-memory polymers for potential biomedical applications. Science 296, 1673–1676.
Luciano, V., Sardini, E., Serpelloni, M., Baronio, G., 2012. Analysis of an electromechanical generator implanted in a human total knee prosthesis. In: Proceedings of the IEEE Sensors Applications Symposium (SAS), University of Brescia, Brescia, Italy.
Ly, R., Rguiti, M., D'Astorg, S., Hajjaji, A., Courtois, C., Leriche, A., 2011. Modeling and characterization of piezoelectric cantilever bending sensor for energy harvesting. Sensors and Actuators A: Physical 168, 95–100.
Mann, R., Burgess, R., 1990. An instrumented prosthesis for measuring pressure on acetabular cartilage *in vivo*. In: Bergmann, G., Graichen, F., Rohlmann, A. (Eds.), Implantable Telemetry in Orthopaedics. Freie Universität Berlin, pp. 65–75.
McGibbon, C., Krebs, D., Trahan, C., Trippel, S., Mann, R., 1999. Cartilage degeneration in relation to repetitive pressure—case study of a unilateral hip hemiarthroplasty patient. Journal of Arthroplasty 14, 52–58.
Mitcheson, P., Green, T., Yeatman, E., Holmes, A., 2004. Architectures for vibration-driven micropower generators. Journal of Microelectromechanical Systems 13, 429–440.
Morais, R., Frias, C., Silva, N., Azevedo, J., Serôdio, C., Silva, P., Ferreira, J., Simões, J., Reis, M., 2009. An activation circuit for battery-powered biomedical implantable systems. Sensors and Actuators A-Physics 156, 229–236.

Morais, R., Silva, N., Santos, P., Frias, C., Ferreira, J., Ramos, A., Simões, J., Baptista, J., Reis, M., 2010. Permanent magnet vibration power generator as an embedded mechanism for smart hip prosthesis. Procedia Engineering 5, 766–769.
Morais, R., Silva, N., Santos, P., Frias, C., Ferreira, J., Ramos, A., Simões, J., Baptista, J., Reis, M., 2011. Double permanent magnet vibration power generator for smart hip prosthesis. Sensors and Actuators A-Physical 172, 259–268.
Morgado, M., Morgado, L., Henriques, E., Silva, N., Santos, P., Santos, M., Ferreira, J., Reis, M., Morais, R., 2012. Nonlinear modeling of vibrational energy harvesters for smart prostheses. Procedia Engineering 47, 1089–1092.
Morris, D., Youngsman, J., Anderson, M., Bahr, D., 2008. A resonant frequency tunable, extensional mode piezoelectric vibration harvesting mechanism. Smart Materials and Structures 17, 065021.
Moss, S., Barry, A., Powlesland, I., Galea, S., Carman, G., 2011. A broadband vibro-impacting power harvester with symmetrical piezoelectric bimorph-stops. Smart Materials and Structures 20, 045013.
Ong, K., Lau, E., Suggs, J., Kurtz, S., Manley, M., 2010. Risk of subsequent revision after primary and revision total joint arthroplasty. Clinical Orthopaedics and Related Research 468, 3070–3076.
Pan, X., Mao, X., Cheng, T., Peng, X., Zhang, X., Liu, Z., Wang, Q., Chen, Y., 2012. Up-regulated expression of MIF by interfacial membrane fibroblasts and macrophages around aseptically loosened implants. Journal of Surgical Research 176, 484–489.
Parvizi, J., Antoci, V., Hickok, N., Shapiro, I., 2007. Selfprotective smart orthopaedic implants. Expert Reviews of Medical Devices 4, 55–64.
Platt, S., Farritor, S., Haider, H., 2005a. On low-frequency electric power generation with PZT ceramics. IEEE/ASME Transactions on Mechatronics 10, 240–252.
Platt, S., Farritor, S., Garvin, K., Haider, H., 2005b. The use of piezoelectric ceramics for electric power generation within orthopedic implants. IEEE/ASME Transactions on Mechatronics 10, 455–461.
Puers, R., Catrysse, M., Vandevoorde, G., Collier, R., Louridas, E., Burny, F., Donkerwolcke, M., Moulart, F., 2000. A telemetry system for the detection of hip prosthesis loosening by vibration analysis. Sensors and Actuators A—Physical 85, 42–47.
Rasouli, M., Phee, L., 2010. Energy sources and their development for application in medical devices. Expert Reviews of Medical Devices 7, 693–709.
Reis, J., Frias, C., Castro, C., Botelho, M., Marques, A., Simões, J., Silva, F., Potes, J., 2012. A new piezoelectric actuator induces bone formation *in vivo*: a preliminary study. Journal of Biomedicine and Biotechnology 2012, 1–7.
Rohlmann, A., Gabel, U., Graichen, F., Bender, A., Bergmann, G., 2007. An instrumented implant for vertebral body replacement that measures loads in the anterior spinal column. Medical Engineering & Physics 29, 580–585.
Rohlmann, A., Petersen, R., Schwachmeyer, V., Graichen, F., Bergmann, G., 2012. Spinal loads during position changes. Clinical Biomechanics 27, 754–758.
Rydell, N., 1966. Forces acting in the femoral head-prosthesis. A study on strain gauge supplied prostheses in living persons. Acta Orthopaedica Scandinavica 440, 1–132.
Saha, C., O'Donnell, T., Wang, N., McCloskey, P., 2008. Electromagnetic generator for harvesting energy from human motion. Sensors and Actuators A 147, 248–253.
Sakai, M., Vonderheit, A., Wei, X., Küttel, C., Stemmer, A., 2009. A novel biofuel cell harvesting energy from activated human macrophages. Biosensors and Bioelectronics 25, 68–75.
Schneider, E., Michel, M., Genge, M., Zuber, K., Ganz, R., Perren, S., 2001. Loads acting in an intramedullary nail during fracture healing in the human femur. Journal of Biomechanics 34, 849–857.
Shah, A., Taylor, S., Hua, J., 2006. Correlation of radiographic and telemetric data from massive implant fixations. Journal of Biomechanics 39, 1304–1314.
Silva, N., Santos, P., Ferreira, J., Santos, M., Reis, M., Morais, R., 2012. Multi-purpose and multi-source energy management system for biomedical implants. Procedia Engineering 47, 722–725.
Silva, N., Santos, P., Ferreira, J., Soares dos Santos, M., Ramos, A., Simões J., Reis, M., Morais, R., 2013. Power management architecture for smart hip prostheses comprising multiple energy harvesting systems. Sensors and Actuators A—Physical, in press.
Soares dos Santos, M., Ferreira, J., Simões, J., Ramos, A., Morais dos Santos, R., Silva, N., Reis, M., Santos, P., 2012. Design methodology for the development of long-term hip prosthesis survival. Journal of Biomechanics 45, S106.
Soares dos Santos, M., Ferreira, J., Ramos, A., Pascoal, R., Morais dos Santos, R., Silva, N., Simões, J., Reis, M., Festas, A., Santos, P., 2013. Multi-source harvesting systems for electric energy generation on smart hip prostheses. In: Gabriel, J., et al. (Eds.), Communications in Computer and Information Science, vol. 357. Springer-Verlag, Berlin Heidelberg, p. 2013.
Sue, C., Tsai, N., 2012. Human powered MEMS-based energy harvest devices. Applied Energy 93, 390–403.
Taylor, S., 1996. A telemetry system for measurement of forces in massive orthopaedic implants *in vivo*. In Proceedings of the 18th Annual International Conference of the IEEE Engineering in Medicine and Biology Society, vol. 1, Amsterdam, pp. 290–292.
Taylor, S., Walker, P., Perry, J., Cannon, S., Woledge, R., 1998. The forces in the distal femur and the knee during walking and other activities measured by telemetry. Journal of Arthroplasty 13, 428–437.
Taylor, S., Walker, P., 2001. Forces and moments telemetered from two distal femoral replacements during various activities. Journal of Biomechanics 34, 839–848.
Wacharasindhu, T., Kwon, J., Meier, D., Robertson, J., 2009. Radioisotope microbattery based on liquid semiconductor. Applied Physics Letters 95, 014103.
Wei, X., Liu, J., 2008. Power sources and electrical recharging strategies for implantable medical devices. Frontiers of Energy and Power Engineering in China 2, 1–13.
Weischenfeldt, J., Porse, B., 2008. Bone marrow-derived macrophages (BMM): isolation and applications. Cold Spring Harbor Protocols 3, 1–6.
Westerhoff, P., Graichen, F., Bender, A., Halder, A., Beier, A., Rohlmann, A., Bergmann, G., 2009a. *In vivo* measurement of shoulder joint loads during activities of daily living. Journal of Biomechanics 42, 1840–1849.
Westerhoff, P., Graichen, F., Bender, A., Rohlmann, A., Bergmann, G., 2009b. An instrumented implant for *in vivo* measurement of contact forces and contact moments in the shoulder joint. Medical Engineering & Physics 31, 207–213.
Yoshida, H., Faust, A., Wilckens, J., Kitagawa, M., Fetto, J., Chao, E., 2006. Three-dimensional dynamic hip contact area and pressure distribution during activities of daily living. Journal of Biomechanics 39, 1996–2004.
Zhao, K., Luo, H., Chen, H., Liu, M., Wang, Z., 2012. A SoC for pressure balance measurement application in total knee arthroplasty. AASRI Procedia 1, 267–275.
Zhu, D., Tudor, M., Beeby, S., 2010. Strategies for increasing the operating frequency range of vibration energy harvesters: a review. Measurement Science and Technology 21, 022001.

Chapter 4

Cosurface-based capacitive stimulation of bone remodeling

Previous chapters highlight that instrumented implants and biophysical stimulators already developed are not suitable for designing instrumented active implants capable of administrating therapeutic trajectories from uncontrolled to controlled osseointegration. Up to date, only instrumented passive implants have been implemented and no effective biophysical stimulation systems (including those based on electrical and/or magnetic field stimulation) were engineered with potential to ensure a high controllability over the peri-implant bone structures and bone-implant integration. Hence, a new concept model for instrumented active implants must be developed: *instrumented active implant with ability to deliver controlled and personalized biophysical stimuli to target tissue areas*. Such aim will be only achieved if electrical and/or magnetic stimulation systems meets the following demands:

1. to deliver non-cytotoxic and non-genotoxic stimuli;
2. to be able to deliver controlled and personalized stimuli, such that time-dependent stimuli (varying waveform, strength, frequency, periodicity, stimulation exposure, etc.) can be applied to various regions of target tissue;
3. to ensure everlasting operation throughout the lifetime of patients, such that revision procedures can be avoided;
4. to be able to apply therapeutic stimuli according to the osseointegration states;
5. to allow miniaturized, stretchable and exible integration inside the implant system;
6. to require low electric power consumption.

From the three different methods of administering electromagnetic fields to bone (direct current, inductive coupling and capacitive coupling), the capacitive-based electrical stimulation emerge as the most feasible to fulfil these demands. Noteworthy, the use

of electrodes in parallel configurations require stepped implants' surfaces, which are not the most appropriated to optimize the bone-implant fixation. Therefore, non-parallel configurations, which can be embedded in active implantable devices, have to be designed and their osteogenic effects start to be evaluated. Promising results on the potential of therapeutic actuation driven by cosurface-based capacitive stimulation were achieved. They are reported in a study entitled "New cosurface capacitive stimulators for the development of active osseointegrative implantable devices" , which was already submitted to a peer-reviewed international journal (*Scientific Reports* - Nature Publishing Group).

New cosurface capacitive stimulators for the development of active osseointegrative implantable devices

Marco P. Soares dos Santos[1,2], Ana Marote[3], João Torrão[1,2], Sandra I. Vieira[3], Odete A. B. da Cruz e Silva[3], A. Ramos[1,2], José A. O. Simões[2], Jorge A. F. Ferreira[1,2]

[1] Centre for Mechanical Technology and Automation, Universidade de Aveiro, 3810-193 Aveiro, Portugal.
[2] Department of Mechanical Engineering, Universidade de Aveiro, 3810-193 Aveiro, Portugal.
[3] Institute for Biomedicine (iBiMED), Department of Medical Sciences, Universidade de Aveiro, 3810-193 Aveiro, Portugal

Corresponding author: Marco P. Soares dos Santos
Email: marco.santos@ua.pt

Abstract

Non-drug strategies based on biophysical stimulation have been emphasized for the treatment and prevention of musculoskeletal conditions. However, to date, no effective stimulation system was ever proposed for intracorporeal therapies. This is particularly true for active intramedullary implants aiming to optimize osseointegration. The increasing demand of these implants, particularly for hip and knee replacements, drives the design of innovative stimulation systems truly effective in bone-implant integration. A new concept of a cosurface-based capacitive system is here proposed for the design of implantable devices that deliver controllable and personalized electric field stimuli to target tissues. The concept of cosurface-based delivery system was studied, a prototype architecture was constructed for *in vitro* tests, and its ability to deliver controllable stimuli was numerically analysed. Successful results on osteoblastic proliferation and differentiation were obtained in the *in vitro* tests. This work provides for the first time a design of a stimulation system that can be embedded in active implantable devices for controllable bone-implant integration and regeneration. This unique insight, in the form of a cosurface design, proposes a truly new line for implementing future personalized stimulatory therapies based on the delivery of electric fields to bone cells.

Keywords: Regenerative medicine; personalized therapy; electrical stimulation; instrumented active implant; capacitive coupling.

Musculoskeletal (MSK) conditions are the second cause of global disability, affecting more than 20% of the world population [1,2]. Increasing incidences of MSK disorders have been observed in developed and developing countries over the last 20 years [2]. Included is osteoarthritis, a major health problem with a global prevalence around 4%, and the most common indication for both total hip and knee replacements [2–4]. Although both of these are already among the most worldwide performed surgical procedures, upsurges in their incidences are predicted in the forthcoming decades [3–6]. Sustained increases in the incidences of knee and hip replacements are mainly due to the observed significant increases in the aged, sedentary and obese population. Current and prospectively, these surgeries represent a burden for individuals, for health systems and for social care systems [3,4,6]. Worsening this scenario, surgical revisions of hip and knee replacements are usually more complex and more invasive than primary replacements, and their revision rates may exceed 10% [7–9]. Hence, implants must be projected to minimize disability and avoid failures throughout the patients' lifetime, which may represent implant lifetimes higher than 50 years. The requirement of such improved duration implants is also emphasized by the higher deterioration risks of the mid and long term fixed cemented implants and by a significant increasing number of more active and younger patients[10].

Asymptomatic long-term fixation of orthopaedic implants requires their osseointegration [10, 11]. Interlocking between bone and implant surfaces should be accomplished at the micrometer and nanometer scale levels [11, 12]. However, bone loss is a frequent phenomenon that turns the bone-implant fixation unstable [10, 13]. This is mainly caused by adverse bone remodeling in response to wear debris and stress-shielding and can result in aseptic loosening [10, 13]. To avoid this cause of implant failure [3, 4], effective regeneration of the peri-prosthetic bone stock is required to ensure a correct biologic interplay at nano- to macro-scale levels. The bone-implant topography and the presence of osseointegrative stimuli have a significant influence over this outcome, given their known influence on the biointegration mechanisms [11, 13]. For optimum osseointegration to be achieved, these positive osseointegrative cues should be optimized and according to personalized interventions, due to the inherent complexity of this process and to the patients' idiosyncrasies.

Pre-optimization of the implants' design is a current methodology used to improve their performance. Micro and nanometer-scale texture design of the implants' surfaces, and custom-made geometries, are sophisticated methods aiming to maximize the host-implant responses [12, 14]. Advanced biomaterials, inert and nearly-inert, have been sintered to improve the mechanical properties of the bone-implant interface, including bioceramics and biocompatible metals and alloys [15]. These approaches are nevertheless used to optimize passive implants, i.e., implants without resources to promote bioactivity. However and regardless of their materials, design, rehabilitation protocols, or surgical procedures used, these passive implants were recently demonstrated to be unable to minimize failures throughout the implants' lifetime [16]. For optimal performances to be achieved, novel implants should also be able to perform trajectories from failure states to without-failure states [16]. By consequence, they must be biologically active throughout their lifetime [16]. Actuation systems based on biomaterials and drug-delivery systems are being explored

to produce clinically-useful active implant systems. Innovative bioactive biomaterials for coating uncemented implants have been exhaustively researched [17–19]. Another promising approach to enhance osseointegration and prevent peri-operative infections is to impregnate coatings with drugs (gentamicin, tobramycin and vancomycin, etc.) and/or biomolecules (growth factors, collagen and proteins, etc.) [17, 20–22]. These solutions can however present important drawbacks for bone-implant optimal bonding, namely: (i) extremely complex designs may be required, mainly for multifunctional coatings [17]; (ii) their controllability is reduced, as their behavior can not be changed after implant insertion; (iii) their delivery dynamics do not consider current biochemical and biomechanical states of the target bone tissues; (iv) their ability to perform personalized delivery is quite limited; (v) long-term release of bioactive substances by these implants is currently unfeasible and will most likely be quite difficult to implement in the forthcoming years; (vi) the simultaneous delivery of different stimuli to different and nearby tissue areas is hard to achieve; (vii) these solutions are unable to perform controlled time-dependent trajectories of the bone formation process.

To date, only instrumented passive systems were implanted in human patients [8, 9]. Their operations have been restricted to measure biomechanical and thermodynamic quantities (forces, moments, deformations and temperatures) *in vivo* [23–25]. Instrumented implants that can ultimately control bone regrowth are highly desirable, particularly when designed to comprise inner monitoring and delivery systems. In this scope, efforts have been focused on the development of biophysical stimulation systems, to exploit the potential of organic adaptation to exogenous excitations. Encouraging results were found *in vivo* by mechanical stimulation driven by piezoelectric actuators [26], but there is an increased risk of weakening the bone-implant interface bonding if the stimulators are located in the implants' surface. However, no technological solutions to stimulate target tissues were found that used stimulators housed inside implants. Ultrasound stimulation is hard to accomplish by instrumented implants: besides the high complexity of the required implant's designs, they may demand a hollowed structure that increases the implant fracture risks. When intramedullary implants were modified to deliver magnetic field (MF) stimuli induced by permanent magnets, a notable bone formation was observed around the implant [27]. Since these are static stimuli, not suitable for controllable and personalized tissue responses, their substitution by electromagnetic-stimulating hip systems has been proposed; these would permit to deliver a controllable electric field (EF) stimulation [28]. This solution is still not able to deliver different stimuli to very close targets and, consequently, unable to geographically control the evolution of the bone formation process. This results from the following: (i) the stimulators' electrodes are attached to the implant's surface; and (ii) the electrical fields are obtained using extracorporeally-induced magnetic fields. Indeed, the current clinical practice that uses biophysical stimulation for bone remodeling is focused on delivering extracorporeal stimuli. This method does not concentrate the stimuli density over the bone-implant interface, as desirable, but mainly on the tissues surrounding the skin. Another method of delivering EF/electromagnetic (EMF) stimulation, with proved *in vitro* osteogenic responses [29, 30] is the capacitive coupling (CC) stimulation. Up-regulatory effects on various cellular mechanisms that underlie bone

formation can be obtained when using CC stimulators to deliver stimuli to osteoblasts in vitro (cell lines, stem cells and primary cells) [31–34]. Extracorporeally-induced CC stimulation has also been used in clinical trials; its ability to improve the treatment of nonunions and osteoarthritis, as well as to minimize post-treatment complications, have been reported [29]. Nevertheless, the CC most common architecture uses electrodes in parallel (Fig. 1) and cannot be integrated into instrumented implants, since the resulting stepped implant's surface would most likely hinder bone-implant integration.

Significant advances in the scope of active implants will be achieved if solutions for long-term, highly controllable and personalized bone-implant bonding are developed. In this paper, we propose a novel therapeutic delivery system with potential to meet these demands.

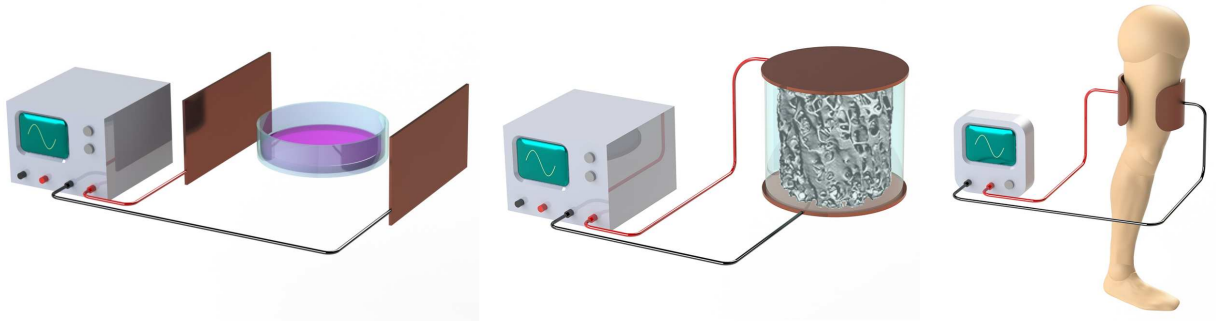

Fig. 1: CC stimulation apparatus using electrodes in parallel configuration: a. *in vitro* stimulation of bone cells. **b.** *In vitro* stimulation of bone tissues. **c.** Clinical usage of CC stimulation.

The concept of cosurface-based capacitive delivery system

Optimized osteogenic responses can be achieved if the stimulation systems fulfil the following requirements:

(a) to deliver non-cytotoxic and non-genotoxic stimuli;

(b) to be able to deliver controllable stimuli, such that different stimuli (varying waveform, strength, frequency, periodicity, stimulation exposure, etc.) can be applied to various regions of target tissue;

(c) to allow defining time-dependent stimulation for personalized medicine;

(d) to ensure everlasting operation throughout the lifetime of patients, such that revision procedures can be avoided;

(e) to be able to apply therapeutic stimuli according to the osseointegration states;

(f) to allow miniaturized, stretchable and/or flexible integration inside the implant system.

To our best knowledge, the methodologies proposed so far are unfeasible for effective bone remodeling. We here propose a new concept for delivering EF stimuli that complies with the six requirements above described: the cosurface-based CC delivery system. This is a non-complex and cost-effective system, with a non-parallel architecture, capable of delivering EF stimuli using electrodes in the same surface, regardless its topology. It can comprise as many electrodes as required, which may function independently, allowing the delivery of EF stimuli to tissue areas in both a quasi-homogeneous and a heterogeneous manner. Further, the electrodes can be shaped with arbitrary geometries and separated from the adjacent electrodes by variable gaps. The solution here presented is in the form of a stimulator composed by a set of identical stripe-shaped electrodes, separated from each other by identical gaps (Fig. 2).

The strategy to fulfil the above describe requirement is as follows. EFs and EMFs do not introduce toxic chemicals and do not induce immunogenic responses to foreign bodies [35], although autophagy is significantly induced by very high EFs. Further, most of studies analyzing potential EFs/EMFs genotoxic effects have not reported damage of the genetic material [36]. Hence, requirement (a) will be most likely fulfilled if the field strength-dependent toxicity of the delivered stimulus is taken in consideration.

Arbitrary and time-dependent excitations can be applied to each pair of electrodes, including different waveforms (sinusoidal, square, triangular or sawtooth, as well as arbitrary periodic or even non-periodic arbitrary ones), amplitudes, frequencies, periodicities, daily stimulation exposures, resting time and total therapy duration. Various regions of a target tissue can be differentially stimulated by defining the most appropriated locations to embed the stimulators inside implants, by choosing optimized stimuli parameters for each region, as well as by optimizing the cosurface architecture. Numerical field analysis can be used to predict EFs/EMFs that are delivered to the peri-implant bone volume, as a function of imposed excitations to electrodes, as well as to optimize the stimulators' design previously to the implant's body insertion. Besides, homogeneity of the delivered EF can be controlled by choosing which sets of electrodes pairs will be delivering stimuli to an area(s) of the tissue. All these degrees of freedom provide the ability to produce customized stimuli for personalizing the administration of either prophylactic or corrective therapies. The stimuli controllability can be even increased since its delivery can be made controlled by clinicians through the use of wireless communication between the implant and extracorporeal systems [16]. Using these approaches, this new therapeutic design is able to comply with requirements (b) and (c).

An everlasting operation, as required in (d), can be accomplished by designing self-powered instrumented implants. Osseointegration states must be monitored for optimal performance of implants [16]. Measurement operations can be performed by the instrumented active implants (via monitoring systems housed inside implants) and/or extracorporeally (through imaging techniques) [16]. These monitoring systems will allow obeying requirement (e), and will establish a feedback control over the stimuli delivery.

Stimulators must be positioned inside the implant, close to the implant's surface, and a biocompatible coating must be used to ensure an absolutely safe encapsulation, as highlighted in Fig. 2a. The conformal integration of these stimulators with instrumented implants, in a way that it withstands mechanical deformations and as stated by requirement (f), is already feasible due to the current advances on materials, mechanics, and manufacturing engineering [37].

An example of application of this concept is to embed stimulators in the proximomedial region of instrumented active hip prosthesis, as illustrated by Fig. 2b. In this type of prosthesis, stress distribution is usually reduced following arthroplasty, which can result in bone loss and consequent implant failure [13]. This concept can also be used on other intracorporeal implants and to stimulate many other tissues.

Results

This study provides a novel cosurface architecture for CC stimulators, a numerical model for prediction of EFs/EMFs delivered to cell cultures, and the first osteogenic *in vitro* responses obtained with such an apparatus. The less complex stimulation apparatus that highlights the potential of this new approach was established by positioning cell culture-containing petri dishes over the stimulators, which in turn are glued a polycarbonate substrate (Fig. 2c,d). In this way, the petri dishes thickness (0.5 mm) avoids cell-electrode contacts and allows a macro-scale mimicking of the stimulators embedded into active implants (close to the implant's surface). Stimulators are composed by 12 stripe-shaped copper electrodes of 2 mm wide, 1 mm thick and different lengths (2× 12 mm, 2× 20 mm, 2× 25 mm, 2× 28 mm, 2× 30 mm, 2× 31 mm). A 0.5 mm gap between electrodes was set. This geometry was specified for stimulating cell cultures on petri dishes of 35 mm of diameter. Two equally charged electrodes were never laid one after the other (anodes are always surrounded by cathodes) such that EF homogeneity can be maximized.

Biological *in vitro* experiments were carried out to analyse the three principal stages of bone remodeling (cellular proliferation, matrix maturation and matrix mineralization) [38]. MC3T3 cells were chosen due to their inherent capability to reproduce osteoblastic proliferation and differentiation, similar to *in vivo* bone formation [39]. Stimulators were powered by excitations that were chosen on the following bases: the parameters chosen have proved osteogenic effects in studies *in vitro* using parallel CC stimulators; data from our pilot experiments was taken into consideration, as this capacitive stimulation method was never tested before; likewise, constraints imposed by instrumented active implants to electrically power the cosurface stimulators were also considered. To our best knowledge, the osteogenic effects of only three different stimuli, delivered *in vitro* to MC3T3 cells, are reported in the literature [31, 40, 41]. These stimulation assays were nevertheless not designed to assess the three stages of osteogenesis, and are only reported to enhance the proliferation rates of these cells [31, 40]. Generally, among the EFs already used to *in vitro* stimulate bone cells, many of them have used strengths lower than 1 V/mm and electrodes' excitations up to 10 V, and at least one osteogenic stage of bone remodeling was

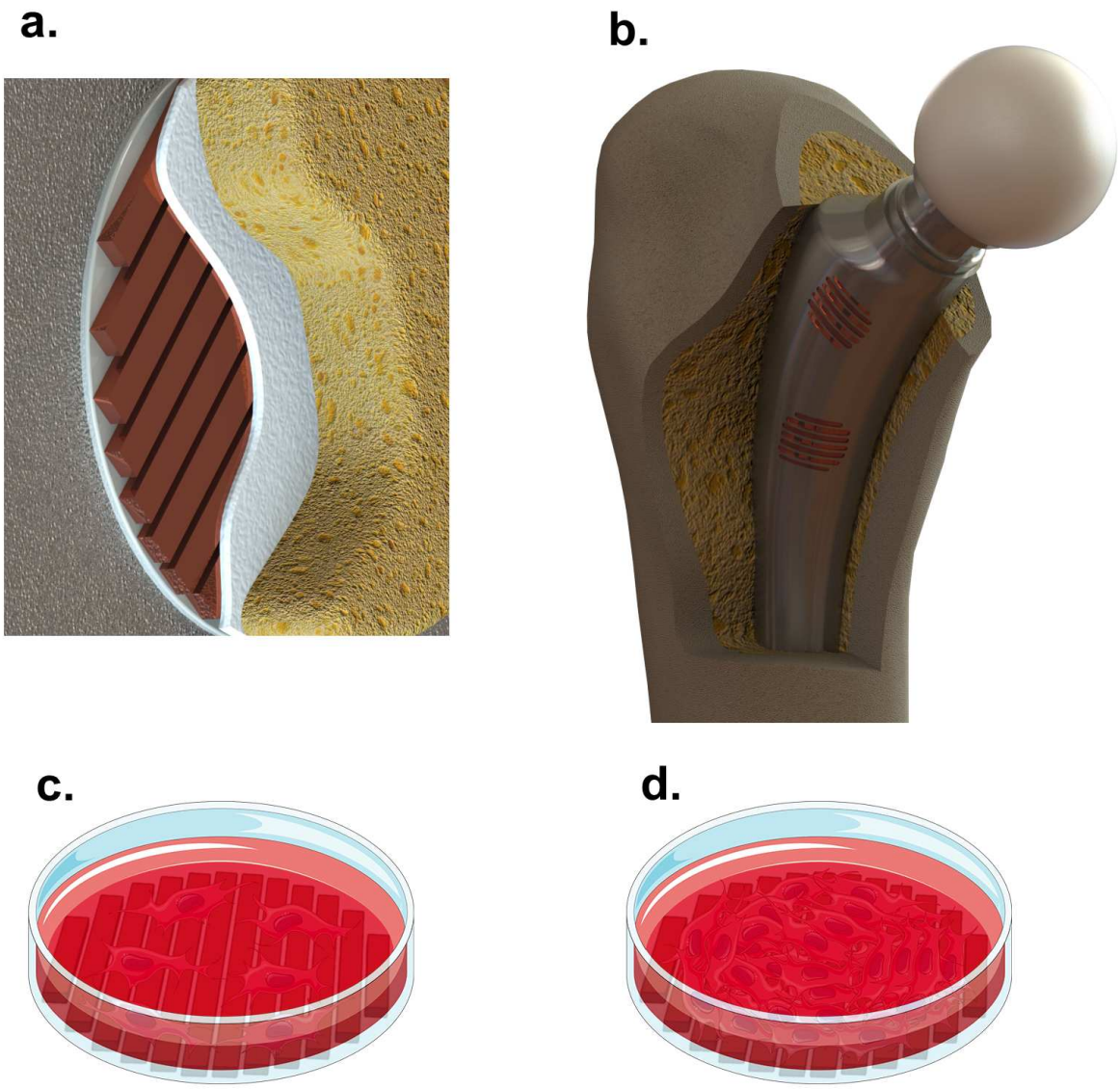

Fig. 2: Cosurface-based CC stimulators according to a striped pattern: a. Embedded for operating inside implant systems. **b.** Example of instrumented hip prosthesis with ability to control osteoregeneration using these stimulators. **c.** Apparatus for analysing the osteogenic results *in vitro* in the pre-confluent cell culture (MED2). **d.** Apparatus for analysing the osteogenic results *in vitro* in the confluent cell culture (MED3).

---

up-regulated in each study [31, 34, 38, 41–43]. Much higher EF strengths (up to 21 V/mm) also enhance osteogenic effects, but very high voltages (hardly achievable by instrumented implants) are required to electrically supply the stimulators [33, 44]. Hence, appropriated voltages that generate EFs capable of enhancing osteogenesis were tested in MC3T3 cells with our cosurface CC apparatus. Frequency is among the main parameters that influence the osteogenic outcome [29, 35]. Since increased osteogenesis has been reported mainly for

low frequencies (lower than 16 Hz) [33,40,45], but also for high frequencies (60 kHz) [41,46], two frequencies within these ranges were also analysed using the cosurface CC stimulator. Given that a large number of studies on EF/EMF-induced bone cells stimulation have powered electrodes with sinusoidal excitations [30,31,41,42], this tested stimulus' waveform was also elected. The daily exposures were defined from other in vitro studies, where these parameters revealed to be osteogenic [38, 43, 47, 48]. Cosurface CC stimulators were thus supplied by two excitations, according to the following parameters:

- **LF EX**: $5 - 5\cos(28\pi t)$ V (sinusoidal waveform, 10 V amplitude, 14 Hz frequency), 4 h/day exposure, 21 days of exposure;
- **HF EX**: $5 - 5\cos(120 \times 10^3 \pi t)$ V (sinusoidal waveform, 10 V amplitude, 60×10^3 Hz frequency), 0.5 h/day exposure, 21 days of exposure.

The Marxell's equations governing the dynamics of EF and MF fields were solved by numerical analysis. The spatially distributed EF and MF strengths were identified when delivered to:

(a) An empty plate, only filled with air (MED1);

(b) A plate with a pre-confluent cell culture (MED2) (Fig. 2c), considering this as an approximation of two homogeneous phases, one above the other: 1) a cellular layer (of 10 μm thickness) adherent to the bottom surface of petri dishes, because of the high percentage of adhesion of MC3T3 cells to polystyrene surfaces [49]; covered by 2) the cell culture medium (a liquid solution of 1 mm thickness);

(c) A confluent cell culture (MED3) similar to MED2 (Fig. 2d), but now assuming the adherent organic layer as resembling an organized cellular tissue of 20 μm thickness, composed by MC3T3 cells and collagen type-I (since this protein corresponds to $\approx$90% of the bone organic matrix).

Such analyses were carried out to characterize how cell cultures are stimulated throughout proliferation (pre-confluent and confluent cultures) and differentiation (fully confluent culture) stages, as well as to study the influence of the dielectric properties of each phase (air, organic, liquid) on the stimuli delivery. Noteworthy, a model to predict EFs and MFs that stimulate cells during the matrix mineralization stage was not conducted in this study.

As illustrated in Figs. 3a,b, EFs ranging between 0.027-9 V/mm are found 0.5 mm above electrodes on MED1 at π rad of LF EX and HF EX. Higher EFs are concentrated above the gaps (fields in the range between 5-7 V/mm in z =0.5 mm), and according to sinusoidal dynamics 100% cross-correlated with the excitations' dynamics (CC = 100%), as shown in Figs. 4a,b. Negligible H-fields (lower than 1.6×10^{-11} A/m, resulting in B-fields lower than 2×10^{-17} T) through the air are registered (Figs. 3c,d). Supplementary Fig. S1 provide a selected set of simulation results that highlight the ability of the cosurface stimulator to deliver controllable stimuli to target regions on MED1. As shown, arbitrary

(sinusoidal, squared, triangular, sawtooth, etc) EFs can be generated by this stimulator at a required frequency. The EF dynamics is quite similar to the excitation dynamics, as it can be also observed by cross-correlations near 100% between the generated EF waveforms and the excitation waveforms. Besides, required EF strengths can be obtained by defining proper excitation amplitudes, as fields' strengths are directly related to the excitation amplitudes (Supplementary Fig. S2a).

Throughout the proliferation stage (MED2), MC3T3 cells will be approximately stimulated with EFs lower than 0.6 V/mm (Figs. 3e,f and Supplementary Fig. S3a,b,i,j). In contrast to EFs distributions through MED1, the highest EFs on the cellular layer of MED2 are situated above the electrodes, due to the high electrical conductivity of the cell culture medium. Quite similar stimuli are then delivered to most cells located in z $\in$ [0.5 0.51] mm (Figs. 3e,f, 4c,d) according to a frequency-dependent behavior (CC = 100%). Most cells are stimulated with maximum EFs around 0.16 V/mm for LF EX, and around 0.36 V/mm for HF EX. The cellular layers are stimulated with different EFs when electrodes are excited with HF EX, although small differences are noticed [lower than 0.025 V/mm on the midpoint located at (x, y) = (1.25, 0) mm above an electrode (Fig. 4d)]. Noteworthy, the highest EF strengths are found in the midplane (z=0.505 mm) of a cellular layer. The B-fields (Figs. 3g,h) are more than 10×10^{10} fold lower than the lowest observed osteogenic magnetic fields reported in literature (either at low or high frequency)[50] and will most likely induce neglecting osteogenic effects. Hence, the following two stimuli were approximately delivered to cells in the pre-confluency stage:

- **LF ST**: $0.08 - 0.08\cos(28\pi t)$ V/mm (sinusoidal waveform, 0.16 V/mm amplitude, 14 Hz frequency), 4 h/day exposure, unto 21 days of exposure;
- **HF ST**: $0.18 - 0.18\cos(120 \times 10^3\pi t)$ V/mm (sinusoidal waveform, 0.36 V/mm amplitude, 60 kHz frequency), 0.5 h/day exposure, unto 21 days of exposure.

The biological effects of these stimuli on the viability and proliferation of the pre-osteoblastic MC3T3 cells were then analysed. The non-toxic resazurin method was used to monitor cell viability with time in culture. 1.8×10^4 cells.cm^{-2} cells were plated and followed by various days in vitro (DIV) (Fig. 5a). Since no significant differences were observed at this initial cell density, and major alterations in cell proliferation usually occur at the pre-confluent period, lower initial cell densities were tested afterwards (1×10^3, 5×10^3 and 10×10^3 cells.cm^{-2}). In this test, cells were directly scored after 1 DIV (24 h) using an exclusion dye (Fig. 5b). Both LF ST and HF ST tended to increase cell number in these conditions, but more consistently and significantly at the lowest cell density (1×10^3 cells.cm^{-2}) (Fig. 5b).

During MC3T3 cells differentiation (MED3), which occurs following culture confluency and cell division arrest, quite similar EFs are approximately delivered to the cells (z $\in$ [0.5 0.52] mm), as shown in Figs. 3i,j, 4e,f and Supplementary Fig. S3e,f,m,n. Small differences between the EF strengths stimulating the first layer of cells and the other layers are envisaged in the responses to HF EX [approximately 0.06 V/mm on the midpoint

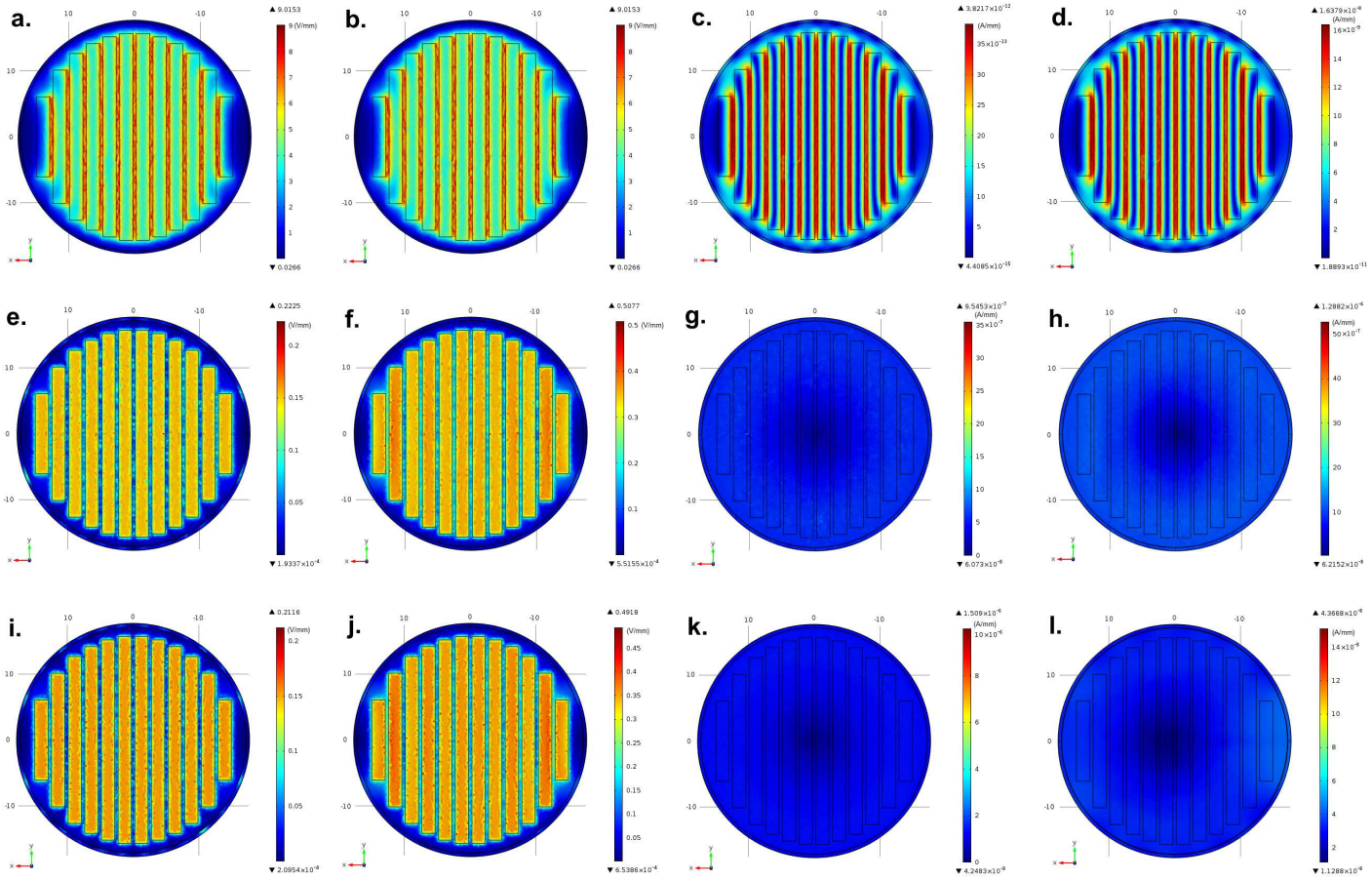

Fig. 3: Simulation results of EF and MF distributions and strengths. **a**. 2D EFs stimulating cells at π rad: LF ST, MED1. **b**. 2D EFs stimulating cells at π rad: HF ST, MED1. **c**. 2D MFs stimulating cells at π rad: LF ST, MED1. **d**. 2D MFs stimulating cells at π rad: HF ST, MED1. **e**. 2D EFs stimulating cells at π rad: LF ST, MED2. **f**. 2D EFs stimulating cells at π rad: HF ST, MED2. **g**. 2D MFs stimulating cells at π rad: LF ST, MED2. **h**. 2D MFs stimulating cells at π rad: HF ST, MED2. **i**. 2D EFs stimulating cells at π rad: LF ST, MED3. **j**. 2D EFs stimulating cells at π rad: HF ST, MED3. **k**. 2D MFs stimulating cells at π rad: LF ST, MED3. **l**. 2D MFs stimulating cells at π rad: HF ST, MED3. 2D EFs and MFs reported for MED1, MED2 and MED3 refer respectively to the strengths on z=0.5 mm, z=0.505 mm and z=0.51 mm above electrodes.

---

located at (x, y) = (1.25, 0) mm above an electrode (Fig. 4f)]. B-fields stimulating cells also present similar strengths as the ones observed for MED2. Consequently, these MFs are most likely not a driving factor enhancing osteogenesis. It should also be noted that the stimuli delivered to MC3T3 cells throughout matrix formation and maturation are similar to those delivered during cell proliferation. Hence, hereafter LF ST and HF ST will be referred as the biophysical stimuli enhancing osteogenic effects during these two first stages of bone remodeling.

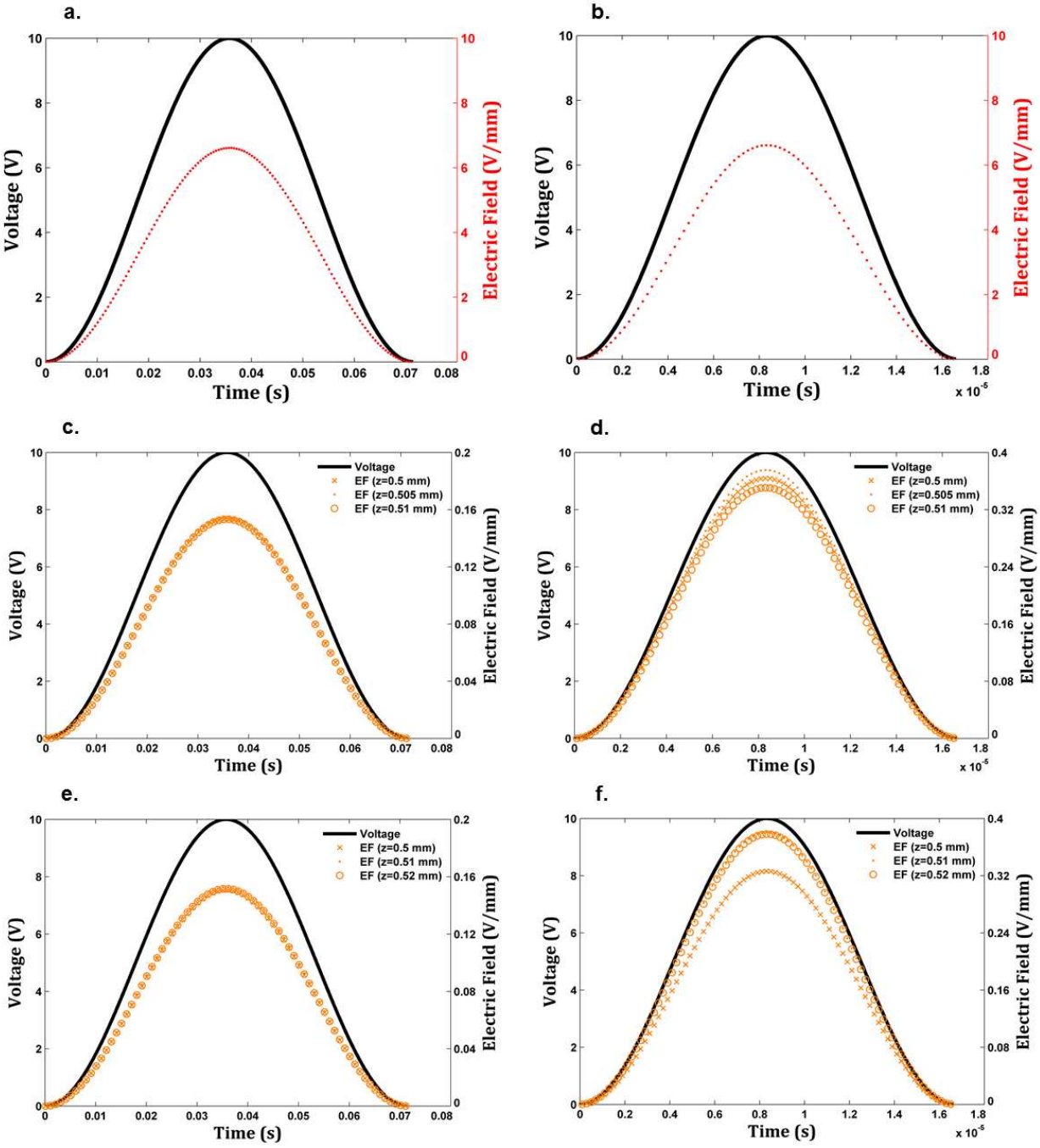

Fig. 4: Simulation results of EF strengths on the midpoint (x, y)=(1.25, 0) mm above a gap. **a**. EFs in [0 2π] rad: LF ST, MED1, z=0.5 mm (CC =100%). **b**. EFs in [0 2π] rad: HF ST, MED1, z=0.5 mm (CC =100%). **c**. EFs in [0 2π] rad: LF ST, MED2 (CC =100% for z=0.5 mm, z=0.505 mm and z=0.51 mm). **d**. EFs in [0 2π] rad: HF ST, MED2 (CC =100% for z=0.5 mm, z=0.505 mm and z=0.51 mm). **e**. EFs in [0 2π] rad: LF ST, MED3 (CC =100% for z=0.5 mm, z=0.51 mm and z=0.52 mm). **f**. EFs in [0 2π] rad: HF ST, MED3 (CC =100% for z=0.5 mm, z=0.51 mm and z=0.52 mm).

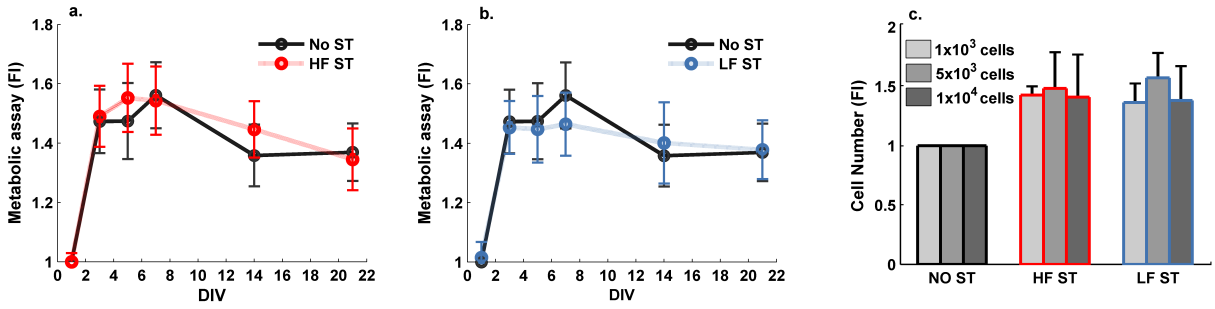

Fig. 5: Influence of the LF ST and HF ST on the number of viable pre-osteoblastic cells. MC3T3 cells were seeded at 1.8×10^4 cells.cm^{-2} and daily exposed to: **a.** NO ST and LF ST or **b.** NO ST and HF ST. The number of viable cells was indirectly accessed by the metabolic reversible resazurin assays at the indicated days in vitro (DIV) (n=6). **c.** The number of viable cells was directly scored 24 h upon seeding the MC3T3 cells at increasing cell densities: 1×10^3, 5×10^3 and 10×10^3 cells.cm^{-2}. Cell number was scored using Trypan blue, a membrane exclusion dye (n=7-15). All data are presented as fold increases (FI) over control (NO ST) levels at 1 DIV.

The biological outcomes resulting from delivering the LF and HF stimuli during the differentiation stage were evaluated. The production and secretion of collagen type-I ('collagen-I') and of a noncollagenous protein (osteonectin) were monitored. These are widely used early biomarkers of osteoblastic differentiation, together with the activity of the alkaline phosphatase (ALP) enzyme. When analysing the cellular (Fig. 6a) and secreted (Supplementar Fig. S4) levels of osteonectin, no differences were detected between the control cells (NO ST) and under LF/HF stimuli at various DIV. When assaying for cellular ALP activity at 15 DIV, a time period of matrix maturation, again no significant differences were detected (Fig. 6b). However, when collagen type-I levels were evaluated and quantified in WB assays, a major increase (1.8-2.7 times) was observed at 7 DIV, and particularly at 14 DIV, for cells daily exposed to the LF and HF stimuli (Fig. 6c,d). All procollagen forms, from α monomers, β dimers, γ trimers, to collagen fibers were elevated. The levels of secreted procollagen were also monitored, where at 14 DIV the LF and HF stimuli also tended to increase the procollagen secretion (Supplementar Fig. S4).

Distribution of the cells and their collagen in the osteoblastic population was analysed by confocal microscopy at 21 DIV. This is a period usually associated with matrix maturation and the onset of matrix mineralization. Intracellular and matrix collagen-I was immunostained (in green); filamentous actin (F-actin, in red) was detected to evidence the cellular contours and cell-to-cell contacts (Fig. 7). Stimulation of cells by cosurface stimulators appeared to present a more organized cellular tissue, with better-defined cell-to-cell contacts (Fig. 7), F-actin staining). When daily stimulated with the LF and HF stimuli for 21 DIV, cells presented a higher content of collagen-I than control cells. This is visible not only inside cells but also at the extracellular matrix (dotted staining in Fig. 7 zoomed-in ROIs). At this period, the highest intensity of the matrix collagen

appeared to result from LF stimulation.

Since a recently developed organic matrix needs to be mineralized to generate a functional mature bone matrix (stage three), the status of matrix mineralization was further assessed. Alizarin Red, a dye that stains calcified extracellular matrices, was used. Figure 8 photographs of representative Alizarin Red-stained circular plates and zoomed-in microphotographic insets reveal that the different frequencies had opposite effects on matrix mineralization. While stimulus induced by LF stimulus tended to maintain or even slightly

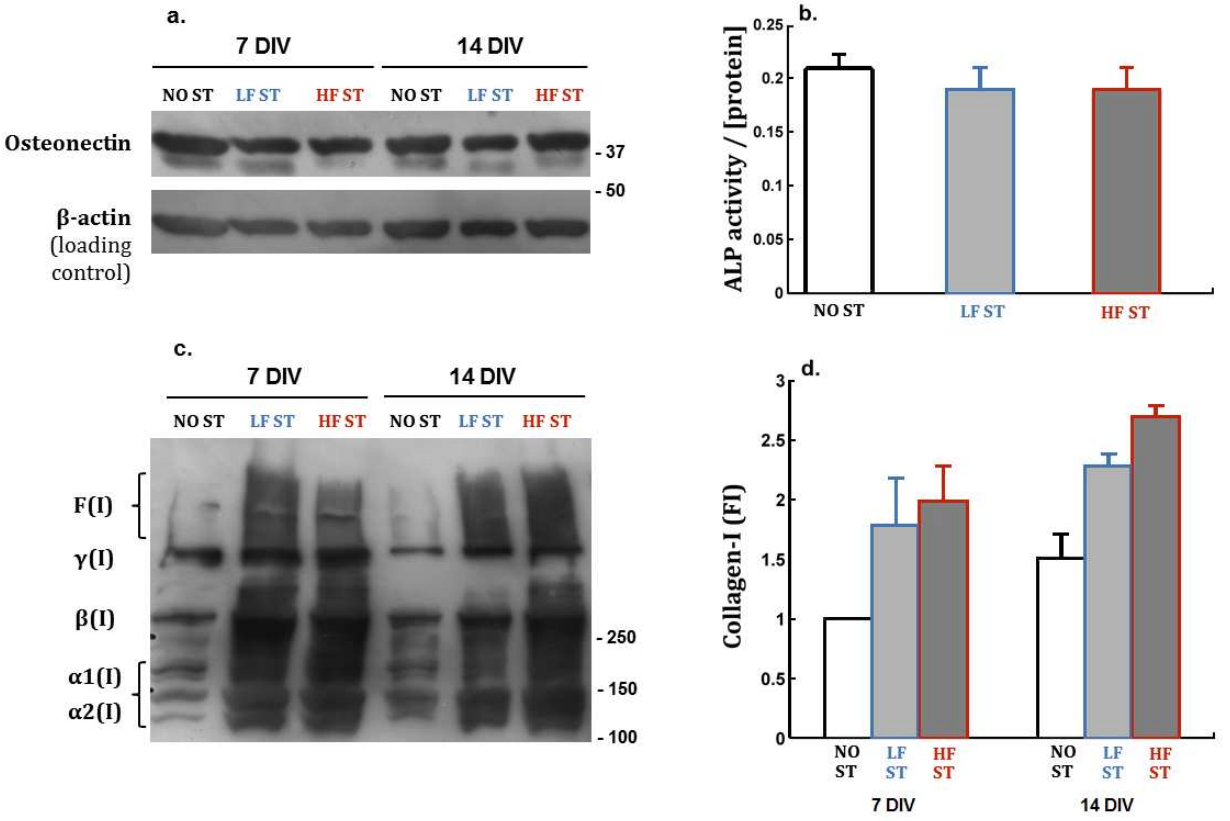

Fig. 6: Relative expression and activity of three matrix maturation protein markers. a. Immunoblot analysis of the osteonectin expression in MC3T3 cells exposed for 7 and 14 DIV *in vitro* to NO ST, LF ST and HF ST. β-actin was used as loading control; no differences were observed in between the experimental conditions. **b.** The intracellular ALP activity was quantified in 1.8×10^4 cells.cm^{-2} MC3T3 cells daily exposed to the LF ST and HF ST for 15 DIV. ALP activity values, determined by measuring the conversion of the ALP substrate (p-Nitrophenyl phosphate) at 405 nm by cells lysates, were divided by the total protein concentration of each lysate. **c.** and **d.** The expression of cell-associated collagen-I was analyzed by immunobloting the lysates of LF ST and HF ST stimulated cells (**c.**) and the levels of collagen-I bands quantified for each condition (**d.**). NO ST, no electromagnetic stimuli. Collagen-I forms: unprocessed and processed α1(I) and α2(I) procollagen monomeric chains (130-160 kDa); β(I), procollagen dimeric forms ($\approx$270 kDa); γ(I), procollagen trimeric forms ($\approx$400 kDa); F(I), collagen fibrils.

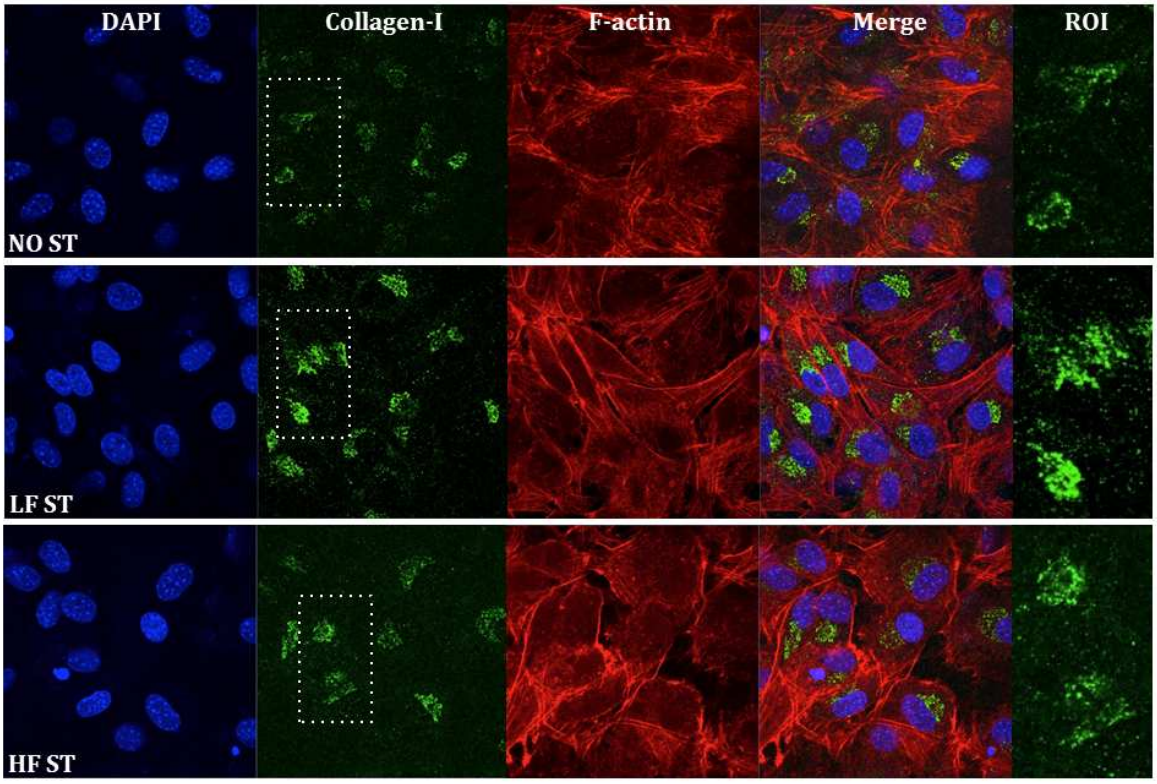

Fig. 7: Confocal microscopy analysis of intracellular collagen-I in MC3T3 cells exposed to LF ST and HF ST for 21 DIV. Fixed cells were subjected to immunocytochemistry procedures in order to detect type-I collagen distribution (green fluorescence). The cytoskeleton constituent filamentous actin (F-actin; labeled with red fluorescing phalloidin) and nucleic acids (labeled with blue fluorescing DAPI) were used as cellular counterstaining. NO ST, no electromagnetic stimuli. Bar, 10 μm. ROI is the region of interest of the green (collagen-I) channel (zoomed 2×).

---

increase matrix mineralization, daily stimulation with the high frequency stimulus led to a decrease in cellular mineralization (Fig. 8).

Although only the LF ST and HF ST were biologically tested in this work, the ability of the cosurface stimulator to deliver other required stimuli to target regions during the first two stages of bone remodeling is also demonstrated. As shown in Supplementary Fig. S5, EFs with required arbitrary waveform, field strength and frequency can be delivered to the cellular layers. Further, different and nearby tissue areas can be simultaneously and differently stimulated by supplying electrodes with different excitations, as illustrated by Supplementary Fig. S6.

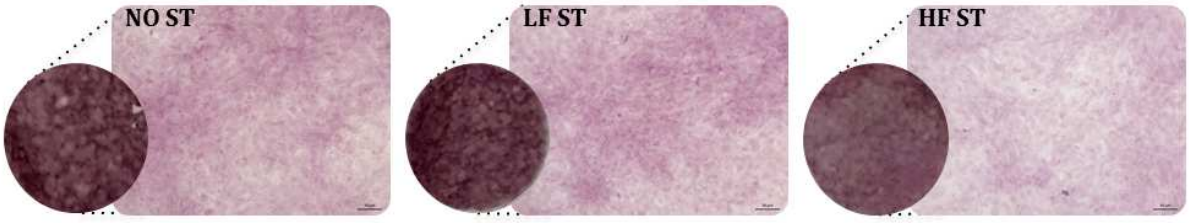

Fig. 8: Visual analyses of the levels of matrix mineralization in MC3T3 cells exposed to EMFs generated by LF and HF stimuli for 21 DIV. Fixed cells in 35 mm culture plates were subjected to cytochemistry procedures with Alizarin Red, which marks calcified extracellular matrices. Photographs of representative Alizarin Red-stained circular plates are shown, together with zoomed in insets taken with a light microscope under a 10× objective (right rectangles). NO ST, no electromagnetic stimuli. Bar, 50 μm.

Discussion

Stimulation of osseointegration is an essential capability of implants [10]. Although the primary stability following implantation is obtained by mechanical press-fit, secondary stability requires optimized bone remodeling, both on host bone and implant surfaces (distance and contact osteogenesis) [10]. Control of the peri-prosthetic bone stock is mandatory to avoid surgical revisions caused by adverse bone remodeling, due to alterations on bone stress distribution that can occur after implant insertion [10, 13]. We here started to analyse the potential of delivering EMF stimuli via cosurface CC stimulators to control osseointegration, and began to monitor their effectiveness in delivering desirable EF stimuli to target regions and in enhancing bone (re)growth. By only testing two stimuli, promising results were achieved on the capability of the cosurface stimulators to induce positive osteogenic responses to different stages of bone remodeling. The cosurface stimulation apparatus was effective in inducing cellular proliferation at early time points and when the culture was at low cell densities. Subsequently, both LF and HF stimuli highly induced cellular collagen-I at the matrix maturation period (7-21 DIV), including its incorporation at the extracellular matrix (21 DIV). Regarding the third stage of osteogenesis, this CC architecture was observed to maintain or even slightly increase matrix mineralization (delivering the LF stimuli) or to postpone it (delivering the LF stimuli). The success obtained in terms of osteoblastic proliferation and differentiation supports the future application of cosurface stimulators in personalized biophysical-based therapies for bone-implant integration. Such purpose requires further research to identify the interplays between the stimuli parameters and their osteogenic outcomes. More systematic studies must be conducted, analysing how bone cell model systems (as immortalized lines, stem cells, and primary cultures) respond to the various stimuli generated by the cosurface architectures. Biological readouts should include cell proliferation, production of structural and regulatory matrix proteins (collagen type-I, fibronectin, alkaline phosphatase, etc.),

and matrix maturation and mineralization markers (as osteopontin, osteocalcin, bone sialoprotein, hydroxyapatite mineral crystals, etc.). An extensive understanding of these cellular responses to electrical and magnetic fields is essential for optimizing stimuli parameters to be used in therapeutic stimulation of the bone tissue.

Since this study portrays the first analysis of cosurface CC stimulation when delivering EFs and MFs to bony cells, and due to their inherent more complex dynamics when compared to parallel CC stimulation, we have considered the less complex models that could make an approximate prediction of how MC3T3 cells were stimulated by EFs and MFs. Three assumptions were then taken into account: (1) during the proliferation stage, the cellular phase is approximately homogeneous and mainly composed by MC3T3 cells; (2) the achieved cellular tissue formed after cell confluency and before matrix mineralization is also nearly homogeneous and mainly composed by MC3T3 cells and collagen-I; (3) the dielectric properties of MC3T3 cells and hydrated collagen are similar. Undoubtedly, further research efforts must be conducted to develop more complex models. Nevertheless, under the conditions here established to carry out the stimulation tests, minor influences on EFs and MFs are expected as a result of the low concentrations of the physiological culture medium around cells, the time-dependent dielectric properties of the cellular medium due to dynamics associated to the proliferation and differentiation stages, and the heterogeneity of the different phases, among others. However, more complex dielectric structures will most likely be observed as higher concentrations of inorganic components of the bone matrix are deposited extracellularly, which will require the development of more complex models. The use of numerical models is also envisaged in future research aiming to investigate the capability of the cosurface stimulator to deliver desirable EFs to target regions of the cancellous bone tissue, namely by designing accurate models defining the inhomogeneity of trabecular structures resulting from their liquid content and crystalline and amorphous mineral and organic phases. Finally, numerical analysis can also enable the geometric optimization of cosurface architectures, such that required surface shapes can be designed to optimize stimuli parameters such as EF strengths, directions, homogeneity, etc. The final aim is to embed these novel cosurface CC stimulators into self-powered instrumented active implants for controlling the peri-implant bone volume. Such methodology may achieve a superior implant performance due to its potential for tracking optimized spatio-temporal trajectories of osteoblasts proliferation, matrix maturation and mineralization [16]. These future implants will be ultimately controlled by a clinician. Besides the innovations carried out to design an efficient therapeutic delivery system, which is the subject of this paper, other significant technological advances have been achieved that optimize other systems required to the full operation of instrumented active implants, namely their communication, monitoring and powering systems. Telemetric systems have been developed for establishing communication between instrumented implants and extracorporeal systems [8,23–25]. This communication can be optimized for monitoring the osseointegration status and establish a therapeutic stimulation based on the decisions of the clinician. Instrumented implants can thus be designed as slave systems commanded by master systems located outside the patients' body, allowing to define and modify time-dependent therapeutic commands [16]. Hence, the stimuli parameters, such as field strength, frequency, periodicity, activation

time, resting time, supply duration, field homogeneity, among others, can be changed after implanted and according to the patients' idiosyncrasies.

Research has been also conducted to develop self-powered instrumented implants for everlasting stimuli delivery [44, 51]. Electromagnetic and piezoelectric energy harvesting systems and power management architectures have been optimized for such purpose [52]. Such capability can enable a superior implant performance as the stimuli delivery can be performed autonomously throughout the routine activities of patients [16]. In parallel, some breakthroughs involving acoustic sound analyses and motion-driven piezoelectric sensing [8] have appeared and will support the development of instrumented implants capable of aseptic loosening detection. Finally, electrodes can now be projected to ensure outstanding electric conductivity properties under large mechanical deformations, which is highly desirable for designing stretchable and flexible cosurface stimulators [37].

Materials and Methods

Construction of the co-surface CC stimulator and numerical modulation

Electrodes were fabricated in copper due to their very high electrical conductivity. Stripes were machined by conventional technology. The polystyrene dishes and polycarbonate substrates were chosen due to their very high electrical resistivity. Thicknesses of 0.4 mm and 0.5 mm for polycarbonate substrates and polystyrene dishes were respectively used.

The finite element method was used to solve the constituent Marxell's equations governing the dynamics of EFs and MFs. The numerical model was developed using the AC/DC module of COMSOL Multiphysics® (v. 4.4, COMSOL). The finite elements were assembled by creating refined 3D 'extra fine' tetrahedral mesh (1.5×10^6 elements) to tessellate the entire geometry of materials and media used to simulate the delivery of EFs and MFs. The dielectric properties of MC3T3 cells were considered as previously reported by Ozawa *et al.* [40] and Wiesmann *et al.* [32]. Similar dielectric properties of MC3T3 cells and hydrated collagen were assumed based on studies conducted by Tomaselli and Shamos [53, 54]. Electric conductivity and permittivity of the physiological medium were established respectively as reported by Pucihar *et al.* [55] and Ozawa *et al.* [40]. The full list of dielectric and magnetic properties of materials and media are summarized in Table I. Simulations were carried out using the Newton iterative method due to its convergence effectiveness and efficiency.

Cell culture stimulation

The osteoblastic MC3T3-E1 cell line (ATCC, Barcelona, Spain; CRL-2593), established from C57BL/6 mouse calvaria, is widely used as a model for studying the various stages of osteogenesis in vitro and due to the similarity to primary calvaria osteoblasts. Cells were

maintained in a humidified atmosphere at 37°C/5% CO_2, in 2 mM glutamine-containing Minimum Essential α-Medium in Eagle's balanced salt solution, supplemented with 10% (v/v) fetal bovine serum, 1% (v/v) of a 100 $U.mL^{-1}$ penicillin and 100 $mg.mL^{-1}$ streptomycin solution (Gibco BRL, Invitrogen, Life Technologies, Carlsbad, CA, USA), and 3.7 $g.L^{-1}$ $NaHCO_3$. Cellular subcultures were performed using 0.05% trypsin/EDTA (Gibco BRL, Invitrogen). Stimulation of cells was carried out inside a CO_2 incubator (Galaxy 14S, New Brunswick Scientic) featuring a communication port that was employed to deliver electric signals to electrodes.

Excitations to power stimulators were congured using a real-time application that was developed using Simulink (v. 7.3, Mathworks) and the Real Time Workshop (v. 7.3, Mathworks) and run using the Real Time Windows Target (v. 3.3, Mathworks) kernel. Excitations were generated by an IO card (MF 624, Humusoft).

Resazurin metabolic and Trypan blue cell score assays

The resazurin colorimetric assay, which analyses the amounts of NADH/NADPH produced by metabolic active cells, was used to determine the effect of LF ST and HF ST on cell viability (as previously described [56]). Briefly, at 1, 3, 5, 7, 14 and 21 DIV, cells were incubated for 4h with a 10% resazurin (Sigma-Aldrich) in MEM medium solution. Resazurin reduction was spectrophotometrically measured at 570 and 600 nm (Infinite M200 PRO, Tecan); the OD 570/OD 600 nm ratio was calculated for each condition [56] and presented as fold increases over control cells (NO ST) levels at 1 DIV. The trypan blue (Sigma-Aldrich) membrane exclusion assay was used in direct cell scoring to assess cell proliferation. Briefly, cells (1×10^3, 5×10^3, 1×10^4) were plated into 35 mm dishes ($\approx$10 cm^2) with 1 mL fresh media. Upon 24 h in culture at 5% CO_2/37°C (either on the cosurface CC stimulators or not), the number of viable cells was scored (as previously

Table I: Dielectric and magnetic properties of materials and media used to simulate EF and MF stimulations.

	Relative electric permittivity	**Electric conductivity (S/m)**	**Relative magnetic permeability**
Electrodes	1	6×10^7	1
Petri dish	2.6	6.7×10^{-14}	1
Substrate	3	6.7×10^{-14}	0.866
Air	1	0	1
Cellular medium (MED1 and MED2)	73	1.6	1
Physiological medium (MED1 and MED2)	73	1.2×10^{-7}	1

reported [56]).

Alkaline phosphatase activity

ALP is an enzyme that hydrolyzes organic phosphates to increase phosphate concentration and prepare the cell for matrix mineralization by hydroxyapatite crystals. Intracellular ALP activity was measured at 15 DIV using ALP substrate (p-Nitrophenyl phosphate, Merck Chemicals). Briefly, cells were washed with PBS, collected in Triton X-100 1% and incubated at 4°C, 200 rpm. After sonication on ice (30 sec), the cellular content was homogenized and an aliquot (20 μl) transferred to a 96-well plate in triplicate. After incubation with 200 μl of the ALP substrate (1 h at 37°C in dark), the enzymatic reaction was quantified in a microplate reader at 405 nm.

Western blot analyses

At 7 and 14 DIV, cells and conditioned media were harvested into SDS 1% solutions and subjected to a 5-20% gradient (cells lysates) or 7.5% (cell media) SDS-PAGE and to western blot (WB) analyses (as previously described [57]). Previous to WB, ponceau S reversible staining was first used for detection of total protein content on nitrocellulose membranes [58]. After overnight incubation at 4°C with the primary antibodies [rabbit anti-collagen type I (1:1000); rabbit anti-osteonectin (1:500); mouse anti-β-Actin (1:1000), all from Novus Biologicals, Germany], horseradish peroxidase-linked (GE Healthcare, Chalfont St. Giles, UK) antibodies for enhanced chemiluminescence (ECL) detection were incubated 2 h/RT. Protein bands were scanned and quantified (GS-800® Calibrated Densitometer and Quantity One densitometry software, Bio-Rad), and WB data corrected to the respective ponceau loading control (as previously reported [58]).

Morphological confocal microscopy analysis

MC3T3 cells grown on coverslips-containing 35 mm petri dishes and subjected for 21 DIV to LF and HF stimulation were fixed in 4% paraformaldehyde (PFA) for 20 min and permeabilized with 0.1% Triton X-100 in PBS (15 min/RT). Immunocytochemistry of collagen-I, F-actin staining with phalloidin, and nuclear staining with DAPI was as previously described [59]. The anti-type-I collagen I antibody (1:250 in 3% BSA-PBS), a FITC-conjugated secondary antibody (1:300 in 3% BSA-PBS), and red fluorescing Alexa 568-labelled Phalloidin (1:500) were used. Images were acquired with a plan-Neofluor 40×/1.30 oil objective in a LSM 510 META confocal microscope (Zeiss, Jena, Germany) (as previously described [59]), in the iBiMED's Imaging Facility, a node of PPBI (Portuguese Platform of BioImaging).

Alizarin red staining (ARS) visualization and quantification

Matrix mineralization was analysed as previously described [60]. Briefly, cells were washed in PBS, fixed in 4% PFA/20 min, washed in dH_2O and incubated with Alizarin red solution (40 mM, pH4.1, Sigma; 20 min/RT). Non-incorporated staining was removed and cells thoroughly washed before image acquisition.

Acknowledgments

This work is funded by FEDER funds through the Operational Programme Competitiveness Factors (COMPETE) and the Portuguese Foundation for Science and Technology (FCT) - grant reference SFRH/BD/78414/2011 and project reference EXPL/EMS-SIS/2128/2013.

Additional information

Competing financial interests: The authors declare no competing financial interests.

References

[1] K-M. Chan, C. G. Rolf, L. Qin, L. Felländer-Tsai, R. M. Castelein, D. B. Saris, J. Malda, G. Richards, S. B. Goodman, R. S. Tuan, W. Maloney, L. Lidgren, C. Hopkins, S-C. Fu, G. Li, M. Ding, T. Tang, X. Zhang, L. Wei, H. B. Sun, H. Ouyang, Musculoskeletal regeneration research network: A global initiative, Journal of Orthopaedic Translation 3(4) (2015) 160-165.

[2] L. March, E. U. Smith, D. G. Hoy, M. J. Cross, L. Sanchez-Riera, F. Blyth, R. Buchbinder, T. Vos, A. D. Woolf, Burden of disability due to musculoskeletal (MSK) disorders, Best Practice & Research Clinical Rheumatology 28(3) (2014) 353-366.

[3] R. Pivec, A. J. Johnson, S. C. Mears, M. A. Mont, Hip arthroplasty, Lancet 380 (2012) 1768-1777.

[4] A. J. Carr, O. Robertsson, S. Graves, A. J. Price, N. K. Arden, A. Judge, D. J. Beard, Knee replacement, Lancet 379 (2012) 1331-1340.

[5] B. H Kapadia, R. A. Berg, J. A. Daley, J. Fritz, A. Bhave, M. A. Mont, Periprosthetic joint infection, Lancet, in press.

[6] S. Kurtz, K. Ong, E. Lau, F. Mowat, M. Halpern, Projections of primary and revision hip and knee arthroplasty in the United States from 2005 to 2030, The Journal of Bone & Joint Surgery 89(4) (2007) 780-785.

[7] G. Labek, M. Thaler, W. Janda, M. Agreiter, B. Stöckl, Revision rates after total joint replacement - cumulative results from worldwide joint register datasets, The Journal of Bone & Joint Surgery 93-B(3) (2011) 293-297.

[8] M. P. Soares dos Santos, J. A. Ferreira, A. Ramos, J. A. Simões, R. Morais, N. M. Silva, P. M. Santos, M. C. Reis, T. Oliveira, Instrumented hip joint replacements, femoral replacements and femoral fracture stabilizers, Expert Review of Medical Devices 11(6) (2014) 617-635.

[9] J. Torrão, M. P. Soares dos Santos, J. A. Ferreira, Instrumented knee joint implants: innovations and promising concepts, Expert Review of Medical Devices 12(5) (2015) 571-584.

[10] V. Goriainov, R. Cook, J. M. Latham, D. G. Dunlop, R. O. Oreffo, Bone and metal: An orthopaedic perspective on osseointegration of metals, Acta Biomaterialia 10(10) (2014) 4043-4057.

[11] P. G. Coelho, R. Jimbo, Osseointegration of metallic devices: current trends based on implant hardware design, Archives of Biochemistry and Biophysics 561 (2014) 99-108.

[12] P. G. Coelho, T. Takayama, D. Yoo, R. Jimbo, S. Karunagaran, N. Tovar, M. N. Janal, S. Yamano, Nanometer-scale features on micrometer-scale surface texturing: A bone histological, gene expression, and nanomechanical study, Bone 65 (2014) 25-32.

[13] D. R. Sumner, Long-term implant fixation and stress-shielding in total hip replacement, Journal of Biomechanics 48(5) (2015) 797-800.

[14] E. E. Pakos, K. S. Stafilas, A. E. Tsovilis, J. N. Vafiadis, N. K. Kalos, T. A. Xenakis, Long term outcomes of total hip arthroplasty with custom made femoral implants in patients with congenital disease of hip, The Journal of Arthroplasty, 30(12) (2015) 2242-2247.

[15] J.F. Bartolomé, J. S. Moya, R. Couceiro, C.F. Gutiérrez-González, F. Guitián, A. Martinez-Insua, In vitro and in vivo evaluation of a new zirconia/niobium biocermet for hard tissue replacement, Biomaterials 76 (2016) 313-320 (2016).

[16] M. P. Soares dos Santos, J. A. Ferreira, A. Ramos, J. A. Simões, Active orthopaedic implants: Towards optimality, Journal of the Franklin Institute 352(3) (2015) 813-834.

[17] S. B. Goodman, Z. Yao, M. Keeney, F. Yang, The future of biologic coatings for orthopaedic implants, Biomaterials 34(13) (2013) 3174-3183.

[18] B. G. Zhang, D. E. Myers, G. G. Wallace, M. Brandt, P. F. Choong, Bioactive coatings for orthopaedic implants - recent trends in development of implant coatings, International Journal of Molecular Sciences 15(7) (2014) 11878-11921.

[19] J. H. Goosen, A. J. Kums, B. J. Kollen, C. C. Verheyen, Porous-coated femoral components with or without hydroxyapatite in primary uncemented total hip arthroplasty: a systematic review of randomized controlled trials, Archives of Orthopaedic and Trauma Surgery 129(9) (2009) 1165-1169.

[20] J. A. Lyndon, B. J. Boyd, N. Birbilis, Metallic implant drug/device combinations for controlled drug release in orthopaedic applications, Journal of Controlled Release 179 (2014) 63-75.

[21] J. He, T. Huang, L. Gan, Z. Zhou, B. Jiang, Y. Wu, F. Wu, Z. Gu, Collagen-infiltrated porous hydroxyapatite coating and its osteogenic properties: In vitro and in vivo study, Journal of Biomedical Materials Research Part A 100A (7) (2012) 1706-1715.

[22] Q. Xu, Y. Tanaka, J. T. Czernuszka, Encapsulation and release of a hydrophobic drug from hydroxyapatite coated liposomes, Biomaterials 28(16) (2007) 2687-2694.

[23] F. Graichen, G. Bergmann, A. Rohlmann, Hip endoprosthesis for in vivo measurement of joint force and temperature, Journal of Biomechanics 32(10) (1999) 1113-1117.

[24] P. Damm, F. Graichen, A. Rohlmann, A. Bendera, G. Bergmann, Total hip joint prosthesis for in vivo measurement of forces and moments, Medical Engineering & Physics 32(1) (2010) 95-100.

[25] G. Bergmann, F. Graichen, J. Dymke, A. Rohlmann, G. N. Duda, P. Damm, High-tech hip implant for wireless temperature measurements in vivo, PLoS One 7(8) (2012) e43489.

[26] J. Reis, C. Frias, C. Canto e Castro, M. L. Botelho, A. Torres Marques, J. A. Simões, F. Capela e Silva, J. Potes, A new piezoelectric actuator induces bone formation in vivo: a preliminary study, Journal of Biomedicine and Biotechnology 2012 (2012) 1-7.

[27] N. Aydin, M. Bezer, The effect of an intramedullary implant with a static magnetic field on the healing of the osteotomised rabbit femur, International Orthopaedics 35(1) (2011) 135-141.

[28] C. Schmidt, U. Zimmermann, U. van Rienen, Modeling of an optimized electro-stimulative hip revision system under consideration of uncertainty in the conductivity of bone tissue, IEEE Journal of Biomedical and Health Informatics 19(4) (2015) 1321-1330.

[29] R. Balint, N. J. Cassidy, S. H. Cartmell, Electrical Stimulation: A Novel Tool for Tissue Engineering, Tissue Engineering Part B: Reviews 19(1) (2013) 48-57.

[30] W. Zhenyu, C.C. Clark, C. T. Brighton, Up-regulation of bone morphogenetic proteins in cultured murine bone cells with use of specific electric fields, The Journal of Bone & Joint Surgery 88(5) (2006) 1053-1065.

[31] C. T. Brighton, W. Wang, R. Seldes, G. Zhang, S. R. Pollack, Signal transduction in electrically stimulated bone cells, The Journal of Bone & Joint Surgery 83-A(10) (2001) 1514-1523.

[32] H-P. Wiesmann, M. Hartig, U. Stratmann, U. Meyer, U. Joos, Electrical stimulation influences mineral formation of osteoblast-like cells in vitro, Biochimica et Biophysica Acta (BBA) - Molecular Cell Research 1538(1) (2001) 28-37.

[33] M. Hartig, U. Joos, H. P. Wiesmann, Capacitively coupled electric fields accelerate proliferation of osteoblast-like primary cells and increase bone extracellular matrix formation in vitro, European Biophysics Journal 29(7) (2000) 499-506.

[34] M. Griffin, S. A. Iqbal, A. Sebastian, J. Colthurst, A. Bayat, Degenerate wave and capacitive coupling increase human MSC invasion and proliferation while reducing cytotoxicity in an in vitro wound healing model, PLoS One 6(8) (2011) e23404.

[35] M. Hronik-Tupaj, D. L. Kaplan, A Review of the responses of two- and three-dimensional engineered tissues to electric fields, Tissue Engineering Part B: Reviews 18(3) (2012) 167-180.

[36] Vijayalaxmi, G. Obe, Controversial cytogenetic observations in mammalian somatic cells exposed to extremely low frequency electromagnetic radiation: a review and future research recommendations, Bioelectromagnetics 26(5) (2005) 412-430.

[37] M-S. Lee, K. Lee, S-Y. Kim, H. Lee, J. Park, K-H. Choi, H-Ki. Kim, D-G. Kim, D-Y. Lee, S. Nam, J-U. Park, High-performance, transparent, and stretchable electrodes using graphene-metal nanowire hybrid structures, Nano Letters 13(6) (2013) 2814-2821.

[38] M. Griffin, A. Sebastian, J. Colthurst, A. Bayat, Enhancement of differentiation and mineralisation of osteoblast-like cells by degenerate electrical waveform in an in vitro electrical stimulation model compared to capacitive coupling, PLoS One 8(9) (2013) e72978.

[39] L. D. Quarles, D. A. Yohay, L. W. Lever, R. Caton, R. J. Wenstrup, Distinct proliferative and differentiated stages of murine MC3T3-E1 cells in culture: an in vitro model of osteoblast development, Journal of Bone and Mineral Research 7(6) (1992) 683-92.

[40] H. Ozawa, E. Abe, Y. Shibasaki, T. Fukuhara, T. Suda, Electric fields stimulate DNA synthesis of mouse osteoblast-like cells (MC3T3-El) by a mechanism involving calcium ions, Journal of Cellular Physiology 138(3) (1989) 477-483.

[41] H. Zhuang, W. Wang, R. M. Seldes, A. D. Tahernia, H. Fan, C. T. Brighton, Electrical stimulation induces the level of TGF-β1 mRNA in osteoblastic cells by a mechanism involving calcium/calmodulin pathway, Biochemical and Biophysical Research Communications 237(2) (1997) 225-229.

[42] R. J. Fitzsimmons, D. D. Strong, S. Mohan, D. J. Baylink, Low-amplitude, low-frequency electric field-stimulated bone cell proliferation may in part be mediated by increased IGF-II release, Journal of Cellular Physiology 150(1) (1992) 84-89.

[43] R. J. Fitzsimmons, J. R. Farley, W. R. Adey, D. J. Baylink, Frequency dependence of increased cell proliferation, in vitro, in exposures to a low-amplitude, low-frequency

electric field: evidence for dependence on increased mitogen activity released into culture medium, Journal of Cellular Physiology 139(3) (1989) 586-591.

[44] M. P. Soares dos Santosa, J. A. Ferreira, A. Ramos, J. A. Simões, R. Morais, N. M. Silva, P. M. Santos, M. J. Reis, T. Oliveira, Instrumented hip implants: Electric supply systems, Journal of Biomechanics 46(15) (2013) 2561-2571.

[45] C. M. Creecy, C. F. O'Neill, B. P. Arulanandam, V. L. Sylvia, C. S. Navara, R. Bizios, Mesenchymal stem cell osteodifferentiation in response to alternating electric current, Tissue Engineering Part A 19(3-4) (2013) 467-474.

[46] M. Hronik-Tupaj, W. L. Rice, M. Cronin-Golomb, D. L. Kaplan, I. Georgakoudi, Osteoblastic differentiation and stress response of human mesenchymal stem cells exposed to alternating current electric fields, BioMedical Engineering OnLine 10(9) (2011) 1-22.

[47] N. Selvamurugan, S. Kwok, A. Vasilov, S. C. Jefcoat, N. C. Partridge, Effects of BMP-2 and pulsed electromagnetic field (PEMF) on rat primary osteoblastic cell proliferation and gene expression, Journal of Orthopaedic Research 25(9) (2007) 1213-1220.

[48] J. Zhou, L-G. Ming, B-F. Ge, J-Q. Wang, R-Q. Zhu, Z. Wei, H-P. Ma, C. J. Xian, K-M. Chen, Effects of 50 Hz sinusoidal electromagnetic fields of different intensities on proliferation, differentiation and mineralization potentials of rat osteoblasts, Bone 49(4) (2011) 753-761.

[49] S. Lavenusa, P. Pilet, J. Guicheux, P. Weiss, G. Louarn, P. Layrolle Behaviour of mesenchymal stem cells, fibroblasts and osteoblasts on smooth surfaces, Acta Biomaterialia 7(4) (2011) 1525-1534.

[50] R. J. Fitzsimmons, J. T. Ryaby, S. Mohan, F. P. Magee, D. J. Baylink, Combined magnetic fields increase insulin-like growth factor-II in TE-85 human osteosarcoma bone cell cultures, Endocrinology 136(7) (1995) 3100-106 (1995).

[51] M. P. Soares dos Santos, J. A. Ferreira, J. A. Simões, R. Pascoal, J. Torrão, X. Xue, E. P. Furlani, Magnetic levitation-based electromagnetic energy harvesting: a semi-analytical non-linear model for energy transduction, Scientific Reports 6 (2016) 18579.

[52] N. M. Silva, P. M. Santos, J. A. Ferreira, M. P. Soares dos Santos, A. Ramos, J. A. Simões, M. J. Reis, R. Morais, Power management architecture for smart hip prostheses comprising multiple energy harvesting systems, Sensors and Actuators A: Physical 202(1) (2013) 183-192.

[53] V. P. Tomaselli, M. H. Shamos, Electrical properties of hydrated collagen. I. Dielectric properties, Biopolymers 12(2) (1973) 353-366.

[54] V. P. Tomaselli, M. H. Shamos, Electrical Properties of Hydrated Collagen. II. Semiconductor Properties, Biopolymers 13(12) (1974) 2423-2434.

[55] G. Pucihar, T. Kotnik, M. Kandušer, D. & Miklavčič, The influence of medium conductivity on electropermeabilization and survival of cells in vitro, Bioelectrochemistry 54(2) (2001) 107-115.

[56] S. Pina, S. I. Vieira, P. M. Torres, F. Goetz-Neunhoeffer, J. Neubauer, O. A. da Cruz e Silva, E. F. da Cruz e Silva, J. M. Ferreira, In vitro performance assessment of new brushite-forming Zn- and ZnSr-substituted β-TCP bone cements, Journal of Biomedical Materials Research Part B: Applied Biomaterials 94(2) (2010) 414-420.

[57] A. G. Henriques, S. I. Vieira, E. F. da Cruz e Silva, O. A. Cruz e Silva, Aβ hinders nuclear targeting of AICD and Fe65 in primary neuronal cultures, Journal of Molecular Neuroscience 39 (1-2) (2009) 248-255.

[58] J. F. Rocha, O. A. da Cruz e Silva, S. I. Vieira, Analysis of the Amyloid Precursor Protein (APP) role in neuritogenesis reveals a biphasic SH-SY5Y neuronal cell differentiation model, Journal of Neurochemistry 134(3) (2015) 288-301.

[59] P.M. Torres, S.I. Vieira, A. R. Cerqueira, S. Pina, O. A. da Cruz Silva, J. C. Abrantes, J. M. Ferreira, Effects of Mn-doping on the structure and biological properties of β-tricalcium phosphate, Journal of Inorganic Biochemistry 136 (2014) 57-66.

[60] C. A. Gregory, W. G. Gunn, A. Peister, D. J. Prockop, An Alizarin red-based assay of mineralization by adherent cells in culture: comparison with cetylpyridinium chloride extraction, Analytical Biochemistry 329(1) (2004) 77-84.

Chapter 5

Self-powering systems for instrumented implants

Instrumented active implants must be suitably powered with electric energy to ensure their control operations over the peri-implant bone volume. As noticed in the literature review (section 3.3), these implants have been electrically supplied only by inductive powering or battery systems. According to the requirements that must be fulfilled to ensure a controlled and personalized osseointegration (section 4), self-powering systems must be designed to support the everlasting operation of the actuation, monitoring, communication and processing systems. Furthermore, their ability to readily provide electric power is a fundamental criterion to ensure that any of the stimulatory therapies chosen by the clinician are performed, although there are always constraints that confine the power consumption. Nevertheless, energy harvesting and storage systems must allow the therapeutic actuation throughout the routine activities of patients. Such requirements for powering instrumented active implants demand further advances on the optimization of energy harvesting systems. Promising results on the potential of motion-driven electromagnetic and piezoelectric energy harvesters were achieved.

5.1 Electric energy harvested from hip motions

There are important advantages using magnetic levitation to harvest electric energy: (a) harvesters are low-cost, maintenance-free, non-complex and easy to manufacture; (b) harvesters operate autonomously with stable performance during long time periods; (c) intelligent control algorithms can control the position of their components according to the excitations' characteristics. These advantages can be explored to power instrumented hip implants. As highlight the viability analysis reported in section 3.1, this motion-driven method is among the most promising ones to effectively supply these implants. To start analysing if hip motions of human patients can be used to power instrumented hip implants during normal daily activities, an experimental test was designed to determine the amount of energy harvested by a magnetic levitation-based electromagnetic energy harvester during walking. Preliminary results were achieved without geometric optimization of harvesters prior to fabrication or intelligent control algorithms to maximize the energy harvesting. This study is entitled "An electical power supply system for instrumented hip joint prostheses" and is published in the *Proceedings of the 7th World Congress of Biomechanics*[1].

[1]As the content of this study is already published, the formatting rules established by the organizing committee of the *7th World Congress of Biomechanics* are used.

AN ELECTRICAL POWER SUPPLY SYSTEM FOR INSTRUMENTED HIP JOINT PROSTHESES

Marco P. Soares dos Santos[1,2], Jorge A. F. Ferreira[2] , Daniel R. Fernandes[2], A. Ramos[1,2], José A. O. Simões[2]

[1] Biomechanics Research Group, Centre for Mechanical Technology and Automation, University of Aveiro, Campus Universitário de Santiago, 3810-193 Aveiro, Portugal.

[2] Department of Mechanical Engineering, University of Aveiro, Aveiro, Portugal.

Introduction:

The number of hip replacements (THR), including uncemented ones, is increasing. Revisions are increasing as well. The increasing number of "young" patients subjected to THR is being reported annually. Soares dos Santos et al. (2013) reviewed the power supply systems of the instrumented hip implants (IHI) implanted *in-vivo*. They concluded that: (1) only inductive power links and batteries were used, which constrain the operation of IHI; (2) motion-driven energy harvesters (M-EHS) are promising methods to power IHI, both to detect failures (such as loosening and/or infections) and to apply therapeutic stimuli in the bone-implant interface.

Methods:

A M-EHS, based on magnetic levitation, was implemented (Fig.1a). It was composed by: (i) 3 neodymium magnets: 2 N48 (A), 6 mm diameter, 6 mm height; a N46 (B), 6 mm diameter, 3 mm height; (ii) a coil with 9000 turns, which was enamelled with copper wire (AWG 42, 0,068 mm diameter) around a hollowed Teflon cylinder (HTC). Magnets A were suspended inside the HTC. Magnet B was attached at the lower end of the HTC. This harvester was embedded into the stem of a hollowed Metabloc™ hip prosthesis (Zimmer, EUA). Magnets (A) operate as moving magnets when hip motion occurs, which harvest electric energy.

This self-powered IHI was attached to the left thigh of a human male (22 years old, 814 N weight) wearing hiking boots. The energy harvested was monitored during 2,5 gait cycles of normal walking at 1,05 m/s speed over 4,3 s.

Results:

67,3 μJ of electric energy was harvested throughout the walking trial (Fig.1b). According to the study conducted by M. Morlock (Technical University Hamburg-Harburg) about the duration of everyday activities of patients that underwent THR, patients walk 4386 s per 12 hours (mean values). Thus, 68,65 mJ of electric energy can be harvested each day only by walking (2.06 J each month).

Authors are validating a nonlinear model to predict the energy harvested when the M-EHS moves in the three-dimensional space, in order to optimize the harvester and maximize the energy harvested for each patient.

Reference

Marco P. Soares dos Santos et al. (2013). Instrumented hip implants: Electric supply systems. *Journal of Biomechanics* 46(15) 2561-2571.

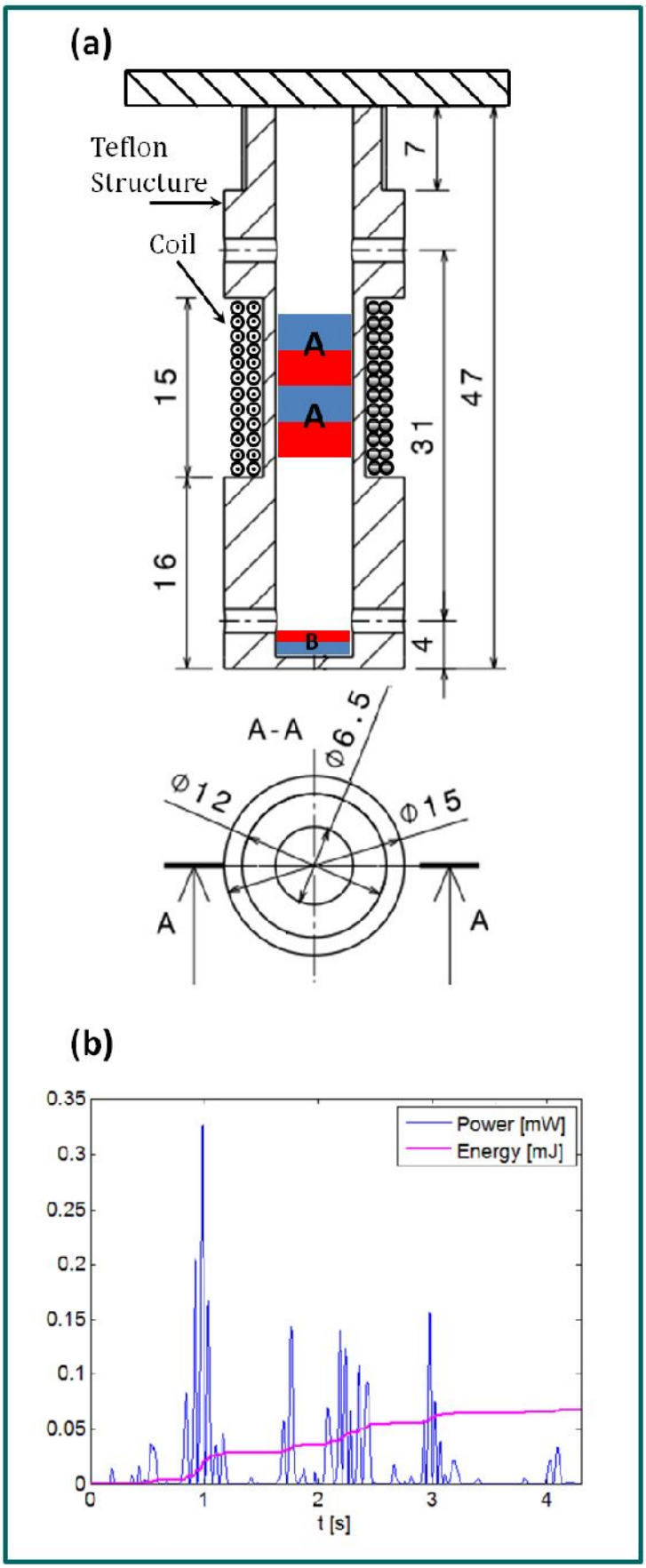

Fig.1: (a) M-EHS (section view); (b) Power and energy harvested.

5.2 The new concept of Multi-source Harvesting System

The reliability of self-powering systems certainly can be improved if multiple harvesting systems operate in true parallel to power the instrumented implant. Such a redundant structure for power supplying is mandatory to ensure the atemporal implant operation. An instrumented hip prosthesis was designed with two electromagnetic harvesters (a translational and a rotational) and a piezoelectric harvester. The validation of this new concept is reported in a chapter entitled "Multi-source Harvesting Systems for Electric Energy Generation on Smart Hip Prostheses", published in the book *Biomedical Engineering Systems and Technologies* (Springer-Verlag Berlin Heidelberg 2013, pp. 80-96)[2].

[2]As the content of this study is already published, the formatting rules established by the Editorial Board of the *Communications in Computer and Information Science* are used.

Multi-source Harvesting Systems for Electric Energy Generation on Smart Hip Prostheses*

Marco P. Soares dos Santos[1], Jorge A.F. Ferreira[1], A. Ramos[1], Ricardo Pascoal[1], Raul Morais dos Santos[2,3], Nuno M. Silva[2], José A.O. Simões[1], M.J.C.S. Reis[4], António Festas[1], and Paulo M. Santos[2]

[1] Department of Mechanical Engineering, University of Aveiro, Aveiro, Portugal
[2] UTAD - University of Trás-os-Montes e Alto Douro, Vila Real, Portugal
[3] Center for the Research and Technology of Agro-Environmental and Biological Sciences, Vila Real, Portugal
[4] Institute of Electronics and Telematics Engineering of Aveiro/UTAD, Vila Real, Portugal
marco.santos@ua.pt

Abstract. The development of smart orthopaedic implants is being considered as an effective solution to ensure their everlasting life span. The availability of electric power to supply active mechanisms of smart prostheses has remained a critical problem. This paper reports the first implementation of a new concept of energy harvesting systems applied to hip prostheses: the multi-source generation of electric energy. The reliability of the power supply mechanisms is strongly increased with the application of this new concept. Three vibration-based harvesters, operating in true parallel to harvest energy during human gait, were implemented on a $Metabloc^{TM}$ hip prosthesis to validate the concept. They were designed to use the angular movements on the flexion-extension, abduction-adduction and inward-outward rotation axes, over the femoral component, to generate electric power. The performance of each generator was tested for different amplitudes and frequencies of operation. Electric power up to 55 μJ/s was harvested. The overall function of smart hip prostheses can remain performing even if two of the generators get damaged. Furthermore, they are safe and autonomous throughout the life span of the implant.

1 Introduction

1.1 Scope of the Problem and Background

Currently, there is no cure for most causes of failure of total joint replacement, except surgical revision [1]. Although drug administration, such as through antimicrobial therapy, suppressive antibiotic therapy, outpatient parenteral antimicrobial therapy and antibiotic prophylaxis, are being used to hinder progressive failure following joint replacement [2], surgical revisions have been the only "medical prescription" for most causes of failure [1]. However, these surgical procedures are not therapeutic methods which are performed to cure or to prevent early failures, but only to relieve pain and to

* The authors would like to thank the Portuguese Foundation for Science and Technology (FCT) for their financial support under the Grant PTDC/EME-PME/ 105465/2008.

J. Gabriel et al. (Eds.): BIOSTEC 2012, CCIS 357, pp. 80–96, 2013.

improve joint function [3]. The ordinary methodology to improve prostheses' function has been based on the research of new designs, new materials, new fixation techniques and new surgical techniques [4–6]. Although the everlasting life span is an essential requirement for the next healthcare bio-systems generations, the 20-year revision rate of current orthopaedic prostheses is still higher than 20%. Demographic changes and scientific breakthroughs are the main reasons ascribed to the increase in the number of primary and revision joint replacements [3], as well as the strong demand for joint replacements and revisions predicted for the coming years [7]. After the first revision procedure, the risk of failure increases even more [8]. Furthermore, the increase in the number of inpatients less than 65 years due to joint disorders [9] is also being considered an important reason that supports the hypothesis of developing a new methodology to design prostheses with the ability to control their own life span. Current hip prostheses are passive implants because they are not smart enough to promote maximal bone-implant interaction. They match their design methodology with a design "not to know" and "not to act against".

Instrumented prostheses have been developed since the 60's of the 20th century [10]. Their methodological basis is to perform *in-vivo* measurement and data storage functions to optimize passive implants, surgical procedures, preclinical testing and physiotherapy programs [11, 12]. They have been used to validate models of the physiological environment and customize physiotherapy programs [13, 14]. Contact forces and moments in the joint, temperature distribution along the implant, articular motions, misalignments and detection of hip loosening [15–22] are the main quantities which have been collected by instrumented implants. Telemetric platforms for orthopaedic implants are being optimized to minimize electric energy consumption [22, 23]. Also, activation circuits to wake up deep sleep electronics have already been developed to instrument hip prostheses [24].

Several causes of implant failures were already identified [25]. Loosening, infection, instability, heterotopic ossification or fractures not only can conduct to pain and inability to walk, to self-care and to perform activities of daily living, but also can cause cardiovascular, pulmonary, renal, arterial, nerve or infectious complications, or even malignancy. More than 80% of the non-success surgical procedures are due to loosening of the prosthetic stem and cup [26]. Methods for hip loosening detection in hip implants, as well as to identify the regions impaired by this progressive failure throughout the implant's life span, are currently being proposed [19, 26]. Efficient power management circuits were designed to energize telemetric system of smart hip implants [27]. Even though the number of methods and configurations to transduce energy from the surrounding environment into electric energy is increasing [28–32], few research efforts have been conducted to provide electric power supply for instrumented hip prosthesis. Vibration-based energy harvesting is being considered the most appropriate method to generate electric energy to supply the active elements of instrumented prostheses [27]. In order to enable loosening detection, an electromagnetic power transducer was recently proposed by Morais et al. [27] to harvest electrical energy from the human gait to supply smart hip prostheses. However, it was designed only with a single generator, which decreases the reliability of the electric power generation because it is not a redundant structure for power supplying. No studies have been reported about methods to ensure high reliability of the electric energy generation on instrumented prostheses.

1.2 Method

Three vibration-based energy harvesting systems were designed to implement a reliable electric power supply of a smart hip prosthesis. Linear models were developed in order to analyse their accuracy predicting the energy generation. Each generator was independently tested. Voltage generation was acquired from different rotational and translational movements.

1.3 Paper Contribution

This paper's main contribution is to validate the multi-source generation concept applied to smart hip prostheses. The main goal in the implementation of these harvesting systems is to enable a multifunctional ability of the hip prosthesis, namely to monitor and report failures, and carry out mechanical-based therapeutic prescriptions.

1.4 Main Conclusions

This study shows that it is possible to implement high reliability electric power supplies for active hip prostheses. It was also concluded that linear models of the generators are very inaccurate in this particular application. Experimental results show that they must be optimized in order to maximize their performance during typical walking speeds and to reduce their volume, which demands for accurate non-linear models to predict the energy generation for multi-displacements of the hip prostheses.

1.5 Outline

The new concept of smart hip prosthesis is introduced in section 2. The design of the three power generator prototypes is detailed in section 3. Experimental and simulation results are presented in section 4. Discussion and conclusions are stated respectively in sections 5 and 6.

2 The New Concept of Smart Hip Prosthesis

Passive prostheses are orthopaedic implants without active components implemented to overcome failures that may occur over time. They are designed: (1) without information about themselves, about the physiological environment that surrounds them and about how to fix their own problems; (2) without resources to eliminate causes of failures; (3) without a "true" connection with medical specialists. The ineffectiveness of this method to overcome complications after primary joint replacement is caused by this passivity, because a maximal interaction with the surrounding physiological environment is not taken into account. The concept of smart orthopaedic implant was proposed to be based on a *smartness-to-measure* methodology [33], but is becoming obsolete as the concept of individualized therapy evolves for accommodating patient physiologic idiosyncrasies [34]. Several studies have contributed to identify the function of strain,

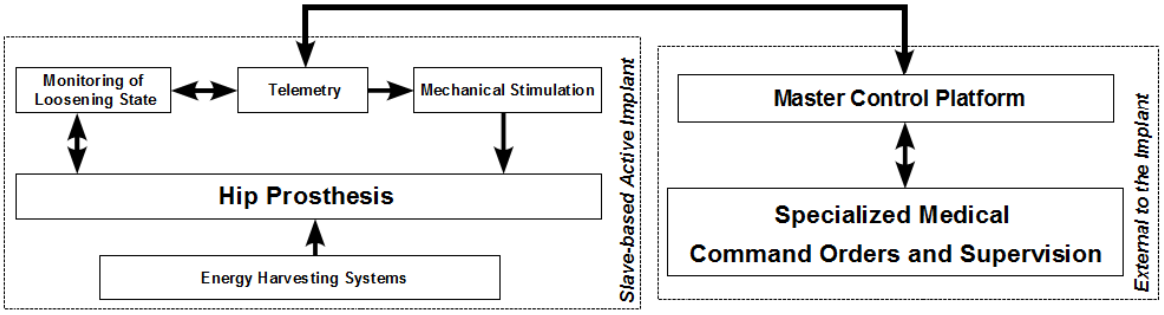

Fig. 1. Block diagram of the new concept of smart orthopaedic implant

load and frequency of mechanical stimulus on the osteogenic responses [35–37], which contributed to hypothesize that the implementation of mechanisms to carry out artificial stimulation programs on bone cells can be an effective and efficient solution to overcome hip loosening. The new concept is based on the *smartness-to-act* methodology in order to prevent and cure failures following primary arthroplasty, avoiding the need of revision procedures. Smart orthopaedic devices must ensure personalized therapy, through: (1) remote communication with external systems outside the human body; (2) monitoring of physical and biological states which can be used to detect early causes of failure; (3) decision-making ability when causes of failure are detected; (4) mechanical actuation-based therapy in the physical and biological states which have a decisive influence on the lifetime of the implant, depending on medical supervision. This long-term survivability biosystem is based on the *tip-of-the-spear* methodology [34], envisioning the application of Paul Ehrlich's *magic bullet* concept [38] to orthopaedic devices: implants must have enough "knowledge" and tools to administer the therapy in the most suitable place and at the most suitable time. To validate the concept, a prototype is being developed, according to the Fig. 1, in order to enable the early detection and cure of aseptic loosening throughout the life span of the hip prosthesis. The methodology is based on the implementation of mechanical micro-stimulation to remodel the bone surrounding the implant in the regions where loosening is detected. Several subsystems were already implemented by this research team toward the validation of a new concept of smart hip prostheses, namely: (1) a generator of electric energy based on double permanent magnet vibration, as well as power management schemes [27]; (2) a telemetric architecture [24, 27, 39]; (3) a piezoresistive-based mechanism to detect prosthetic loosening [26]; (4) a piezoelectric-based stimulation mechanism [35, 40, 41].

3 Material and Methods

3.1 Hip Prosthesis Prototype

A *Metabloc*^{TM} straight stem system (*Zimmer* Corporate, Warsaw, Indiana, EUA), size 10, was hollowed to design a hip prosthesis prototype comprising three vibration-based electric power generators (Fig. 2). Fatigue tests on hollow bone implants were already conducted [16], which have proved the safety of the approach.

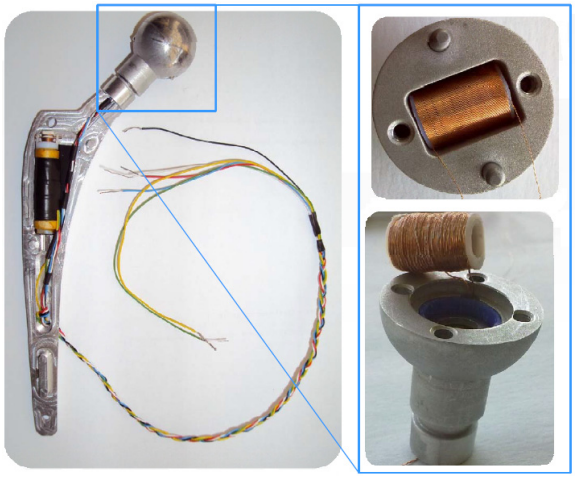

Fig. 2. Multiple Energy harvesting systems for a hip prosthesis prototype

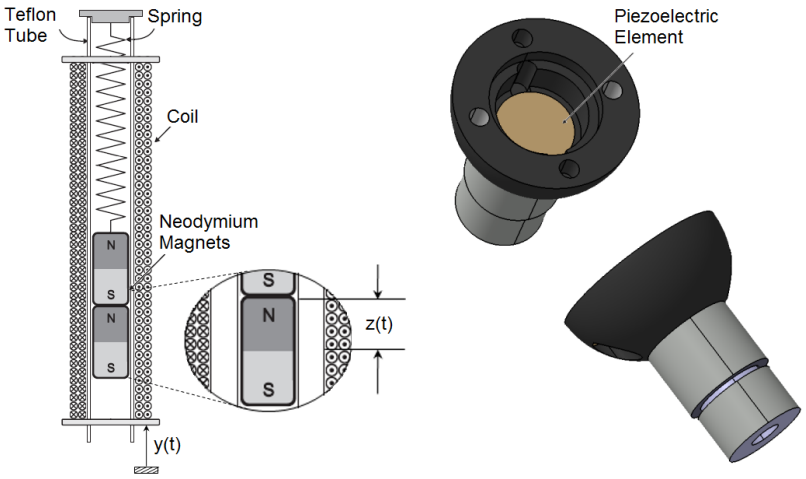

Fig. 3. (Left) Scheme of the TEEH generator; (Right) CAD of the PEH generator

3.2 Translation-Based Electromagnetic Power Generator (TEEH)

Power Generator Prototype Design. An electromagnetic power transducer was designed in the body of the hip prosthesis, as shown in Fig. 3 (left). It transduces mechanical movements, from the abduction-adduction and flexion-extension axes, into electric energy. The generator prototype comprises an extension coil spring ($K = 2.45$ N/m, 5 mm of diameter and 0.2 mm^2 of wire section) and 2 neodymium disc magnets N35 (6 mm of diameter, 6 mm of height and 1.22 T of magnetic field). These magnets are suspended inside a Teflon tube ($c_m = 0.04$) where enamelled copper wire (0.1 mm of diameter, 27 mm of length and 1.72×10^{-8} Ωm of electrical resistivity) was wound ($N = 2000$ turns, 124.4 Ω of total wire resistance), which in turn was attached to the hip prosthesis fixture. The coil and the prosthesis make up the body frame. A relative displacement $z(t)$ between the magnets and the frame comes up due to the hip displacements $y(t)$, which are transmitted by the body frame.

Linear Model of the TEEH System. Linearly, vibration-based generators can be modelled as second-order mass-spring-damper systems [29, 42, 43], as described by equation (1). The mechanical structure can be modelled as an inertial frame where a suspended mass is coupled to a spring, which in turn is coupled to a damping element. The mass represents a set of magnets and the damper represents the sum of the comprising parasitic losses and the electrical energy extracted by the transducer [42].

$$m\ddot{z}(t) + c\dot{z}(t) + kz(t) = -m\ddot{y}(t) \tag{1}$$

m is the mass of the magnets, k the stiffness of the spring and c is the damping coefficient. When this damping system is excited by an external sinusoidal vibration $y(t) = Y\sin(\omega t)$, the solution of (1) is given by (2). $\omega_n = (k/m)^{1/2} = 4.98$ Hz is the natural frequency and $\zeta = c/2m\omega_n = 0.256$ its total damping ratio.

$$z(t) = \frac{Y\omega^2}{\left(\left(\omega_n^2 - \omega^2\right)^2 + \left(2\zeta\omega_n\omega\right)^2\right)^{1/2}} \sin\left(\omega t - arctg\left(\frac{2\zeta\omega_n\omega}{\omega_n^2 - \omega^2}\right)\right) \tag{2}$$

3.3 Rotation-Based Electromagnetic Power Generator (REEH)

Power Generator Prototype Design. An electromagnetic transducer was designed using the modular ball head of the hip prosthesis and the acetabular component. Energy is harvested from the rotation around the flexion-extension axis and around the inward-outward. The ball head was hollowed to comprise a circular winding of enamelled copper wire (AWG 42, 0.063 mm of diameter), which was coiled ($N = 4710$ turns, 682 Ω of total wire resistance, 117.1 m of total length of the coil, 7.92 mm of average diameter) around a Teflon tube (5.8 mm of diameter, 12 mm of length), whose core was designed to be a steel cylinder (4 mm of diameter, 14 mm of length, 100 of relative permeability). 24 neodymium disc magnets N52 (6 mm of diameter, 2 mm of height and 1.48 T of magnetic field) were placed on the structure of an acetabular component, in order to set the magnetic field lines over the volume of the upper half of the ball head, as presented by Fig. 4 (right). 6 groups of 2 magnets, positioned equidistantly, were settled symmetrically in the acetabulum with 6 other groups of 2 magnets, which were also equidistantly positioned. Figure 4 (left) illustrate a scheme of the REEH generator.

Linear Model of the REEH System. The total harvested energy is the total sum of the energy that can be harvested from the rotation around the flexion-extension axis and the energy acquired from the rotation around the inward-outward axis, according to equation (3).

$$V_{emf}^{\hat{x}\hat{z}} = -\pi R^2 NB\frac{d\alpha_{\hat{z}}}{dt}sin(\alpha_{\hat{z}}) - \pi R^2 NB\frac{d\alpha_{\hat{x}}}{dt}sin(\alpha_{\hat{x}}) \tag{3}$$

3.4 Piezoelectric Power Generator (PEH)

Power Generator Prototype Design. A piezoelectric power generator was designed to harvest energy from the axial load over the hip joint. Figure 3 (right) provides a CAD

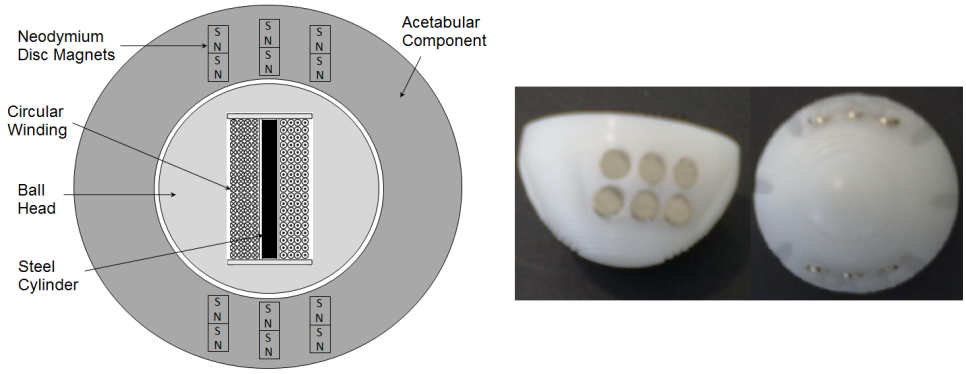

Fig. 4. (left) Scheme of the REEH transducer; (right) Acetabulum of high density polyethylene

modulation of the PEH generator. A piezoelectric ceramic diaphragm (ref. 7BB-12-9, *muRata* Corporate, Kyoto, Japan) with 9 mm of diameter and 0.22 mm of thickness (12 mm of plate size, 0.1 mm of plate thickness and 9.0 ± 1.0 kHz of resonant frequency) was placed on the lower half of ball head of the hip prosthesis.

Neural Network Model of the PEH System. Piezoelectric energy harvesters can be modelled as mechanical damping systems [29, 43]. Because the piezoelectric element is attached to the hip prosthesis structure, the mechanical damping ratio and proof mass are very difficult to find due to the geometry of the prosthesis. An artificial neural network (ANN) model was developed to predict the power and energy generation [44]. A multilayer "feed-forward" ANN was trained to perform the matching between a series of pairs of the frequency and amplitude of sinusoidal axial forces, and the average power and peak-to-peak voltage generation. The ANN consists of one input layer, with two neurons, two hidden layers, with seven neurons each, and one output layer, with two neurons, as shown in figure 5 and predicted by equation (4). The Levenberg-Marquardt's algorithm was used as the training algorithm and the mean square error of 1.0×10^{-20} as the convergence criteria for the network training. Sigmoid functions (Tansig) for the hidden layers and linear function (Purelin) for the output layer were used as the transfer functions.

$$\mathbf{y}_N = f_L\Big(\mathbf{LW}_2 f_S\big(\mathbf{LW}_1 f_S\big(\mathbf{IW}_1 \mathbf{i}_N + \mathbf{b}_1\big) + \mathbf{b}_2\big) + \mathbf{b}_3\Big) \tag{4}$$

Here, $\mathbf{y}_N$ is the output 2×1 matrix, $\mathbf{i}_N$ is the 2×1 input matrix, $\mathbf{IW}_1$ is a input weight 7×2 matrix, $\mathbf{LW}_1$ and $\mathbf{LW}_2$ are respectively layer weight 7×7 and 2×7 matrices, and $\mathbf{b}_1$, $\mathbf{b}_2$ and $\mathbf{b}_3$ are respectively bias 7×1, 7×1 and 2×1 matrices. f_L and f_S are linear and sigmoid functions, respectively.

4 Experimental and Simulation Results

The experimental average and peak power, energy and peak-to-peak voltage generation were analysed. These experimental results were compared with the linear models reported in sections 3.2, 3.3 and 3.4.

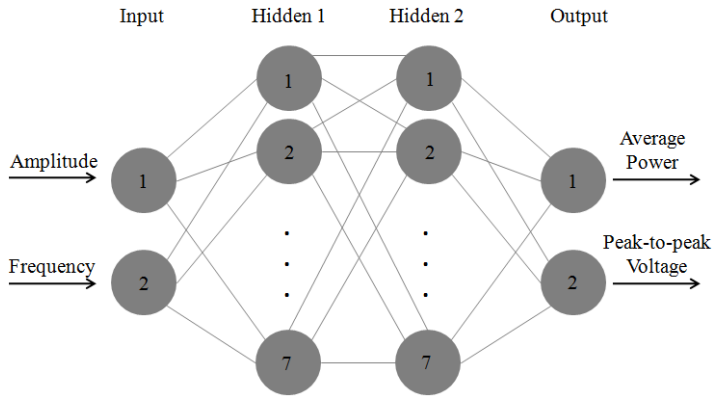

Fig. 5. ANN used to model the average power and peak-to-peak voltage of the PEH generator

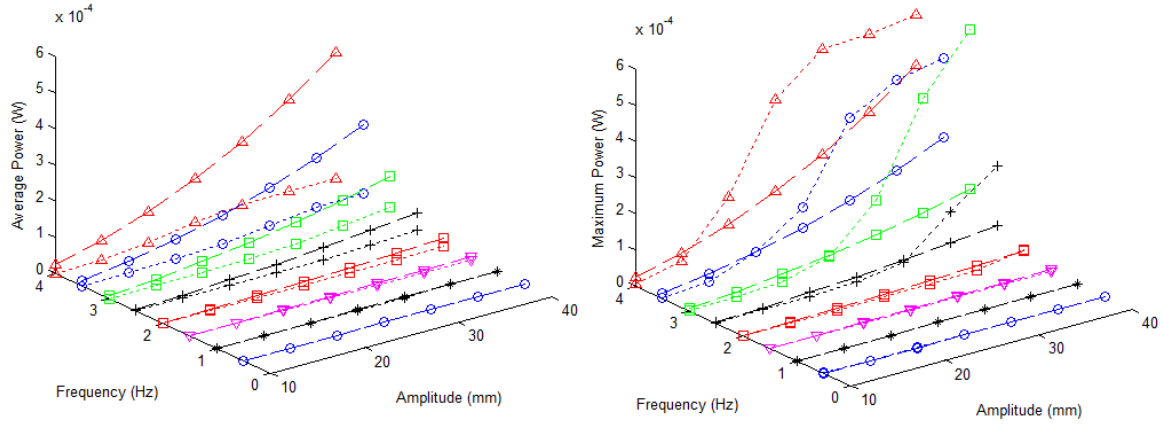

Fig. 6. Experimental (dotted line) and simulated (dashed line) average (in the left) and maximum (in the right) power harvested from the TEEH transducer

4.1 TEEH Results

A load resistance of 979 Ω was used to enable the energy transfer when sinusoidal input vibrations, with amplitudes in the range 10 mm to 40 mm and frequencies in the range 0.5 Hz to 4 Hz, were applied to this generator. Figure 6 shows the results of the experimental and simulated average and maximum power, whereas Fig. 7 highlights the results of the experimental and simulated energy and peak-to-peak voltage. Tables 1 to 4 report the modulation errors. The maximum energy harvested was 53.7 μJ/s when the sinusoidal function has an amplitude of 40 mm and a frequency of 4 Hz. This harvester is able to provide 567.4 μW of instantaneous peak power when the input is excited with an amplitude of 40 mm and a frequency of 3 Hz.

4.2 REEH Results

A load resistance of 8.98 kΩ was used to enable energy transfer of this generator when sinusoidal rotations in the flexion-extension axis, with amplitudes in the range 50° to 70° and frequencies in the range 0.5 Hz to 2.5 Hz, were applied to the generator. Using the magnetic field in the winding measured at the ends of the winding (80 mT), the experimental and simulated results are reported in Fig. 8 and Fig. 9. Tables 5 to 8 report

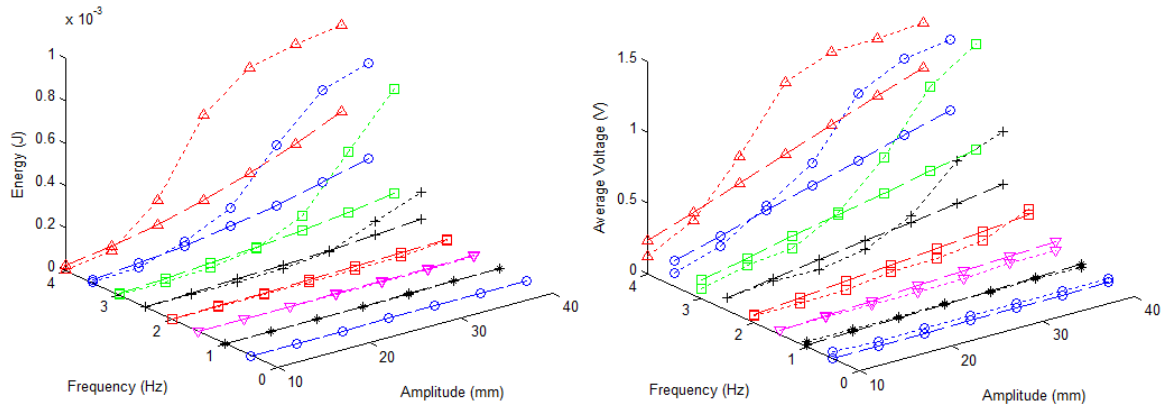

Fig. 7. Experimental (dotted line) and simulated (dashed line) energy (in the left) and peak-to-peak voltage (in the right) harvested from the TEEH transducer

Table 1. TEEH generator — modulation error (W) of the average power

Amplitude (mm)	Frequency (Hz) 0.5	1	1.5	2	2.5	3	3.5	4
10	$0.06^{(1)}$	$0.009^{(2)}$	$0.05^{(2)}$	$0.02^{(3)}$	$0.04^{(3)}$	$0.08^{(3)}$	$0.02^{(4)}$	$0.03^{(4)}$
15	$0.02^{(1)}$	$0.02^{(2)}$	$0.11^{(2)}$	$0.04^{(3)}$	$0.08^{(3)}$	$0.18^{(3)}$	$0.03^{(4)}$	$0.05^{(4)}$
20	$0.13^{(1)}$	$0.04^{(2)}$	$0.20^{(2)}$	$0.06^{(3)}$	$0.15^{(3)}$	$0.31^{(3)}$	$0.05^{(4)}$	$0.09^{(4)}$
25	$0.26^{(1)}$	$0.06^{(2)}$	$0.31^{(2)}$	$0.10^{(3)}$	$0.23^{(3)}$	$0.47^{(3)}$	$0.08^{(4)}$	$0.12^{(4)}$
30	$0.43^{(1)}$	$0.09^{(2)}$	$0.44^{(2)}$	$0.14^{(3)}$	$0.32^{(3)}$	$0.62^{(3)}$	$0.10^{(4)}$	$0.18^{(4)}$
35	$0.62^{(1)}$	$0.12^{(2)}$	$0.60^{(2)}$	$0.19^{(3)}$	$0.39^{(3)}$	$0.71^{(3)}$	$0.14^{(4)}$	$0.26^{(4)}$
40	$0.85^{(1)}$	$0.15^{(2)}$	$0.78^{(2)}$	$0.24^{(3)}$	$0.48^{(3)}$	$0.85^{(3)}$	$0.19^{(4)}$	$0.35^{(4)}$

$^{(1)} \times 10^{-7}$; $^{(2)} \times 10^{-5}$; $^{(3)} \times 10^{-4}$; $^{(4)} \times 10^{-3}$.

Table 2. TEEH generator — modulation error (W) of the maximum power

Amplitude (mm)	Frequency (Hz) 0.5	1	1.5	2	2.5	3	3.5	4
10	$0.70^{(1)}$	$0.03^{(2)}$	$0.01^{(2)}$	$0.01^{(3)}$	$0.001^{(4)}$	$0.01^{(4)}$	$0.01^{(4)}$	$0.02^{(4)}$
15	$0.30^{(1)}$	$0.02^{(2)}$	$0.06^{(2)}$	$0.03^{(3)}$	$0.003^{(4)}$	$0.01^{(4)}$	$0.02^{(4)}$	$0.02^{(4)}$
20	$0.54^{(1)}$	$0.01^{(2)}$	$0.15^{(2)}$	$0.05^{(3)}$	$0.01^{(4)}$	$0.02^{(4)}$	$0.0002^{(4)}$	$0.08^{(4)}$
25	$0.53^{(1)}$	$0.0002^{(2)}$	$0.27^{(2)}$	$0.07^{(3)}$	$0.02^{(4)}$	$0.003^{(4)}$	$0.06^{(4)}$	$0.26^{(4)}$
30	$0.48^{(1)}$	$0.05^{(2)}$	$0.35^{(2)}$	$0.11^{(3)}$	$0.004^{(4)}$	$0.09^{(4)}$	$0.23^{(4)}$	$0.29^{(4)}$
35	$0.37^{(1)}$	$0.04^{(2)}$	$0.39^{(2)}$	$0.13^{(3)}$	$0.09^{(4)}$	$0.32^{(4)}$	$0.25^{(4)}$	$0.22^{(4)}$
40	$0.69^{(1)}$	$0.12^{(2)}$	$0.64^{(2)}$	$0.03^{(3)}$	$0.17^{(4)}$	$0.44^{(4)}$	$0.22^{(4)}$	$0.14^{(4)}$

$^{(1)} \times 10^{-6}$; $^{(2)} \times 10^{-5}$; $^{(3)} \times 10^{-4}$; $^{(4)} \times 10^{-3}$.

the modulation errors. The maximum energy harvested was 0.77 μJ/s. The "plus" sign refers to peak-to-peak amplitudes in the range $-10°$ to $60°$, $-10°$ to $50°$ and $-10°$ to $40°$; the "square" sign refers to peak-to-peak amplitudes in the range $-20°$ to $50°$, $-20°$ to $40°$ and $-20°$ to $30°$.

Table 3. TEEH generator — modulation error (J) of the energy

Amplitude (mm)	Frequency (Hz) 0.5	1	1.5	2	2.5	3	3.5	4
10	$0.17^{(1)}$	$0.01^{(2)}$	$0.03^{(2)}$	$0.01^{(3)}$	$0.003^{(4)}$	$0.01^{(4)}$	$0.01^{(4)}$	$0.02^{(4)}$
15	$0.16^{(1)}$	$0.01^{(2)}$	$0.10^{(2)}$	$0.03^{(3)}$	$0.01^{(4)}$	$0.01^{(4)}$	$0.02^{(4)}$	$0.02^{(4)}$
20	$0.14^{(1)}$	$0.02^{(2)}$	$0.18^{(2)}$	$0.06^{(3)}$	$0.01^{(4)}$	$0.02^{(4)}$	$0.02^{(4)}$	$0.11^{(4)}$
25	$0.13^{(1)}$	$0.04^{(2)}$	$0.29^{(2)}$	$0.08^{(3)}$	$0.02^{(4)}$	$0.01^{(4)}$	$0.08^{(4)}$	$0.40^{(4)}$
30	$0.11^{(1)}$	$0.07^{(2)}$	$0.42^{(2)}$	$0.12^{(3)}$	$0.01^{(4)}$	$0.07^{(4)}$	$0.29^{(4)}$	$0.50^{(4)}$
35	$0.09^{(1)}$	$0.10^{(2)}$	$0.53^{(2)}$	$0.14^{(3)}$	$0.06^{(4)}$	$0.29^{(4)}$	$0.44^{(4)}$	$0.47^{(4)}$
40	$0.06^{(1)}$	$0.14^{(2)}$	$0.69^{(2)}$	$0.07^{(3)}$	$0.13^{(4)}$	$0.49^{(4)}$	$0.45^{(4)}$	$0.41^{(4)}$

$^{(1)} \times 10^{-6}$; $^{(2)} \times 10^{-5}$; $^{(3)} \times 10^{-4}$; $^{(4)} \times 10^{-3}$.

Table 4. TEEH generator — modulation error (V) of the peak-to-peak voltage

Amplitude (mm)	Frequency (Hz) 0.5	1	1.5	2	2.5	3	3.5	4
10	0.05	0.02	0.003	0.01	0.003	0.06	0.08	0.11
15	0.03	0.02	0.01	0.04	0.01	0.05	0.08	0.06
20	0.04	0.01	0.03	0.06	0.07	0.08	0.04	0.19
25	0.03	0.01	0.04	0.05	0.06	0.02	0.16	0.51
30	0.03	0.01	0.05	0.08	0.05	0.25	0.47	0.52
35	0.03	0.01	0.04	0.06	0.30	0.60	0.55	0.41
40	0.03	0.02	0.06	0.04	0.38	0.74	0.50	0.31

Table 5. REEH generator — modulation error (W) of the average power [error ("plus" test) | error ("square" test)]

Amplitude (°)	Frequency (Hz) 0.5	1	1.5	2	2.5
50	$0.11^{(1)}$ | $0.06^{(1)}$	$0.04^{(2)}$ | $0.25^{(1)}$	$0.09^{(2)}$ | $0.06^{(2)}$	$0.18^{(2)}$ | $0.10^{(2)}$	$0.33^{(2)}$ | $0.22^{(2)}$
60	$0.16^{(1)}$ | $0.11^{(1)}$	$0.06^{(2)}$ | $0.49^{(1)}$	$0.22^{(2)}$ | $0.10^{(2)}$	$0.40^{(2)}$ | $0.19^{(2)}$	$0.54^{(2)}$ | $0.29^{(2)}$
70	$0.30^{(1)}$ | $0.17^{(1)}$	$0.11^{(2)}$ | $0.78^{(1)}$	$0.24^{(2)}$ | $0.14^{(2)}$	$0.44^{(2)}$ | $0.41^{(2)}$	$0.32^{(2)}$ | $0.22^{(2)}$

$^{(1)} \times 10^{-7}$; $^{(2)} \times 10^{-6}$.

Table 6. REEH generator — modulation error (W) of the maximum power [error ("plus" test) | error ("square" test)].

Amplitude (°)	Frequency (Hz) 0.5	1	1.5	2	2.5
50	$0.07^{(2)}$ | $0.36^{(1)}$	$0.24^{(2)}$ | $0.09^{(2)}$	$0.05^{(3)}$ | $0.18^{(2)}$	$0.08^{(3)}$ | $0.03^{(3)}$	$0.17^{(3)}$ | $0.09^{(3)}$
60	$0.13^{(2)}$ | $0.45^{(1)}$	$0.31^{(2)}$ | $0.20^{(2)}$	$0.11^{(3)}$ | $0.32^{(2)}$	$0.23^{(3)}$ | $0.08^{(3)}$	$0.24^{(3)}$ | $0.13^{(3)}$
70	$0.22^{(2)}$ | $0.75^{(1)}$	$0.58^{(2)}$ | $0.36^{(2)}$	$0.11^{(3)}$ | $0.59^{(2)}$	$0.22^{(3)}$ | $0.18^{(3)}$	$0.18^{(3)}$ | $0.12^{(3)}$

$^{(1)} \times 10^{-7}$; $^{(2)} \times 10^{-6}$; $^{(3)} \times 10^{-5}$.

Table 7. REEH generator — modulation error (J) of the energy [error ("plus" test) | error ("square" test)]

Amplitude (°)	Frequency (Hz) 0.5	1	1.5	2	2.5
50	$0.16^{(1)}$ | $0.09^{(1)}$	$0.06^{(2)}$ | $0.04^{(2)}$	$0.14^{(2)}$ | $0.08^{(2)}$	$0.28^{(2)}$ | $0.15^{(2)}$	$0.49^{(2)}$ | $0.33^{(2)}$
60	$0.24^{(1)}$ | $0.16^{(1)}$	$0.09^{(2)}$ | $0.07^{(2)}$	$0.34^{(2)}$ | $0.15^{(2)}$	$0.59^{(2)}$ | $0.29^{(2)}$	$0.81^{(2)}$ | $0.43^{(2)}$
70	$0.44^{(1)}$ | $0.26^{(1)}$	$0.16^{(2)}$ | $0.12^{(2)}$	$0.35^{(2)}$ | $0.21^{(2)}$	$0.65^{(2)}$ | $0.61^{(2)}$	$0.48^{(2)}$ | $0.33^{(2)}$

$^{(1)} \times 10^{-6}$; $^{(2)} \times 10^{-5}$.

Table 8. REEH generator — modulation error (V) of the peak-to-peak voltage [error ("plus" test) | error ("square" test)]

Amplitude (°)	Frequency (Hz) 0.5	1	1.5	2	2.5
50	0.03 | 0.02	0.05 | 0.03	0.08 | 0.04	0.11 | 0.05	0.14 | 0.09
60	0.04 | 0.02	0.06 | 0.04	0.12 | 0.05	0.16 | 0.07	0.15 | 0.09
70	0.05 | 0.02	0.08 | 0.06	0.11 | 0.06	0.13 | 0.11	0.09 | 0.06

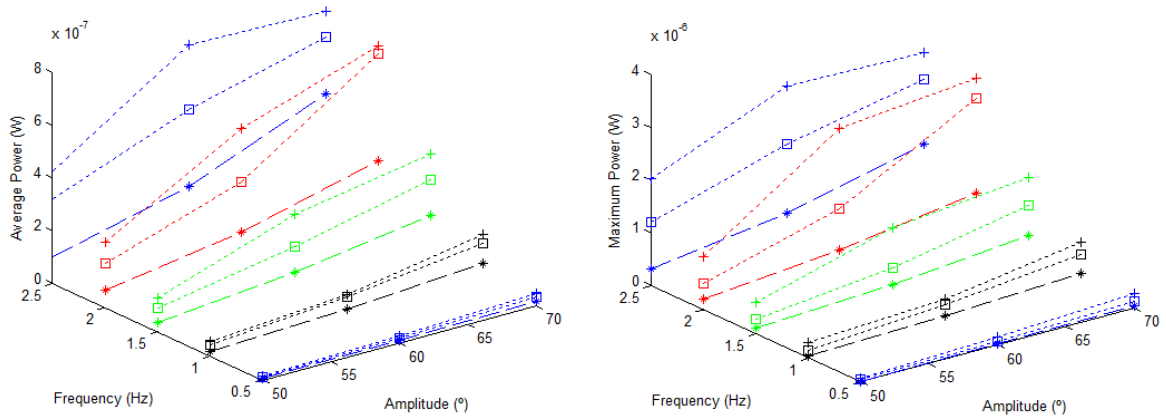

Fig. 8. Experimental (dotted line) and simulated (dashed line) average (in the left) and maximum (in the right) power harvested from the REEH generator

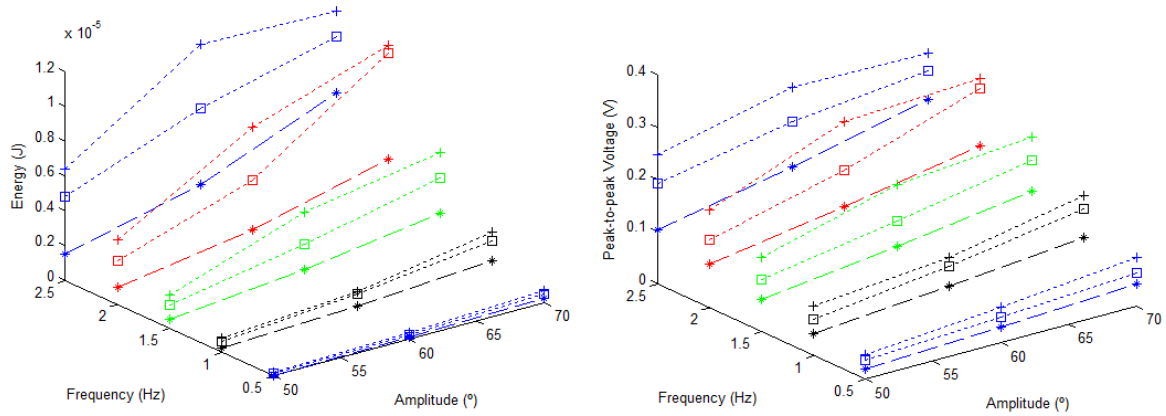

Fig. 9. Experimental (dotted line) and simulated (dashed line) energy (in the left) and peak-to-peak voltage (in the right) harvested from the REEH generator

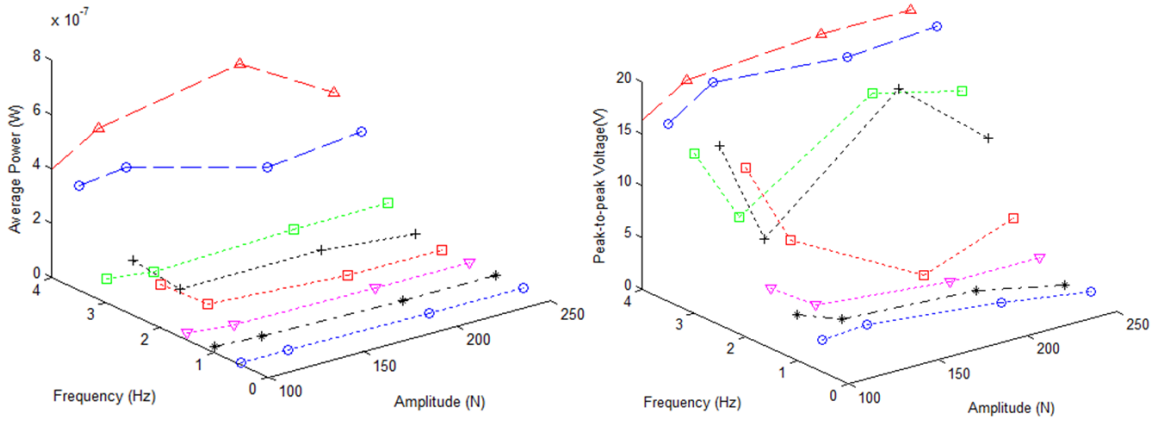

Fig. 10. Experimental average power and peak-to-peak voltage results harvested from the PEH

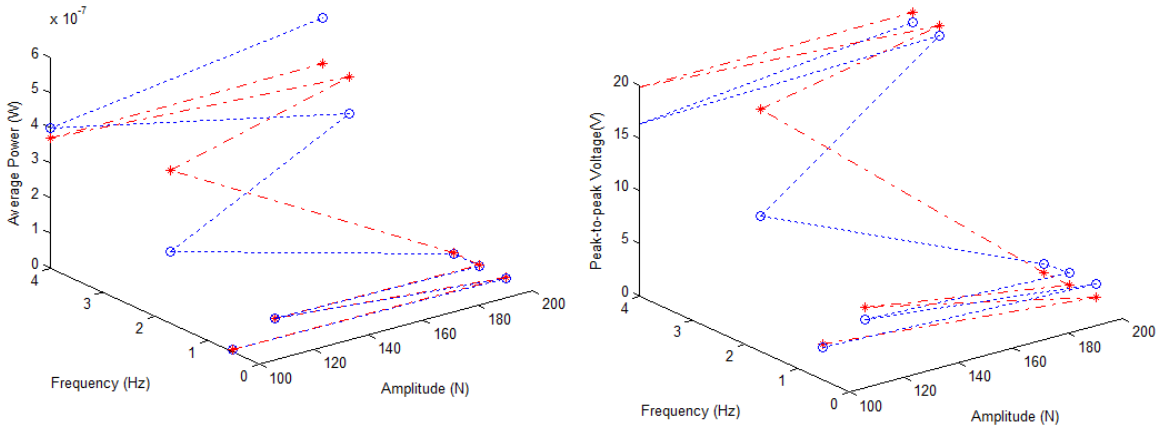

Fig. 11. Validation of the average power harvested from the PEH generators (dash-dot line refers to the network output)

4.3 PEH Results

External sinusoidal forces, with amplitudes in the range 100 N to 250 N and frequencies in the range 0.5 Hz to 4 Hz, were applied to the generator. A load of 1 MΩ was used to enable the energy transfer. Figure 10 reports the experimental average power and peak-to-peak voltage results, whereas Fig. 11 introduces the validation results of the "feed-forward" ANN, using only data not used in the training process. Tables 9 to 10 report the modulation errors. The maximum energy harvested was 0.6 μ J/s.

5 Discussion

5.1 Need for Multi-source Harvester Systems

The high reliability of the electric energy generation system is a necessary condition to ensure high reliability of the therapy based on mechanical stimulation. It is technologically possible to implement active implants with the ability to monitor failures, to communicate the states of its surrounding physiological environment to the medical specialist and carry out mechanical-based therapeutic prescriptions ordered by the specialist. These operations demand a full availability of electric energy.

Table 9. PEH generator — modulation error of the average power

Frequency (Hz)	0.5	0.5	1	1	1.5	3	3.5	4	4
Amplitude (N)	100	200	125	200	200	125	200	100	200
Absolute error (W)[(1)]	0.0004	0.003	0.0003	0.003	0.002	0.23	0.11	0.03	0.13

[(1)] $\times 10^{-6}$.

Table 10. PEH generator — modulation error of the peak-to-peak voltage

Frequency (Hz)	0.5	0.5	1	1	1.5	3	3.5	4	4
Amplitude (N)	100	200	125	200	200	125	200	100	200
Absolute error (W)	0.32	1.18	1.22	1.18	0.80	10.19	0.98	3.49	0.88

5.2 Choice of the Energy Harvesting Method

There are several methods to harvest electric energy from the surrounding environment. Biofuel cells, magnetic induction, thermoelectric and vibration are some of the main sources used to harvest energy. Vibration-based generation is being considered the most appropriate solution to harvest electrical energy on prostheses [45]. Although there are no studies supporting this hypothesis, their ease of implementation, their ability of being fully autonomous and operating without maintenance, ensuring safety throughout the life span of the implant, were relevant features taken into consideration to validate this new concept of energy harvesting systems applied to hip prostheses.

5.3 Performance of the Linear Models

Linear models can only ensure accuracy within a narrow window of the systems' operating range. The modulation errors, presented in sections 4.1, 4.2 and 4.3, confirm the inaccuracy of the linear models of the generators, especially those used to model the behaviour of the TEEH generator. The real translational and rotational hip displacements, the friction and gravity forces acting on these systems, the non-linearity behavior of inductors and transduction damping coefficients were jeopardized from linear models. Because experimental results show a higher performance of the TEEH generator in this particular application, it is mandatory the development of non-linear models for high accuracy prediction of electric energy generation considering a broad specter of the generators' operation.

5.4 Optimization of the Multi-source Harvester System

Each transducer must be optimized in order to maximize electric generation during typical walking speeds, namely in the range between 0.5 Hz and 2 Hz. The optimization of the TEEH and PEH generators demands for a "perfect" match between the frequency of the hip kinematics and their resonant frequencies. The implementation of a continuous-matching system is very complex [46] because the duration and frequency of every-day human activities are unpredictable [47]. New methods must be developed to ensure high performance tracking of the hip kinematics' frequency. Each generator must be

optimized to supply as much electric energy as demanded by the active mechanics of smart prostheses, even though they may require different periods to generate the same amount of energy.

6 Conclusions

A therapeutic methodology to cure failures of hip prostheses following primary artroplasty, based on a personalized approach, would be of great importance for the quality of life of many patients. Multi-source electric energy generation systems for orthopaedic implants contribute forward the implementation of individualized medicine approaches in the scope of embedded smart bone implants. This new concept was validated with the use of three vibrational energy harvesters: two electromagnetic generators and a piezoelectric. Experimental results confirm the inaccuracy of the generators' linear models operating on hip prostheses fixtures, which invalidates their use in optimization routines.

There is ongoing work to:

1. Develop non-linear models of vibrational energy harvesters. The main goal is to reduce the volume of each generator and maximize their performance;
2. Identify the most appropriate method to generate electrical energy on hip implants;
3. Design a new method to ensure an effective tracking of the frequency of the hip kinematics. The set of generators must be synchronized with the hip dynamics in order to ensure all energy requirements demanded by active elements of the smart prostheses;
4. Design an energy management system for a multitude of power sources;
5. Design of energy harvesting systems which are independent of failures due to contact stresses (for instance, magnetically levitated generators);
6. Design of a redundant multi-source harvester structure. Such a redundant ability, along with the requirements introduced in the previous number and in section 5.4, are sufficient to ensure reliability of the electric energy generation system.

References

1. Ren, W., Blasier, R., Peng, X., Shi, T., Wooley, P.H., Markel, D.: Effect of oral erythromycin therapy in patients with aseptic loosening of joint prostheses. Bone 44(4), 671–677 (2009)
2. Esposito, S., Leone, S.: Prosthetic joint infections: microbiology, diagnosis, management and prevention. International Journal of Antimicrobial Agents 32(4), 287–293 (2008)
3. Dreinhöfer, K.E., Dieppe, P., Günther, K.P., Puhl, W.: EUROHIP - Health Technology Assessment of Hip Arthroplasty in Europe. Springer, New York (2009)
4. Ramos, A., Completo, A., Relvas, C., Simões, J.: Design process of a novel cemented hip femoral stem concept. Materials and Design 33, 313–321 (2012)
5. Jun, Y., Choi, K.: Design of patient-specific hip implants based on the 3D geometry of the human femur. Advances in Engineering Software 41(4), 537–547 (2010)
6. Simões, J.A., Marques, A.T.: Design of a composite hip femoral prosthesis. Materials and Design 26(5), 391–401 (2005)

7. Fehring, T.K., Odum, S.M., Troyer, J.L., Iorio, R., Kurtz, S.M., Lau, E.C.: Joint replacement access in 2016: A supply side crisis. The Journal of Arthroplasty 25(8), 1175–1181 (2010)
8. Ong, K.L., Lau, E., Suggs, J., Kurtz, S.M., Manley, M.T.: Risk of subsequent revision after primary and revision total joint arthroplasty. Clinical Orthopaedics and Related Research 468(11), 3070–3076 (2010)
9. Kurtz, S.M., Lau, E., Ong, K., Zhao, K., Kelly, M., Bozic, K.J.: Future young patient demand for primary and revision joint replacement. Clinical Orthopaedics and Related Research 467(10), 2606–2612 (2009)
10. Rydell, N.W.: Forces acting on the femoral head-prosthesis. A study on strain gauge supplied prostheses in living persons. Acta Orthopaedica Scandinavica 37(88), 1–132 (1966)
11. Damm, P., Graichen, F., Rohlmann, A., Bender, A., Bergmann, G.: Total hip joint prosthesis for in vivo measurement of forces and moments. Medical Engineering & Physics 32(1), 95–100 (2010)
12. Boyle, C., Kim, I.Y.: Comparison of different hip prosthesis shapes considering micro-level bone remodeling and stress-shielding criteria using three-dimensional design space topology optimization. Journal of Biomechanics 44(9), 1722–1728 (2011)
13. Nikooyan, A.A., Veeger, H.E., Westerhoff, P., Graichen, F., Bergmann, G., van der Helm, F.C.: Validation of the delft shoulder and elbow model using in-vivo glenohumeral joint contact forces. Journal of Biomechanics 43(15), 3007–3014 (2010)
14. Rohlmann, A., Gabel, U., Graichen, F., Bender, A., Bergmann, G.: An instrumented implant for vertebral body replacement that measures loads in the anterior spinal column. Medical Engineering & Physics 29(5), 580–585 (2007)
15. Puers, R., Catrysse, M., Vandevoorde, G., Collier, R., Louridas, E., Burny, F., Donkerwolcke, M., Moulart, F.: A telemetry system for the detection of hip prosthesis loosening by vibration analysis. Sensors and Actuators A: Physical 85(1-3), 42–47 (2000)
16. Heinlein, B., Graichen, F., Bender, A., Rohlmann, A., Bergmann, G.: Design, calibration and pre-clinical testing of an instrumented tibial tray. Journal of Biomechanics 40, S4–S10 (2007)
17. Almouahed, S., Gouriou, M., Hamitouche, C., Stindel, E., Roux, C.: Design and evaluation of instrumented smart knee implant. IEEE Transactions on Biomedical Engineering 58(4), 971–982 (2011)
18. Graichen, F., Bergmann, G., Rohlmann, A.: Hip endoprosthesis for in vivo measurement of joint force and temperature. Journal of Biomechanics 32(10), 1113–1117 (1999)
19. Marschner, U., Grätz, H., Jettkant, B., Ruwisch, D., Woldt, G., Fischer, W.J., Clasbrummel, B.: Integration of a wireless lock-in measurement of hip prosthesis vibrations for loosening detection. Sensors and Actuators A: Physical 156(1), 145–154 (2009)
20. Rowlands, A., Duck, F.A., Cunningham, J.L.: Bone vibration measurement using ultrasound: Application to detection of hip prosthesis loosening. Medical Engineering & Physics 30(3), 278–284 (2008)
21. Bergmann, G., Graichen, F., Rohlmann, A., Westerhoff, P., Heinlein, B., Bender, A., Ehrig, R.: Design and calibration of load sensing orthopaedic implants. Journal of Biomechanical Engineering 130(2), 021009 (2008)
22. Graichen, F., Arnold, R., Rohlmann, A., Bergmann, G.: Implantable 9-channel telemetry system for in vivo load measurements with orthopedic implants. IEEE Transactions on Biomedical Engineering 54(2), 253–261 (2007)
23. Valdastri, P., Rossi, S., Menciassi, A., Lionetti, V., Bernini, F., Recchia, F.A., Dario, P.: An implantable ZigBee ready telemetric platform for *in vivo* monitoring of physiological parameters. Sensors and Actuators A: Physical 142(1), 369–378 (2008)

24. Morais, R., Frias, C.M., Silva, N.M., Azevedo, J.L.F., Serôdio, C.A., Silva, P.M., Ferreira, J.A.F., Simões, J.A.O., Reis, M.C.: An activation circuit for battery-powered biomedical implantable systems. Sensors and Actuators A: Physical 156(1), 229–236 (2009)
25. Kim, P.R., Beaulé, P.E., Laflamme, G.Y., Dunbar, M.: Causes of early failure in a multicenter clinical trial of hip resurfacing. The Journal of Arthroplasty 23(6), 44–49 (2008)
26. Alpuim, P., Filonovich, S.A., Costa, C.M., Rocha, P.F., Vasilevskiy, M.I., Lanceros-Mendez, S., Frias, C., Marques, A.T., Soares, R., Costa, C.: Fabrication of a strain sensor for bone implant failure detection based on piezoresistive doped nanocrystalline silicon. Journal of Non-Crystalline Solids 354(19-25), 2585–2589 (2008)
27. Morais, R., Silva, N.M., Santos, P.M., Frias, C.M., Ferreira, J.A.F., Ramos, A.M., Simões, J.A.O., Baptista, J.M.R., Reis, M.C.: Double permanent magnet vibration power generator for smart hip prosthesis. Sensors and Actuators A: Physical 172(1), 259–268 (2011)
28. Wei, X., Liu, J.: Power sources and electrical recharging strategies for implantable medical devices. Frontiers of Energy and Power Engineering in China 2(1), 1–13 (2008)
29. Kaźmierski, T.J., Beeby, S.: Energy Harvesting Systems - Principles, Modeling and Applications. Springer, New York (2011)
30. Kerzenmacher, S., Ducrée, J., Zengerle, R., von Stetten, F.: Energy harvesting by implantable abiotically catalyzed glucose fuel cells. Journal of Power Sources 182(1), 1–17 (2008)
31. Carmo, J.P., Ribeiro, J.F., Silva, M.F., Goncalves, L.M., Correia, J.H.: Thermoelectric generator and solid-state battery for stand-alone microsystems. Journal of Micromechanics and Microengineering 20(8), 1–8 (2010)
32. Lu, M., Guang Zhang, G., Fu, K., Hao Yu, G., Su, D., Feng Hu, J.: Gallium nitride schottky betavoltaic nuclear batteries. Energy Conversion and Management 52(4), 1955–1958 (2011)
33. Burny, F., Donkerwolcke, M., Moulart, F., Bourgois, R., Puers, R., Schuylenbergh, K.V., Barbosa, M., Paiva, O., Rodes, F., Bégueret, J.B., Lawes, P.: Concept, design and fabrication of smart orthopedic implants. Medical Engineering & Physics 22(7), 469–479 (2000)
34. Sakamoto, J.H., van de Ven, A.L., Godin, B., Blanco, E., Serda, R.E., Grattoni, A., Ziemys, A., Bouamrani, A., Hu, T., Ranganathan, S.I., Rosa, E.D., Martinez, J.O., Smid, C.A., Buchanan, R.M., Lee, S.Y., Srinivasan, S., Landry, M., Meyn, A., Tasciotti, E., Liu, X., Decuzzi, P., Ferrari, M.: Enabling individualized therapy through nanotechnology. Pharmacological Research 62(2), 57–89 (2010)
35. Frias, C., Reis, J., e Silva, F.C., Potes, J., Simões, J., Marques, A.T.: Polymeric piezoelectric actuator substrate for osteoblast mechanical stimulation. Journal of Biomechanics 43(6), 1061–1066 (2010)
36. Tanaka, S.M., Li, J., Duncan, R.L., Yokota, H., Burr, D.B., Turner, C.H.: Effects of broad frequency vibration on cultured osteoblasts. Journal of Biomechanics 36(1), 73–80 (2003)
37. Bacabac, R.G., Smit, T.H., Loon, J.J.W.A.V., Doulabi, B.Z., Helder, M., Klein-Nulend, J.: Bone cell responses to high-frequency vibration stress: does the nucleus oscillate within the cytoplasm? The FASEB Journal 20(7), 858–864 (2006)
38. Winau, F., Westphal, O., Winau, R.: Paul Ehrlich - in search of the Magic Bullet. Microbes and Infection 6, 786–789 (2004)
39. Morais, R., Silva, N., Santos, P., Frias, C., Ferreira, J., Ramos, A., Simões, J., Baptista, J., Reis, M.: Permanent magnet vibration power generator as an embedded mechanism for smart hip prosthesis. Procedia Engineering 5, 766–769 (2010)
40. Frias, C., Reis, J., e Silva, F.C., Potes, J., Simões, J., Marques, A.T.: Piezoelectric actuator: Searching inspiration in nature for osteoblast stimulation. Composites Science and Technology 70(13), 1920–1925 (2010)
41. Reis, J.C.: The Bone/Implant Interface: New Approaches to Old Problems. PhD thesis, University of Évora (2010)
42. Beeby, S.P., Tudor, M.J., White, N.M.: Energy harvesting vibration sources for microsystems applications. Measurement Science and Technology 17, R175–R195 (2006)

43. Priya, S., Inman, D.J.: Energy Harvesting Technologies. Springer, New York (2009)
44. Kalogirou, S.: Applications of artificial neural-networks for energy systems. Applied Energy 67, 17–35 (2000)
45. Yuen, S.C., Lee, J.M., Li, W.J., Leong, P.H.: An AA-sized vibration-based microgenerator for wireless sensors. IEEE Pervasive Computing 6(1), 64–72 (2007)
46. Zhu, D., Tudor, M.J., Beeby, S.P.: Strategies for increasing the operating frequency range of vibration energy harvesters: a review. Measurement Science and Technology 21(2), 1–29 (2010)
47. Morlock, M., Schneider, E., Bluhm, A., Vollmer, M., Bergmann, G., Müller, V., Honl, M.: Duration and frequency of every day activities in total hip patients. Journal of Biomechanics 34(7), 873–881 (2001)

5.3 Modeling and simulation of electromagnetic energy harvesting using magnetic levitation

Motion-driven energy harvesters for instrumented implants seem to be more easily implemented by magnetic levitation-based harvesting than using piezoelectric transducers. These harvesters using levitated hard-magnetic elements also seem to harvest more electric energy. The results retrieved from the previous study have also confirmed that linear models are not able to accurately predict the electromagnetic energy harvesting. Although low levels of energy are harvested in the recovery period following THR and when patients are not able to perform their routine activities (such as due to the ageing process or injury), a conclusive demonstration of the (in)effectiveness of this method to power instrumented implants requires to evaluate the maximum energy they are able to harvest according to the gait patterns of patients. Such analysis must consider that energy harvesting must be personalized. This purpose require the geometric optimization of the harvesters (prior to implant insertion) and the ability of the instrumented implant to control the position of their components (the fixed magnet(s) and coil(s)), according to the hip movements of patients during their routine activities. These demands can only be fulfilled if non-linear models are developed for accurate prediction of the energy harvesting considering 3D motions of the harvesters. Currently, due to the inherent complexity to validate such a model, a semi-analytical non-linear model that enables accurate and efficient analysis of energy transduction was already validated for vertical excitations of the harvester. This study is entitled "Magnetic levitation-based electromagnetic energy harvesting: a semi-analytical non-linear model for energy transduction". It is published in the *Scientific Reports (Nature Publishing Group)* (volume 6, 18579)[3].

[3]As the content of this study is already published, the formatting rules established by the journal *Scientific Reports (Nature Publishing Group)* are used.

SCIENTIFIC REPORTS

OPEN

Magnetic levitation-based electromagnetic energy harvesting: a semi-analytical non-linear model for energy transduction

Received: 03 August 2015
Accepted: 20 November 2015
Published: 04 January 2016

Marco P. Soares dos Santos[1,2], Jorge A. F. Ferreira[1,2], José A. O. Simões[2], Ricardo Pascoal[3], João Torrão[2], Xiaozheng Xue[4] & Edward P. Furlani[4,5]

Magnetic levitation has been used to implement low-cost and maintenance-free electromagnetic energy harvesting. The ability of levitation-based harvesting systems to operate autonomously for long periods of time makes them well-suited for self-powering a broad range of technologies. In this paper, a combined theoretical and experimental study is presented of a harvester configuration that utilizes the motion of a levitated hard-magnetic element to generate electrical power. A semi-analytical, non-linear model is introduced that enables accurate and efficient analysis of energy transduction. The model predicts the transient and steady-state response of the harvester a function of its motion (amplitude and frequency) and load impedance. Very good agreement is obtained between simulation and experiment with energy errors lower than 14.15% (mean absolute percentage error of 6.02%) and cross-correlations higher than 86%. The model provides unique insight into fundamental mechanisms of energy transduction and enables the geometric optimization of harvesters prior to fabrication and the rational design of intelligent energy harvesters.

Motion-driven electromagnetic energy harvesting systems have been used to provide self-powering for a wide range of technologies, such as remote sensors and actuators, mobile electronics, wearable devices and biomedical implants[1–7]. When dominant excitations are known a priori in a constrained range, the harvesters' characteristics can be optimized prior to fabrication using accurate models. For unknown, broadband and time-varying vibration spectra, new tunable mechanisms and broadband harvesting designs have been proposed[8–14]. However, these harvesters are usually complex and their use is often impractical due to dimensional constraints. Besides, the tuning mechanisms must be subject to constraints and, thus, practical applications require geometric optimization. Moreover, broadband harvesters cannot ensure optimal performances if intelligent control is not used to optimize the adaptive mechanism[15,16]. Consequently, modelling of the energy transduction is essential for design optimization prior to fabrication, as well as to fulfil demanding adaptability requirements. However, such modeling is problematic because of the highly non-linear behavior of most harvesters.

Magnetic levitation has been used to implement low-cost and maintenance-free electromagnetic energy harvesters, with the ability to operate autonomously with stable performance for long periods of time[17–19]. Their non-complex design is effective in many applications involving severe dimensional constraints[19]. Besides, intelligent control algorithms can be developed to control the position of their components according to the excitations' characteristics (for example, amplitude and frequency). Geometric optimization prior to fabrication and adaptive positional control of components cannot be accomplished using linear system models because they are not sufficient to adequately predict levitation-based energy harvesting, as such systems exhibit highly nonlinear behavior[20,21]. The Finite Element Method (FEM) has been used to solve the differential equations that govern the dynamics of these systems, taking into account effects such as the magnetic levitation forces between magnets and magnetic

[1]Centre for Mechanical Technology & Automation, TEMA, University of Aveiro, 3810-193 Aveiro, Portugal. [2]Department of Mechanical Engineering, University of Aveiro, 3810-193 Aveiro, Portugal. [3]Institute of Electronics and Informatics Engineering of Aveiro, IEETA, 3810-193 Aveiro, Portugal. [4]Department of Chemical and Biological Engineering, University at Buffalo, SUNY, Buffalo, NY, US. [5]Department of Electrical Engineering, University at Buffalo, SUNY, Buffalo, NY, US. Correspondence and requests for materials should be addressed to M.P.S.D.S. (email: marco.santos@ua.pt)

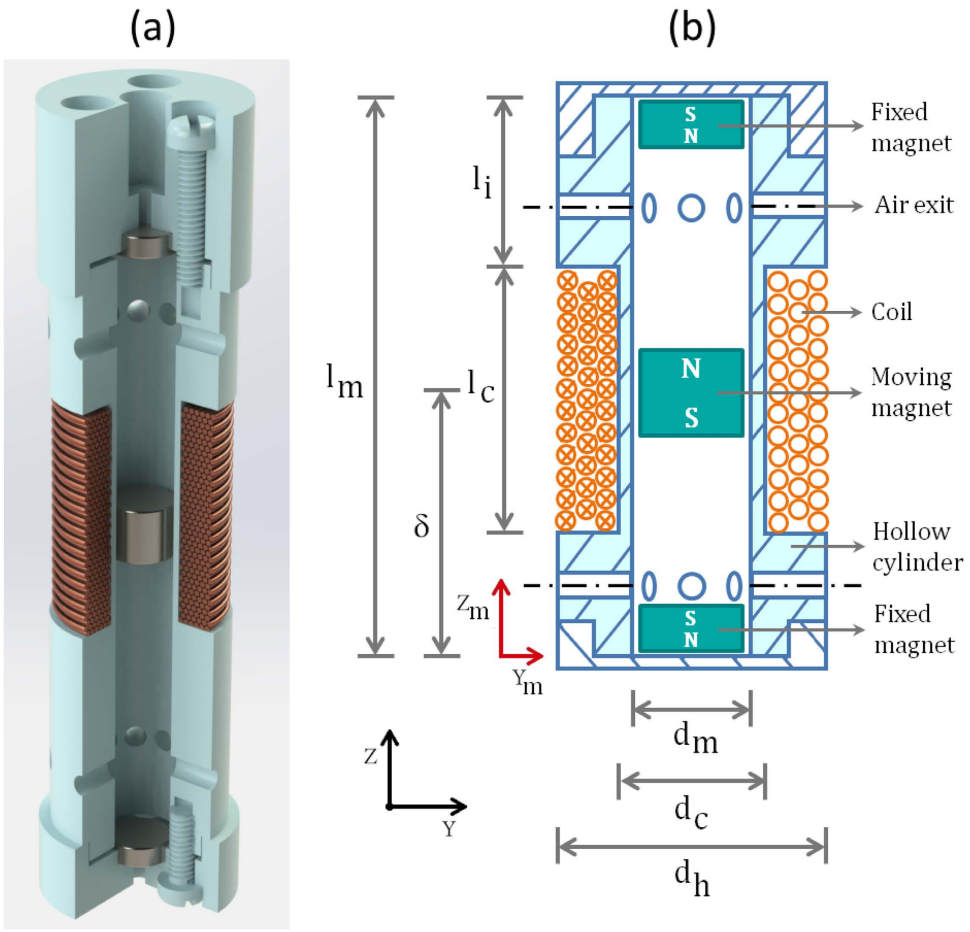

Figure 1. Section-views of the levitation-based harvester.

field (MF) distributions, etc.[21–24]. A combined approach using FEM and analytical or semi-analytical modeling has also been proposed[22,24]. However, the computational cost of FEM analysis is usually much greater than that of semi-analytical methods[21], cumbersome and often impractical for system optimization. In contrast, analytical analysis readily enables complexity minimization and accuracy maximization of the computation[21,25,26]. Several analytical and semi-analytical non-linear models have been developed for modeling magnetic levitation-based energy harvesting systems[20,21,24]. So far, modeling of harvester architectures with mechanical friction has been conducted by either identifying models that are only valid for specific experimental setups (i.e. those that include mechanical and/or electrical damping identification) and, hence, not suitable for design optimization; or disregarding either the electric or the mechanical behavior; or neglecting the inductive effects of coil(s) on energy harvesting, including highly non-linear effects associated with multilayered coil(s)[20–24]. Some phenomena occurring in these harvesting systems have also been modeled using semi-analytical techniques for diamagnetic levitation systems[27–30]. Their inherent nonlinearities have not yet been observed in detail due to their insufficient levitation gaps. Besides, many applications require self-powering technology in which levitation must be stable for a broad range of orientations (with respect to the acceleration of gravity) and for unconstrained motion amplitudes of the moving magnet[7,17], which is hard to accomplish by diamagnetic levitation. Moreover, no configuration has been developed to allow motion of the levitating magnet along most of the harvester length using this levitation method[27–30]. Hence, the potential of harvester architectures using tight-fit containers with very low friction contact must be further explored. To our best knowledge, no models have been demonstrated with the following functionalities: (a) use only analytical or semi-analytical equations to accurately predict both electrical and mechanical behavior; (b) take into account the main nonlinearities of forces that oppose magnet motion, including those due to mechanical contact between container and levitated magnet; (c) have been experimentally validated with different motional excitations (amplitude and frequency) and loads; and (d) are well-suited to be used in geometric optimization of the harvester and in intelligent harvesting for unconstrained motion amplitudes and arbitrary orientations of the harvester over a broad range of frequencies. In this paper, we introduce and demonstrate for the first time a validated semi-analytical model that addresses all these considerations.

Semi-analytical Model

We have developed a semi-analytical model for predicting the behavior of compact magnetic levitation-based harvesters of the form shown in Fig. 1(a). These comprise a hollow cylindrical structure that houses three disc-type cylindrical permanent magnets. A portion of the cylinder is wrapped in a multilayered coil. Two of the magnets are

attached to the end extremities of the container. The third magnet moves within the container between the fixed magnets and experiences a repulsive (levitation) force from each magnet. The coil is formed by winding enamelled wire around the outer surface of the container.

The MF distribution of the cylindrical magnet can be predicted using a number of analytical and semi-analytical methods[31–34]. In this work, we used the "equivalent" surface current model[31] and discretize the magnet into a finite set of current loop elements. We then superimpose the MFs of the constituent current loops to obtain the magnetic field of the magnet[25,26]. Equations (1–6) are used to compute the axial component of the MF, $B_z(r, z) = \mathbf{B}(r, z) \cdot \hat{\mathbf{z}}_m$ as a function of radial and axial distances (r and z) to the center of the moving magnet.

$$B_z = \mu_0 \frac{M_m}{2\pi} \int_{P_z+\delta-\frac{1}{2}L_m}^{P_z+\delta+\frac{1}{2}L_m} f(z, z')[Z_t(z, z')E(k) + K(k)]\,\mathrm{d}z' \tag{1}$$

$$E(k) = \int_0^{\frac{\pi}{2}} \sqrt{1 - k^2 sin^2(\phi)}\,\mathrm{d}\phi \tag{2}$$

$$K(k) = \int_0^{\frac{\pi}{2}} \frac{1}{\sqrt{1 - k^2 sin^2(\phi)}}\mathrm{d}\phi \tag{3}$$

$$f(z, z') = \frac{1}{\sqrt{(R_m + r)^2 + (z - z')^2}} \tag{4}$$

$$k = \sqrt{\frac{4rR_m}{(R_m + r)^2 + (z - z')^2}} \tag{5}$$

$$Z_t = \frac{R_m^2 - r^2 - (z - z')^2}{(R_m - r)^2 + (z - z')^2} \tag{6}$$

In these equations, P_z and δ are as defined below; L_m, R_m and M_m are the length, radius and saturation magnetization of the moving magnet, respectively; μ_0 is the free-space magnetic permeability; and $E(k)$ and $K(k)$ are complete elliptic integrals of the first and second kind. The use of analytical analysis to compute $B_z(r, z)$ is superior to the more commonly used numerical field analysis, both in terms of accuracy and computational efficiency[25,26].

The Maxwell-Faraday equation can be used to model the electromotive force induced in the coil by the time-varying magnetic flux that permeates it. One can obtain an approximate solution for predicting voltage harvesting by considering the coil as a set of single circular turns (N_r turns of the coil in the radial direction for each z; N_z turns of the coil in the axial direction for each r) and a 3D surface bounded by a closed contour defined by each of these turns. Using the Kelvin-Stokes theorem, and assuming that the spatial distribution of turns along the coil is uniform, one obtain the following Equation for computing the output voltage V as the magnet moves within the container.

$$V = 2\pi \frac{\partial}{\partial t}\left(\sum_{k=1}^{N_z}\sum_{j=1}^{N_r}\int_0^{r_j} B_z(r, z_k) r\mathrm{dr}\right) \tag{7}$$

In this equation, r_j is the radius r of the j'th turn; z_k is the distance z of layer k; and t is the integration sample time. The voltage V induces a current I in each turn of the coil through a circuit loop composed of the impedances of the harvester and load, as expressed by Eq. (8). The load is assumed to be purely resistive (R_l) and only the coil resistance (R_w) and inductance (L_w) are considered[21].

$$\frac{dI}{dt} = \frac{V - I(R_w + R_l)}{L_w} \tag{8}$$

The induced current I gives rise to a magnetic force (Lorentz force) that opposes the motion of the moving magnet, as given by:

$$F_{lz} = 2\pi I \sum_{k=1}^{N_z}\sum_{j=1}^{N_r} B_r(r_j, z_k) r_j \tag{9}$$

The magnetic force between two magnets as a function of their axial separation was computed by taking the derivative of their interaction energy with respect to the distance between them[35,36]. Equation (10) was used to compute the axial force $F_{mu_z} = \mathbf{F}_{mu}(r, z) \cdot \hat{\boldsymbol{z}}_m$ between the moving magnet and the fixed magnet located at the top of the harvester,

$$F_{mu_z} = \mu_0 \pi R_u R_m M_u M_m \int_0^\infty J_1(\varepsilon R_u) J_1(\varepsilon R_m) [e^{-\varepsilon (S_u + L_u)} + e^{-\varepsilon (S_u + L_m)} - e^{-\varepsilon (S_u)} - e^{-\varepsilon (S_u + L_u + L_m)}] \varepsilon^{-1} \mathrm{d}\varepsilon \quad (10)$$

where R_u is the radius, M_u is the saturation magnetization and L_u is the length, all pertaining to the fixed magnet at the top. S_u is the distance between the moving magnet and the fixed magnets at the top and J_1 is the 1st-order Bessel function. Equation (10) can also be used to compute the force $F_{md_z} = \mathbf{F}_{md}(r, z) \cdot \hat{\boldsymbol{z}}_m$ between the moving magnet and the fixed magnet located at the bottom, but using R_d, M_d, L_d and S_d. The assumption that the magnets are coaxially positioned is taken into account.

For any global coordinate system (x, y, z), the position $\mathbf{P}_m$ and orientation of $\hat{\boldsymbol{z}}_m$ of the moving magnet can be computed by establishing the forward kinematics for translations $(P_x, P_y, P_z + \delta)$ and rotations $(\theta_x, \theta_y, 0)$ of the container about a (fixed) space system reference frame (δ is the distance between P_z and the center of mass of the moving magnet, as shown in Fig. 1(b)). Extrinsic Euler angles $z - y - x$ were used to define a geometric matrix transformation $\mathbf{Q}$ that expresses $\mathbf{P}_m$ and the orientation of $\hat{\boldsymbol{z}}_m$.

$$\mathbf{Q} = \mathbf{T}_{(z,P_z)} \mathbf{T}_{(y,P_y)} \mathbf{T}_{(x,P_x)} \mathbf{R}_{(y,\theta_y)} \mathbf{R}_{(x,\theta_x)} \mathbf{T}_{(z,\delta)} \quad (11)$$

$$\mathbf{P}_m = \left[P_x + \delta \cos(\theta_x) \sin\left(\theta_y\right)\right] \hat{\boldsymbol{x}} + \left[P_y - \delta \sin(\theta_x)\right] \hat{\boldsymbol{y}} + \left[P_z + \delta \cos(\theta_x) \cos\left(\theta_y\right)\right] \hat{\boldsymbol{z}} \quad (12)$$

$$\hat{\boldsymbol{z}}_m = \cos(\theta_x) \sin\left(\theta_y\right) \hat{\boldsymbol{x}} - \sin(\theta_x) \hat{\boldsymbol{y}} + \cos(\theta_x) \cos\left(\theta_y\right) \hat{\boldsymbol{z}} \quad (13)$$

where $\mathbf{T}_{(x,P_x)}$, $\mathbf{T}_{(y,P_y)}$, $\mathbf{T}_{(z,P_z)}$ are the transformation matrices for translating P_x, P_y and P_z in (x, y, z); and $\mathbf{R}_{(x,\theta_x)}$ and $\mathbf{R}_{(y,\theta_y)}$ are the transformation matrices for rotating θ_x and θ_y around (x, y). $\mathbf{Q}$ was defined considering that the influence of rotations around (x_m, y_m, z_m) and θ_z is negligible. One can use Eqs (12) and (13) to find the axial acceleration $\frac{d^2 P_m}{dt^2} = \frac{d^2 \mathbf{P}_m}{dt^2} \cdot \hat{\boldsymbol{z}}_m$ of the moving magnet. After simplification, and considering P_x, P_y, θ_x and θ_y to be constant, the following algebraic equation was obtained:

$$\frac{d^2 P_m}{dt^2} = \frac{d^2 \delta}{dt^2} + \frac{d^2 P_z}{dt^2} \cos(\theta_x) \cos\left(\theta_y\right) \quad (14)$$

The axial component of the gravitational force F_{gr} is:

$$F_{gr} = mg\hat{\boldsymbol{z}} \cdot \hat{\boldsymbol{z}}_m = mg \cos(\theta_x) \cos\left(\theta_y\right) \quad (15)$$

where m is the mass of the moving magnet and g is the acceleration due to gravity. The friction force F_{fr} between the moving magnet and the container's inner surface was modelled by using the Karnopp friction model[37]:

$$F_{fr} = \begin{cases} f_{re} & \text{if } -f_{bw_n} < f_{re} < f_{bw_p} \\ f_{co_p} + k_{v_p} \frac{d\delta}{dt} & \text{if } \frac{d\delta}{dt} > v_{min} \\ -f_{co_n} + k_{v_n} \frac{d\delta}{dt} & \text{if } \frac{d\delta}{dt} < -v_{min} \end{cases} \quad (16)$$

$$f_{re} = m \frac{d^2 P_m}{dt^2} - F_{gr} - F_{mu_z} + F_{md_z} - F_{lz} \quad (17)$$

This friction model takes into account the following effects: (i) different viscous friction coefficients for negative (k_{v_n}) and positive (k_{v_p}) speeds $\frac{d\delta}{dt}$; (ii) different break-away forces for negative (f_{bw_n}) and positive (f_{bw_p}) speeds; (iii) different Coulomb forces for negative (f_{co_n}) and positive (f_{co_p}) speeds; and (iv) a low speed region $-v_{min} \leq \frac{d\delta}{dt} \leq v_{min}$, where one can consider $\frac{d\delta}{dt} = 0$. These effects can emerge due to processes used to fabricate the container.

Two differential equations are required to model the interplay between the electrical and mechanical dynamics of the moving magnet. The electrical behavior is governed by Eq. (8); the motion of the moving magnet is given by:

$$\frac{d^2 \delta}{dt^2} = -\frac{d^2 P_z}{dt^2} \cos(\theta_x) \cos\left(\theta_y\right) - \frac{F_{lz}}{m} + \frac{F_{md_z}}{m} - \frac{F_{mu_z}}{m} - \frac{F_{gr}}{m} - \frac{F_{fr}}{m} \quad (18)$$

Results

A harvester was implemented with the characteristics described in Table 1 (Fig. 1(b)). Two resistive loads were chosen: $R_l = 89.3\,\mathrm{k}\Omega$, for analyzing a quasi open-circuit voltage; and $R_l = 3.5\,\mathrm{k}\Omega$, for maximizing the power transfer to the load. To accurately analyze the nonlinearities on energy transduction of this harvester architecture, open-load conditions were discarded, such that the current dynamics could be computed for consequent analysis

Characteristics	Value	Units
l_m	58×10^{-3}	m
l_c	20×10^{-3}	m
l_i	23.5×10^{-3}	m
d_h	16×10^{-3}	m
d_c	8.2×10^{-3}	m
d_m	6.2×10^{-3}	m
R_m	3×10^{-3}	m
R_u	3×10^{-3}	m
R_d	3×10^{-3}	m
L_m	6×10^{-3}	m
L_u	1×10^{-3}	m
L_d	1×10^{-3}	m
M_m	8×10^5	A/m
M_u	7.61×10^5	A/m
M_d	7.61×10^5	A/m
m	1.24×10^{-3}	kg
$N_r N_z$	15000	—
Coil wire diameter	6.8×10^{-5}	m
R_w	3.63	kΩ
L_w	1.009	H
R_l	89.3|3.5	kΩ

Table 1. Harvester's characteristics.

of friction on physical contact between the moving magnet and the container. Neodymium magnets were chosen to provide a substantial magnetic flux $\frac{\partial \Phi}{\partial t}$ through the coils, where $\Phi = \int_0^{r_j} B_z(r, z_k) r \mathrm{d}r$. The coils were formed using enamelled copper with a very small diameter to accommodate a large number of turns. The coil was positioned so that the moving magnet is surrounded by the coil when the harvester is stationary, i.e., absent excitation. The cylindrical container was machined out of PTFE (Seal & Design Inc.) due to its low coefficients of friction.

The harvester was attached to a testing machine with servo-motors that can produce arbitrary vertical displacements. $\theta_y = \pi/9$ rad and $\theta_x = 0$ rad were then imposed to the experimental apparatus to ensure that $F_{fr} \neq 0$. Several free fall tests (using only the moving magnet and the fixed magnet at the bottom of the container) were conducted to identify the friction coefficients. By performing a global search to find the minimum difference between experimental and simulated responses, the following coefficients were obtained: $f_{co_p} = 3.68 \times 10^{-3}$ N, $f_{co_n} = 5.79 \times 10^{-4}$ N, $f_{bw_p} = 4.05 \times 10^{-3}$ N, $f_{bw_n} = 6.37 \times 10^{-4}$ N, $k_{v_p} = 9.89 \times 10^{-5}$ N s / m, $k_{v_n} = 5.51 \times 10^{-5}$ Ns/m, $v_{min} = 5 \times 10^{-3}$ m/s. The undisturbed position of the levitated magnet was determined using both experimental tests and simulation and found to be approximately $\delta = 38.3 \times 10^{-3}$ m.

Our system model was validated by comparing predictions with measurements with the harvester subjected to sinusoidal motion. This choice of excitation was made due to the fact that a large number of applications use cyclic motion to harvest energy. Measurements were taken for frequencies in the 3–10 Hz range. Very low voltage output was obtained for frequencies lower than 3 Hz (mean absolute voltages lower than 0.3 V for $R_l = 89.3$ kΩ and 0.15 V for $R_l = 3.5$ kΩ), and voltages exceeding the analog input range of the acquisition board (upper and lower saturation values: 10 V and −10 V) was obtained for frequencies higher than 10 Hz. The steady-state and transient responses of the energy harvester were analysed. The results of the steady-state analysis are shown in Fig. 2 and Table 2. These results demonstrate that the model accurately predicts the highly non-linear behavior of the harvester. Note that very good agreement between experimental and simulation results were achieved with energy errors lower than 14.15% (mean absolute percentage error is 6.02%) and cross-correlations higher than 86%. Similar results were obtained for the transient response, as shown in Fig. 3, i.e., the same energy errors and cross-correlations were obtained.

Discussion

One of the main goals of this study was to develop the less complex model that could ensure very good validation results. These were achieved by neglecting: (a) the non-concentricity between the moving magnet and the fixed magnets; (b) the dynamic effects of the friction force; (c) the effects of non-axiality and non-uniformity of the friction force along the overall length of the inner wall of the container; and (d) the several components of viscous fluidic damping and air compressibility. Although further research efforts may be conducted to develop more complex models, the model presented in this paper can be used for achieving very good predictions of the energy harvesting in nonlinear regimes.

The careful selection of appropriate materials, surface finish and container architecture is also required to maximize the harvester performance. Container materials should have friction coefficients as low as possible, and with negligible magnetic permeability. PTFE is among the materials that meet such requirements. Harvester

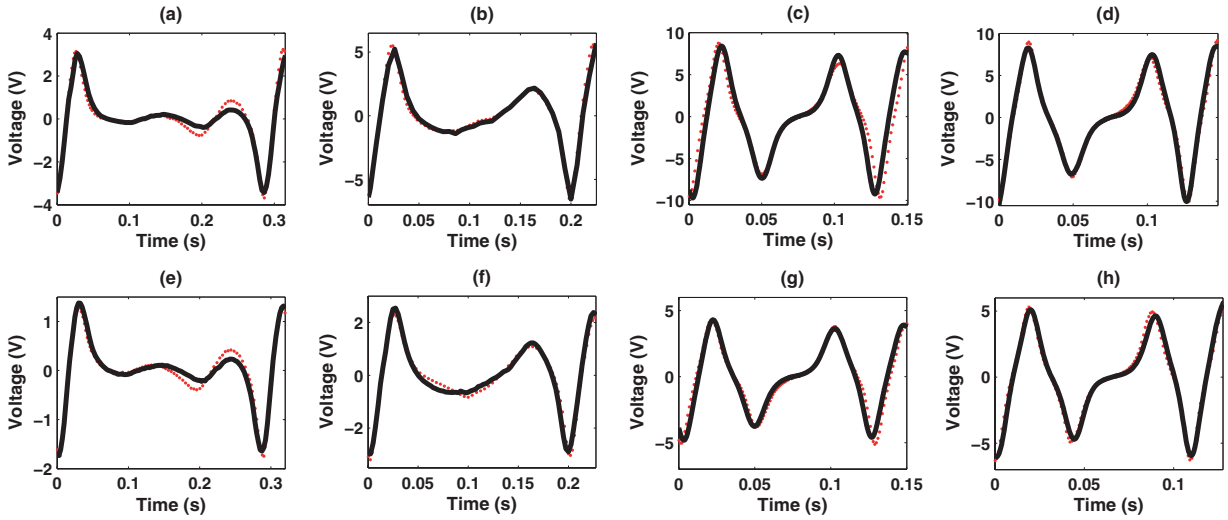

Figure 2. Steady-state analysis (experimental (red dots) and simulation (solid black lines)) for experiments: (**a**) T2; (**b**) T4; (**c**) T6; (**d**) T8; (**e**) T1; (**f**) T3; (**g**) T5; (**h**) T7.

Exp.	P_z (mm)[c]	R_l (kΩ)	CC (%)	EE (%)	ST (sec)[d]
T1	17 *sin* (7πt)	3.5	86.20	9.31	≈12.5
T2	17 *sin* (7πt)	89.3	88.30	4.26	≈12.4
T3	12.25 *sin* (10πt)	3.5	98.24	6.38	≈9.3
T4	12.25 *sin* (10πt)	89.3	88.03	2.46	≈9.1
T5	7.75 *sin* (15πt)	3.5	92.78	0.59	≈5.8
T6	7.75 *sin* (15πt)	89.3	90.63	14.15	≈5.9
T7	6 *sin* (18πt)	3.5	88.53	4.72	≈5.1
T8	7 *sin* (16πt)	89.3	94.79	6.27	≈5.9

Table 2. Validation results[a,b]. [a]Abbreviations: CC - Cross-correlation; EE - Energy error; ST - Simulation time. [b]Results are referred to a cycle in steady state responses. [c]$P_x = 0$ m, $P_y = 0$ m, $\theta_x = 0$ rad, $\theta_y = \pi/9$ rad. [d]2.5 GHz CPU, 8 GB RAM, Windows 7 operating system.

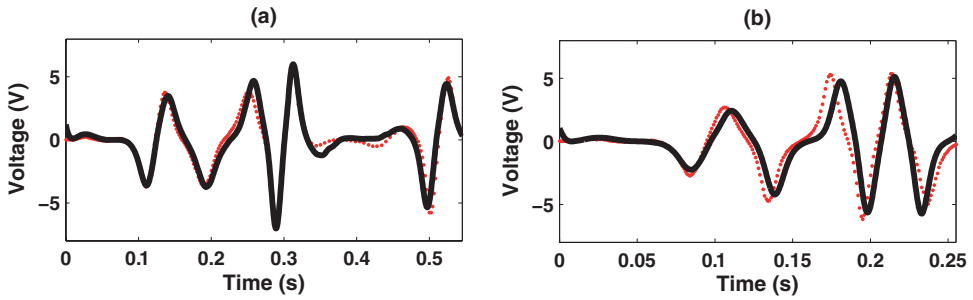

Figure 3. Transient analysis (experimental (red dots) and simulation (solid black lines)) for experiments: (**a**) T4, CC = 93.85%, EE = 7.51%; (**b**) T7, CC = 88.62%, EE = 6.23%.

architectures using a tight-fit container-magnet interface are superior to other architectures, as they minimize the coil-magnet distance, maximizing the magnetic flux through the coils. More complex nonlinearities will most likely be observed if loose-fit container-magnet interfaces are used, due to the increasing effects of non-axiality of the moving magnet on friction force. The use of square containers and cylindrical magnets minimize the friction forces (due to the lower contact areas), but the magnetic flux through the coils would be lower. Manufacturing methods that minimize the surface roughness, ensuring similar friction coefficients along its area, also minimize nonlinearities of contact friction. Conventional machining will most likely produce worse surface finish than using chemical processes. The model proposed here can be used as a predictive tool if the requirement for harvesting

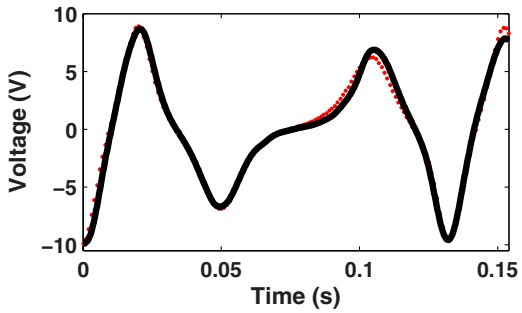

Figure 4. Steady-state analysis (experimental (red dots) and simulation (solid black lines)) for experiment T6 considering $M_m = 8.1 \times 10^5$ A/m and $\delta = 38.5 \times 10^{-3}$ m: CC = 99.24%, EE = 4.55%.

performance optimization described above are taken into account. If the same materials, architectures and manufacturing methods are used, similar results will most likely be achieved.

EEs lower than 10% were achieved for most of the experiments. Only the T6 experiment exceeded this error range. To identify the most probable causes for this deviation, we hypothesized that very small errors in the identified model's parameters and/or nonlinear effects of friction force not accurately modeled can result in higher energy errors for specific excitations. Considering the highly nonlinear behavior of B_z, the resulting effects of using a non-optimal M_m were analyzed. The steady-state analysis of the T6 experiment for $M_m = 8.1 \times 10^5$ A/m (value also within bounds reported by the manufacturer) was carried out, which change the undisturbed position of the levitated magnet in 0.2 mm (to $\delta = 38.5 \times 10^{-3}$ m). An energy error lower than 5% was observed, as shown in Fig. 4. Similar errors were also achieved for the other excitations analyzed in this study by applying these parameters. Hence, we can infer that non-optimal identification of the magnetization saturations can cause increasing energy errors for specific excitations. These results also suggest that a more accurate model for the friction force must be found. The proposed Karnopp friction model does not take into account the dynamic stick-slip motion of the moving magnet for PTFE-NdFeB contact surfaces and possible roughness differences that may be found along the container's inner surface. Besides, even harvester architectures based on tight-fit container-magnet interfaces always require a time-dependent non-axiality degree of the moving magnet for levitation stability. All these effects may set differing initial conditions among experiments (the position, orientation and velocity of the moving magnet, the surface roughness, among others), mainly when successive experimental tests are conducted. We cannot also dismiss possible manifestations of chaoticity in these behaviors.

Few similarities are found between the semi-analytical model proposed here and those recently developed for diamagnetic levitation-based harvesting (DLH)[29,30], namely: (a) the moving magnet is modeled as a finite set of thin current loops; (b) multilayered coil(s) are modeled as a finite set of thin circular turns; (c) the effects of the coil inductance on the current dynamics were also considered. Although DLHs are friction-free architectures, their accurate analysis requires modeling of other complex dynamics not existent in levitation systems using tight-fit containers, such as the damping forces between the moving magnet and the diamagnetic structure[29,30]. To our best knowledge, the proposed model that explores in more detail the fundamental transduction mechanisms of DLHs needs further improvement if it is to be used for harvester design optimization[30]. DLHs were tested only using very small excitations amplitudes[27–30]. Their insufficient levitation gaps have only allowed analyzing nonlinearities for very constrained motions of the moving magnet[27–30]. So far, stable levitation using different orientations of the harvester has been only achieved by different DLH designs[30,38]. However, the harvesting architecture studied in this paper and our semi-analytical model enables the analysis of energy transduction nonlinearities for wide range of motion amplitudes of the moving magnet, as well as for arbitrary orientations of the harvester.

The solver used in this work is considered one of the best global fixed-step solvers for physical systems, but it can be computationally more intensive than other solvers. Still, computing time efficiency is well demonstrated by results expressed in Table 2. Computational efficiency could be further improved if the algorithm was fully implemented in compiled code and run in dedicated computing platforms. Better selection of the fixed-step size could also improve the simulation time. The increase in computational efficiency compared to FEM was not quantified because, to our knowledge, the time to simulate FEM-based models has not yet been reported.

For known and narrowband excitations, the harvester's characteristics described in Table 1 can be optimized prior to fabrication. This model can be used to optimize the self-powering capability of a broad range of technologies, including those that impose hard dimensional constraints, unconstrained motion amplitudes and arbitrary orientations of the harvester. Intelligent levitation-based broadband harvesting can also be achieved using such an accurate model. Intelligent control algorithms can be developed to find the most suitable positions of the fixed magnets and coil(s) for each narrowband of amplitude and frequency. It should be noted that the governing equations presented for this levitation-based harvester can also be used to model many other motion-driven electromagnetic energy harvesters, as well as to maximize the energy they can be harvested for narrow or broadband excitations. They can also be used to develop models for arbitrary tri-dimensional trajectories of harvesters.

Methods

The hollow cylindrical structure of the harvester was machined by conventional technology. The harvester output voltage was monitored and servo-motors were controlled by a DSP board (DS1102 from dSPACE). I/O modules

of DS1102 were initialized and configured in Simulink R13 (v. 5.0, Mathworks) by the Real Time Workshop (v. 5.0, Mathworks) and Real Time Interface (v. 4.4, dSPACE). An application was developed in ControlDesk (v. 2.3, dSPACE) to interact with the real-time application and to control the experiments. V was computed by discretizing $B_z(r, z)$ (incremental steps equal to the wire diameter) and, then, numerically integrating the resulting mesh. The 1st-order Bessel function J_1 was computed as proposed by Deun and Cools[39]. In order to improve the computational efficiency, $B_z(r, z)$, $B_z(r, z_k)r$, $\int_0^{r_j} B_z(r, z_k)\,r\mathrm{d}r$, F_{mu_z} and F_{md_z} were stored in 3D Look-up Tables. Equations (7) and (9) were compiled by using Matlab S-Functions API.

The simulations were carried out using Simulink R2014a (v. 8.3, Mathworks). Equations (8) and (18) were solved via numerical integration using global Simulink fixed-step solver ode14x (fixed-step size: 2.5 ms; solver jacobian method: 'full perturbation'; extrapolation order: 4) so that high solution accuracy and computational efficiency could be achieved. A global search algorithm from Matlab R2014a ('GlobalSearch' solver; 'fmincon' to find the minimum of the constrained squared error function) was used to find the friction coefficients. The same algorithm was used to compute the saturation magnetizations of magnets: firstly, the force between the moving magnet and each of the fixed magnets were experimentally determined within the interval of possible distances between the two faces of the magnets (0.1 to 50 mm); finally, the matching of the experimental measurements to the theoretical prediction given by Eq. 10 was carried out (the sets of lower and upper bounds of saturation magnetizations reported by the manufacturer were considered in the constrained optimization).

The energy errors and cross-correlations were computed using the following equations[40]:

$$EE = \frac{\left|\int_0^{t_1} \frac{V_{l_e}^2(t)}{R_l}\mathrm{d}t - \int_0^{t_1} \frac{V_{l_s}^2(t)}{R_l}\mathrm{d}t\right|}{\int_0^{t_1} \frac{V_{l_e}^2(t)}{R_l}\mathrm{d}t} \times 100 \tag{19}$$

$$R_{l_e l_s}(\beta) = \begin{cases} \sum_{\alpha=1}^{\Omega-\beta} V_{l_e}(\alpha+\beta)\, V_{l_s}(\alpha) & \text{if } \beta \geq 0 \\ R_{l_s l_e}(-\beta) & \text{if } \beta < 0 \end{cases} \tag{20}$$

$$CC = 100 \times \max \frac{R_{l_e l_s}(\beta - \Omega)}{\sqrt{\sum_{\alpha=1}^{\Omega} V_{l_s}^2(\alpha) + \sum_{\alpha=1}^{\Omega} V_{l_e}^2(\alpha)}}, \quad \beta = 1, 2, \ldots, 2\Omega - 1 \tag{21}$$

where $V_{l_e}(t)$ and $V_{l_s}(t)$ are respectively the experimental and simulated voltage harvested on the load R_l in the time domain; $V_{l_e}(\alpha)$ and $V_{l_s}(\alpha)$ are the discrete counterparts of $V_{l_e}(t)$ and $V_{l_s}(t)$ (length: Ω; $1 \leq \alpha \leq \Omega$); t_1 is the end of the cycle time. The trapezoidal numerical integration was used to compute Eq. 19.

References

1. Dewan, A., Ay, S. U., Karim, M. N. & Beyenal, H. Alternative power sources for remote sensors: A review. *J. Power Sources* **245(1),** 129–143 (2014).
2. Khaligh, A., Zeng, P. & Zheng, C. Kinetic Energy Harvesting Using Piezoelectric and Electromagnetic Technologies - State of the Art. *IEEE T. Ind. Electron.* **57(3),** 850–860 (2010).
3. Harb, A. Energy harvesting: State-of-the-art. *Renew. Energ.* **36(10),** 2641–2654 (2011).
4. Paradiso, J. A. & Starner, T. Energy scavenging for mobile and wireless electronics. *Pervasive Comput.* **4(1),** 18–27 (2005).
5. Mitcheson, P. D., Yeatman, E. M., Rao, G. K., Holmes, A. S. & Green, T. C. Energy harvesting from human and machine motion for wireless electronic devices. *Proc. IEEE* **96(9),** 1457–1486 (2008).
6. Beeby, S. P., Tudor, M. J. & White, N. M. Energy harvesting vibration sources for microsystems applications. *Meas. Sci. Technol.* **17(12),** R175–R195 (2006).
7. Teng, X.-F., Zhang, Y.-T., Poon, C. C.& Bonato, P. Wearable medical systems for p-health. *IEEE Rev. Biomed Eng.* **1,** 62–74 (2008).
8. Zhang, C. L. & Chen, W. Q. A wideband magnetic energy harvester. *Appl. Phys. Lett.* **96,** 123507-1–123507-3 (2010).
9. Jang, S., Kim, I., Jung, H. & Lee, Y. A tunable rotational energy harvester for low frequency vibration. *Appl. Phys. Lett.* **99,** 134102-1–134102-3 (2011).
10. Ward, J. K. & Behrens, S. Adaptive learning algorithms for vibration energy harvesting. *Smart Mater. Struct.* **17,** 035025 (2008).
11. Mallick, D. & Roy, S. Bidirectional electrical tuning of FR4 based electromagnetic energy harvesters. *Sensor. Actuat A-Phys.* **226,** 154–162 (2015).
12. Shariati, N., Rowe, W. S., Scott J. R. & Ghorbani, K. Multi-Service Highly Sensitive Rectifier for Enhanced RF Energy Scavenging. *Sci. Rep.* **5,** 9655 (2015).
13. Zhu, D., Tudor, M. J. & Beeby, S. P. Strategies for increasing the operating frequency range of vibration energy harvesters: a review. *Meas. Sci. Technol.* **21,** 022001 (2010).
14. Harne, R. L. & Wang K. W. A review of the recent research on vibration energy harvesting via bistable systems. *Smart Mater. Struct.* **22,** 023001 (2013).
15. Sussmann, H. J. *Nonlinear Controllability and Optimal Control* (Marcel Dekker INC, 1990).
16. Boltyansky, V. G. Sufficient conditions for optimality and the justification of the dynamic programming method. *SIAM J. Control* **4(2),** 326–361 (1966).
17. Soares dos Santos, M. P. *et al.* Instrumented hip implants: Electric supply systems. *J. Biomech.* **46(15),** 2561–2571 (2013).
18. Soares dos Santos, M. P. *et al.* Instrumented hip joint replacements, femoral replacements and femoral fracture stabilizers. *Expert Rev. Med. Devices* **11(6),** 617–635 (2014).
19. Morais, R. *et al.* Double permanent magnet vibration power generator for smart hip prosthesis. *Sensor. Actuat A-Phys.* **172(1),** 259–268 (2011).
20. Mann, B. P. & Sims, N. D. Energy harvesting from the nonlinear oscillations of magnetic levitation. *J. Sound Vib.* **319(1-2),** 515–530 (2009).

21. Avila Bernal, A. G. & Linares García, L. E. The modelling of an electromagnetic energy harvesting architecture. *Appl. Math. Model.* **36(10),** 4728–4741 (2012).
22. Dallago, E., Marchesi, M. & Venchi, G. Analytical Model of a Vibrating Electromagnetic Harvester Considering Nonlinear Effects. *IEEE Trans. Power Electron.* **25(8),** 1989–1997 (2010)
23. Saha, C. R., O'Donnell, T., Wang, N. & McCloskey, P. Electromagnetic generator for harvesting energy from human motion. *Sensor. Actuat A-Phys.* **147(1),** 248–253 (2008).
24. Munaz, A. Lee, B. & Chung, G. A study of an electromagnetic energy harvester using multi-pole magnet. *Sensor. Actuat A-Phys.* **201,** 134–140 (2013).
25. Furlani, E. P. & Xue, X. Field, force and transport analysis for magnetic particle-based gene delivery. *Microfluid. Nanofluid.* **13(4),** 589–602 (2012).
26. Xue, X. & Furlani, E. P. Template-assisted nano-patterning of magnetic core-shell particles in gradient fields. *Phys. Chem. Chem. Phys.* **16(26),** 13306–13317 (2014).
27. Liu, L. & Yuan, F. G. Nonlinear vibration energy harvester using diamagnetic levitation. *Appl. Phys. Lett.* **98(20),** 203507 (2011).
28. Liu, L. & Yuan, F. G. Diamagnetic levitation for nonlinear vibration energy harvesting: theoretical modeling and analysis. *J. Sound Vib.* **332(2),** 455–464 (2013).
29. Wang, X. Y., Palagummi, S., Liu, L. & Yuan, F. G. A magnetically levitated vibration energy harvester. *Smart Mater. Struct.* **22(5),** 055016 (2013).
30. Palagummi, S. & Yuan, F. G. An optimal design of a mono-stable vertical diamagnetic levitation based electromagnetic vibration energy harvester. *J. Sound Vib.* **342,** 330–345 (2015).
31. Furlani, E. P. In *Permanent Magnet and Electromechanical Devices: Materials, Analysis and Applications* (Academic Press, 2001).
32. Furlani, E. P. A method for predicting the field in permanent magnet axial-field motors. *IEEE Trans. Mag.* **28(5),** 2061–2066 (1992).
33. Furlani, E. P. Computing the field in permanent-magnet axial-field motors. *IEEE Trans. Mag.* **30(5),** 3660–3663 (1994).
34. Furlani, E. P. A formula for the levitation force between magnetic disks. *IEEE Trans. Mag.* **29(6),** 4165–4169 (1993).
35. Craik, D. J. In *Magnetism: principles and applications*. 342–244 (John Wiley, 1995).
36. Vokoun, D., Beleggia, M., Heller, L. & Šittner, P. Magnetostatic interactions and forces between cylindrical permanent magnets. *J. Magn. Magn. Mater.* **321(22),** 3758–3763 (2009).
37. Karnopp, D. Computer simulation of stick-slip friction in mechanical dynamic systems. *J. Dyn. Syst.-T ASME* 107(1), 100–103 (1985).
38. Palagummi, S., Zou, J. & F. Yuan, F. A horizontal diamagnetic levitation based low frequency vibration energy harvester. *J. Vib. Acoust.* **137(6),** 061004 (2015).
39. Deun, J. V. & Cools, R. Integrating products of Bessel functions with an additional exponential or rational factor, *Comput. Phys. Commun.* **178,** 578–590 (2008).
40. Orfanidis, S. J. *Optimum Signal Processing: An Introduction* 2nd edn, Ch. 1-2 (Prentice Hall, 1996).

Acknowledgements

The authors would like to thank the Portuguese Foundation for Science and Technology (FCT) for their financial support POPH/FSE under the project EXPL/EMS-SIS/2128/2013 and the grant SFRH/BD/78414/2011. Work of author Ricardo Pascoal has been partially funded by Portuguese National Funds through FCT, in the context of the projects UID/CEC/00127/2013 and Incentivo/EEI/UI0127/2014. Authors Furlani and Xue acknowledge financial support from the U.S. National Science Foundation, through award number CBET-1337860.

Author Contributions

M.P.S.D.S., J.A.F.F., R.P., X.X. and E.P.F. developed the model; E.P.F., J.A.F.F. and J.A.O.S. managed and supervised the research project; M.P.S.D.S. and J.T. designed and fabricated the harvester; M.P.S.D.S., J.A.F.F. and J.T. implemented the experimental apparatus; M.P.S.D.S. performed the theoretical calculations, model simulation and data analysis; all the authors contributed in writing the manuscript.

Additional Information

Competing financial interests: The authors declare no competing financial interests.

How to cite this article: Santos, M. P. S. *et al.* Magnetic levitation-based electromagnetic energy harvesting: a semi-analytical non-linear model for energy transduction. *Sci. Rep.* **6**, 18579; doi: 10.1038/srep18579 (2016).

Chapter 6

Discussion

This thesis proposes a novel approach to minimize implant failures: to use instrumented implants capable of controlling the bone-implant integration. The architectures of these implants fulfil the necessary and sufficient requirements to ensure performance optimality preventing deficient bone remodelling. Cosurface-based capacitive stimulators allow to deliver a wide range of electric fields to target tissue areas. The stimulators' geometry (electrodes and gaps), the amount of stimulators and their locations can also be optimized to allow that required therapy-based stimuli delivery can be performed. Noteworthy, this technology allows to deliver therapy actuations along the entire implants' surface and even control them in a network scheme. Besides, they can be controlled by clinicians by establishing a communication link between implant and extracorporeal systems, which provide the ability to deliver controllable stimuli after implant insertion. Personalized therapies can then be administrated to patients of all ages and according to their idiosyncrasies. The rational design of intelligent control algorithms can be useful to adjust postoperatively the moving electrodes from their initial positioning, extending the operability range of the stimulatory system. A superior controllability over osseointegration can be even obtained if its states are monitored. Additionally, everlasting stimuli delivery can be achieved using self-powering technologies to supply instrumented implants. It should be noted that stimulation, monitoring, processing and communication systems can be disabled, such that implants only operate passively. Hence, this new concept of instrumented active implant can be explored to reach a controllability level (over osteoblast proliferation, matrix maturation and matrix mineralization) that cannot be attained by other approaches proposed so far.

This new approach give the opportunity to develop instrumented active implants with a wide range of new means of therapeutic actuations. The clinicians' expertise can be used to administrate appropriated stimulatory therapies, taking advantage of decision-making based on previous research studies and on outcomes obtained from other patients [1]. Further sophistication may be attained if active implants are designed with the ability to autonomously define the stimulatory therapies. Nowadays, available technology allows transferring the human knowledge to data storage systems located inside instrumented implants, and artificial intelligence algorithms can learn from the inherent variability of

the osseointegration states of each patient [1]. Included as controllable states might be the cell adhesion on implants' surface, the expression of extracellular matrix proteins and mineralization proteins, the mechanical behavior and topological characterization of the bone-implant interface, among others. Should not be dismissed that may exist stimulation-based treatments, ensuring trajectories from failure states to without-failure states, such that there is no need of monitoring the osseointegration states. This scenario may most likely occur for preventive actuations. The potential of cosurface stimulators to avoid the need of bioactive coatings must be referred when analysing the interaction between these methodologies. When implants are not coated with bioactive materials, this biophysical stimulator can only optimize the host bone adherence to implants' surface. Nevertheless, their stimuli delivery can be exploited as the main method to avoid implant failures, although they can be programmed as an adjuvant strategy to enhance the potentiality of bioactive coatings [2] or to deliver drugs and/or other bio-agents [3]. The capability of osteogenic, osteoconductive and osteoinductive stimulations are thus inherent to instrumented active implants.

This new concept model of Instrumented Active Implant also present some constraints. Stimuli delivered by cosurface stimulators to mid-regions between electrodes and a target region are dependent of the required stimuli that must be delivered to that target region. Such limitation may not be however an obstacle for controlling bone remodeling. Besides, it is unknown to what extend different stimuli can be delivery to nearby tissue areas. As proved in chapter 2, monitoring of the osseointegration states is required to obtain optimized trajectories of osteoblast proliferation, matrix formation and maturation and matrix mineralization [1]. The decision-making of clinicians is not error-free, and the probability to be administrated a non-optimized therapy increases as the number of monitored states decreases. Other risks cannot be disregarded, such as the cytotoxic and genotoxic risks related to implant fractures, which are significantly higher when implant systems are biointegrated in young/active patients. Biocompatible cosurface stimulators can be already constructed [4], but manufacturing of biocompatible sensing, processing, energy storage, and communication systems is still a hot topic in chemistry and material sciences [5]. A risk minimization can be carried out if some electronic systems and energy harvesters were fully encapsulated using biocompatible materials, as well as by miniaturizing these inner systems to minimize the hollowed structures inside implants. As far we are aware, possible genotoxic effects resulted from the delivery of electromagnetic fields cannot be overlooked, as shown in chapter 4. The above described geometry optimization of stimulators and energy harvesters prior to arthroplasty may be a sophistication level hard to accomplish. The ability of adaptive mechanisms to adjust the electrodes positioning will most likely be rather limited after implant insertion. Therefore, the most reliable scheme seems to be the identification of the peri-implant regions of more pronounced bone loss (such as the proximomedial region of total hip replacements) and of the most effective architectures and geometries for each patient's profile. Another important issue is the inherent osteogenic effects that can be promoted by extracorporeally-induced magnetic fields stimulating the bone-implant interface when communication and/or powering operations are performed [6].

Although it seems reasonable to assume much lower exposure times to these stimuli when comparing with those delivered for therapeutic actuation, these extracorporeally-originated stimuli can interfere with administrated control trajectories imposed to bony proliferation, differentiation and mineralization. Finally, instrumented active implants will be more complex and expensive than passive implants, although they have a huge potential to minimize the personal and societal burden of disability due to osseointegration problems, as analysed in this thesis.

Various difficulties will arise in the development of instrumented active implants. Promising results on the potential of cosurface-based capacitive stimulation to control bone remodeling were achieved, but the osteogenic effects of a wide variety of stimuli are still unknown. *Per se*, administrating EF delivery trajectories may not be enough to ensure effective implant fixation to host bone, in particular if patients suffer from severe bone remodeling disorders (e.g. osteoporosis). Moreover, the patients' idiosyncrasies may difficult the identification process towards optimality of therapeutic actuations. To ensure everlasting operation of active implants, complex self-powering and monitoring systems may have to be designed. Motion-driven electromagnetic energy harvesting seems the most promising method to power instrumented implants [7]. However, such harvesters must be designed considering: the geometric optimization prior to fabrication, taken into account the tridimensional hip joint motions during the routine activities of patients and according to their ageing processes; rational design of intelligent harvesters, in order to be adaptable to the intrinsic variability of patients' motions that significantly reduce their performance [7, 8]. In this scope, the work here presented is a solid basis for future research aiming to investigate the effectiveness of this strategy to power instrumented implants. Indeed, the amount of energy harvested may impose limits on the EF strengths that can be delivered to the peri-implant bone volume and, consequently, the amount of therapeutic actuation trajectories may be more reduced than expected. Storage systems will most likely be necessary [9], mainly for powering implants during the perioperative period, in old ages and when demanding therapies are required (e.g., several hours of daily stimulation). Even so, it should not be discarded that extracorporeal systems may be needed to electrically supply implants. Regarding to the design of monitoring systems, in addition to the complexity to track the osseointegration states, their operation may produce adverse effects on the bone-implant fixation. Because monitoring systems must be located as close as possible to the stimulatory systems, the design complexity increases as increases the number of sensors and actuators. Projecting instrumented implants capable of delivering bio-agents in the bone-implant interface without weaken the bone-implant integration will be also challenging. As these implants always have to be constructed with inner hollowed structures, it is imperative to research new materials with bulk properties that can minimize fracture risks. To conclude this enumeration of difficulties that must be handled, it must be also referred that stimulation therapies can no longer be modified if the communication system stops working properly.

All technological breakthroughs accomplished to date in this research area are not enough to develop instrumented active systems that can be already implanted in human patients. In the forthcoming years, the ability of cosurface stimulators to

promote controlled and personalized bone remodeling must be deeply explored. The interrelationships between stimuli parameters and their osteogenic outcomes require to perform a large number of stimulation assays *in vitro* and *in vivo*. Biological tests must be conducted using various bone cell models and bone structures. Systematic analyses of EF strength distributions throughout the highly inhomogeneous trabecular structures are thus crucial. Besides, effects due to cosurface-based stimulation on cells' homeostasis and adherence to the implant surface must be studied. The shared use of the cosurface capacitive apparatuses to stimulate organic structures and to monitor changes in the osseointegration state will most likely be considered. Additionally, the use of these stimulators as a method to improve the performance of bioactive coatings will be most likely analysed in detail. Research efforts must be also focused on developing non-linear models for predicting energy harvesting considering 3D excitations of the harvesters caused by hip motions of patients. The accurate and efficient analysis of other motion-based energy transductions is also envisaged, such as the rotational electromagnetic and piezoelectric harvesting. Nevertheless, innovative harvesting solutions not dependant on the mechanical work expended by patients (e.g. femoral motions) are also expected. Finally, the development of measurement systems to accurately monitor the osseointegration state must be strongly encouraged.

References

[1] Marco P. Soares dos Santos, Jorge A. F. Ferreira, António Ramos, José A. O. Simões. Active orthopaedic implants: towards optimality, Journal of the Franklin Institute 352(3) (2015) 813-834.

[2] Milena Fini, Ruggero Cadossi, Valerio Cane, Francesco Cavani, Gianluca Giavaresi, Adriano Krajewski, Lucia Martini, Nicolo Nicoli Aldini, Antonio Ravaglioli, Lia Rimondini, Paola Torricelli, Roberto Giardino, The effect of pulsed electromagnetic fields on the osteointegration of hydroxyapatite implants in cancellous bone: a morphologic and microstructural in vivo study, Journal of Orthopedic Research 20(4) (2002) 756-763.

[3] James H. Prescott, Sara Lipka,Samuel Baldwin, Norman F. Sheppard, John M. Maloney, Jonathan Coppeta, Barry Yomtov, Mark A. Staples, John T. Santini, Chronic, programmed polypeptide delivery from an implanted, multireservoir microchip device, Nature Biotechnology 24 (2006) 437-438.

[4] Haiqun Chen, Marc B. Müller, Kerry J. Gilmore, Gondon G. Wallace, Dan Li, Mechanically strong, electrically conductive, and biocompatible graphene paper, Advanced Materials 20(18) (2008) 3557-3561.

[5] Dae-Hyeong Kim, Roozbeh Ghaffari, Nanshu Lu, John A. Rogers, Flexible and stretchable electronics for biointegrated devices, Annual Review of Biomedical Engineering 14 (2012) 113-128.

[6] Marco P. Soares dos Santos, Jorge A. F. Ferreira, António Ramos, José A. O. Simões, Raul Morais, Nuno M. Silva, Paulo M. Santos, Manuel C. Reis, Tatiana Oliveira, Instrumented hip joint replacements, femoral replacements and femoral fracture stabilizers, Expert Reviews of Medical Devices, 11(6) (2014) 617-635.

[7] Marco P. Soares dos Santos,Jorge A. F. Ferreira, A. Ramos, José A. O. Simões, Raul Morais, Nuno M. Silva, Paulo M. Santos, M. J. C. S. Reis, T. Oliveira, Instrumented hip implants: electric supply systems, Journal of Biomechanics 46(15) (2013) 2561-2571.

[8] Marco P. Soares dos Santos, Jorge A. F. Ferreira, José A. O. Simões, Ricardo Pascoal, João Torrão, Xiaozheng Xue, Edward P. Furlani, Magnetic levitation-based electromagnetic energy harvesting: a semi-analytical non-linear model for energy transduction, Scientific Reports 6 (2016) 18579.

[9] Nuno M. Silva, Paulo M. Santos, Jorge A. F. Ferreira, Marco P. Soares dos Santos, A. Ramos, José A. O. Simões, M. J. C. S. Reis, Raul Morais, Power management architecture for smart hip prostheses comprising multiple energy harvesting systems, Sensors and Actuators A: Physical 202(1) (2013) 183-192.

Chapter 7

Conclusions

The design of implants with advanced materials (including for bioactive coatings), sophisticated geometries and inner instrumentation (for measurement and therapeutic actuation) are among the most relevant approaches already proposed to optimize osseointegration for long-term implant fixation. However, increasing incidences of primary and revision THRs and TKRs have been observed, and recent previsions estimate even higher increasing rates in the forthcoming years. This thesis demonstrates that a new concept model for orthopaedic implants must be developed with ability to control the peri-implant bone structures. The concept of *self-powered instrumented active implant with ability to deliver controlled and personalized biophysical stimuli to target tissue areas* is here proposed after:

1. Analysing the advantages and drawbacks of instrumented and non-instrumented implants;

2. Carrying out literature reviews focusing on the major breakthroughs already attained in several instrumented implants (namely hip joint replacements, femoral replacements, femoral fracture stabilizers and knee joint replacements);

3. Analysing the potential of several biophysical stimulation systems to be embedded in active implantable devices for controllable bone-implant integration and regeneration;

4. Investigating the various stimulators used to deliver electromagnetic fields to bone cells in culture, and correlating the stimuli parameters with observed biological outcomes;

5. Formulating the architecture and operation of both passive and active orthopaedic implants;

6. Demonstrating the inability of non-instrumented passive implants and instrumented passive implants to perform optimal trajectories from states of failure to states of without-failure;

7. Demonstrating the ability of instrumented active implants to optimize the bone-implant fixation;

8. Starting to investigate the potential of cosurface capacitive stimulators to control bone remodeling. It was inferred that this stimulatory system can simultaneously deliver different stimuli to different tissue areas, as well as to enhance osteogenic responses *in vitro* throughout several bone remodeling stages;

9. Accomplishing various advances for the development of self-powering systems to ensure everlasting operation of instrumented active implants.

This work then provides, for the first time, promising results that highlight the ability of instrumented active orthopaedic implants to promote controlled and personalized bone-implant integration.

Chapter 8

Supplementary Material - Chapter 3.1

EXPERT REVIEWS

Instrumented knee joint implants: innovations and promising concepts

Expert Rev. Med. Devices 12(5), 571–584 (2015)

João ND Torrão[1], Marco P Soares dos Santos*[1,2] and Jorge AF Ferreira[1]

[1]*Department of Mechanical Engineering, University of Aveiro, Campus Universitário de Santiago, 3810-193 Aveiro, Portugal*
[2]*Biomechanics Research Group, Centre for Mechanical Technology and Automation, Campus Universitário de Santiago, 3810-193 Aveiro, Portugal*
**Author for correspondence:*
Tel.: +351 234 370 830
marco.santos@ua.pt

This article focuses on *in vivo* implementations of instrumented knee implants and recent prototypes with highly innovative potential. An in-depth analysis of the evolution of these systems was conducted, including three architectures developed by two research teams for *in vivo* operation that were implanted in 13 patients. The specifications of their various subsystems: sensor/transducers, power management, communication and processing/control units are presented, and their features are compared. These systems were designed to measure biomechanical quantities to further assist in rehabilitation and physical therapy, to access proper implant placement and joint function and to help predicting aseptic loosening. Five prototype systems that aim to improve their operation, as well as include new abilities, are also featured. They include technology to assist proper ligament tensioning and ensure self-powering. One can conclude that the concept of instrumented active knee implant seems the most promising trend for improving the outcomes of knee replacements.

KEYWORDS: energy harvesting • instrumented orthopedic implant • knee arthroplasty • knee joint replacement • load measurement • medical device • orthopedics • telemetry • therapeutic actuator

As life expectancy is increasing over the past decades, thanks to social and scientific advances, the human body is exposed to wear for longer periods than in previous generations. In terms of structure, bones and joints can be susceptible to medical conditions that the aging body cannot recover from without advanced medical care.

The knee joint experiences several types of loads, such as compressive forces, lateral forces and moments, among others. Changes in the body's weight can adversely affect these loads, which can lead to osteoarthritis (OA) and cartilage degeneration (CD) [1,2]. OA is, in fact, the main cause for total knee replacement (TKR), accounting between 94 and 97%. It can be caused by changes in bone density and morphology, meniscal derangement, hormones or trauma, but the more critical factors remain age and obesity [2,3].

The solution to severe conditions lies in performing TKR procedures [4]. In the USA more than 650,000 TKR procedures take place every year [2], with similar rates being reported by other national databases. In the UK, during 2012, there were 90,842 knee replacement-related procedures, 6.5% of which were revisions, which represents an increase of 7.3% in comparison with the previous year [5]. Norway reports 11% increase in TKR surgeries in 2009, 8.3% of overall for revision procedures [6]. Other studies have also presented similar results, stating that standard TKR have a survivability rate of well over 90% up to 15 years [5–9]. However, Labek *et al.* [10] reported recently that 6% of all implants require revision after 5 years, a number that doubles up to 12% after 10 years. It was also reported that the risk of subsequent revisions is five- to six-times greater after the first revision procedure [11]. One must highlight that these values are predicted to increase 673% for primary procedures and 601% for revisions cases by 2030 [4], This prediction is mainly based on the rising obesity rates and the increasing life expectancy, which means that patients will outlive the implant lifespan but will develop other medical conditions, such as osteoporosis [4].

There are several factors for TKR revision surgery. According to the US national joint registry, infection (26.2%) and aseptic

 10.1586/17434440.2015.1068114 ISSN 1743-4440

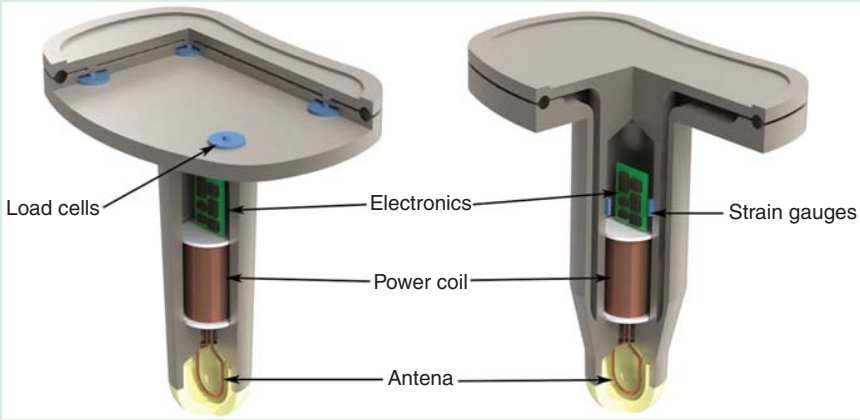

Figure 1. 3D representation of SiT (Sensors in Tray) and SiS (Sensors in Stem) instrumented tibial tray architectures.

loosening (24.3%) are the main causes [4], while the UK registry reports the aseptic loosening (32%), infection (22%), patient pain (15%), instability (12%) and wear of the polymer insert (10%). These statistics are also corroborated by the Norwegian registry report, both also stating that the number of revision procedures is rising [5,6].

Implant instability is a common problem after TKR. It is due to several operative factors, such as improper fixation or misalignment of the knee implant, but primarily due to a lack of proper medial and lateral ligament tensioning [12,13]. While placement and alignment are carefully planned on the preoperative stage, ligament tensioning relies primarily on the surgeon's skill [12,13].

To improve the lifespan of implants and reduce their shortcomings, novel technological breakthroughs are necessary. *In vivo* data are preferable for the optimization of implants, since analytical and/or finite element models are inaccurate due to their inherent simplifications, and experimental data from cadaver joints can introduce significant errors due to the deterioration and/or lack of soft tissues, such as muscles and ligaments.

The first researcher to measure biomechanical quantities *in vivo* was Rydell [14] in 1966. Although his instrumented hip implant was a very important breakthrough, it was based on an invasive method due to the use of percutaneous wires connected to an external system. It was only in 1979 that English and Kilvington [15] developed and deployed an enclosed instrumented hip implant system, battery powered and equipped with a telemetry system capable of wireless communication, allowing other researchers to develop and test new approaches for the hip, knee and shoulder joints [16]. The first instrumented implant to measure *in vivo* loading quantities of the knee joint was proposed by Taylor *et al.* [17,18] in 1996. It is a massive instrumented femoral replacement combined with a tibial tray, which is used to acquire axial forces on two different locations along the femoral axis. Its telemetry system uses remote powering via magnetic field coupling instead of batteries. An instrumented implant similar to a standard TKR prosthesis would only be intraoperatively tested in 2001 [19] and implanted in 2004 [20].

Some architectures have been developed and tested *in vivo* and used to monitor data to optimize and calibrate the mathematical models for joint mechanics and component wear, as well as for aiding in the development of prototype systems to address the causes for revision procedures.

Review scope & reading guide

This work focuses on analyzing the modifications that standard knee prosthesis undergo to design them as instrumented implants. A comparison between the architectures implemented for *in vivo* operation and their subsystems is provided for analyzing the features of their monitoring, power supply and communication systems. New prototypes that have not been tested *in vivo*, but present innovative features to minimize TKR-related failures, were also analyzed.

The design features, architectures, functions, achievements and the potential of new breakthroughs of instrumented knee implants were identified from the collection of selected publications. No time-period restriction was introduced in the search parameters because there is no previously published in-depth review about this subject. The collection was completed in February 2015.

Instrumented knee joint implants validated *in vivo*

Overview

Although many efforts have been conducted on this topic, to date, only two research teams have concluded the development and preclinical trials of instrumented TKR implants used in human patients. These groups have produced three distinct architectures that were implanted in 13 patients. They are arranged chronologically as follows:

1. D'Lima *et al.* [20–32] designed two architectures for instrumented endoprostheses: [20–26]: for the first generation and [27–32] the second generation.
2. Heinlein *et al.* [33–43] developed an architecture for instrumented knee implants.

These three architectures consist of instrumented tibial tray designs customized for monitoring operations. They can be classified into two different types, according to the location of sensors: those located in the plate ('SiP') or those located in the stem ('SiS') as seen in Figure 1.

SiP architectures were first considered. In 1996, Kaufman *et al.* [44] developed such an architecture for *in vivo* measurement of compressive forces via percutaneous wiring, by using four transducers, one at each quadrant of the

plate of the modified tibial tray (N.K. Biotechnical Corporation).

D'lima *et al.* [20–26] implemented the first SiP-based architecture. A prototype was intraoperatively tested in 2001 during a revision procedure. However, it was removed afterwards, becoming the first system to measure compressive forces on the knee joint wirelessly. Subsequently, this system was implanted on a patient in 2004. The first-generation implants developed by D'lima *et al.* [20–26] was based on a customization of a standard commercial titanium alloy implant (DePuy Johnson and Johnson). The following main modifications were accomplished: hollowing of the stem, where the circuitry was housed; customization of the plate to hold four load cells; and, finally, the addition of an upper plate connected to the lower plate by four posts. These developments have enabled the measurement of compressive forces *in vivo* after conducting fatigue tests, calibration procedures and *in vitro* testing using cadaveric materials. Because it was the first implanted architecture, it presents several novelties, such as:

1. first TKR implant using a SiP configuration;
2. first TKR implant capable of measuring compressive axial loads on the tibia;
3. first TKR implant with a telemetry system;
4. first TKR implant remotely powered via an inductive power link.

The second architecture by D'lima *et al.* [27–32] was developed shortly after to improve the first generation, namely by adding new technology to measure other quantities than compressive loads. It is SIS based and composed by two tibial trays: a thinner standard inner tray (NKII, Zimmer) that was hollowed and fitted inside a custom made outer tray such that both are fixed together at the bottom most part of the outer stem. Instead of load cells, this second generation uses four rosettes of three strain gauges each. These 12 sensors are embedded in the inner stem, 16 mm below the plate, which enable measuring three orthogonal forces, both compression and extension, as well as three moments about the orthogonal axes. Before carrying out the required procedures for *in vivo* operation, it was tested and calibrated on a simulator. Their breakthroughs include development of the:

1. first instrumented TKR implant using a SiS based design;
2. first TKR implant to measure three orthogonal forces and moments;
3. TKR implant with most sensing elements (12).

The implant developed by Heinlein *et al.* [33–43] is a SiS design based on a modification of an Innex Fixuc prosthesis (Zimmer). The inner tray was hollowed to house the circuitry. A larger tray was hollowed as well to be used as the outer tray (as opposed to the custom-made part in the second-generation implant developed by D'Lima *et al.* [27–32]). Both trays were electron beam welded along the base of the stem. This instrumented implant uses six strain gauges that allowed it to measure three orthogonal forces and moments. It also features a temperature sensor to properly compensate errors due to temperature sensitivity of the strain gauges. It underwent several demanding fatigue and calibration tests to comply with the safety criteria required by ISO 14879-1 and ASTM F1800-04 standards.

These authors were the first to develop an instrumented knee implant with the ability to monitor the operating temperature of the circuit boards. One must also highlight that this implant has been the most used one to date.

Measurement features

Table 1 lists the instrumentation features of the three architectures experimentally validated *in vivo*. Loads and moments over knee implants have been the main monitored quantities. Resistive methods using strain gauges are used in all architectures. Only the knee system developed by Heinlein *et al.* [33–43] uses a thermistor to monitor the temperature inside the tibial tray. This system also features the highest sampling rate (250 Hz) and the maximum accuracy error (2%), while the first-generation implant developed by D'Lima *et al.* [20–26] measures loads at rates up to 70 Hz with a mean absolute error of 1.5%.

Sensors, for both the second-generation implants developed by D'Lima *et al.* [27–32] and Heinlein *et al.* [33–43], are embedded in the inner wall of the stem. Not similarly, for the first generation by D'Lima *et al.* [20–26], sensors were embedded on the plate of the tibial tray. The second generation proposed by D'Lima *et al.* [27–32] contains the highest number of sensors (12).

No architecture reports any type of data storage and/or processing system for diagnosing failure states of the implants. None of these instrumented knee systems are able to monitor the physiological characteristics of tissues around the implants.

Communication features

Table 2 presents the comparison between the communication systems' characteristics of the different architectures. All systems use radiofrequency (RF) telemetric systems embedded in the stem, whereas antennas were located inside a polyethylene cap at the distal tip.

The first-generation system designed by D'Lima *et al.* [20–26] used the Strainlink© system developed by Townsend and MicroStrain™ [21]. It supports up to five data channels and transmission frequency of 916.5 MHz. The communication is performed by pulse-code modulation (PCM), due to its lower susceptibility to noise than pulse width modulation (PWM) and pulse interval modulation (PIM). The second generation [27–32] uses a modified version of the Strainlink® (418 MHz PCM), to comply with the need of 12 channels for the 12 embedded sensors.

The architecture designed by Heinlein *et al.* [33–43] uses the communication system developed by Graichen *et al.* [45], which was extensively tested by the Orthoload group [46]. By supporting nine channels and using 125 MHz PIM, six strain gauges, the temperature sensor and the voltage supply system could be

Table 1. Instrumented knee joint replacements – measurement features[†].

Features	D'Lima *et al.* [20–32]	Heinlein *et al.* [33–43,45,46]
Measuring method	(1,2) Resistive (Wheatstone bridges)	Resistive
Components of measurement systems	(1) 4 load cells (strain gauges); (2) 12 gauges (4 rosettes of 3 gauges each)	6 strain gauges, 1 NTC thermistor
Locations of components	(1) One in each quadrant of the lower plate of the tibial tray; (2) on the stem of the tibial component, 16 mm beneath the plate	Inside the stem of the tibial component
Measured quantities	(1) Compressive medial and lateral loads; (2) 6 tibial loads (3 orthogonal forces plus 3 moments)	Mediolateral force (FML), anteroposterior force (FAP), axial compressive force (Faxial), flexion–extension moment (Mflex/ex), varus–valgus moment (Mvar/val) and internal–external moment (Mint/ext)
Transmitted quantities[‡]	All measured quantities were transmitted	All measured quantities were transmitted
Sampling period	(1) 70 Hz; (2) N/D	125 Hz
Errors	(1) Mean absolute error of 1.5% (2) N/D	Maximum accuracy error (load): 2%

[†]Terminology: (n): implant of the nth generation.
[‡]They were transmitted to signal acquisition systems outside the patients' body.
N/D: Information not reported.

monitored. The communication module is housed inside a metallic cylinder shell for mechanical and magnetic protection.

The *in vivo* data transmitted to receiver stations outside the patient's body were analyzed afterward for validating biomechanical models and other gait-related research [22–26,28–32,34–43].

Supply features

Table 3 provides the comparative analysis of the power supplies that enable the implants to operate. Because it is a more recent technology, instrumented knee implants have profited from the knowledge acquired in the development of other instrumented implants extensively tested *in vivo*, such as those designed for the hip joint [16]. All three architectures use remote electrical powering via an inductive magnetic link. Batteries have not been used to avoid autonomy faults and the presence of potential harmful substances inside the patient's body.

D'Lima *et al.* [20–32] uses the same power supply of the Strainlink© system [21] for both architectures. A current is induced in a secondary coil located inside the stem by a primary coil around the patient's lower leg. However, since the secondary coil is inside the implant's titanium, which in turn is surrounded by bone and soft tissue, the power transfer efficiency of about 0.04% (only 40 mW is acquired when 1.6 kHz 100 W power oscillation is driven by the primary coil). The induced alternating current (AC) is then rectified by a power regulation circuit, embedded inside the implants, to provide the 40 mW steady DC voltage for powering all the instrumentation.

Heinlein *et al.* [33–43,45] use a similar system based on the power supply system developed by the Orthoload Group to power instrumented hip implants [46]. An external 4 kHz power oscillator is used to drive the primary coil around the patient's leg. A voltage sensor measures if electronic systems inside the implant are being powered suitably and relays that information to the controller's workstation (located outside the patients' body). One can find similar low power transfer efficiency for the other designs (from 0.04 to 0.1%). The overall energy consumption required to power the implant is not reported, but the communication system alone requires 5 mW of electrical power.

Power requirements are relatively low since instrumented TKR systems were not designed to comprise data storage, real-time processing of data measured *in vivo* or real-time therapeutic actuation. However, similar architectures composed of higher number of sensors, and other subsystems requiring electric power, may demand significant energy amounts.

The main limitations of these inductive power systems are as follows:

1. the period between data monitoring operations is limited, as the remote powering system is too cumbersome, disrupting the patient daily activities;
2. when developing such devices, safe operation must be guaranteed, meaning that the RF fields need to be within those acceptable to humans [47] and according to standards in the Active Implantable Medical Device Directive (AIMDD-EU Directive 90/385/EWG) and the Medical Device Directive (MDD-EU Directive 93/42/EWG). The Orthoload group reported that their implants were developed taking into account such norms [46].

In vivo operation details

Table 4 compares significant postoperative details about patient characteristics, time and type of data acquisition events and their purpose. Data were only acquired in the laboratorial environment because all devices only operate (monitoring and data communication) when they are powered by an inductive

power system and other transmission/reception systems, which were only available outside the patients' bodies. The first patient received an instrumented implant in 2004. By customizing a standard commercial titanium implant as the first generation developed by D'Lima *et al.* [20–26], data were acquired throughout the first postoperative days and following weeks of rehabilitation. Subsequently, data obtained up to 7 years after implantation has been reported, making it the longest data acquisition period performed by the instrumented knee architectures implanted by this research group. To overcome the limitation of the *in vivo* measurement of only compressive loads, another three patients received a second-generation architecture between 2006 and 2008 [27–32], which was able to measure all six orthogonal loads (three Cartesian forces and three moments). Data acquisition started at the rehabilitation stage (3 weeks postoperatively) and was performed up to 1 year after implantation.

Even though the implant developed by Heinlein *et al.* [33–43] is the most recent architecture, it had been implanted into nine patients between 2007 and 2010. Worthy of note is the fact that a large amount of data from the Orthoload group is publically available on their database. It comprises the largest amount of *in vivo* data of any of the three architectures, which can be accessed through their website [46]. For one of the patients (K3R), data have been obtained up to 85 months postoperatively, the longest data acquisition period of all six knee joint loads. It has benefited from the developments in instrumented hip and shoulder implants already used by this group, namely by using the 'MATRIX' method that they proposed to measure three orthogonal forces plus three moments by using six sensors [48].

A common goal for most studies conducted by both research teams was to use the data acquired to validate and adjust existing numerical models for the knee joint [22–24,26,28–31,34–36,38–43,49]. Other research works include the study of the influence of footwear on knee loads [25,37,39] and assessment of

Table 2. Instrumented knee joint replacements – communication features[†].

Features	D'Lima *et al.* [20–32]	Heinlein *et al.* [33–43,45,46]
Method of communication	(1,2) Telemetric (radio transmission of inductive link): radio transmission of data from implants to a receiver	Telemetric (radio transmission of inductive link): radio transmission of data from implants to a receiver
Components of communication systems	(1) 5-channel 916.5 MHz PCM transmitter; antenna; (2) 12-channel 418 MHz PCM transmitter; antenna	9-channel 120–170 MHz PIM transmitter; antenna
Locations of components	(1,2) Circuitry: inside the stem, antenna: distal tip, covered by a polyethylene cap	Circuitry: inside the stem, antenna: distal tip, covered by a polyethylene cap
Acquisition mode[‡]	(1,2) During tests	During tests[§]
Resolution	(1) 22 bits; (2) 12 bits	12 bits

[†]Terminology: (n): implant of the n^{th} generation.
[‡]Period between data monitoring operations.
[§]Communication with implants was only carried out in the research laboratory.
PCM: Pulse-code modulation; PIM: Pulse-interval modulation.

Table 3. Instrumented knee joint replacements – supply features[†].

Features	D'Lima *et al.* [20–32]	Heinlein *et al.* [33–42,45,46]
Type of supply	(1,2) Electric energy	Electric energy
Method for power supply	(1,2) Inductive powering, using a 1.5 kHz modulation	Inductive powering using a 4 kHz modulator
Components of supply systems inside the patient's body	(1,2) (Secondary) power coil; regulation systems (microcontroller)	(Secondary) power coil; regulation systems (microcontroller)
Locations of components inside the patients' body	(1,2) All components are located in the tibial tray; power coil: bottom of the stem; circuitry: middle of the stem	All components are located in the tibial tray; power coil: middle of the stem; circuitry: bottom of the stem
Components of supply systems outside the patients' body	(1,2) 1.6 kHz power oscillator plus 100 W amplifier; (primary) coil (around shin)	4 kHz power oscillator; (primary) coil (around shin); antenna, RF receiver and controllers
Power regulation circuitries	(1,2) Inside the implant: circuitry to regulate output voltage; outside the implant: N/D	Inside the implant: circuitry to regulate output voltage; outside the implant: circuitry to control the oscillator power/frequency and to compensate displacements between the coils
Power generation	(1) 40 mW (9 mW minimum for sensors); (2) 40 mW	N/D (5 mW for communication operations)
Life span	(1,2) N/D	N/D
Efficiency	(1,2) Approximately 0.04%	Between 0.04% and 0.1%

[†]Terminology: (n): implant of the n^{th} generation.
N/D: Information not reported.

Table 4. Instrumented knee joint replacements – *in vivo* operating details[†].

Features	D'Lima *et al.* [20–32]						Heinlein *et al.* [33–43,45,46]				
Patients	Designation		Age	Weight	Gender	Knee	Designation	Age	Weight	Gender	Knee
	(1)	P0[‡]	79	75.7 kg	Male	Left	K1L	63	100 kg	Male	Left
		JW	80	68 kg	Male	Right	K2L	71	93 kg	Male	Left
	(2)	PS	83	74 kg	Male	Left	K3R	70	92 kg	Male	Right
		DM	81	70 kg	Male	Right	K4R	63	97 kg	Female	Right
		SC	67	89 kg	Female	Left	K5R	60	100 kg	Male	Right
							K6L	65	76 kg	Female	Left
							K7L	74	70 kg	Female	Left
							K8L	70	74 kg	Male	Left
							K9L	75	100 kg	Male	Left
Total patients with implants	(1) 1 patient; (2) 3 patients						9 patients				
Reported post-operative data acquisition events	JW- 1 d, 3 d, 6 d, 3 w, 6 w, 8 m, 1.5 y, 3.5 y, 7 y PS: 3 w, 3 m, 1 y DM: 3 w, 7 m, 1 y SC: 3 w, 5 m, 1 y						K1: 1 d–2 w, 3 w, 1 m, 2.3 m, 4 m, 6–10 m, 18 m, 20 m, 24 m, 27 m, 35 m, 44 m K2: 1–10 d, 3 w, 6 m, 16 m, 23 m, 33 m, 39.5 m, 46 m K3: 7 m, 8 m, 13 m, 16 m, 24 m, 31 m, 85 m K4: 7.5 m K5: 1 w, 6 m, 11 m, 17 m, 18 m, 24 m, 30 m K6: 7.5 m, 12 m, 30 m K7: 12 m, 21 m, 31 m K8: 12 m, 13 m, 18 m, 25 m, 34 m K9: 12 m, 14.5 m, 16 m, 24 m				
Data acquisition situations	Treadmill walking, rowing machine, leg press machine, leg extension with resistance, stationary cycling; ascending/descending stairs, knee lunge; sitting/standing						Standard physiotherapy; walking; ascending/descending stairs, stationary cycling, squatting; sitting/standing; deep knee bend; treadmill jogging and walking; Walking activities included use of regular footwear, wedge footwear or wedge insoles, ankle orthosis, valgus braces or walking aides (such as crutches)				
Objective of studies	Validation of numerical models; Measurement of standard joint loads for implant testing; Study of the load evolution during rehabilitation; Study of the shoe influence in cartilage deterioration; Study of the influence of gait modification and walking poles in rehabilitation; Study of the influence of wedge shoes on knee loads						Validation of numerical models; Measurement of standard joint loads for implant testing; Study of the load evolution during rehabilitation; Study of the influence of wedge shoes on knee loads; Study of the influence of ankle orthosis on knee loads; Study of the internal-external abduction moment and medial force correlation during gait; Measurement of loads during 3 point and 4 point walking; Study of the effect of valgus braces on knee loads				

[†]Terminology: (n): implant of the n^{th} generation.
[‡]Intra operative test patient (P0) was replaced by a standard model after successful testing instrumented TKR.

physiotherapy techniques with or without braces and other aids [24–26,29–31,34–41,43].

The TKR designed by D'Lima *et al.* [20–32] differ from those designed by Heinlein *et al.* [33–43] not only due to their embedded systems but also in the type of implant in which their architectures are based. The first group used a cruciate ligament-retaining system, while the second is a cruciate sacrificing system that uses an ultracongruent tibial insert. Different implant types can affect the joint behavior [50,51], which in turn can affect the magnitude and direction of forces that are measured by instrumented TKRs.

D'lima *et al.* [30] reported low shear forces during operation of their second-generation implant, which attributed to the cruciate retaining system usage. Since all architectures have a gap between the upper and lower plates of the tibial tray, connective tissue can grow within this space. Therefore, different measurements can be obtained in comparison with tibial trays effectively sealed. Even though both D'Lima *et al.* [27] and Heinlein *et al.* [33] express their concern about this matter, only the latter have reported the usage of a round plastic sealant along the gap circumference positioned between the upper and the lower plates.

No revision procedures for these implants have been reported.

Novel breakthroughs in instrumented knee implants

Overview

To improve the autonomy and longevity of instrumented TKRs, some prototypes were proposed by five research groups, focusing on self-powering, kinematic measurement systems and ligament tensioning assistance. These systems are still in their development/experimental stage and none of them was already tested on human patients.

Almouahed and Lahuec *et al.* [52–55] addressed the issue of dependence on an external power supply by proposing a self-powered architecture based on the first generation (SiT architecture) tested by D'Lima *et al.* [20–26]. They used piezoceramic load cells to both measure compressive forces and harvest electric energy for powering the implant subsystems. Luciano *et al.* [56,57] also presented a contribution for self-powering of the implants. They developed a motion-driven electromagnetic harvesting system that uses the relative motion between a coil and 12 magnets to harvest electric energy. The power-generating elements (coils, magnets and regulation electronics) are located in the polyethylene insert, as well as in the femoral component of the TKR.

Arami *et al.* [58–60] developed an instrumented TKR insert to measure the internal–external and flexion–extension rotations to allow measuring knee kinematics more accurately and without the need of (quite expensive) external equipment, which in turn allow the monitoring of data during the daily activities of patients.

Two approaches were already proposed to ensure proper ligament tensioning: Crottet *et al.* [61,62] developed an intraoperative tool, similar to a TKR insert, to measure loads in real time for aiding the surgeon; Collo *et al.* [63,64] produced two tibial tray prototypes that are able to perform slight changes in their geometry to ensure proper tensioning of the medial and lateral ligaments after implantation.

Self-powering solutions

Table 5 lists significant features of the self-powered implant systems already proposed. Almouahed and Lahuec *et al.* [52–55] proposed a SiT-based architecture capable of measuring anteromedial, anterolateral, posteromedial and posterolateral compressive loads, featuring its own telemetry radio communication system. They used piezoceramic elements as power-generating elements. They conclude that an average of 1.8 mW can be harvested to power the telemetry system, at typical walking speed. However, this approach for self-powering is highly dependent on the loads on the tibial tray. This prototype is still at an optimization stage to minimize its power requirements and to maximize the power output of its harvesting components. The authors have not reported if their prototype is a customization of a commercially available model.

The proposal presented by Luciano *et al.* [56,57] relies on knee motions to harvest electric energy, rather than on the use of knee loads, to power an autonomous sensor unit. By placing two sets of magnets with interchanged polarity orientation, one along each condyle, and a wire coil in the insert pin between them, such that its axis is perpendicular to the sagittal plane, the motion of the knee joint drives magnetic flux variations to induce voltage on the coil. The system was able to harvest an overall power of about 92 μW during normal walking speeds simulated *in vitro* using a robotic knee simulator, which is capable of self-powering a 1.7 mW sensor unit for 16 ms. This power magnitude is achieved by harvesting a peek voltage ranging from 1.4 V to 2.0 V every 7.6 s. During this interval, compressive loads measured by magnetoresistive elements are transmitted via a 125 kHz telemetry radio. It is based on a NexGen® Legacy® Knee LPS-Flex prosthesis (Zimmer) in which the femoral component and the polyethylene insert were modified to house the magnets, power coil and circuitry.

Kinematic measuring systems

Arami *et al.* [58–60] proposed a knee system to measure *in vivo* knee kinematics, namely internal–external and flexion–extension rotations. This knee system is a customization of the F.I.R.S.T. (Free Insert in Rotation, STabilized) knee prosthesis from Symbios Orthopédie. It was designed comprising the following features:

- three magnetoresistive sensors housed in the insert;
- two permanent magnets, one located in the femoral component and the other in the tibial tray;
- inductive power supply.

The system works by analyzing the variation of the magnetic flux from the motion of permanent magnets. The magnet located in the tibial tray is related to internal–external rotation, while the one in the femoral component accounts for the

Table 5. New instrumented TKR systems – features of self-powering prototypes†.

Features	Almouahed *et al.* [52–54]	Luciano *et al.* [56,57]
Method for power generation	Piezoelectric	Electromagnetic
Power output	1.8 mW	92 μW (1.4 V to 2.0 V at every 7.6 s to power the 1.7 mW telemetry and sensor system for 16 ms)
Components	4 piezoceramic elements, power management unit	2 series of 6 box-shaped magnets; wire coil; power management circuit
Location of components	4 piezoceramic elements on beneath the tray of the tibial component	1 series of 6 magnets in each condyle (femoral component); Wire coil on the polyethylene insert femoral pin; Power management circuitry, sensors and communication system at the center of the insert
Measurement features	4 piezoceramic elements measure compressive loads	3 magneto resistive sensors to measure compressive loads
Communication features	402-405 MHz telemetry radio	125 kHz telemetry radio
Lifespan	N/D	N/D
Efficiency	N/D	10%

†Terminology: N/D: information not reported.

flexion–extension rotation. Measured quantities are obtained by fusing data from the various sensors to estimate angle configurations from the raw data of each sensor. They achieved errors up to 0.9° for internal–external rotations and 1.1 deg for flexion–extension rotations. They have not reported the development of novel breakthroughs for telemetric systems. A later version of this prototype also comprises two strain gauges to measure compressive loads beneath each condyle for identifying polyethylene insert wear. However, it was not described how load values evolve over the course of the insert degradation.

Ligament tensioning tools

Table 6 presents significant features of two prototypes that were designed to assist in lateral ligament tensioning. Crottet *et al.* [61,62] developed an intraoperative tool to measure ligament forces and contact forces. It was designed for replacing the polyethylene insert (between the femoral and tibial components) to support surgeons during procedures related with ligament tensioning, by providing load information in real time. After completion of these procedures, this mechanism is replaced by the insert. The prototype is composed by two separate sensing plates (one for each condyle) with 6 thick-film piezoresistive sensors (three for each plate). Six cadaver knees were used for *in vitro* tests. A mean relative error of 0.5% was achieved.

Collo *et al.* [63,64] proposed a knee system prototype composed by an actuation system with the ability to change the configuration of the upper plate of the tibial tray such that the tension of the ligaments can be adjusted after the surgeon has finished the procedure. They implemented two actuation systems:

1. using a horizontal wedge plate with a lead screw, whose forward motion raises the upper plate of the tibial tray;
2. using a vertical planetary gear train driving screw nuts to move up or down the upper plate, such that an 'optimal' configuration can be achieved.

Both systems are driven by a microstepper motor that is powered by an internal battery, which in turn can be charged via an inductive link. This actuation system is manually controlled by the surgeon since no measurement system was designed to provide feedback. Only 3D printed plastic prototypes have been produced to validate the concept. Authors are planning to develop metallic prototypes in the forthcoming years.

Expert commentary

The instrumented implant architectures validated *in vivo*, presented in this review, were designed as transducers to measure biomechanical loads, in addition to their main function of restoring articular motion. They are medical devices composed by:

- sensing systems;
- signal processing and conditioning systems to extract information from the data acquired by the sensing systems;
- telemetry systems to transmit data between electronic circuits inside and outside the patients' body;
- power supply systems to provide the energy required for operation.

In spite of the importance of these achievements, there are no knee implants yet capable of:

1. monitoring biochemical characteristics of the tissues surrounding the implants;
2. characterizing failures, such as component wear, aseptic loosening or infection;
3. performing personalized therapies in the bone-implant interface;
4. collect data autonomously during daily activities.

Currently, among the main obstacles for developing such systems are those related to space availability for components and their safe encapsulation. Only a limited amount of material can be removed to avoid fractures and maintain mechanical properties. Besides, major design modifications must be avoided to ensure the patient's compliance. Since most embedded components are not biocompatible, they need to be safely

encapsulated and confined to small cavities inside implants. Considering that permanent implants are mostly manufactured using metallic alloys, such that proper osseointegration and moisture protection be achieved, remote powering can only be conducted by using low frequencies (in the kHz range). Data transfer rate is also limited due to this problem. To expand the communication rate to the MHz range, the antenna was located outside the metal encapsulation at the distal tip covered by a plastic cap and connected to the control unit via a lead-through [21–43].

There is, however, a growing trend to implement instrumented implants with sensors capable of measuring quantities other than biomechanical loads. Arami *et al.* [58–60] reported a prototype TKR to measure knee kinematics. The architecture proposed by Heinlein *et al.* [33–43] also includes a temperature sensor, a feature also shared with the hip implants developed by Mann *et al.* [65–67], Davy *et al.* [68,69] and Bergman *et al.* [70–72]. The latter also proposed a hip implant, which was already implanted in five patients, comprising a network of nine temperature sensors to measure the temperatures along the entire implant length, to study how temperature changes (induced by friction) deteriorate osseointegration [71,72]. More recently, the same team proposed a study involving 100 individuals using an implant with one temperature sensor in the neck beneath the ceramic head, designed specifically to study the risk of thermally induced bone necrosis [70].

Table 6. New instrumented TKR systems – features of prototypes for ligament tensioning†.

Features	Crottet *et al.* [61,62]	Collo *et al.* [63,64]
Type	Intra-operative tool	Tibial tray with actuation system
Measurement features	6 deformable bridges with piezo resistive elements.	N/D
Measured quantities	Medial and lateral collateral ligament forces (FML, FLL), medial and lateral contact forces (FMC, FLC), external varus force (FEX)	N/D
Method for power supply	Direct electrical supply	Battery powered with inductive coupling charging system
Actuation systems	N/D	1: Lead-screw wedge 2: Screw nut gear-train
Actuation system components	N/D	1: Horizontal lead screw and wedge to change height and angle of upper plate of tibial tray driven by microstepper motor 2: Vertical planetary gear train driving screw nuts to change configuration of upper plate of tibial tray operated by micro stepper motor
Testing/ development stage	Numerical simulation; Validation in cadaveric joint simulator	Numerical simulation; Proof-of-concept prototype system

†Terminology: N/D: information not reported.

Several innovations have been recently reported such that the lifespan of instrumented TKR systems can be extended. Ruther *et al.* [73] designed a method to use acoustic analysis of sound waves, generated by a mechanical oscillator, to monitor the osseointegration in the interface of cementless orthopedic implants. Hao *et al.* [74] developed a differential variable reluctance transducer to predict aseptic loosening by measuring the migration and micromotion of implants in real time. Alpuim *et al.* [75] proposed a piezoresistive thin film strain sensor to monitor aseptic loosening by monitoring the relative motions in the bone-implant interface. However, these systems still require further optimization and testing for system validation [16].

The autonomy of the instrumented TKR systems to operate throughout patients' daily life requires housing energy harvesters inside the implant. Energy harvesting *in vivo* is the key challenge that must be addressed for developing self-powering implants. To accomplish this purpose, Almoulahed *et al.* [52–55] proposed a TKR using piezoelectric elements to measure loads, as well as to harvest electric energy. Platt *et al.* [76] also proposed a similar piezoelectric harvesting system, but it requires further optimization to increase power output levels. Luciano *et al.* [56,57] contributed with a motion-driven electromagnetic rotation-based energy harvester that was customized for knee implants, while Morais *et al.* [77–79], Morgado *et al.* [80] and Soares dos Santos *et al.* [81–83] proposed translation-based electromagnetic harvesters to power instrumented hip replacements, which could be customized for knee implants. Soares dos Santos [81,82] also developed a multisource harvesting system composed of electromagnetic and piezoelectric harvesters to increase the amount of available energy harvested *in vivo*, as well as to improve the reliability of the power supply. Silva *et al.* [79,84] developed a power management system comprising supercapacitors to store the energy harvested from the operation of the multisource energy harvesting system. A deep discussion about the effectiveness of self-powering systems to supply instrumented orthopedic implants was recently published by Soares dos Santos *et al.* [83]. Although motion-driven self-powering can generate energy without the disadvantages of both inductive supply and batteries systems, their performance is strongly dependent on the physical activities of patients. Since most patients experience reduced mobility during rehabilitation and in their old age, further developments are still required to improve efficiency of the power harvesting and power management systems to maintain implant operation when harvesting is insufficient [83].

Although additional risks by using instrumented TKRs in human patients must be taken into account, *in vivo* data measurements using this method are more reliable than those obtained by in vitro testing of cadaveric joints or by numerical methods [21–43]. Still, all these innovations have been performed to extend the lifespan of instrumented TKR systems in a non-real-time mode, that is, their operation can be only used to optimize the next generations of implants. The ordinary methodology to improve knee implants has focused on the optimization of their design and materials. However, this approach has not ensured long-term survival of implants and, as a consequence, surgical procedures are still required significantly to minimize complications following TKR. However, Soares dos Santos *et al.* [85] studied recently the necessary and sufficient conditions required for optimality of orthopedic implants, and by using the Pontryagin Maximum Principle, they concluded that it is impossible to ensure optimal trajectories from states of failure to states of without-failure for implants without therapeutic actuation and therapeutic programming (whatever its nature), whatever their architectures, implants' optimization, rehabilitation protocols or surgical procedures. They also concluded that if optimal trajectories between states of failure and states of without-failure exist, then instrumented active implants comprise suitable architectures to implement them. The innovation proposed by Collo *et al.* [63,64] can be considered as an instrumented active knee prototype, but it was not designed to apply therapeutic actuations in the bone implant interface such that it can control its biochemical environment. Considering that aseptic loosening and infection are among the most common causes for revision TKR [4–6], research in the design of instrumented active knee systems must be considered as an effective methodology to minimize and/or prevent these causes responsible for revision procedures.

Five-year view

Although instrumented implants are quite important tools to calibrate biomechanical models and monitor patient evolution throughout recovery, they still have much potential that can be explored. Further optimization of the current TKR systems and the inclusion of additional features could be performed to implement them with the ability to detect and even prevent failures in real time.

Solutions for when an external antenna cannot be used can be developed in the forthcoming years, such as using the secondary coil of the power system as the communication antenna. Bergman *et al.* [72] used this method in a recent proposal for a temperature measuring total hip replacement by using a combination of high pass and low pass filters to demodulate signals less than 1 kHz while discarding the 4-kHz power supply modulation, as well as the 50-Hz power mains.

As the miniaturization of electronics advances, low power and high-performance circuits may enable the development of implants embedding actuation systems, as well as the required control architecture, in confined spaces. Furthermore, research in material science may result in the development of materials with appropriate mechanical properties that allows using them in permanent implants minimizing fracture and improving magnetic permeability. Higher frequencies could thus be used for maximizing data transfer rates and remote powering system efficiency. Breakthroughs for monitoring the insert wear, aseptic loosening and infection are expected to be conducted in the forthcoming years, which can be further promoted by such advances in electronics and material sciences. Novel sensing systems for TKRs may be developed such that the influence of friction-induced knee implant temperatures on osseointegration can be identified.

More advanced methods that analyze the implant stability for detecting loosening may be explored and/or implemented in the near future. However, one must also highlight that novel methods based on monitoring molecular markers may be researched [86,87]. The development of sensors to measure failure specific marks in the regions surrounding the implant, such as nitric oxide [86] or peroxynitrite [87], is likely to be considered first. To accomplish this goal, implants will require resource storage capabilities to house the chemicals required for biosensing [88] and even medical drugs for therapeutic purposes [89].

Advancements in rapid prototyping technologies, such as electron beam melting [90], can allow patient-specific implants to be produced at reasonable rates and costs. Manufacturing of instrumented implants using such technologies may facilitate the inclusion of the embedded subsystems required for active instrumented implants.

Power supply systems will require further developments to power more complex implants with additional embedded features. Power generation can be performed by using the movements of patients during their daily activities. Energy harvesting is a promising method to power instrumented knee implants, mainly because it is inexpensive and maintenance-free affordable solution, as well as it ensures long-term energy generation. Additional research will likely be focused on optimization of harvesters considering the gait patterns of patients during their daily activities to maximize their power output as well as in the development of redundant multisource harvester structures [79,84].

Therapeutic actuation systems that have been proposed, but currently are not yet suitable for *in vivo* applications, such as ligament tensioning [63,64] and stimulation systems to improve osseointegration [91,92], may have been engineered and ready for *in vivo* tests. Research to identify the most suitable noninvasive therapeutic stimuli to deliver on the bone-implant interface is likely to be conducted. Moreover, the stimulation parameters that can induce bone tissue growth must be found, such that the osseointegration can be improved.

Financial & competing interests disclosure

The authors were supported by Portuguese Foundation for Science and Technology – project EXPL/EMS-SIS/2128/2013. The authors have no other relevant affiliations or financial involvement with any organization or entity with a financial interest in or financial conflict with the subject matter or materials discussed in the manuscript apart from those disclosed.

Key issues

- Even though considerable research has been conducted to improve implant design, revision rates of TKR are about 6% after 5 years and 12% after 10 years. The number of primary TKR procedures is increasing, especially in a younger demographic.
- Instrumented knee implants are proposed as research tools to measure biomechanical quantities *in vivo*. Their purpose is to collect data (forces and moments) to validate models defining the implants' biomechanical behavior; optimize the mechanical design of standard implants; carry out preclinical testing; and track patient healing and rehabilitation after arthroplasty.
- Three architectures of instrumented TKR, comprising RF telemetry systems and resistive load measuring sensors, powered by an inductive power link, were implanted into 13 human patients.
- Up to 7 years of successful operation and *in vivo* data acquisition have been achieved. No revision procedures or side effects have been reported.
- None of the architectures validated *in vivo* were designed with therapeutic actuation systems. Only one research team proposed a prototype comprising an actuation system to control the lateral ligament tensioning, such that failures in the ligament tensioning can be overcome postoperatively.
- Currently, data acquisition events are limited to laboratorial settings due to the need of external power supply technology and supplementary kinematic measurement systems.
- New developments to acquire other biomechanical quantities, such as those related with kinematics, as well as to include sensors for monitoring critical areas where component wear (polyethylene insert) and loosening (femoral and tibial fixations) may occur.
- Improvement and optimization of electric power supply systems, especially self-powering methods, is mandatory such that the autonomy of instrumented implants can be maximized.
- Further research on patient-specific implants and ligament tensioning assistance tools may help in reducing revision risks and postoperative pain in TKR patients.
- Development of embedded noninvasive stimulation systems (electrical and/or mechanical) for instrumented implants may effectively induce and control bone growth in regions where aseptic loosening occurs.
- The design of instrumented active implants with therapeutic actuation systems seems to be the most promising trend to detect/prevent failure states (aseptic loosening, infection or component wear) in real time.

References

Papers of special note have been highlighted as:
• of interest
•• of considerable interest

1. Felson DT, Zhang Y, Hannan MT, et al. Risk factors for incident radiographic knee osteoarthritis in the elderly: the Framingham Study. Arthritis Rheum 1997;40:728-33
2. Carr A, Robertsson O, Graves S, et al. Knee replacement. The Lancet 2012;379:1331-40
3. Messier SP. Osteoarthritis of the knee and associated factors of age and obesity: effects on gait. Med Sci Sports Exerc 1994;26: 1446-52
4. Paxton EW, Namba RS, Maletis GB, et al. A prospective study of 80,000 total joint and 5000 anterior cruciate ligament reconstruction procedures in a community-based registry in the United States. J Bone Joint Surg 2010;92(2):117-32
5. Porter M, Borroff M, Gregg P, et al. 10th annual report 2013. National Joint Registry for England, Wales and Northern Ireland (2013)
6. Bergen H Report June 2010. The Norwegian Arthroplasty Register (2010)
7. Crowder A, Duffy G, Trousdale R. Long-term Results of Total Knee Arthroplasty in Young Patients With Rheumatoid Arthritis. J Arthroplasty 2005; 20(3):12-16
8. Ito J, Koshino T, Okamoto R, Saito T. 15-year follow-up study of total knee arthroplasty in patients with rheumatoid arthritis. J Arthroplasty 2003;18(8):984-92
9. Duffy G, Crowder A, Trousdale R, Berry D. Cemented Total Knee Arthroplasty Using a Modern Prosthesis in Young Patients With Osteoarthritis. J Arthroplasty 2007;22(6-1): 67-70
10. Labek G, Thaler M, Janda W, et al. Revision rates after total joint replacement - cumulative results from worldwide joint register datasets. J Bone Joint Surg 2011; 93:B(3)):293-7
11. Ong KL, Lau E, Suggs J, et al. Risk of subsequent revision after primary and revision total joint arthroplasty. Clin Orthop Relat R 2010;468(11):3070-6
12. Vail T, Lang J. Surgical techniques and instrumentation in total knee arthroplasty. Surgery of The Knee 2006;1493-8
13. Scuderi G, Tria A. Knee Arthroplasty Handbook: Techniques in Total Knee and Revision Arthroplasty. Springer; 2006
14. Rydell NW Forces acting in the femoral head-prosthesis. A study on strain gauge supplied prostheses in living persons. Acta Orthop Scand 1966;37(Suppl 88):1-132
15. English TA, Kilvington M. In vivo records of hip loads using a femoral implant with telemetric output (a preliminary report). J Biomed Eng 1979;1(2):111-15
16. Soares dos Santos M, Ferreira JAF, Ramos A, et al. Instrumented hip joint replacements, femoral replacements and femoral fracture stabilizers. Expert Rev Med Devices 2014;11(6):617-35
17. Taylor SJ. A telemetry system for measurement of forces in massive orthopaedic implants in vivo. Conf. Proc. 18th IEEE Eng. Med Biol Soc 1996;1: 290-2
18. Taylor SJ, Perry JS, Meswania JM, et al. Telemetry of forces from proximal femoral

replacements and relevance to fixation. J Biomech 1997;30(3):225-34

19. Morris BA, D'Lima DD, Slamin JE, et al. e-Knee: evolution of the electronic knee prosthesis: telemetry technology development. J Bone Joint Surg Am 2001; 83-A(2):62-6
20. D'Lima DD, Townsend CP, Arms CW, et al. An implantable telemetry device to measure intraarticular tibial forces. J Biomech 2005;38:299-304

•• **First instrumented knee implant implanted *in vivo* capable of measuring compressive loads.**

21. Townsend CP, Arms SW, Hamel MJ. Remotely powered, multichannel, microprocessor based telemetry. systems for smart implantable devices and smart structures. Biannual Meeting of the International Society on Biotelemetry, Juneau AK, USA; 9 – 15 May 1999
22. Zhao D, Banks SA, D'Lima DD, et al. In vivo medial and lateral tibial loads during dynamic and high flexion activities. J Orthop Res 2007;25(5):593-602
23. D'Lima DD, Patil S, Steklov N, et al. Paul Award: tibial forces measured in vivo after total knee arthroplasty. J Arthroplasty 2006;21:255-62
24. Mündermann A, Dyrby CO, D'Lima DD, et al. In vivo knee loading characteristics during activities of daily living as measured by an instrumented total knee replacement. J Orthop Res 2008;26(9):1167-72
25. Erhart JC, Dyrby CO, D'Lima D, et al. Changes in in-vivo knee loading with a variable-stiffness intervention shoe correlate with changes in the knee adduction moment. J Orthop Res 2010;28:1548-53
26. Kinney AL, Besier TF, Silder A, et al. Changes in in vivo knee contact forces through gait modification. J Orthop Res 2013;31(3):434-40
27. Kirking B, Krevolin J, Townsend C, et al. A multiaxial force-sensing implantable tibial prosthesis. J Biomech 2006;39:1744-51
28. D'Lima D, Patila S, Steklov N, et al. In vivo knee moments and shear after total knee arthroplasty. J Biomech 2007;40(1): 11-17

•• **First implanted TKR capable of measuring 3D forces and moments *in vivo*.**

29. D'Lima DD, Steklov N, Patil S, et al. The Mark Coventry Award: in vivo knee forces during recreation and exercise after knee arthroplasty. Clin Orthop Relat Res 2008;466:2605-11
30. Varadarajan K, Moynihan A, D'Lima DD, et al. In vivo contact kinematics and contact forces of the knee after total knee arthroplasty during dynamic weight-bearing activities. J Biomech 2008;41(10):2159-68
31. Gerus P, Sartori M, D'Lima DD, et al. Subject-specific knee joint geometry improves predictions of medial tibiofemoral contact forces. J Biomech 2013;46:2778-86
32. Fregly BJ, D'Lima DD, Colwell CW Jr. Effective gait patterns for offloading the medial compartment of the knee. J Orthop Res 2009;27(8):1016-21
33. Heinlein B, Graichen F, Bender A, et al. Design, calibration and pre-clinical testing of an instrumented tibial tray. J Biomech 2007;40(1):4-10
34. Heinlein B, Kutzner I, Graichen F, et al. ESB Clinical Biomechanics Award. 2008: Complete data of total knee replacement loading for level walking and stair climbing measured in vivo with a follow-up of 6-10 months. Clinical Biomechanics 2009;24:315-26

•• **Latest instrumented knee architecture, capable of measuring 3D forces and moments and circuit temperature *in vivo*.**

35. Kutzner I, Heinlein B, Graichen F, et al. Loading of the knee joint during activities of daily living measured in vivo in five subjects. J Biomech 2010;43:2164-73
36. Kutzner I, Küther S, Heinlein et al. The effect of valgus braces on medial compartment load of the knee joint – in vivo load measurements in three subjects. J Biomech 2011;44:1354-60
37. Kutzner I, Damm P, Heinlein B, et al. The effect of laterally wedged shoes on the loading of the medial knee compartment-in vivo measurements with instrumented knee implants. J Orthop Res 2011;29:1910-15
38. Halder A, Kutzner I, Graichen F, et al. Influence of Limb Alignment on Mediolateral Loading in Total Knee Replacement – In Vivo Measurements in Five Patients. J Bone Joint Surg Am 2012; 94(11):1023-9
39. Kutzner I, Stephan D, Dymke J, et al. The influence of footwear on knee joint loading during walking – in vivo load measurements with instrumented knee implants. J Biomech 2013;46:796-800
40. Kutzner I, Heinlein B, Graichen F, et al. Loading of the knee joint during ergometer cycling: telemetric in vivo data. J Orthop Sports Phys Ther 2012;42(12):1032-8
41. Kutzner I, Trepczynski A, Heller MO, et al. Facts about Their Correlation during Gait. PLoS One 2013;8(12):e8103
42. Bergmann G, Bender A, Graichen F, et al. Standardized Loads Acting in Knee Implants. PLoS One 2014;9(1):e86035
43. Trepczynski A, Kutzner I, Bergmann G, et al. Modulation of the relationship between external knee adduction moments and medial joint contact forces across subjects and activities. Arthritis Rheumatol 2014;66(5):1218-27
44. Kaufman KR, Kovacevic N, Irby SE, Colwell CW Jr. Instrumented implant for measuring tibiofemoral forces. J Biomech 1996;29:667-71
45. Graichen F, Arnold R, Rohlmann A, Bergmann G. Implantable 9-channel telemetry system for in vivo load measurements with orthopaedic implants. IEEE T. Bio-med Eng 2007;54(2):253-61
46. Bergmann G. Charit Universitaetsmedizin Berlin "OrthoLoad". Available from: www.orthoload.com [Last accessed March 2015]
47. IEEE-SA Standard Board, C95.1-2005 - IEEE standard for safety levels with respect to human exposure to radio frequency electromagnetic fields, 3 kHz to 300 GHz. Institute of Electrical and Electronics Engineers (2005)
48. Bergmann G, Siraky J, Kölbel R, Rohlmann A. Measurement of joint forces with implants - a new method of instrumentation and its application in sheep. Conf. Proc. Biomechanics Symposium. ASCE Mechanics Conf 1981. 43:225-8
49. Fregly BJ, Besier TF, Lloyd DG, et al. Grand challenge competition to predict in vivo knee loads. J Orthop Res 2012; 30(4):503-13
50. Kolisek FR, McGrath MS, Marker DR, et al. Posterior-stabilized versus posterior cruciate ligament-retaining total knee arthroplasty. Iowa Orthop J 2009;29:23-7
51. Lewandowski PJ, Askew MJ, Lin DF, et al. Kinematics of posterior cruciate ligament-retaining and-sacrificing mobile bearing total knee arthroplasties. An in vitro comparison of the New Jersey LCS meniscal bearing and rotating platform prostheses. J Arthroplasty 1997;12:777-84
52. Almouahed S, Gouriou M, Hamitouche C, et al. Design and Evaluation of Instrumented Smart Knee Implant. IEEE Transactions on Biomedical Engineering 2011;58(4):971-82

•• **Proposal of TKR prototype to simultaneously measure compressive loads and generate energy *in vivo*.**

53. Almouahed S, Gouriou M, Hamitouche C, et al. The use of piezoceramics as electrical energy harvesters within instrumented knee

implant during walking. IEEE/ASME Trans Mechatron 2011;16(5):799-807

54. Lahuec C, Almouahed S, Arzel M, et al. A self-powered telemetry system to estimate the postoperative instability of a knee implant. IEEE Transactions on Biomedical Engineering 2011;58(3):822-5

55. Lahuec C, Arzel M. An analog core computing the center of pressure in a knee replacement prosthesis. IEEE 9th International Conference: New Circuits and Systems, Bordeaux France; 26 – 19 June 2011

56. Luciano V, Sardini E, Serpelloni M, Baronio G. An energy harvesting converter to power sensorized total human knee prosthesis. Meas Sci Technol 2014;25(2): 1-10

57. Crescini D, Sardini E, Serpelloni M. Design and test of an autonomous sensor for force measurements in human knee implants. Sensors and Actuators A Physical 2011; 166(1):1-8

58. Arami A, Miehlbradt J, Aminian K. Accurate internal–external rotation measurement in total knee prostheses: A magnetic solution. J Biomech 2012;45: 2023-7

•• **First instrumented knee prototype proposed to measure kinematics-related quantities *in vivo*.**

59. Arami A, Simoncini M, Atasoy O, et al. Instrumented knee prosthesis for force and kinematics measurements, IEEE trans. Autom Sci Eng 2013;10:615-24

60. Forchelet D, Simoncini M, Arami A, et al. Enclosed electronic system for force measurements in knee implants. Sensors 2014;14(8):15009-21

61. Crottet D, Maeder T, Fritschy D, et al. Development of a force amplitude- and location-sensing device designed to improve the ligament balancing procedure in TKA. IEEE Trans Biomed Eng 2005;52:1609-11

62. Crottet D, Kowal J, Sarfert S. A, et al. Ligament balancing in TKA: evaluation of a force-sensing device and the influence of patellar eversion and ligament release. J Biomech 2007;40(8):1709-15

63. Collo A, Poignet P, Hamitouche C, et al. A miniaturised actuation system embedded in an instrumented knee implant for postoperative ligament imbalance correction. Conf Proc IEEE Eng Med Biol Soc 2014;2014:6211-14

•• **Actuation system prototype to adjust ligament tensioning postoperatively.**

64. Collo A, Poignet P, Hamitouche C, et al. An Active Tibial Component for Postoperative Fine-Tuning Adjustment of Knee Ligament Imbalance. 5th IEEE RAS & EMBS International Conference on Biomedical Robotics and Biomechatronics, São Paulo Brazil; 12 – 15 Aug 2014

65. Tackson SJ, Krebs DE, Harris BA. Acetabular pressures during hip arthritis exercises. Arthrit Care Res 1997;10(5): 308-19

66. McGibbon CA, Krebs DE, Mann RW. In vivo hip pressures during cane and load-carrying gait. Arthrit Care Res 1997; 10(5):300-7

67. McGibbon CA, Krebs DE, Trahan CA, et al. Cartilage degeneration in relation to repetitive pressure - case study of a unilateral hip hemiarthroplasty patient. J Arthroplasty 1999;14(1):52-8

68. Kotzar GM, Davy DT, Goldberg VM, et al. Telemeterized in vivo hip joint force data: A report on two patients after total hip surgery. J Orthop Res 1991;9(5):621-33

69. Kotzar GM, Davy DT, Berilla J, Goldberg VM. Torsional loads in the early postoperative period following total hip replacement. J Orthop Res 1995;13(6): 945-55

70. Graichen F, Bergmann G, Rohlmann A. Hip endoprosthesis for in vivo measurement of joint force and temperature. J Biomech 1999;32(10):1113-17

71. Bergmann G, Graichen F, Rohlmann A, et al. Frictional heating of total hip implants. Part 1- measurements in patients. J Biomech 2001;34(4):431-28

72. Bergmann G, Graichen F, Dymke J, et al. High-tech hip implant for wireless temperature measurements in vivo. PLoS One 2012;7(8):e43489

73. Ruther C, Gabler C, Ewald H, et al. In vivo monitoring of implant osseointegration in a rabbit model using acoustic sound analysis. J Orthop Res 2014;32(4):606-12

74. Hao S, Taylor JT, Bowen CR, et al. Sensing methodology for in vivo stability evaluation of total hip and knee arthroplasty. Sensor Actuat A-Phys 2010; 157(1):150-60

75. Alpuim P, Filonovich SA, Costa CM, et al. Fabrication of a strain sensor for bone implant failure detection based on piezoresistive doped nanocrystalline silicon. J Non-Cryst. Solids 2008;354(19-25): 2585-9

76. Platt SR, Farritor S, Haider H. On low-frequency electric power generation with PZT ceramics. IEEE-ASME T. Mech 2005;10(2):240-52

77. Morais R, Silva N, Santos P, et al. Permanent magnet vibration power generator as an embedded mechanism for smart hip prosthesis. Procedia Engineering 2010;5:766-9

78. Morais R, Silva NM, Santos PM, et al. Double permanent magnet vibration power generator for smart hip prosthesis. Sensor. Actuat. A-Phys 2011;172(1):259-68

79. Silva N, Santos P, Ferreira J, et al. Multi-purpose and multi-source energy management system for biomedical implants. Procedia Engineering 2012;47: 722-5

80. Morgado ML, Morgado LF, Henriques E, et al. Nonlinear modeling of vibrational energy harvesters for smart prostheses. Procedia Engineering 2012;47:1089-92

81. Soares dos Santos M, Ferreira JA, Ramos A, et al. Multi-source energy harvesting power generators for instrumented implants - towards the development of a smart hip prosthesis. Conf Proc 5th BIODEVICES 2012;71-81

82. Soares dos Santos M, Ferreira JA, Ramos A, et al. Multi-source harvesting systems for electric energy generation on smart hip prostheses. Biomedical. Gabriel J, Schier J, Van Huffel S, et al., editors. Engineering Systems and Technologies 357. Springer-Verlag; Berlin Heidelberg: 2013. p. 80-96

83. Soares dos Santos M, Ferreira JA, Ramos A, et al. Instrumented hip implants: Electric supply systems. J Biomech 2013;46(15): 2561-71

84. Silva NM, Santos PM, Ferreira JA. Power management architecture for smart hip prostheses comprising multiple energy harvesting systems. Sensor. Actuat. A-Phys 2013;202:183-92

85. Soares dos Santos M, Ferreira JA, Ramos A, et al. Active orthopaedic implants: Towards optimality. J Franklin Inst 2015;352(3): 813-34

•• **Proof that only instrumented active implants can achieve optimal performances.**

86. Stea S, Visentin M, Donati ME, et al. Nitric oxide synthase in tissues around failed hip prostheses. Biomaterials 2002; 23(24):4833-8

87. Yang F, Wu W, Cao L, et al. Pathways of macrophage apoptosis within the interface membrane in aseptic loosening of prostheses. Biomaterials 2011;32(35): 9159-67

88. Ponmozhi J, Frias C, Marques T, Frazão O. Smart sensors/actuators for biomedical applications: Review. Measurement 2012; 45(7):1675-88

89. Prescott JH, Lipka S, Baldwin S, et al. Chronic, programmed polypeptide delivery from an implanted, multireservoir microchip device. Nat Biotechnol 2006; 24(4):437-8

90. Harrysson O, Cormier D. Direct fabrication of custom orthopedic implants using electron beam melting technology. Advanced Manufacturing Technology for Medical Applications 2006;193-208

91. Hronik-Tupaj M, Kaplan DL. A review of the responses of two- and three-dimensional engineered tissues to electric fields. Tissue Eng Pt B-Rer 2012;18(3):167-80

92. Balint R, Cassidy NJ, Cartmell SH. Electrical stimulation: A novel tool for tissue engineering. Tissue Eng Pt B-Rer 2013; 19(1):48-57

Chapter 9

Supplementary Material - Chapter 3.2

Supplementary material of article:
'**Electromagnetic stimulation of bone remodeling in vitro: a review**'

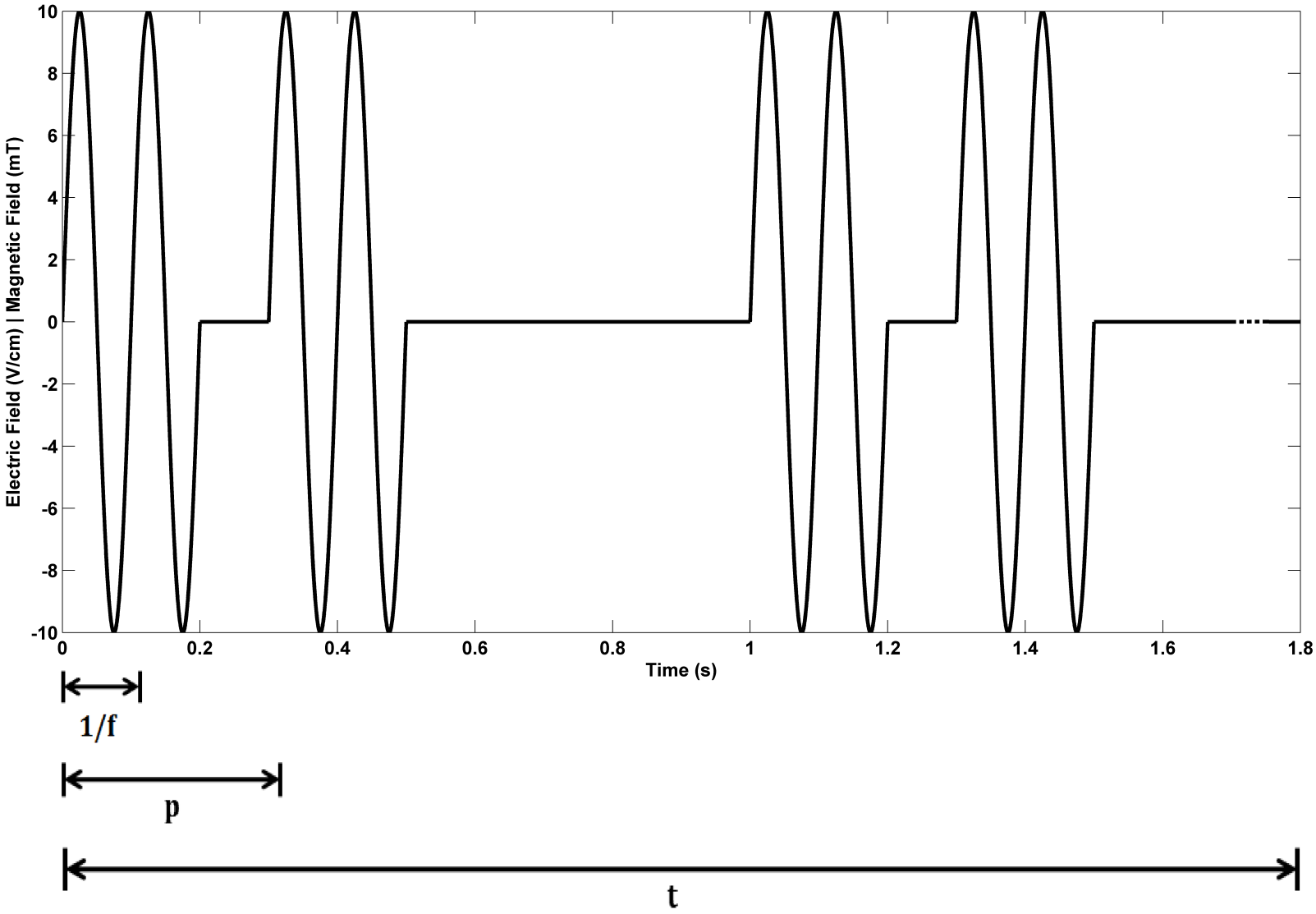

Fig. S1: Identification of the frequency (f), periodicity (p) and expose time (t) of electric and magnetic fields.

Supplementary Tables

Table S1 - Direct current stimulation characteristics and biological outcomes evaluated in different cell lines. ND – not defined; NA – not applicable; Cons. – constant electric field; ES – electric stimulation; $[Ca^{2+}]i$ - intracellular calcium concentration; IA – DNA incorporation assay; EF – electric field.

Cell culture			Stimuli characteristics						Outcomes					Reference
Type	Description	Confluence state	Waveform	Frequency (Hz)	EF strength (V/cm)	Current density ($\mu A/cm^2$)	Exposure time	Assay duration	Proliferation	Differentiation	Mineralization	$[Ca^{2+}]$	Alignment & Migration	
Cell line	**ROS 17/2.8** (rat osteosarcoma cell line)	Non-confluent	Sinusoidal	60	15-20 $x10^{-3}$	300 to 400	34 h	44 to 48 h [10 to 14 h no ES + 34 h ES]	↑ IA (+10 to 40%)	-	-	-	-	[63]
	RCJ 1.20 and RCB 2.2A (rat osteoblast-like cell lines)	Pre-confluent	Cons.	*NA*	1 and 10	*ND*	1h to 17.2 h		-	-	-	-	Cathodal galvanotaxis	[68]
	SaOS-2 (human osteosarcoma cell line)	*ND*	Cons.	*NA*	5 and 14	*ND*	5 min to 5 h		-	-	-	↑$[Ca^{2+}]i$ (at 14 V/cm)	Anodal galvanotaxis	[69]
	MG63 (human osteosarcoma cell line)	*ND*	Cons.	*NA*	7 to 12	*ND*	secs to 80 min		-	-	-	≈ $[Ca^{2+}]_i$	Alignment and elongation perpendicular to EF lines	[65]

Table S2 - Direct current stimulation characteristics and biological outcomes evaluated in stem cells. ND – not defined; NA – not applicable; Cons. – constant electric field; ES – electric stimulation; $[Ca^{2+}]i$ - intracellular calcium concentration; $[Ca^{2+}]m$ – medium calcium concentration; EF – electric field; OM – osteogenic media; MetB – metabolic activity assay; ALPa – Alkaline phosphatase activity; ALPe – Alkaline phosphatase expression; OC – osteocalcin; OPN – osteopontin; Col I – collagen type I; MM – matrix mineralization.

Cell culture			Stimuli characteristics						Outcomes					Reference
Type	Description	Confluence state	Waveform	Frequency (Hz)	EF strength (V/cm)	Current density ($\mu A/cm^2$)	Exposure time	Assay duration	Proliferation	Differentiation	Mineralization	$[Ca^{2+}]$	Alignment & Migration	
Stem cells	**hBM-MSCs** (human Bone Marrow derived Mesenchymal Stem Cells)	*ND*	Cons.	*NA*	$25x10^{-2}$ to 6	*ND*	2h to 10 h		-	-	-	-	Anodal galvanotaxis	[70]
					2	*ND*	2h	28 days [2 h ES + 1 day no ES + 28 days OM]	-	-	≈ MM	-	-	
	hBM-MSCs (human Bone Marrow derived Mesenchymal Stem Cells)	*ND*	Cons.	*NA*	0.1; 1; 10	*ND*	30 min		-	-	-	↓ $[Ca^{2+}]i$ spikes	-	[74]
			Sinusoidal	1	1	*ND*	30 min /day	10 days (+OM)	↑Cell Nr. (+200%)	↑ALPa	↑ MM	-	-	
	mASCs (mouse Adipose Derived Stromal Cells)	*ND*	Square	50	6	*ND*	6 h/day	10 days	≈ Cell Nr. (days 1, 3, 5, 7, 10)	-	-	-	Alignment and elongation perpendicular to field vector	[66]
							6 h/day	7 days (+OM)	-	↑ALPa (+100%); ↑ALPe and OPN (+500%); ↑Col I; Runx2 (+100%)	-	-		
							6 h/day	21 days (+OM)	-	-	≈ OC; ≈ MM	-		
							5 min		-	-	-	↑ $[Ca^{2+}]i$		
	hBM-MSCs (human Bone Marrow derived Mesenchymal Stem Cells)	*ND*	Cons.	*NA*	0.1	*ND*	3 h/day	5 days	↑ MetB (days 0, 2, 3, 5)	-	-	-	↑ rate of cell migration; ↑expression of migration and invasion related	[71]

	Description	Confluence state	Waveform	Frequency (Hz)	EF strength (V/cm)	Current density ($\mu A/cm^2$)	Exposure time	Assay duration	Proliferation	Differentiation	Mineralization	$[Ca^{2+}]$	Alignment & Migration	Reference
	hBM-MSCs (human Bone Marrow derived Mesenchymal Stem Cells)	*ND*	Square	100	*ND*	1.5	24 h/day	6 days [1 day no ES + 5 days ES]	↑ Cell Nr. +78% (day 3), +53.5% (day 5)	-	-	-	-	[87]
								21 days (7 days ES + 14 days no ES) + OM	-	↑ALPa (day 10) ≈ OPN, BSP, Col I	≈ OC; ↑MM (+20%) (day 21)	-	-	
				100	*ND*	15		6 days [1 day no ES + 5 days ES]	↑ Cell Nr. +40% (day 3), +22.5% (day 5)	-	-	-	-	
	hBM-MSCs (human Bone Marrow derived Mesenchymal Stem Cells)	*ND*	Sinusoidal	$60x10^3$	0.02	*ND*	40 min /day	28 days + OM	≈ MetB	↑ ALPe; ↑ Col I; ↑ Col I deposition (days 15, 20)	≈ MM	-	-	[52]

Table S3 - Direct current stimulation characteristics and biological outcomes evaluated in primary cells. ND – not defined; NA – not applicable; VE – Voltage between electrodes; VC - voltage between cells; Cons. – constant electric field; ES – electric stimulation; $[Ca^{2+}]i$ - intracellular calcium concentration; $[Ca^{2+}]m$ – medium calcium concentration; $[Ca^{2+}]ecm$ – extracellular matrix calcium concentration; EF – electric field; EA – exclusion assay.

Cell culture			Stimuli characteristics							Outcomes					References
Type	Description	Confluence state	Waveform	Frequency (Hz)	Periodicity (s)	EF strength (V/cm)	Current density ($\mu A/cm^2$)	Exposure time	Assay duration	Proliferation	Differentiation	Mineralization	$[Ca^{2+}]$	Alignment & Migration	
Primary culture	**Osteoblasts** (Rat calvaria)	Non-confluent	Cons.	*NA*	*NA*	*ND*	100	1h/day	7 days [2 days no ES + 5 days ES]	↑ EA (+28,6%) (day 5)	-	-	-	Parallel orientation of cells to current flow axis	[76]
	Osteoblasts (Rat calvaria)	*ND*	Cons.	*NA*	*NA*	5; 14	*ND*	5 min to 5 h		-	-	-	↑ $[Ca^{2+}]i$ (14 V/cm)	Cathodal migration	[69]
	Osteoblasts (Rat calvaria)	*ND*	Cons.	*NA*	*NA*	*ND*	100; 300	5 min		-	-	-	↑ $[Ca^{2+}]i$ (+130%) (10min after ES)	-	[73]
					NA		100	1h/day	5 days	↑Cell Nr. (+38%)	-	-	-	-	
	Osteoblasts (Bovine)	*ND*	Cons.	*NA*	*NA*	7 to 12	*ND*	80 min		-	-	-	≈ $[Ca^{2+}]i$	Alignment and elongation perpendicular to EF lines	[65]
	Mouse **calvarial organ culture**	*ND*	Cons.	*NA*	*NA*	*ND*	20	72 h		-	-	-	↓ $[Ca^{2+}]m$	-	[64]
	Osteoclasts (Rabbit)	Pre-confluent	Cons.	*NA*	*NA*	1; 10	*ND*	1 h to17.2 h		-	-	-	-	Anodal galvanotaxis	[68]
	Human fetal **osteoblasts** (hFOB 1.19)	Pre-confluent	Cons.	*NA*	*NA*	2	*ND*	30 min		-	-	-	↑ $[Ca^{2+}]i$ (+350%) (20 min)	-	[72]

	Description	Confluence state	Waveform	Frequency (Hz)	Periodicity (s)	EF strength (V/cm)	Current density ($\mu A/cm^2$)	Exposure time	Assay duration	Proliferation	Differentiation	Mineralization	$[Ca^{2+}]$	Alignment & Migration	References
	Osteoblasts (Rat calvaria)	*ND*	Square	$3x10^3$	$3.2x10^{-5}$	*ND*	1.5	6 h/day	3 days [1 day no ES + 2 days ES]	≈ EA	-	-	-	-	[78]
									4 days + OM	-	≈ OPN, Col I, msx2; ↓ALP, cbfa1; no BSP	no OC	-	-	
								24 h/day	3 days [1 day no ES + 2 days ES]	↑ EA (+31%)	-	-	-	-	
									4 days + OM	-	≈ OPN, Col I, ALP, ↓cbfa1, x BSP	no OC	-	-	
	Osteoblasts (Rat calvaria)	Sub-confluent (on polymers)	Square	10	*ND*	*ND*	*ND*	6 h/day	2 days	↑ Cell Nr. (+46%)	≈ OPN,OPG; ↑ Col I (day 1)	-		-	[77]
		Confluent (on polymers)							23 days [2 days no ES + 21 days ES] + OM	-	≈ OPN; ↑ ON, OPG, Col I (day 21)	-	↑$[Ca^{2+}]$ecm (+307%); ↑OC	-	

Table S4 - Capacitive coupling stimulation characteristics and biological outcomes evaluated in cell lines. ND – not defined stimuli characteristic; NA – not applicable; ES – electric stimulation; IA – DNA incorporation assay; MetB – metabolic activity assay; DNA – DNA content; ALPa – Alkaline phosphatase activity (i – intracellular; m – media); ALPe – Alkaline phosphatase expression; MM – matrix mineralization; OPN – osteopontin; Col I – collagen type I; BSP – Bone sialoprotein; ON – osteonectin.

Cell culture			Stimuli characteristics							Outcomes			References
Type	Description	Confluence state	Waveform	Frequency (Hz)	Periodicity (s)	EF strength (V/cm)	Current density (uA/cm^2)	Exposure time	Assay duration	Proliferation	Differentiation	Mineralization	
Cell line	**MC3T3-E1** (mouse osteoblast-like cell line)	Pre-confluent	Square (duty cycle: 2.9%)	10	*ND*	14.5	*ND*	20 h	68 h [24 h no ES + 20 h ES +24 h no ES]	≈ IA	-	-	[79]
						20.3				≈ IA	-	-	
						31.9				↑ IA (+100%)	-	-	
						31.9		5 min; 6 h; 20 h	72 h [24 h no ES, 5 min, 6h, 20h ES --> 48h]	↑ IA (+35-100%)	-	-	
	MC3T3-E1 (mouse osteoblast-like cell line)	2 days Post-confluent	Sinusoidal	$60x10^3$	*ND*	0.02	300	24 h	24h	↑ IA (+18.7%)	-	-	[81]
	TE-85 (human osteosarcoma cell line)	Pre-confluent	Sinusoidal	10	*ND*	$1x10^{-7}$	*ND*	30 min	66,5 h [48 h no ES (24 h Serum + 24 h Serum-free) + 30 min ES + 18 h]	≈ IA	-	-	[80]
				12						≈ IA	-	-	
				14						↑ IA (+30%)	-	-	
				16						≈ IA	-	-	
	MC3T3-E1 (mouse osteoblast-like cell line)	2 days Post-confluent	Sinusoidal	60	*ND*	0.02	300	30 min	24 h [ES 30 min + 23,5 h no ES]	↑ DNA (+17%)	-	-	[82]
								2 h	24 h [ES 2h + 22 h no ES]	↑DNA (+23%)	-	-	
								6 h	24 h [ES 6h + 18h no ES]	↑ DNA (+25%)	-	-	
								24 h	24 h	↑ DNA (+49%)	-	-	
	SaOS-2 (human osteosarcoma cell line)	Non-confluent	Degenerate	*ND*	$62.5x10^{-3}$	0.1	*ND*	4 h	28 h [4 h ES + 20 h no ES + 4 h ES]	↑MetB. A (2h) ↓MetB.A (28h)	↑ALPa(m) (28h), ALPa(i) (2h, 26h, 28h), ALPe; ↑Col I; ↑OPN; ↑ ON; ↑BSP	↑MM (+480%) (28h)	[58]

Table S5 - Capacitive coupling stimulation characteristics and biological outcomes evaluated in stem cells. ND – not defined stimuli characteristic; NA – not applicable; ES – electric stimulation; OM – osteogenic media; MetB – metabolic activity assay; ALPa – Alkaline phosphatase activity; ALPe – Alkaline phosphatase expression; OC – osteocalcin; OPN – osteopontin; Col I – collagen type I; BSP – Bone sialoprotein; MM – matrix mineralization.

Cell culture			Stimuli characteristics							Outcomes			References
Type	Description	Confluence state	Waveform	Frequency (Hz)	Periodicity (s)	EF strength (V/cm)	Current density (uA/cm^2)	Exposure time	Assay duration	Proliferation	Differentiation	Mineralization	
Stem cells	**hBM-MSCs** (human Bone Marrow derived Mesenchymal Stem Cells)	*ND*	Degenerate	*ND*	$62.5x10^{-3}$	0.1	*ND*	3 h/day	5 days	↑ MetB	-	-	[71]
	hMSCs (human Bone Marrow derived Mesenchymal Stem Cells)	(on an hydrogel)	Sinusoidal	10	*ND*	*ND*	*ND*	6 h/day	14 days	-	≈ Runx2; ≈ osterix; ≈ OPN (days 7 and 14)	↑ OC (day 14)	[86]

Table S6 - Capacitive coupling stimulation characteristics and biological outcomes evaluated in primary cells. ND – not defined stimuli characteristic; NA – not applicable; ES – electric stimulation; [Ca^{2+}]ecm - extracellular matrix calcium concentration; OM – osteogenic media; IA – DNA incorporation assay; MetB – metabolic activity assay; EA – exclusion assay; ALPa – Alkaline phosphatase activity (i – intracellular; m – media); ALPe – Alkaline phosphatase expression; OC – osteocalcin; OPN – osteopontin; Col I – collagen type I; ON – osteonectin; BSP – Bone sialoprotein; cbfa1 - Core-binding factor alpha(1); BMP2 - Bone morphogenetic protein; OPG – Osteoprotegerin.

Cell culture			Stimuli characteristics							Outcomes			References
Type	Description	Confluence state	Waveform	Frequency (Hz)	Periodicity (s)	EF strength (V/cm)	Current density (uA/cm^2)	Exposure time	Assay duration	Proliferation	Differentiation	Mineralization	
Primary culture	Bone cells (rat embryo calvaria)	Confluent	Square (duty cycle: $7.5x10^{-3}$%)	3	*ND*	13	*ND*	5 min	24h [5 min ES --> 24 h no ES]	↑ IA (+ 40%)	-	-	[85]
						22	*ND*			≈ IA	-	-	
						54	*ND*			↑ IA (+240%)	-	-	
	Bovine primary cells (osteoblast migration from periosteum explants)	Sub-confluent	Square	16	*ND*	60	*ND*	24 h/day	11 days [4 days no ES + 7 days ES]	↑ Cell Nr. (+ 10-30%) (day 7)	↑ ALP (+200 - 300%)	-	[55]
		Confluent					*ND*		22 days [4 days no ES + 18 days ES]	-	↑ FN, ON, Col I, BSP, OPG (days 9 to 22)	↑OC (days 13 and 18)	
	Bovine primary cells (ostoblast migration from periosteum explants)	Pre-confluent (Confluent before ES application)	Square	16	*ND*	60	*ND*	24 h/day	21 days [7 days no ES + 14 days ES]	-	-	↑[Ca2+]ecm; globular mineralized bodies	[61]
			Square			210	*ND*			-	-	rod-shaped crystals	

Description	Confluence state	Waveform	Frequency (Hz)	Periodicity (s)	EF strength (V/cm)	Current density (uA/cm^2)	Exposure time	Assay duration	Proliferation	Differentiation	Mineralization	References
Bone cells (rat embryo calvaria)	Confluent	Square (duty cycle: $7.5x10^{-3}$%)	3	*ND*	13	*ND*	5 min	24h [5 min ES --> 24 no ES]	↑IA (+ 40%)	-	-	[84]
					24				IA ≈	-	-	
					54				↑ IA (+240%)	-	-	
Osteoblasts (Rat)	(on conducting polymers)	Sinusoidal	100	*ND*	*ND*	*ND*	1 h/day	8 days [1 day no ES + 7 days ES]	↑ MetB	↑ BMP-2, p-Smad4, Col I, ON	-	[138]
Embroynic chick calvarial cells	*ND*	*ND*	8	*ND*	$1x10^{-7}$	*ND*	30 min	18,5h [30 min ES + 18 h no ES]	≈ IA	-	-	[83]
			12						≈ IA	-	-	
			16						↑ IA (+30%)	-	-	
			20						≈ IA	-	-	
			24						≈ IA	-	-	

Table S7 - Inductive coupling stimulation characteristics and biological outcomes evaluated in cell lines. ND – not defined stimuli characteristic; NA – not applicable; AC – alternating voltage; CV - constant voltage; ES – electric stimulation; [Ca2+]ecm - extracellular matrix calcium concentration; OM – osteogenic media; IA – DNA incorporation assay; MetB – metabolic activity assay; DNA – DNA content; EA – exclusion assay; PS – protein synthesis; ALPa – Alkaline phosphatase activity; OC – osteocalcin; OPN – osteopontin; Col I – collagen type I; FN – fibronectin; MM – matrix mineralization.

Cell culture			Stimuli characteristics							Outcomes			References
Type	Description	Confluence state	Waveform	Frequency (Hz)	Periodicity (ms)	MF strength (mT)	EF strength (mV/cm)	Exposure time	Assay duration	Proliferation	Differentiation	Mineralization	
Cell line	**MG63** (human osteosarcoma cell line)	Non-confluent (on polymers)	Square (PEMF)	75	*ND*	2.3	*ND*	12 h /day	7 days [1 day no ES + 3 days ES + 3 days no ES]	↑MetB. (+31%) (day 7)	↑ALP (+21%) (day 4); ↑ 22% Pro-Col I, TGF-β (day 7)	↑OC (+14%) (day 4)	[105]
	MG63 (human osteosarcoma cell line)	*ND*	Square (PEMF)	75	*ND*	2.3	0.02	30 min, 1 h, 3 h, 6 h,12 h, 18 h or 24 h	24 h no Es + 30 min, 1 h, 3 h, 6 h,12 h, 18 h or 24 h ES	↑ IA (1 h to 24 h)	-	-	[121]
	TE-85 (human osteosarcoma cell line)	Non-confluent	CV + Sinusoidal (CMF)	15.3	*ND*	$4x10^{-2}$ AC| $2x10^{-2}$ CV	*ND*	10, 20 or 30 min	24 h No + 10, 20 or 30 min ES + 24 h no ES	↑ IA (+71%)	-	-	[89]
	TE-85 (human osteosarcoma cell line)	Non-confluent	Square (PEMF)	75	*ND*	2.3	0.02	10 min		≈ IA	-	-	[91]
								30 min		↑ IA (+276%)	-	-	
								9h		↑ IA (+284%)	-	-	
								24 h		↑ IA (+355%)	-	-	
	MG63 (human osteosarcoma cell line)							10 min		≈ IA	-	-	
								30 min		↑ IA (+147%)	-	-	
								9 h		↑ IA (+174%)	-	-	
								18/36 h		↑ IA (+182%)	-	-	
	MC3T3-E1 (mouse osteoblast-like cell line)	*ND*	Square (PEMF)	48	*ND*	1.55	*ND*	24 h	24 h	≈ MetB.	no ALP	-	[98]
									48 h [24 h no ES + 24 h ES]	≈ MetB.	no ALP	-	
									48h [24 h ES + 24 h no ES]	≈ MetB.	no ALP	-	
								48h		≈ MetB.	no ALP	-	
	MC3T3-E1 (mouse osteoblast-like cell line)	*ND*	Square (PEMF)	5000	66.7	4	*ND*	30 min/day	3 days [2 days ES + 1 day no ES]	↑MetB.	↑ALP	-	[102]
									3 days [2 days ES + 4 h or 24 h no ES]	-	↑COX-2 (+24 h)	-	

Description	Confluence state	Waveform	Frequency (Hz)	Periodicity (ms)	MF strength (mT)	EF strength (mV/cm)	Exposure time	Assay duration	Proliferation	Differentiation	Mineralization	References
MC3T3-E1 (mouse osteoblast-like cell line)	Non-confluent	Square (PEMF)	6667	66.7	7	*ND*	24 h/day	30 days [5 days ES + 25 days no ES] + OM	↑ DNA +38.5% (day 2); + 7.1% (day 7)	↑ALP	↑ MM (+51%)	[53]
								30 days [10 days no ES + 5 days ES + 15 days no ES] + OM		↑ALP	↑ MM (+35%)	
								30 days [25 days no ES + 5 days ES] + OM		-	↓ MM (-20%)	
								30 days [15 days ES + 15 days no ES] + OM		↑ALP	↑ MM (+ 51%)	
								30 days [15 days no ES + 15 days ES] + OM		-	≈ MM	
								30 days + OM		-	≈ MM	
ROS 17/2.8 (rat osteosarcoma cell line)	Non-confluent	*ND*	30	*ND*	1.8	$6x10^{-3}$	24 h/day	3 days	≈ Cell Nr.	↑ ALP (+108%)	-	[94]
							12 h/day	3 days [2,5 days no ES + 12 h ES]	≈/↓ Cell Nr.	↑ ALP	-	
ROS 17/2.8 (rat osteosarcoma cell line)	Non-confluent	Sinusoidal	30	*ND*	1.8	0.02	24 h/day	5 days	↓ Cell Nr.	↑ ALP	-	[93]
MG63 (human osteosarcoma cell line)	Confluent	Triangular (PEMF)	4444	66.7	1.8	*ND*	8 h/day	4 days	↓ Cell Nr. (-48% at day 4); ↓IA (-37% at day 2)	↑ ALP; ↑ Col I (+160% at day 1)	↑ OC (+260% at day 2)	[92]
MLO-Y4 (osteocyte-like cells)	Non-confluent (collagen coated plate)	Triangular (PEMF)	4444	66.7	1.6	*ND*	8 h/day	4 days	≈ EA	↑ ALP (+200% at day 1)	≈ OC	[107]
ROS 17/23 osteoblast-like cells	Confluent						24 h/day	3 days	≈ EA	-	≈ OC	

Description	Confluence state	Waveform	Frequency (Hz)	Periodicity (ms)	MF strength (mT)	EF strength (mV/cm)	Exposure time	Assay duration	Proliferation	Differentiation	Mineralization	References
SaOS-2	Non-confluent	Square (PEMF)	5000	66.7	*ND*	9	4 h/day	3 days [2 days no ES + 4 h ES +16 h no ES]	≈ MetBA; ≈ Cell Nr.	-	-	[106]
	Confluent							3 days [20 h no ES + 4 h ES]	-	↑ALP (+85% day 1; +43% day 2; +80% day 3)	-	
								3 days [20 h no ES + 4 h ES] + OM	-	↑ALP (+ 90%)	↑MM	
TE-85 osteosarcoma cells	Non-confluent	CV +Sinusoidal (CMF)	15.3	*ND*	$40x10^{-3}$ AC| $20x10^{-3}$ CV	*ND*	30 min	18.5h [30 min ES + 18h No ES]	↑ IA (+58%)	-	-	[90]
SaOS-2	Non-confluent	Square (PEMF)	$1x10^{6}$	66.7	0.1	*ND*	24 h/day	21 days	↑MetB (11days)	-	-	[126]
SaOS-2	Non-confluent	Triangular (PEMF)	4000	66.7	1.3	*ND*	8 h/day	3 days	↓ PS (-9% to 14%)	↑ ALP (+12% to 16%)	-	[87]
							24 h/day	3 days [1 day ES + 2 days no ES]	↓ PS (- 11%)	↑ ALP (+14% to 20%)	-	
								3 days [1day no ES + 1 day ES + 1 day no ES]	≈ PS	↑ ALP (+19% to 38%)	-	
								3 days [2 days no ES + 1 day ES]	↓ PS (-17%)	↑ALP (0 to +22%)	-	

Table S8 - Inductive coupling stimulation characteristics and biological outcomes evaluated in stem cells. ND – not defined stimuli characteristic; NA – not applicable; ES – electric stimulation; [Ca^{2+}]ecm - extracellular matrix calcium concentration; OM – osteogenic media; IA – DNA incorporation assay; MetB – metabolic activity assay; DNA – DNA content; EA – exclusion assay; ALPa – Alkaline phosphatase activity; OC – osteocalcin; MM – matrix mineralization.

Cell culture			Stimuli characteristics							Outcomes			References
Type	Description	Confluence state	Waveform	Frequency (Hz)	Periodicity (ms)	MF strength (mT)	EF strength (mV/cm)	Exposure time	Assay duration	Proliferation	Differentiation	Mineralization	
Stem cells	**hBM-MSCs** (human Bone Marrow derived Mesenchymal Stem Cells)	Non-confluent	Sinusoidal	200	5000	1000	*ND*	3 min /day	5 days [1 day no ES + 4 days ES]	↑ IA	-	-	[96]
		Pre-confluent							25 days (+OM 7 to 25 days)	-	↑ ALP	↑MM	
									25 days [7 days ES + 18 days no ES (+OM)]	-	↑ ALP	↑MM	
	hBM-MSCs (human Bone Marrow derived Mesenchymal Stem Cells)	Non-confluent	Square (PEMF)	4444	66.7	1.8	*ND*	8 h/day	10 days	↑ Cell Nr. (+20 to 60%)	-	-	[95]
									24 days [3 days ES + 21 days no ES (+OM)]	-	≈ ALP	≈MM	
	hBM-MSCs (human Bone Marrow derived Mesenchymal Stem Cells)	Non-confluent	Square (PEMF)	7.5	*ND*	0.13	2	2 h/day	7 days	≈ DNA	-	-	[88]
									15 days [1 day no ES + 14 days ES]+OM	↓ DNA (-75% at day 7); ↑ DNA (+62% at day 10)	↑ALPa (+82% day 7); ↓ALPa (-123% day 10); ↑Runx2/Cbfa1 (day 7); ↓Runx2/Cbfa1 (day 10)	↑MM (day 28)	
	hBM-MSCs (human Bone Marrow derived Mesenchymal Stem Cells)	Confluent	Triangular (PEMF)	4444	66.7	1.6	*ND*	8 h/day	24 days + OM + BMP-2	↓Cell Nr.	↑ ALP	↑OC	[97]
	hBM-MSCs (human Bone Marrow derived Mesenchymal Stem Cells)	*ND*	Triangular (PEMF)	4444	66.7	1.8	*ND*	3 h/day	5 days	↑ MetB.	-	-	[71]
	C3H10T1/2 (pluripotent stem cells isolated from mouse embryo osteocarcoma)	*ND*	Square (PEMF)	1000	0.1	*ND*	0.1	24 h/day	14 days	≈ MetB.	↑ ALP (at days 3, 9, 12)	↑ OC (days 7,10); ↑ MM (day 14)	[113]

Description	Confluence state	Waveform	Frequency (Hz)	Periodicity (ms)	MF strength (mT)	EF strength (mV/cm)	Exposure time	Assay duration	Proliferation	Differentiation	Mineralization	References
hBM-MSCs (human Bone Marrow derived Mesenchymal Stem Cells)	*ND*	Square (PEMF)	4444	66.7	1.8	*ND*	8 h/day	11 days	↑Cell nr (+34.8%, + 29.8% (+ OM) at day 1)	↑ALP (at days 1 and 4); ↓Col I (day 4); ↑Col I (day 7); ↑cbfa-1 (day 2); ↓ cbfa-1 (day 4); ↓BMP-2 (day 2); ↑BMP-2 (at days 4 and 7)	↑OC (day 4); ↑MM (day 11)	[114]
BMSCs (Human bone marrow stromal cells)	*ND*	Square (PEMF)	200 $x10^3$	66.7	0.1	*ND*	24 h/day	14 days	↓IA (day 14)	≈ ALP, Col I and ON; ↑BMP-2 (at days 5 and 9); ↑TGF-β (day 9); ↑OPG (at days 5 and 9); ↑OC I (day 9)	↑MM (days 9 and 14)	[104]
hBM-MSCs (human Bone Marrow derived Mesenchymal Stem Cells)	Non-confluent	Square (PEMF)	$1x10^6$	66.7	0.1	*ND*	24 h/day	21 days	↑MetB (+13% at day 7, +16% at day 14)	↑Col-1 (+120% at day 14, + OM); ↑ALP (+80% at day 21, +OM)	-	[126]
hBM-MSCs (human Bone Marrow derived Mesenchymal Stem Cells)	Non-confluent	Square (PEMF)	5	*NA*	1.1	*ND*	30min /day	21 days	-	≈ ALP (days 3, 6, 9); ↑ ALP (days 12, 15)	↑OC; ↑MM (day 21)	[108]
			25						-	≈ ALP (day 3); ↑ ALP (days 6, 9, 12, 15)	↑OC; ↑MM (day 21)	
			50						-	↑ ALP (days 3, 6, 9, 12, 15)	↑↑OC (day 21); ↑MM (day 21)	
			75						-	≈ ALP (day 3); ↑ ALP (days 6, 9, 12, 15)	↑OC; ↑MM (day 21)	
			100						-	≈ ALP (day 3); ↑ ALP (days 6, 9, 12, 15)	↑OC; ↑MM (day 21)	
			150						-	≈ ALP (days 3, 6, 9); ↑ ALP (days 12, 15)	↑OC; ↑MM (day 21)	
hBM-MSCs (human Bone Marrow derived Mesenchymal Stem Cells)	Pre-confluent	Square (PEMF)	75	*NA*	2	*ND*	10min /day	7 days + OM	= MetB	= ON, BSP, OPN, Runx2	-	[123]
								21 days + OM	= MetB ↑DNA	↑ ON, BSP, OPN, Runx2, DC, FN, Col, aALP and ALP	↑ q[Ca^{2+}] (day 21)	
ASCs (human Adipose-derived mesenchymal stem cells)								7 days + OM	= MetB	= ON, BSP, OPN, Runx2	-	
								21 days + OM	= MetB; ↑DNA	↑ OSN, BOSP, aALP; = OPN, Runx2, DC, FN, Col, and ALP	↑ q[Ca^{2+}] (day 21)	

	Description	Confluence state	Waveform	Frequency (Hz)	Periodicity (ms)	MF strength (mT)	EF strength (mV/cm)	Exposure time	Assay duration	Proliferation	Differentiation	Mineralization	References
	ASCs (human Adipose-derived mesenchyme stem cells)	*ND*	Sinusoidal	7.5	*NA*	0.1	*ND*	8 h/day	20 days	-	↓ ALP levels (day 7; NM and OM)	-	[103]
				10							↑ (OM) and = or ↓ (NM) ALP levels (day 7)		
				15							↑ (OM) and = or ↓ (NM) ALP levels (day 7)		
				30							↑ (OM) and = or ↓ (NM) ALP levels (day 7)		
				45							↑ (OM) and = or ↓ (NM) ALP levels (day 7)		
				60							↑ (OM) and = or ↓ (NM) ALP levels (day 7)		
				75							↓ ALP levels (day 7; NM and OM)		
				7.5		1					↓ ALP levels (day 7, NM and OM), ALPai (day 10) ↓ Runx2, COL-I, OC, OSX (day 4 and 7, NM and OM),	↓ $[Ca^{2+}]$ (NM and OM)	
				10							↑ ALP levels (day 7; NM and OM)	-	
				15							↑ ALP levels (day 7; NM and OM)		
				30							↑ ALP levels (day 7, NM and OM) and ↑ ALPai (day 10), ↑ Runx2, COL-I, OC, OSX (day 4 and 7, NM and OM)	↑ MM (day 20) ↑ $[Ca^{2+}]$ (day 20) (NM and OM)	
				45							↑ ALP levels (day 7, NM and OM) and ↑ ALPai (day 10), ↑ Runx2, COL-I, OC, OSX (day 4 and 7, NM and OM)	↑ $[Ca^{2+}]$ (day 20) (NM and OM)	
				60							↑ (OM) and = or ↓ (NM) ALP levels (day 7)	-	
				75							↑ (OM) and = or ↓ (NM) ALP levels (day 7)	-	

	Description	Confluence state	Waveform	Frequency (Hz)	Periodicity (ms)	MF strength (mT)	EF strength (mV/cm)	Exposure time	Assay duration	Proliferation	Differentiation	Mineralization	References
	ASCs (human Adipose-derived mesenchyme stem cells)	*ND*	Sinusoidal	7.5	*NA*	2	*ND*	8 h/day	20 days	-	↓ ALP levels (day 7; NM and OM)	-	[103]
				10							↑ (OM) and = or ↓ (NM) ALP levels (day 7)		
				15							↑ (OM) and = or ↓ (NM) ALP levels (day 7)		
				30							↑ ALP levels (day 7, NM and OM)		
				45							↑ ALP levels (day 7, NM and OM)		
				60							↑ (OM) and = or ↓ (NM) ALP levels (day 7)		
				75							↑ (OM) and = or ↓ (NM) ALP levels (day 7)		
				7.5		3					↑ (OM) and = or ↓ (NM) ALP levels (day 7)	-	
				10							↑ (OM) and = or ↓ (NM) ALP levels (day 7)		
				15							↑ (OM) and = or ↓ (NM) ALP levels (day 7)		
				30							↑ (OM) and = or ↓ (NM) ALP levels (day 7)		
				45							↑ (OM) and = or ↓ (NM) ALP levels (day 7)		
				60							↑ (OM) and = or ↓ (NM) ALP levels (day 7)		
				75							↓ ALP levels (day 7; NM and OM)		

Table S9 - Inductive coupling stimulation characteristics and biological outcomes evaluated in primary cultures. ND – not defined stimuli characteristic; NA – not applicable; AC – alternating voltage; CV - constant voltage; ES – electric stimulation; Cons. – constant magnetic field; $[Ca^{2+}]$ecm - extracellular matrix calcium concentration; OM – osteogenic media; IA – incorporation assay; MetB – metabolic activity assay; DNA – DNA content; EA – exclusion assay; PS – protein synthesis; ALPa – Alkaline phosphatase activity; OC – osteocalcin; OPN – osteopontin; Col I – collagen type I; MM – matrix mineralization.

Cell culture			Stimuli characteristics							Outcomes			References
Type	Description	Confluence state	Waveform	Frequency (Hz)	Periodicity (ms)	MF strength (mT)	EF strength (mV/cm)	Exposure time	Assay duration	Proliferation	Differentiation	Mineralization	
Primary culture	**iCALs** (immortalized calvarial cells)	*ND*	Square (PEMF)	1000	0.1	*ND*	0.1	24 h/day	14 days	≈ MetB.	↑ ALP (days 3, 7, 9)	↑ MM (day 14)	[113]
	Osteoblasts (rat calvaria)	*ND*	Square (PEMF)	48	*ND*	1.55	*ND*	24 h/day	24 h	≈ MetB.	↓ ALP	-	[98]
									48 h [24 h no ES + 24 h ES]	↑ MetB. (+12.6%)	≈ ALP	-	
									48 h [24 h ES + 24 h no ES]	↑ MetB. (+19.8%)	≈ ALP	-	
								48h		↑ MetB. (+19.1%)	↑ ALP	-	
	HBC human bone cells	Non-confluent	CV + Sinusoidal (CMF)	15.3	*NA*	$40x10^{-3}$ AC | $20x10^{-3}$ VC	*ND*	30 min	18.5 h [30 min ES + 18 h no ES]	↑ IA (+26%)	NA	-	[90]
	Osteoblasts (human femoral heads)	*ND*	*ND* (PEMF)	14.9	*ND*	0.4	*ND*	24 h/day	10 days	↑ Cell Nr. (+1.8% day 3; +29% day 7; +55.5% day 10)	↑ ALP (+1% day 3; + 20% day 7; + 58% day 10)	-	[101]
	Osteoblasts (rat calvaria)	Non-confluent	Triangular (PEMF)	3800	666.7	*ND*	*ND*	4 h/day	7 days + BMP-2	↑ Cell Nr.	-	-	[100]
									13 days (ES at 9, 11, 13d) + 1 day no ES	-	↑ALP (day 12), ≈ Pro-Col I	↑ OC (day 12)	
									13 days (ES 15, 17, 19d) + 1 day no ES	-	≈ ALP, Pro-Col I	↑ OC (day 18)	
									20 days [1 day no ES + 19 days ES] + BMP-2	-	↑ALP and ↑ Pro-Col I (day 12)	↑ OC; ↑ MM (day 12)	

Description	Confluence state	Waveform	Frequency (Hz)	Periodicity (ms)	MF strength (mT)	EF strength (mV/cm)	Exposure time	Assay duration	Proliferation	Differentiation	Mineralization	References
Osteoblats (rat calvaria)	2 post-confluent	Square (PEMF)	7.5	ND	*ND*	2	2 h/day	1 day	↑ MetB.	-	-	[99]
Osteoblasts (rat calvaria)	Non-confluent	Square (PEMF)	15	~5	0.1	ND	8 h/day	14 days [2 days no ES + 12 days ES]	↑ MetB. (34% day 3; 11.5% day 5; 13.3% day 7); ≈ MetB.A (day 14)	↓ ALP, RANKL; ≈ OPN, Col I	≈ OC; ≈ MM	[59]
Osteoblasts (human trabecular bone - healthy)	On a 3D network	Sinusoidal	20	*NA*	6	0.113	24 h/day	21 days	-	↑Col I (200% day 7; 370% day 14)	-	[110]
Osteoblasts (Ectopic osseus tissue - myositis ossificans)									-	↑Col I (240% day 3; 540% day 7; 120% day 21)	Densely packed ECM; intense Col I and ALP labelling	
Osteoblasts (rat calvaria)	Non-confluent	CV	*NA*	*NA*	160	*ND*	24 h/day	20 days	≈ Cell Nr. (at day 10)	↑ $[Ca^{2+}]$, ALP (day 20)	↑ MM (+50%), ↑OC	[112]
Osteoblasts (rat calvaria)	Non-confluent	Sawtooth (PEMF)	4444	66.7	1.8	*ND*	6 h	6h ES + 21 days OM	-	-	↑ MM (39% nr, 70% larger)	[115]
SV-HFOs (fetal pre-osteoblasts)	Non-confluent	Square (PEMF)	200 x10^3	66.7	0.1	*ND*	24 h/day	14 days	=IA	-	-	[104]

	Description	Confluence state	Waveform	Frequency (Hz)	Periodicity (ms)	MF strength (mT)	EF strength (mV/cm)	Exposure time	Assay duration	Proliferation	Differentiation	Mineralization	References
	Osteoblasts (rat calvaria)	*ND*	sinusoidal	50	*NA*	0.9	*ND*	30 min/day	Up to 15 days	↓MetB (3days)	= ALP (9 days); ↑BMP2 (12, 24, 96h)	= MM (10 days)	[111]
						1.2					↑ ALP (9 days); ↑BMP2 (12, 24, 96h); ↑Col-1 (96h)	↑ MM (10 days)	
						1.5					↑ ALP (9 days); ↑BMP2 (12, 24h); ↑Runx-2 (12h); ↑Col-1 (12h)	↑ MM (10 days)	
						1.8					↑ ALP (9 days); ↑BMP2 (12, 24, 96h); ↑Runx-2 (12, 24h); ↑Col-1 (12, 96h)	↑ MM (10 days)	
						2.1					↑ ALP (9 days); ↑BMP2 (24h); ↑Runx-2 (12h); ↑Col-1 (12h)	↑ MM (10 days)	
						2.4					↑ ALP (9 days); ↑BMP2 (24h); ↑Runx-2 (12h)	↑ MM (10 days)	
						2.7					= ALP (9 days); ↑BMP2 (24h)	↑ MM (10 days)	
						3					= ALP (9 days); ↑BMP2 (12, 24h)	= MM (10 days)	
						3.3					↑ ALP (9 days); ↑BMP2 (12h)	↑ MM (10 days)	
						3.6					↑ ALP (9 days); ↑BMP2 (12, 24, 96h); ↑Runx-2 (12, 24h); ↑Col-1 (12, 96h)	↑ MM (10 days)	
						3.9					↑ ALP (9 days); ↑BMP2 (12, 24h); ↑Col-1 (12h)	↑ MM (10 days)	
						4.2					↑ ALP (9 days); ↑BMP2 (12h);	↑ MM (10 days)	
						4.5					↓ ALP (9 days); ↑BMP2 (12h)	↑ MM (10 days)	
						4.8					↓ ALP (9 days); ↑Col-1 (12h)	↓ MM (10 days)	

Chapter 10

Supplementary Material - Section 4

Supplementary material of article:
'**New cosurface capacitive stimulators for the development of active osseointegrative implantable devices**'

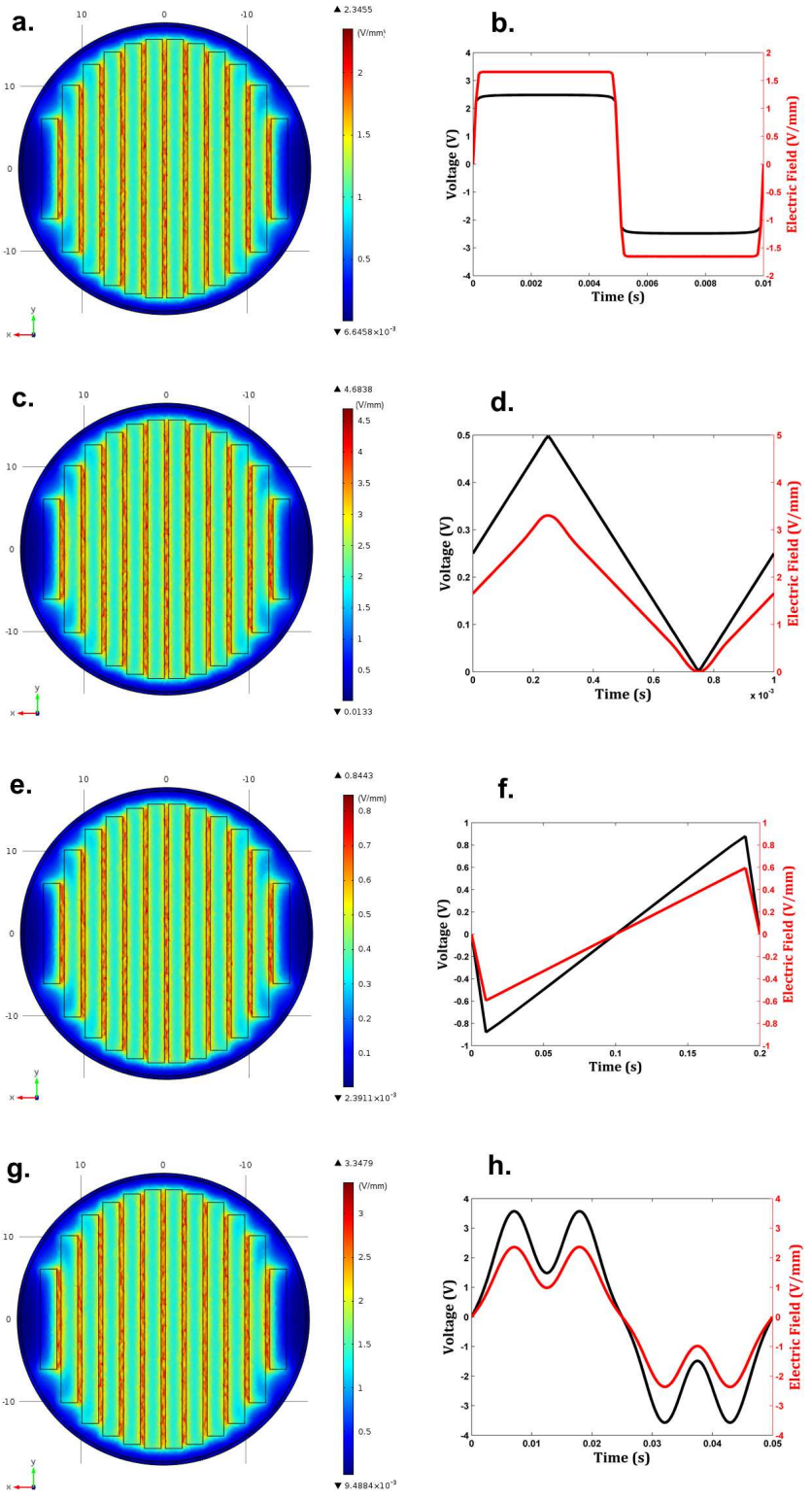

Fig. S1: Simulation results of EF distributions and strengths on MED1 (z=0.5 mm) according to the following periodic excitations applied to stimulator' electrodes: a. 2D EFs: squared excitation (SQ ST) (5 V, 100 Hz). **b**. EFs on a gap midpoint (GM): SQ ST (CC =99.88%). **c**. 2D EFs: triangular excitation (TR ST) (0.5 V, 1 Hz). **d**. EFs on GM: TR ST (CC =99.98%). **e**. 2D EFs: sawtooth excitation (SW ST) (2 V, 5 Hz). **f**. EFs on GM: SW ST (CC =99.99%). **g**. 2D EFs: arbitrary excitation (AR ST) (3.5 V, 20 Hz). **h**. EFs on GM: AR ST (CC =100%). EFs were obtained when voltages reach maximum amplitudes (at $\pi/2$ rad in the triangular waveform). Results shown in 2nd column refer to EFs in [0 2π] rad. The midpoint above a gap is (x, y, z)=(0, 0, 0.5) mm from such horizontal planes.

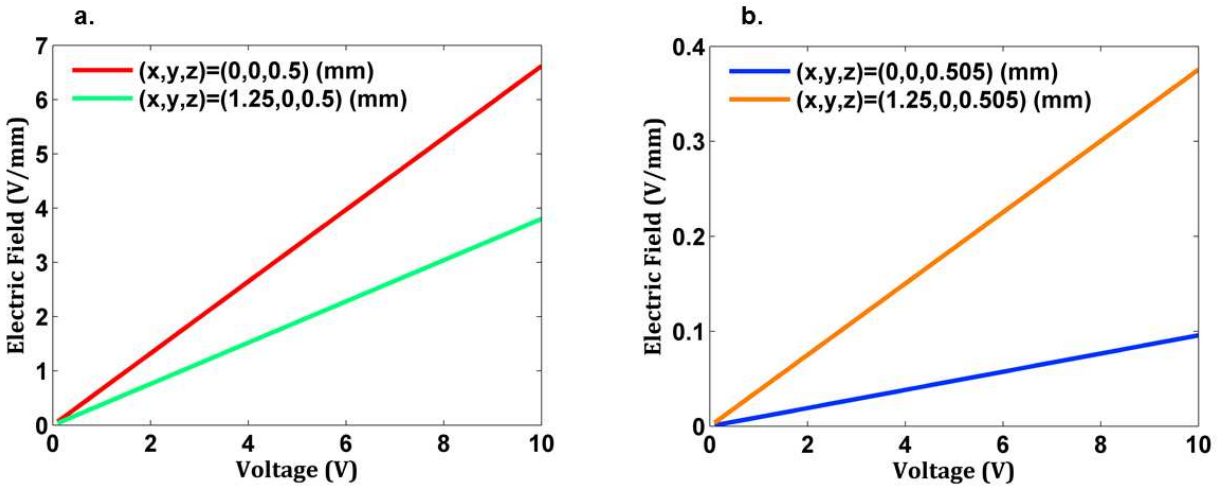

Fig S2: Interrelationships between EF strengths and constant excitations of the stimulator' electrodes. a. EFs in the gap midpoint (x, y, z)=(0,0,0.5) mm and in the electrode midpoint (x, y, z)=(1.25, 0, 0.5) mm on MED1. **b.** EFs in the gap midpoint (x, y, z)=(0, 0, 0.505) mm and in the electrode midpoint (x, y, z)=(1.25, 0, 0.505) mm on MED2.

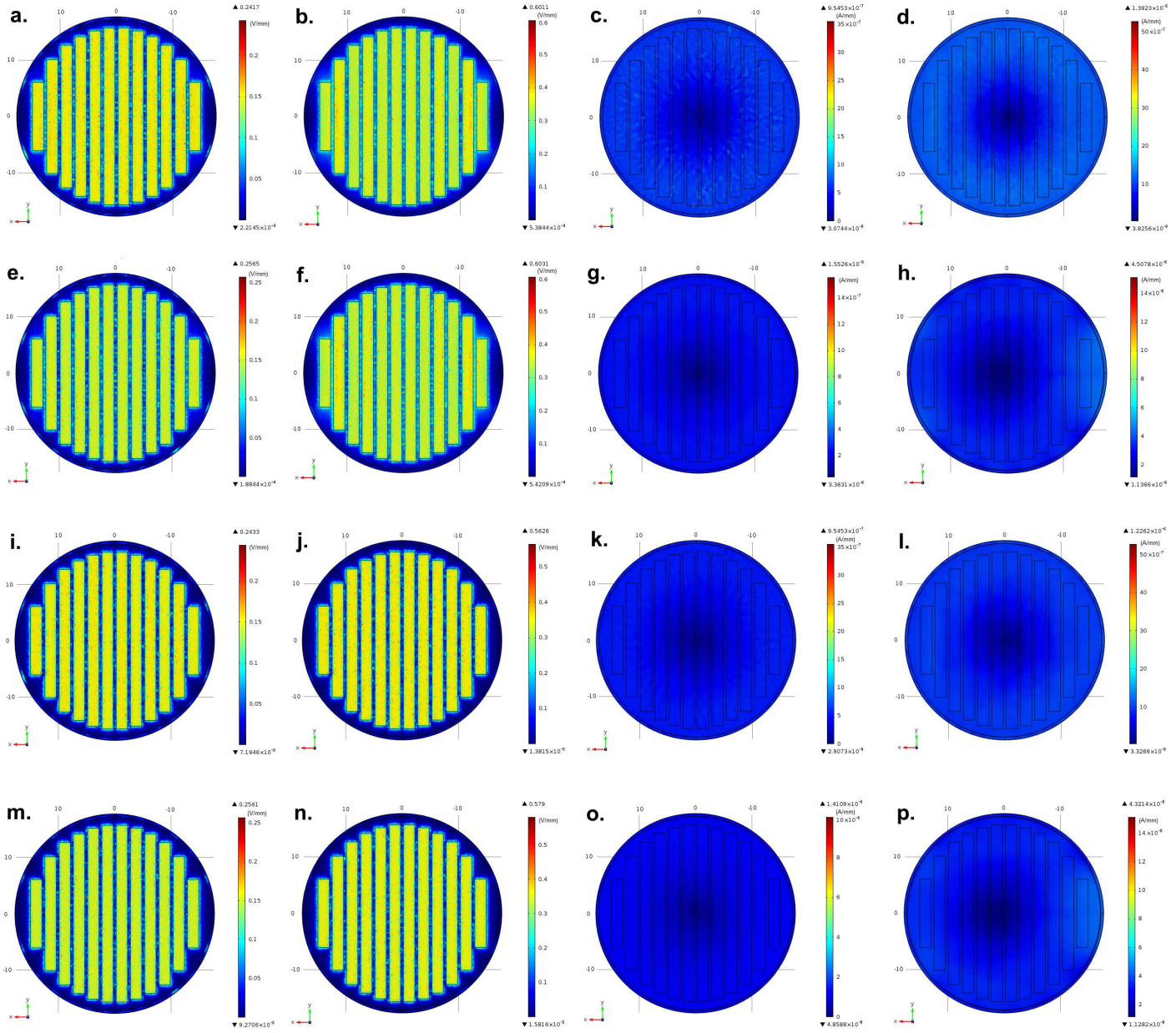

Fig. S3: Simulation results of EF and MF distributions and strengths. **a**. 2D EFs stimulating cells at π rad: LF ST, MED2, z=0.5 mm. **b**. 2D EFs stimulating cells at π rad: HF ST, MED2, z=0.5 mm. **c**. 2D MFs stimulating cells at π rad: LF ST, MED2, z=0.5 mm. **d**. 2D MFs stimulating cells at π rad: HF ST, MED2, z=0.5 mm. **e**. 2D EFs stimulating cells at π rad: LF ST, MED3, z=0.5 mm. **f**. 2D EFs stimulating cells at π rad: HF ST, MED3, z=0.5 mm. **g**. 2D MFs stimulating cells at π rad: LF ST, MED3, z=0.5 mm. **h**. 2D MFs stimulating cells at π rad: HF ST, MED3, z=0.5 mm. **i**. 2D EFs stimulating cells at π rad: LF ST, MED2, z=0.51 mm. **j**. 2D EFs stimulating cells at π rad: HF ST, MED2, z=0.51 mm. **k**. 2D MFs stimulating cells at π rad: LF ST, MED2, z=0.51 mm. **l**. 2D MFs stimulating cells at π rad: HF ST, MED2, z=0.51 mm. **m**. 2D EFs stimulating cells at π rad: LF ST, MED3, z=0.52 mm. **n**. 2D EFs stimulating cells at π rad: HF ST, MED3, z=0.52 mm. **o**. 2D MFs stimulating cells at π rad: LF ST, MED3, z=0.52 mm. **p**. 2D MFs stimulating cells at π rad: HF ST, MED3, z=0.52 mm

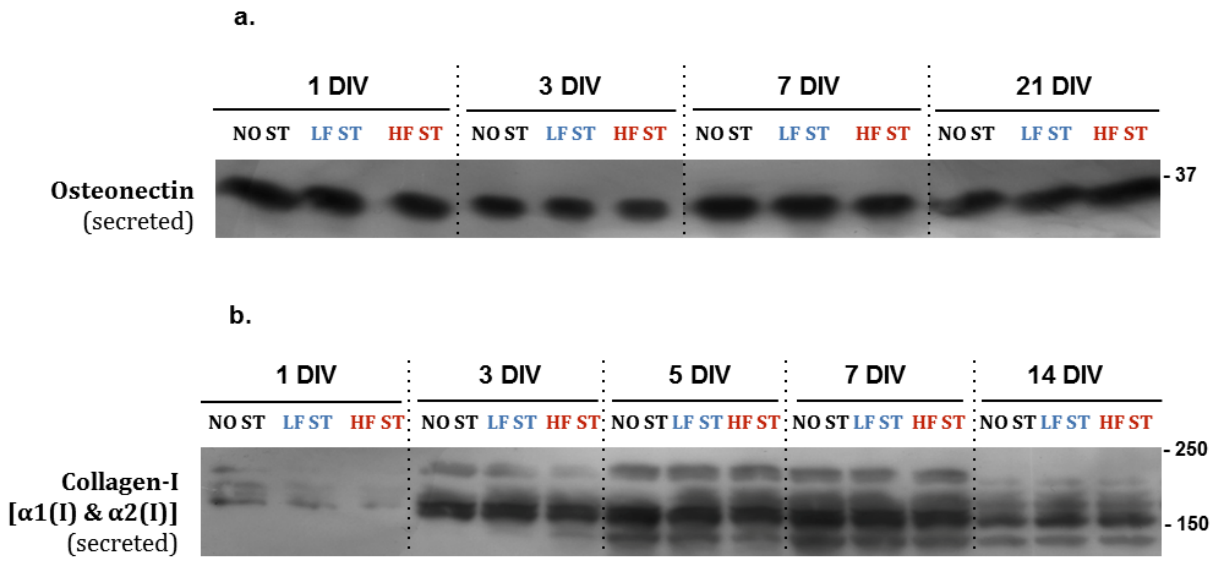

Fig. S4: Secretion of two matrix maturation markers into the cells conditioned media upon LF and HF stimuli Immunoblot analysis of the levels of: **a.** osteonectin (a 35 kDa protein); and **b.** collagen-I [unprocessed and processed α1(I) and α2(I) procollagen monomeric chains of 130-160 kDa)], secreted into the medium by MC3T3 cells exposed for various days in vitro (DIV) to NO ST, LF ST and HF ST. Migration of molecular weight markers is indicated to the right.

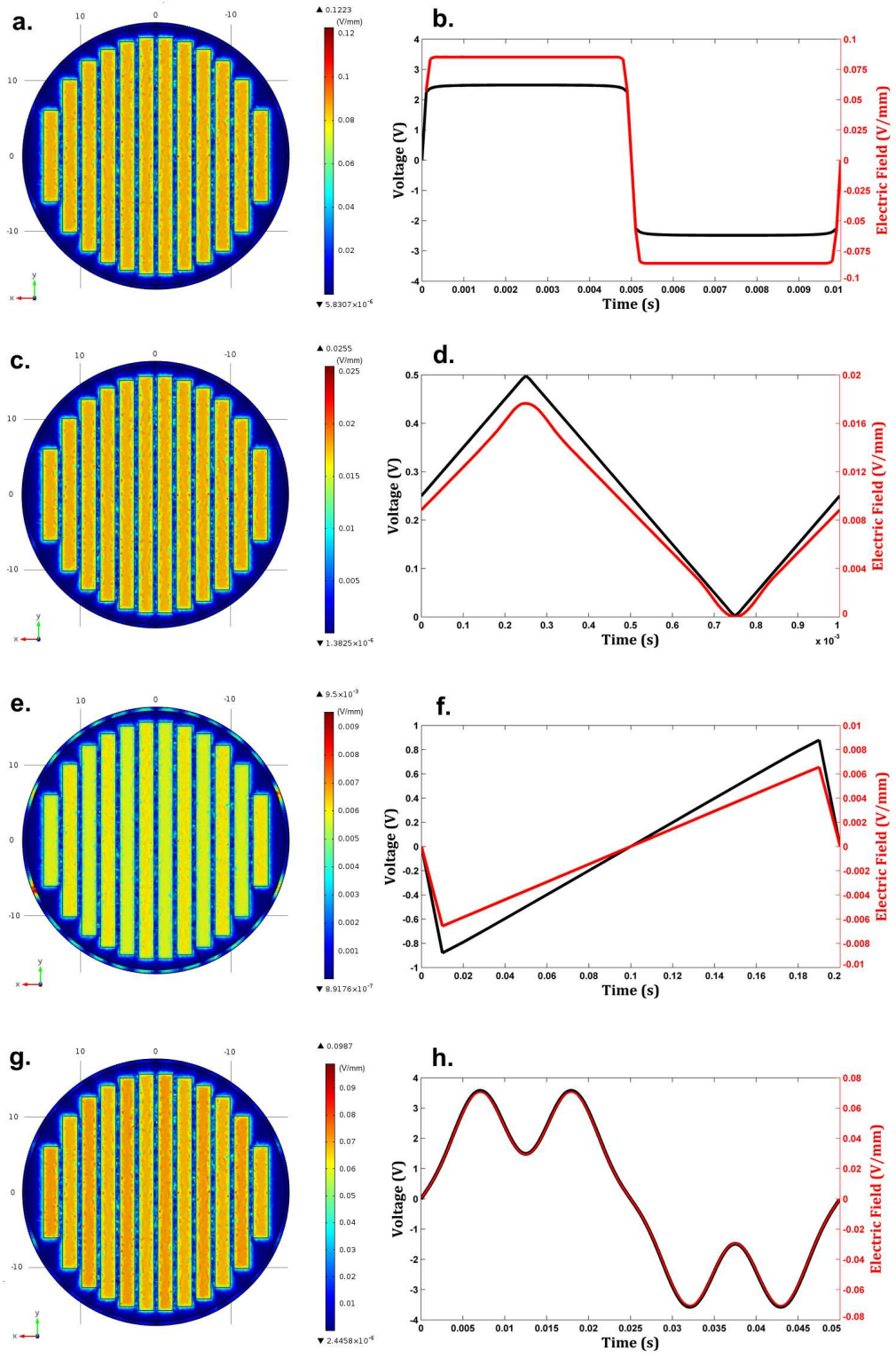

Fig. S5: Simulation results of EF distributions and strengths on MED2 (z=0.505 mm) according to the following periodic excitations applied to stimulator' electrodes: a. 2D EFs: squared excitation (SQ ST) (5 V, 100 Hz). **b**. EFs on a midpoint above a gap (GM): SQ ST (CC =99.88%). **c**. 2D EFs: triangular excitation (TR ST) (0.5 V, 1 Hz). **d**. EFs on GM: TR ST (CC =99.98%). **e**. 2D EFs: sawtooth excitation (SW ST) (2 V, 5 Hz). **f**. EFs on GM: SW ST (CC =99.99%). **g**. 2D EFs: arbitrary excitation (AR ST) (3.5 V, 20 Hz). **h**. EFs on GM: AR ST (CC =100%). EFs were obtained when voltages reach maximum amplitudes (at $\pi/2$ rad in the triangular waveform). Results shown in 2nd column refer to EFs in [0 2π] rad. The midpoint above a gap is (x, y, z)=(0, 0, 0.5) mm from such horizontal planes.

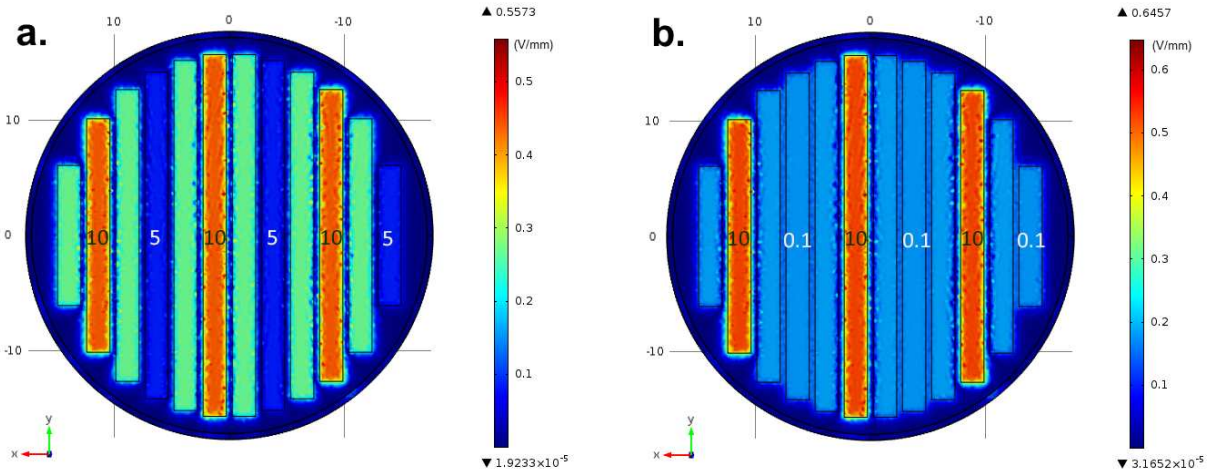

Fig. S6: Simulation results of EF distributions and strengths on MED3 (z=0.510 mm) when electrodes are differently supplied by static excitation: a. 2D EFs: 10 V and 5 V excitations. **b**. 2D EFs: 10 V and 0.1 V excitations. The voltage supplying each pair of electrodes is illustrated.